Mapping Multiplexing Technique (MMT): A Novel Intensity Modulated Transmission Format For High-Speed Optical Communication Systems

MOHAMED ASAAD ELSHERIF, MSc

Thesis submitted to The University of Nottingham,
Department of Electrical and Electronic Engineering,
Faculty of Engineering, for the degree of
Doctor of Philosophy, May 2016

Abstract

There is a huge rapid growth in the deployment of data centers, mainly driven from the increasing demand of internet services as video streaming, e-commerce, Internet Of Things (IOT), social media, and cloud computing. This led data centers to experience an expeditious increase in the amount of network traffic that they have to sustain due to requirement of scaling with the processing speed of Complementary metal–oxide–semiconductor (CMOS) technology. On the other side, as more and more data centers and processing cores are on demand, as the *power consumption* is becoming a challenging issue. Unless novel power efficient methodologies are innovated, the information technology industry will be more liable to a future power crunch. As such, low complex novel transmission formats featuring both power efficiency and low cost are considered the major characteristics enabling large-scale, high performance data transmission environment for short-haul optical interconnects and metropolitan range data networks.

In this thesis, a novel high-speed Intensity-Modulated Direct-Detection (IM/DD) transmission format named "*Mapping Multiplexing Technique (MMT)"* for high-speed optical fiber networks, is proposed and presented. Conceptually, MMT design challenges the high power consumption issue that exists in high-speed short and medium range networks. The proposed novel scheme provides low complex means for increasing the power efficiency of optical transceivers at an impactful tradeoff between power efficiency, spectral efficiency, and cost. The novel scheme has been registered as a patent (*Malaysia PI2012700631*) that can be employed for applications related but not limited to, short-haul optical interconnects in data centers and Metropolitan Area networks (MAN).

A comprehensive mathematical model for N-channel MMT modulation format has been developed. In addition, a signal space model for the N-channel MMT has been presented to serve as a platform for comparison with other transmission formats under optical channel constraints. Especially, comparison with M-PAM, as meanwhile are of practical interest to expand the capacity for optical interconnects deployment which has

been recently standardized for *Ethernet IEEE 802.3bs 100Gb/s* and in today ongoing investigation activities by *IEEE 802.3 400Gb/s Ethernet Task Force*.

Performance metrics have been considered by the derivation of the average electrical and optical power for N-channel MMT symbols in comparison with Pulse Amplitude Modulation (M-PAM) format with respect to the information capacity. Asymptotic power efficiency evaluation in multi-dimensional signal space has been considered. For information capacity of 2, 3 and 4 bits/symbol, 2-channel, 3-channel and 4-channel MMT modulation formats can reduce the power penalty by 1.76 dB, 2.2 dB and 4 dB compared with 4-PAM, 8-PAM and 16-PAM, respectively. This enhancement is equivalent to 53%, 60% and 71% energy per bit reduction to the transmission of 2, 3 and 4 bits per symbol employing 2-, 3- and 4-channel MMT compared with 4-, 8- and 16-PAM format, respectively.

Beside the power efficiency advantage, N-channel MMT data capacity multiplexing feature enhances the eligibility for scaling the baud rate with the limitations that exists in electronic and optical components operating at a fraction of the aggregated data rate. Therefore, 2-channel MMT has the feature to scale its baud rate to 1/2 of its aggregated bitrate compared with OOK. While, 3-channel MMT has a baud rate equivalent to 1/3 of its aggregated bitrate compared with OOK. Also, 4-channel MMT is capable of decreasing the electronic requirement of its components to a baud rate equivalent to 1/4 of the aggregated bit rate compared with OOK.

One of the major dependable parameters that affect the immunity of a modulation format to fiber non-linearities, is the system baud rate. The propagation of pulses in fiber with bitrates in the order > 10G, is not only limited by the linear fiber impairments, however, it has strong proportionality with fiber intra-channel non-linearities (Self Phase Modulation (SPM), Intra-channel Cross-Phase Modulation (IXPM) and Intra-channel Four-Wave Mixing (IFWM)). Hence, in addition to the potential application of MMT in short-haul networks, the thesis validates the practicality of implementing N-channel MMT system accompanied by dispersion compensation methodologies to extend the reach of error free transmission (BER $\leq 10^{-12}$) for Metro-networks. In chapter 5, N-Channel MMT has been validated by real environment simulation results to outperform the performance of M-PAM in tolerating fiber non-linearities.

By the employment of pre-post compensation to tolerate both residual chromatic dispersion and non-linearity, performance above the error free transmission limit at 40Gb/s bit rate have been attained for 2-, 3- and 4-channel MMT over spans lengths of up to 1200Km, 320 Km and 320 Km, respectively. While, at an aggregated bit rate of 100 Gb/s, error free transmission can be achieved for 2-, 3- and 4-channel MMT over spans lengths of up to 480 Km, 80 Km and 160 Km, respectively.

At the same spectral efficiency, 4-channel MMT has realized a single channel maximum error free transmission over span lengths up to 320 Km and 160 Km at 40Gb/s and 100Gb/s, respectively, in contrast with 4-PAM attaining 240 Km and 80 Km at 40Gb/s and 100Gb/s, respectively.

Keywords:-

Optical Interconnects, Intensity-Modulated Direct-Detection Systems (IM/DD), Mapping Multiplexing Technique (MMT), Metropolitan Area Networks (MAN) and Fiber Non-Linearities.

Acknowledgments

First of all, I would like to thank my supervisor Prof. Amin Malek Mohammadi for his insights, guidance and support over the years. I have benefitted from the numerous opportunities, advices and experiences he provided me. It was a great pleasure working under his supervision. I would like also to thank my co-supervisor Dr. Wee Gin Lim for his fruitful discussions during the PhD. In addition, I would like to thank my internal examiner Dr. Gnanam Gnanagurunathan for her time and willingness to examine my work. I also want to thank my colleague and friend Nguyen Dong-Nhat for the productive collaboration and useful discussions we had together.

Both, the Ministry of Science, Technology and Innovation (MOSTI) Malaysia and The University of Nottingham, financially funded this research work. Thanks to them.

I would like to express my deepest gratitude and special thanks to both, Dr. Ashraf Abdelraouf & Dr. Lamia Khashan for their continuous all-time support, encouragement and valuable advice since the start of my bachelor degree studies and up until this moment. This work would not have been realized without their motivation.

I would also like to take the opportunity to thank all my professors, colleagues and friends in the Department of Electronics and Communication Engineering, Misr International University.

My warmest and sincere thanks go to my parents Mr. & Mrs. Asaad Elsherif and my sisters, for their continuous never ending love, support and patience. I thank my father and mother for raising me with good values and without whom I would not be the person that I am today.

Finally, I am dedicating this work to my beloved wife and life-partner Dina Kouta, without her love, support and patience; I do not even imagine how it would have been done. Also, I owe a thank you to my father and mother in law Mr. & Mrs Alsaid Kouta for their encouragement and support.

Contents

List of Abbreviations

100GBase-ER4	100G Ethernet – Extended Range-4-channels
40Gbase-LR4	40G Ethernet – Long Range-4-channels
40Gbase-SR4	40G Ethernet – Short Range-4-channels
ADC	Analog to Digital Converter
ASIC	Application Specific Integrated Circuits
ANSI	American National Standards Institute
ASE	Amplified Spontaneous Emission
AS	Aggregate Switch
AWGN	Additive White Gaussian Noise
BER	Bit Error Rate
CGR	Cumulative Growth Rate
CS	Core Switch
CMOS	Complementary metal–oxide–semiconductor
CD	Chromatic Dispersion
CENELEC	European Committee for Electro-technical Standardization
CW	Continuous Wave
DAC	Digital to Analog Converter
DML	Directly Modulated Laser
DCF	Dispersion Compensation Fiber
DSF	Dispersion Shifted Fiber
DC	Direct Current
EML	Externally Modulated Laser
EM	External Modulator
EDFA	Erbium Doped Fiber Amplifier
FEC	Forward Error Correction
FPGA	Field Programmable Gate Arrays
GVD	Group Velocity Dispersion
HBTs	Heterojunction Bipolar Transistors
HSSG	High Speed Study Group
IM	Intensity Modulated
IP	Internet Protocol
ITU	International Telecommunication Union
ISI	Inter-symbol-interference
IXPM	Intra-channel Cross-Phase Modulation
IFWM	Intra-channel Four-Wave Mixing
IEEE	Institute of Electrical and Electronics Engineers

IM/DD	Intensity-Modulated/Direct-Detection
InP	Indium Phosphide
InGaAs	Indium Gallium Arsenide
LED	Light Emitting Diode
LD	Laser Diode
MCML	MOS Current Mode Logic
MZM	Mach-Zehnder Modulator
MQW-MZM	Multiple-Quantum-Well Mach-Zehnder Modulator
MMT	Mapping Multiplexing Technique
MMF	Multi-Mode Fiber
MAN	Metropolitan Area Networks
ML	Maximum Likehood
MAP	Maximum A Posteriori
MLSD	Maximum Likehood Sequence Detection
NLS	Non-linear Schrodinger
NRZ-OOK	Non Return to Zero ON-OFF Keying
NZDF	Nonzero Dispersion Fiber
NF	Noise Figure
OTN	Optical Transport Networks
OOK	On-Off Keying
OSI	Open System Interconnection
PRBS	Pseudo Random Bit Sequence
PDF	Probability Density Function
PPM	Pulse Position modulation
PAM	Pulse Amplitude Modulation
PHY	Physical Layers
PIN	PIN photodiode
PWM	Pulse Width Modulator
RDF	Reverse Dispersion Fiber
RIN	Relative Intensity Noise
RZ-OOK	Return to Zero On-Off Keying
RMS	Root-Mean-Square
SBS	Stimulated Brillouin Scattering
SPM	Self-Phase Modulation
SMF	Single Mode Fiber
SONET	Synchronous Optical Networking
SDH	Synchronous Digital Hierarchy
SNR	Signal To Noise Ratio
SiP	Silicon Photonics
TOR	Top of Rack switch
TDM	Time Division Multiplexed
TIA	Trans-Impedance Amplifier
VLC	Visible Light Communication
VCSEL	vertical-cavity surface-emitting laser
WAN	Wide Area Network
WDM	Wavelength Division Multiplexing

List of Figure

List of Tables

1. Chapter 1: Introduction

1.1 Overview

1.1.1 Fiber optic solutions for Metro and Short Range Networks

Recently, optical transmission systems have received much interest as one of the major and dominant solutions for metropolitan and short-range area networks. This was stimulated by the growing desire for bandwidth and speed, enabled by the high-speed optical transmission systems. In 2014, Cisco Forecast and Methodology study has estimated that metro traffic demand for metropolitan area networks will be twice as fast as long-haul networks and will account for 62% of the global IP traffic demand in 2018 as shown in figure 1.1[1]. At 2015, the same research group released its study estimating an increased share for metro networks and reported that it will account to 66% in 2019 [2]. This is due to the incremental role of content delivery networks, which are transmitted through metro networks and bypassed by long-haul networks. Figure 1.2 shows the exponential increase in the data traffic per month for metropolitan networks compared to long-haul networks where the estimated growth factor will be doubled by 2018. Studies have predicted 560% increase in metropolitan area network traffic demand between (2012-2017)[3]. As such, this rapidly increasing demand is driving researchers to look into possible capacity expansion solutions for high speed metropolitan and optical access networks.

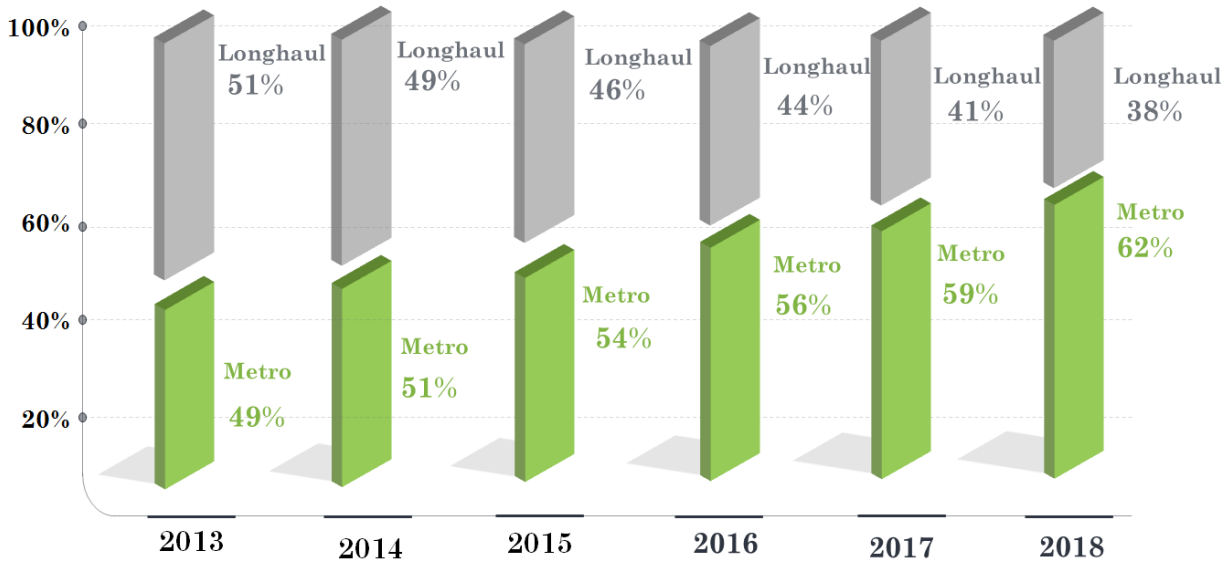

Figure 1.1 Global IP data traffic growth percentage for metropolitan and long-haul networks[1].

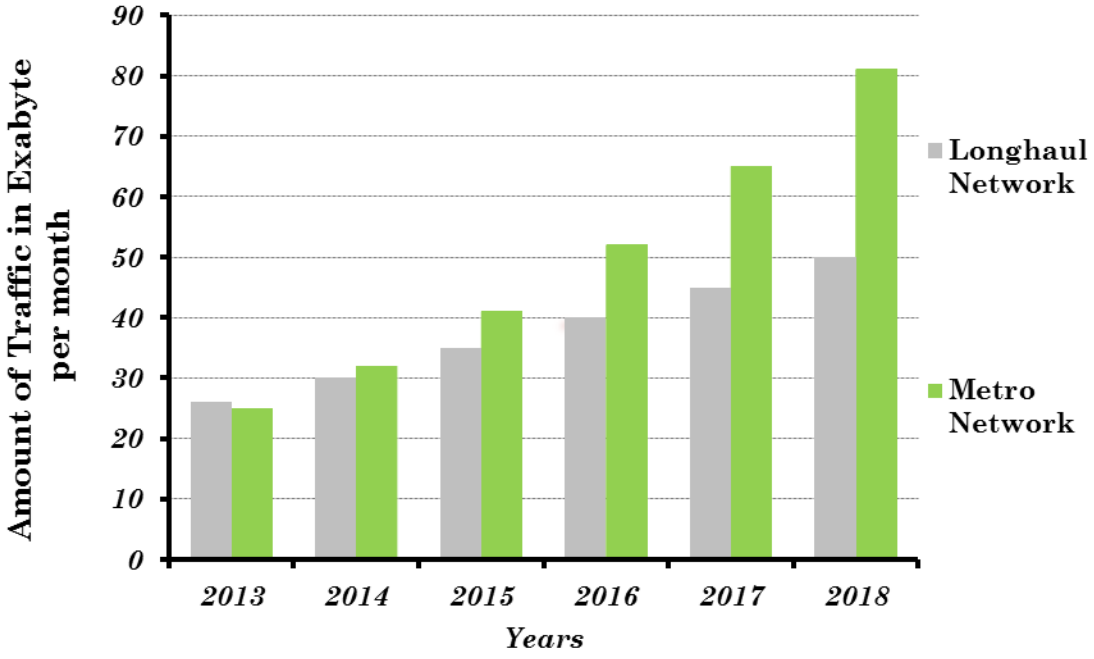

Figure 1.2 Global IP data traffic growth for metropolitan and long-haul networks between 2013-2018[1].

1.1.2 Ethernet

There are three main standards for short and medium range optical links; Ethernet, Fiber Channel and Infiniband. Ethernet is considered the major and the widest spread of them, which standardize links over copper and fiber optic links.

The IEEE standards include many forms that support variable distances and throughput speeds. To date, figure 1.3 shows clearly all supported IEEE standardization with respect to link bitrates, transmission distances and fiber type, enabling high speed data connectivity for short and medium range links. In 1995, 100 Mbit/s speed has been standardized in *IEEE802.3u* and known at that time as "Fast Ethernet" and referred to it as (100Base-SX)[4]. In 2001, Gigabit Ethernet has been released through *IEEE 802.3z* standardization, which was referred to it as (1000Base-LX "Long Range" and 1000Base-SX "Short Range"). In 2002, *IEEE 802.ae* standard has been issued to announce the emerge of 10Gigabit Ethernet and was referred to it as (10Gbase-SX and 10Gbase-LR [5]. In 2009, a collaborative work has started between International Telecommunication Union's Telecommunication Standardization (ITU-T) and *IEEE 802.3* working group to provide a standardization for 40Gb/s and 100Gb/s Ethernet for next-generation Optical Transport Networks(OTN) [6]. The working groups objective was to support 40Gb/s and 100Gb/s bitrates for distance at least 10Km and 40 Km using SMF[6]. In 2010, the IEEE 802.3 have released the standardization and referred to it as (40Gbase-SR4, 100Gbase-SR4, 40Gbase-LR4 and 100Gbase-LR4), which was considered at that time the first Ethernet penetration for metropolitan area network and Wide Area Network (WAN) that was dominated by Synchronous Optical Networking (SONET) and Synchronous Digital Hierarchy (SDH) protocols [7]–[9]. The existing 100GBase-ER4 (ER4-Extended Range- 4-channels) and 40GBase-ER4 have been standardized to support the 40 km metro application such as Datacenter to Datacenter links, Metro Ethernet,…etc[10]. As such, the demand is rising for extending the transmission reach of optical metro links utilizing low cost optical link solutions.

Short link distances are necessitated by cost effective cabling solutions being a significant trade-off parameter. For short-range application < 1Km, Multi-Mode Fiber (MMF) is employed for IM/DD systems. This is due to its lower cost and relatively good performance for this kind of applications performance requirement. However, multi-mode fibers are limited by the low bandwidth distance product, which leads to a limitation in both system throughput and link distance. In 2014, 400Gigabit Ethernet Task force has started the investigation for SMF and MMF links through its standardization *IEEE P802.3bs*. However, it deduced that MMF is not able support intra data centers connectivity at bit rate of 400Gb/s. Hence, started its investigation for 400Gb/s over 500m SMF[11], [12].

Hence, Single Mode fiber (SMF) is considered a perfect optimum alternative for longer transmission distances links aided by its superiority in supporting higher capacities. One of the significant high consumers for these sort of links; are data centers point-to-point optical interconnects.

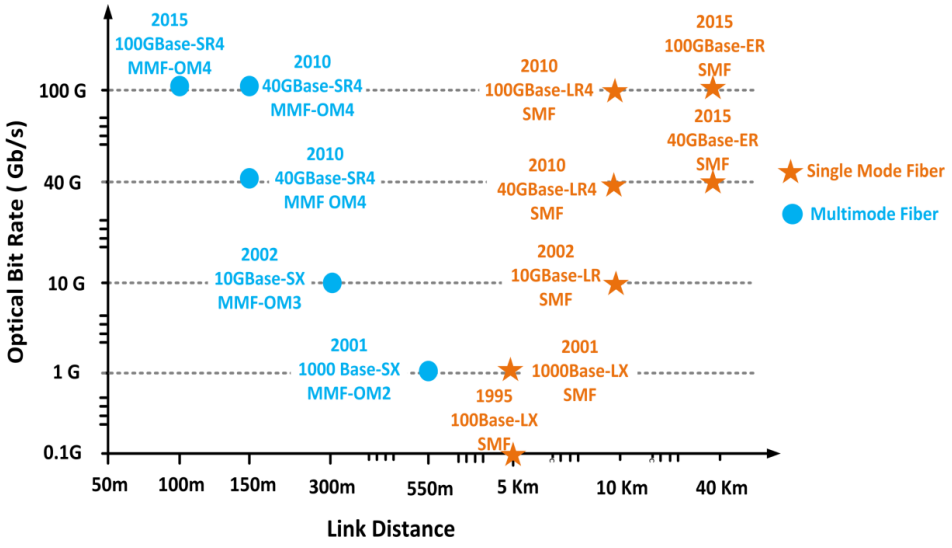

Figure 1.3 IEEE Standards for Ethernet with respect to link distance, transmission speed and fiber type.

1.2 Problem statement and Research Motivation

1.2.1 Data Center Power Consumption

On the other side, as more and more data centers and processing cores are on demand, as the power consumption is becoming a challenging issue. Greenpeace's Maker IT Green report [13], estimates that the global demand for electricity from data centers was around 330bn kWh in 2007. This demand is projected to triple by 2020 (more than 1000bn kWh). The typical electrical consumption of this class of data centers are in the order of tens of megawatt, equivalent to supply a small size city with electricity and the total electricity consumed by data centers are equivalent to the fifth country whole consumption of electricity [14]–[18]. In 2013, power demand for data centers alone grew 40GWatt[19]. Although, the United States is the largest consumer of data center power globally, followed by Japan, UK, Germany and France, however, there are fast emerging markets for data centers in countries such as China, Singapore ,Malaysia, Egypt, etc.. This is aided by the virtualization and cloud computation widespread in which recent studies predicted that in 2019, 86% of the workload will be handled and stored in cloud data centers, while just 14% will be processed in conventional localized data centers[20].

SMART 2020 is a report that quantifies the role and efforts of the Information Communication Technology (ICT) industry sector in overcoming the environmental negative impacts of carbon excess usage[21]. In addition, SMART2020 evaluates the energy saving efforts through the utilization of green technology in reducing the harmful emissions from the ICT sector. From the environmental perspective, SMART2020 annual report has accounted data centers responsible for 14% of the total gas emissions from the information technology sector in 2007 [21]. SMART 2020 encourages an upgrade and optimization in ICT sector infrastructure utilizing energy efficient methodologies. It reported that a huge energy saving can be achieved by employing smart motor systems, smart logistics, smart buildings and smart grids.

Innovative methodologies to lower the power consumption of data centers in every aspect (i.e, cooling infrastructure, devices heat dissipation, data transmission efficiency, etc..), which is mostly classified to be green technologies, are under active research interest [15], [18], [22]–[27]. Recent act from worldwide organizations is taking place to produce annual reports monitoring the progress of big data centers hosts in terms of their efforts in turning their data centers facilities to employ Green power technologies [19].

1.2.2 Data Center Optical Interconnection

The rapid growth in network traffic demand has motivated the continual development in 100G, 400G technologies in the context of next generation Multi-Giga Ethernet for short-haul and metropolitan data networks[1]. One of the significant IP consumers in metropolitan area network are data centers in which the data centers traffic demand will reach 10.4 Zettabyte per year by 2019 with a CGR of 25% [20]. Figure 1.4 shows the data center medium range links with cloud applications in metropolitan area architecture.

In order to a give an insightful close analysis to these data, it is worth noting that in 2014, 75.4% of the data traffic remained inside the data center , while 17.8% was from data center to user and 6.8% from data center to data center[20]. This level of network traffic inside the data centers with thousands of servers and rigorous requirement for low latency, scalable and high throughput solutions, has turned the attention to the employment of power efficient optical interconnects to replace the electrical ones[28].

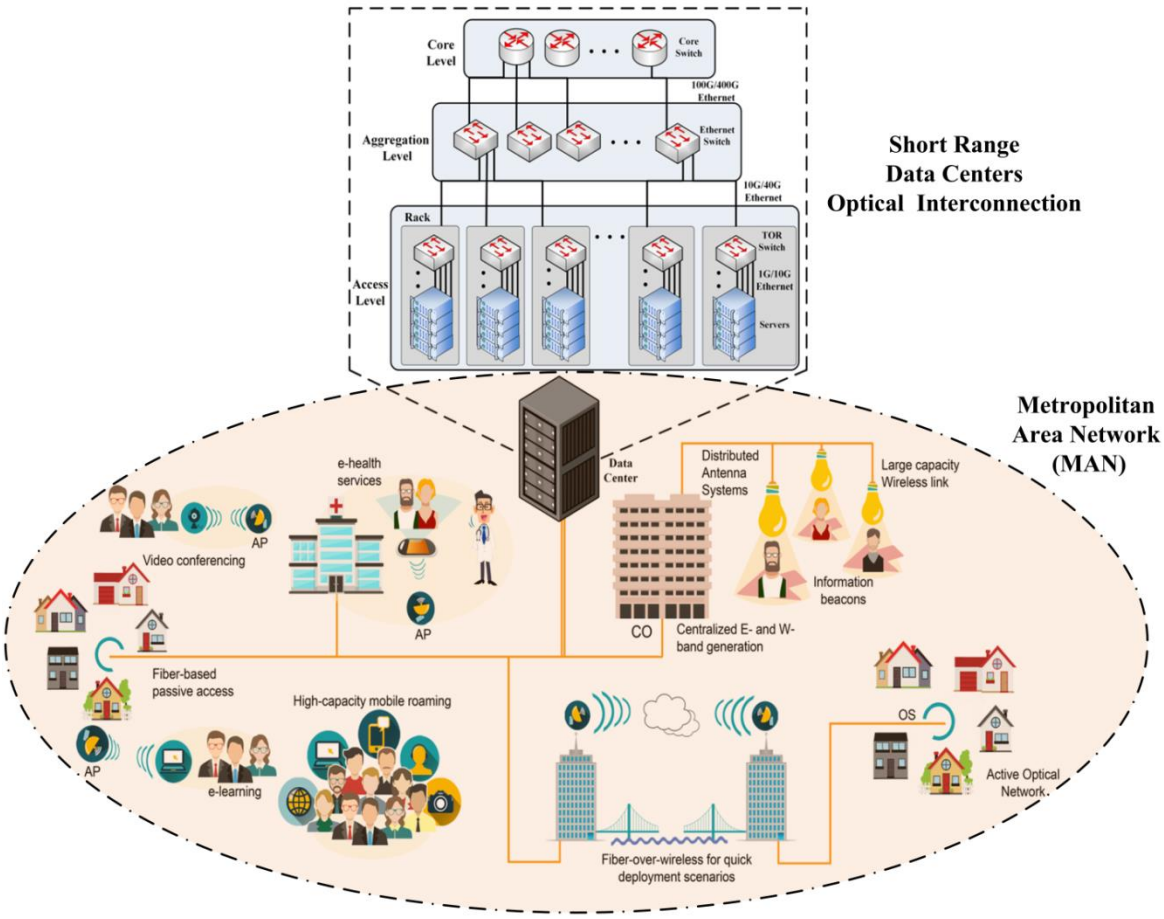

Figure 1.4 Data center optical medium range links with cloud applications in a metropolitan area architecture.

Nowadays, data center traffic relies on electronic switching employing point to point high speed optical interconnects[29]. The data centers with thousands of servers are linked in layers by multiple Ethernet switches. Figure 1.5 shows a 3-tier data center architecture interconnected by multiple varied speed Ethernet optical interconnections. First, the Top of Rack switch (TOR) installed and hosting a number of server blades through 1G/10G line rate links. Second layer, interconnecting a number of TOR switches to an Aggregate Switch (AS) with higher multiplexing throughput reaching 10/40G. The AS's are further interconnected to the Core Switch (CS) employing 100G/400G Ethernet.

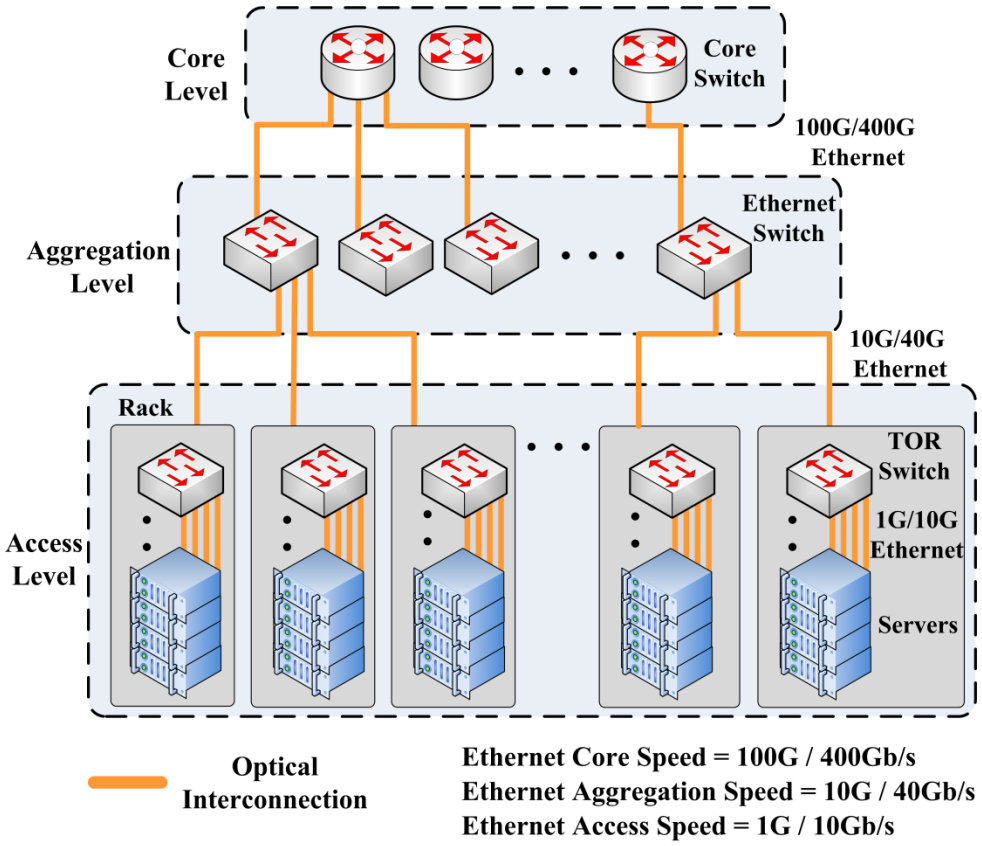

Figure 1.5 Typical 3-Tier data center optical interconnection with multiple Ethernet switches.

As such, aggregated bitrates of 10Gb/s, 40Gb/s, 100Gb/s and 400Gb/s Ethernet speeds are attracting research communities for cost effective optical solutions for next generation data center optical interconnections.

1.2.3 Intensity Modulated Multilevel Transmission Formats

The highest channel transmission rate supported by *IEEE 802.3* electrical interfaces is 25Gbit/s, that is due to the existence of many electronic signal-processing challenges and link losses [12]. One way to increase the bit rate, the employment of one or a plural of different data transmission methodologies as increasing the number of levels, channels, modulation order and baud rate. Wavelength Division Multiplexing (WDM) is one of the classical approaches for expanding the capacity, however, it imposes higher system cost and an increased power consumption, which is due to the number of optical components employed. Optical components have been reported being the dominant cost element in

optical links [30], [31]. Higher order Intensity-Modulated/Direct-Detection (IM/DD) systems with single wavelength have attracted much interest recently due to its low complexity and cost compared with multiple wavelength multiplexing[32], [33]. This is driven by the huge progress in silicon photonics with its advancement in the integration of photonic components with the CMOS manufacturing process[34]–[40]. The IEEE High Speed Study Group (HSSG) is in the process of an extensive investigation for the feasibility of different economic low complex alternatives for next generation 100G and 400G optical Ethernet networks [41].

M-PAM is considered a perfect candidate for systems featuring an optimum trade-off balance between high performance, low cost and complexity for short-haul and metro area applications[42]–[50]. Recently, *IEEE 802.3bm* Task Force (TF) has investigated the technical performance, feasibility and different design aspects for 4-PAM, 8-PAM and 16-PAM multilevel formats on Single Mode Fiber (SMF) to be standardized to the existing 100 GBASE-LR4 [51]. The reports demonstrated the deployment practicality of 4-PAM, and 8-PAM in the context of being an upper boundary limit for the modulation order due to the exponential increase in impairment penalties with the increment in the number of levels[30]. In 2014, *IEEE 802.3bj* standard has approved 4-PAM as a modulation format for 100Gb/s backplane PHY of 100GBASE-KR4[52].

M-PAM has M number of levels for the transmission of $\log_2(M)$ bits of information. Hence, M-PAM is considered a bandwidth limited signaling format, since the spectral requirement is in the order of $1/\log_2(M)$ of On-Off Keying (OOK), while its power penalty is $(M-1)$ of OOK at fixed bandwidth. On the other hand, Pulse Position modulation (M-PPM) divides the symbol duration T_s in to M number of sub intervals with duration T_s/M for the transmission of $\log_2(M)$ bits of information with a two constant distinct levels. Hence, M-PPM is considered a power limited signaling format with a power efficiency advantage, while its spectral requirement is $M/\log_2(M)$. The M-PAM and M-PPM performances have been investigated for intensity modulated direct detection systems (IM/DD) in [50], [53], [54].

As above-mentioned considerations, the thesis interest to propose a solution to the problem of the high power consumption issue that exists in high-speed dense short-haul optical interconnects and metropolitan area networks links. This could be achieved by introducing novel power efficient data transmission alternatives for short and medium range optical links. The essence of the novel transmission format is its capability to meet t8he huge capacity demand simultaneously combined with a reduction in power consumption. This can be realized by reducing the optical sensitivities of error-free high-capacity data transmissions, which consequently reflects a lower cost per transported bit of information.

1.3 Thesis Aims and Objectives

This thesis had an ultimate goal to reach an impactful trade-off between design parameters to overcome the challenges and meet the requirements of high power consumption data intensive applications.

The thesis aims to propose a novel IM/DD transmission format named *"Mapping Multiplexing Technique (MMT)"* that can be practically employed for applications related but not limited to, high-speed short-haul optical interconnects and metropolitan area high-speed links. The MMT features a low-cost, high capacity and power efficient advantages, enabling large-scale high-performance data transmission environment for high-speed optical links.

The main general objectives of this research dissertation are as follows:-

1- Design a novel power efficient and low-cost transmission format for high-speed optical communication systems in short-haul and Metropolitan Area Networks (MAN).
2- Formulate a mathematical model for the structure and properties of the proposed data transmission format.
3- Develop the theory and governing rules for the multiplexing format, transmitter and detection circuits.

4- Evaluation for the performance of the proposed technique in comparison to relevant existing schemes.
5- Comparison between the proposed format and other relevant transmission formats with respect to their power efficiency.
6- To develop a Bit Error Rate (BER) model for the proposed transmission format.

1.4 Scope of Work

As far as the Open System Interconnection (OSI) 7-layer reference model is concerned, the research work proposed through MMT signaling format concerned with its utilization in the physical layer.

This research work incorporated a pragmatic methodology to achieve the desired objectives focusing on three main goals:-

a) Design and development of the theory and rules behind the MMT transceiver under optical channel constraints for non-coherent optical communication systems.
b) Analytical evaluation for N-channel MMT performance by comparing it with existing modulation formats. The incorporated transmission formats is selected based upon their relevance to the proposed transmission technique.
c) Numerical performance investigation of N-channel MMT tolerance to fiber linear and non-linear impairments for future deployment in desired short and medium range applications.

Exhaustive procedures, design aspects and performance evaluation metrics have been executed through the thesis focusing on the three aforementioned main goals to achieve the desired thesis objectives.

1.5 Contribution of this research work

MMT design aspects and performance evaluation metrics considered in this thesis have comprised the following:-

1- Development of signal space model for the first time for N-channel MMT system.

   a) Definition of the basis functions for the signal structure of N-channel MMT *(in section 3.2).*
   b) Derivation for the MMT symbols with respect to the defined basis functions.
   c) Construction for the constellation diagram of N-channel MMT format in a multi-dimensional signal space geometry under optical channel constraints.

2- Transceiver system design included the following :-

   a) Transmitter design with an adequate governing data multiplexing and mapping algorithms. This included the following:-
      i. Definition for the basic properties and waveform synthesis of MMT symbol structure based on the system information capacity (in bits/symbol), which is equivalent to the number of users (or channels) *(in section 3.3).*
      ii. Mathematical formulation for the MMT dual-slot and multilevel waveform generator.
   b) Proposal for two receiver detection designs utilizing:-
      i. Optimal detection receiver, which is based upon Maximum Likehood (ML) criterion *(in section 3.3.3).*
      ii. Threshold detection, which is based upon low complex multiple stage detection algorithm*(in section 3.3.3).*

3- Performance metrics to assess MMT and compare it with other similar modulation formats. This comprised the following:-

   a) Derivation of closed form expressions for calculating the average electrical and optical power for N-channel MMT symbols, based upon MMT signal space constellation. These expressions are governed by the system information capacity or in other words number of channels *(in section 4.1)*.

b) Derivation of an explicit expression for the theoretical BER calculation of N-channel MMT format with respect to the received optical power in the presence of Additive White Gaussian Noise (AWGN) model *(in section 4.2).*

c) Optical power penalty comparison between N-channel MMT and M-PAM modulation formats, relative to OOK with respect to fixed information capacity of 2-, 3- and 4-bits/symbol. The model has encountered the three most relevant noise sources in IM/DD system: shot noise, thermal noise and relative intensity noise at aggregated bit rates of 10Gb/s, 40 Gb/s and 100 Gb/s *(in section 4.2.2).*

d) Development of a bit error rate estimation model for MMT threshold detection receiver based upon MMT Gaussian Probability Density Function (PDF) *(in section 3.4.2).*

e) Establishment for asymptotic power efficiency assessment comparison between N-channel MMT and M-PAM relative to OOK, to verify our BER results presented in (iii) *(in section 4.3).*

f) Derivation of expressions to calculate the theoretical power penalty of N-channel MMT at both, fixed baud rate and fixed aggregated bitrate.

g) Quantitative numerical analysis for N-channel MMT and M-PAM receiver sensitivities in the presence of pre-amplified receiver model utilizing an integrated simulation module between OptiSystem® and MATLAB® *(in section 5.2).*

h) Quantitative comparison between N-channel MMT and M-PAM transmission formats with respect to their tolerance against chromatic dispersion *(in section 5.3.1).*

i) Performance investigation for the impact of linear and nonlinear impairments in the presence of pre-amplified receiver Amplified Spontaneous Emission (ASE) noise, Group Velocity Dispersion (GVD), Self-Phase Modulation (SPM) utilizing post compensation and pre-post compensation methodologies*(in section 5.3.2).*

j) Exploration for the optimal dispersion compensation methodology (Post compensation and Pre-post compensation) to compensate for the residual dispersion in fiber spans for metro network data transmissions*(in section 5.3.2).*

k) Numerical analysis for the immunity of N-channel MMT and M-PAM signal characteristics in tolerating the impact of non-linear fiber impairments. The immunity is translated to a maximum transmission reach tolerating non-linear impairments such as i.e SPM, Intra-channel Four-Wave Mixing (IFWM) and Intra-channel Cross-Phase Modulation (IXPM) *(in section 5.3.2).*

l) Investigation for the maximum achievable error free transmission at 40Gb/s and 100Gb/s systems in the presence of fiber linear and nonlinear impairments *(in section 5.3.2.8).*

m) Investigation for the impact of non-linear inelastic scattering i.e Stimulated Brillouin Scattering (SBS) *(in section 5.3.2.9).*

n) Exploration on the practical applicability and availability of state of art circuit design methodologies that enable future implementation of MMT transceiver *(in chapter6).*

o) Energy Efficiency comparison between MMT and M-PAM presented through the paper "*Energy Efficient Transmission Scheme Alternative to M-PAM for Short Range Data Communication*".

p) Performance enhancement of 4-channel MMT through optical signal processing presented through paper "*Performance Enhancement of Mapping Multiplexing Technique (MMT) Utilizing Dual-Drive Mach-Zehnder Modulator for Metropolitan Area Networks*".

Figure 1.7 Shows N-channel MMT novel transmission format positioned with respect to digital modulation formats. In addition, the figure summarizes the MMT design aspects and performance evaluation metrics discussed in the thesis.

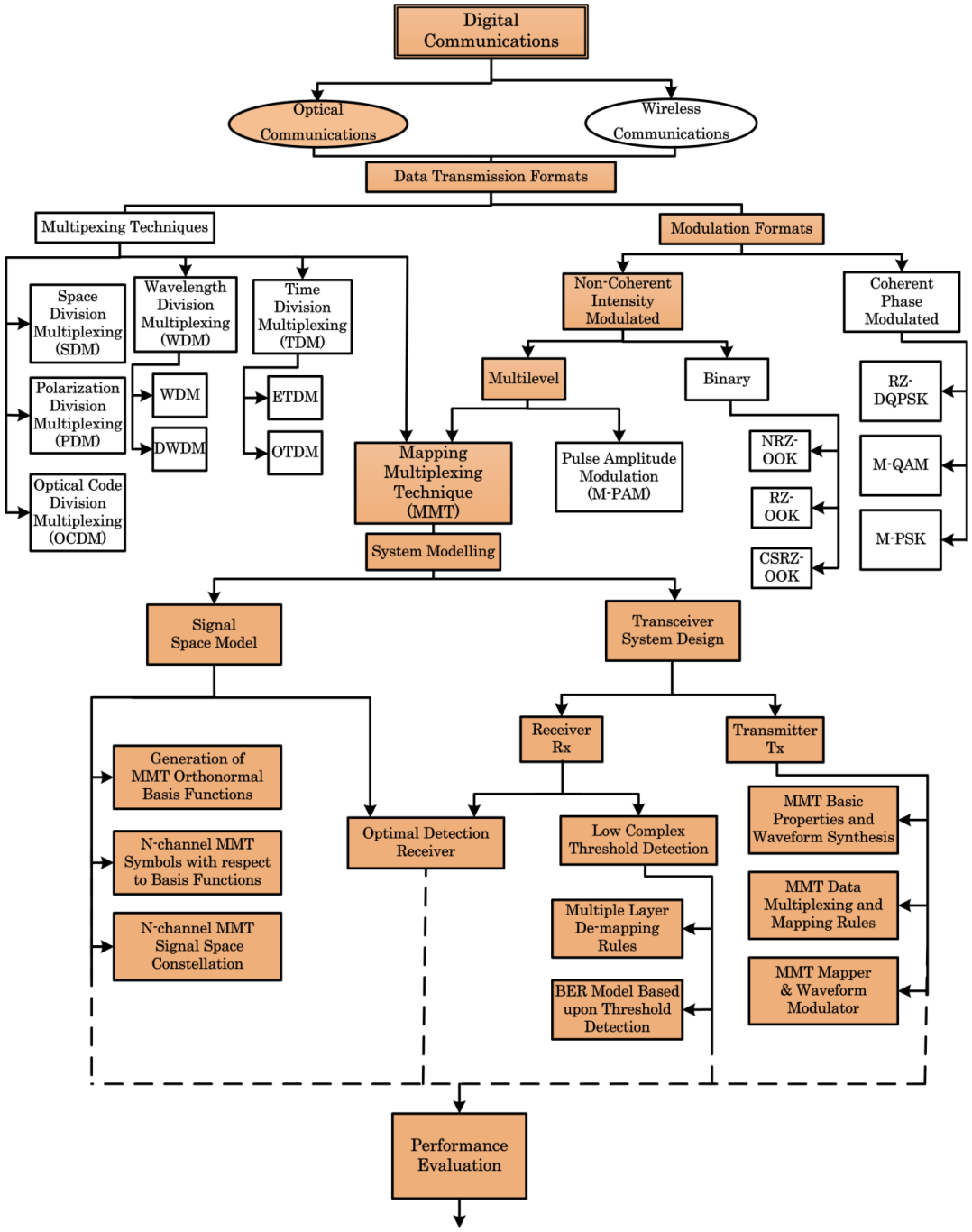
Digital Communications
Optical Communications
Wireless Communications
Data Transmission Formats
Multipexing Techniques
Modulation Formats
Space Division Multiplexing (SDM)
Wavelength Division Multiplexing (WDM)
Time Division Multiplexing (TDM)
Polarization Division Multiplexing (PDM)
Optical Code Division Multiplexing (OCDM)
WDM
DWDM
ETDM
OTDM
Non-Coherent Intensity Modulated
Coherent Phase Modulated
Multilevel
Binary
RZ-DQPSK
M-QAM
M-PSK
NRZ-OOK
RZ-OOK
CSRZ-OOK
Mapping Multiplexing Technique (MMT)
Pulse Amplitude Modulation (M-PAM)
System Modelling
Signal Space Model
Transceiver System Design
Receiver Rx
Transmitter Tx
Generation of MMT Orthonormal Basis Functions
N-channel MMT Symbols with respect to Basis Functions
N-channel MMT Signal Space Constellation
Optimal Detection Receiver
Low Complex Threshold Detection
Multiple Layer De-mapping Rules
BER Model Based upon Threshold Detection
MMT Basic Properties and Waveform Synthesis
MMT Data Multiplexing and Mapping Rules
MMT Mapper & Waveform Modulator
Performance Evaluation

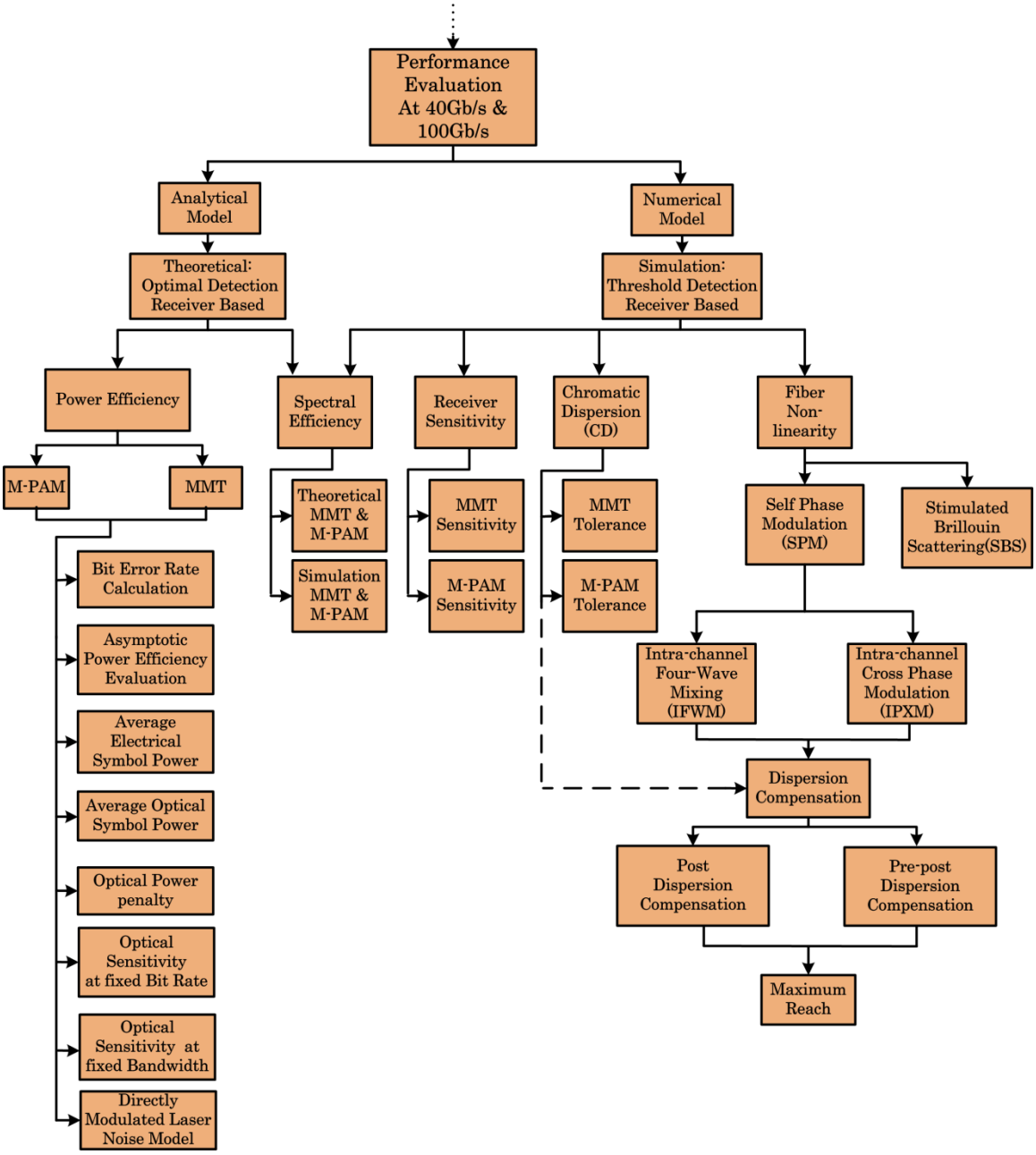

Figure 1.6 N-channel MMT transmission format position in digital communications. The MMT design and performance evaluation aspects discussed in the thesis are highlighted in orange colour.

1.6 Thesis Organization

The structure of the thesis is as follows:-

Chapter 2 "Literature Review": The chapter presents and provides a basic general overview for the fundamentals of modulation formats, fiber impairments, and optical components discussed through the thesis. The basic concepts of IM/DD systems, detection and channel characteristics, are presented. In addition, the chapter describes the main fiber propagation impairments limiting the IM/DD system for short and metro optical communication links.

Chapter 3 "MMT System Model and Performance Metrics": The chapter discusses the methodology behind MMT format structure based upon Shannon channel capacity theory. Afterwards, presents the characteristics and constraints of the IM/DD channel with an overview of N-channel MMT transceiver models. Then, benchmark classical methodology for modulation formats analytical evaluation utilizing signal space analysis for N-channel MMT have been adopted. Moreover, the theory and governing rules behind the data multiplexing and modulation of N-channel MMT system is developed. In this context, the basic properties and waveform synthesis for 2-, 3-, and 4-channel MMT data structures are defined. Furthermore, a proposal for two-receiver detection designs for MMT symbols. The first is an optimal detection based receiver, while, the second is threshold detection based receiver. Then, an illustration for a unique low complex MMT symbol detection and recovery algorithm based upon threshold detection receiver.

Chapter 4 "Analytical Performance Evaluation": In this chapter, analytical performance metrics have been employed to evaluate the performance of N-channel MMT. This included a mathematical derivation for the average electrical and optical power for MMT symbols, based upon signal space constellation. Moreover, mathematical formulation for a closed form expression for theoretical Bit Error Rate (BER) calculation of N-channel MMT. Then, an optical receiver sensitivity comparison between N-channel

MMT and M-PAM at error free transmission is presented. Afterwards, a validation for the results has been executed by performing an asymptotic power efficiency evaluation between N-channel MMT and M-PAM, relative to On-Off Keying format. The comparison between N-channel MMT has been investigated with respect to fixed information capacity, fixed baud rate and fixed bitrate. In addition, explicit expressions to calculate the power penalty at both fixed bitrate and baud rate for N-channel MMT are developed.

Chapter 5 "Numerical Performance Analysis": The chapter presents a numerical investigation on the appropriateness of N-channel MMT for deployment in metropolitan area networks. The investigation comprised a study on the interaction between signal format characteristics and their interplay with fiber linear and nonlinear impairments. An optimization for system settings have been carried to acquire a maximum transmission reach in the presence of fiber intra-channel non-linearities, scattering non-linearity effect and dispersion inherent impairments. The investigation of N-channel MMT and M-PAM immunity to fiber intra-channel non-linearity i.e Self Phase Modulation (SPM), Intra-channel Cross Phase Modulation (IXPM) and Intra-channel Four Wave Mixing (IFWM), is discussed. In addition, an exploration for the impact of Stimulated Brillouin Scattering (SBS) non-linearity on MMT system. Moreover, an exploration for the maximum achievable error free transmission of N-channel MMT and M-PAM at system aggregated bitrates of 40Gb/s and 100Gb/s systems is discussed.

Chapter 6 "MMT Practical Consideration": This chapter addresses the practical applicability, feasibility and availability of state of the art CMOS circuits technology enabling future MMT transceiver implementation. In addition, a comparison between the system requirement for 4-channel MMT, 4-PAM and OOK has been presented.

Chapter 7 "Conclusion and Future Directions": This chapter summarizes the important findings and contributions of the thesis with an outlook on future research directions.

2. Chapter 2: Literature Review

2.1 Introduction

In chapter 2, a basic general overview for the fundamentals of modulation formats, fiber impairments, and optical components that has been discussed through the thesis, is presented. The basic concepts of IM/DD systems, detection and channel characteristics, are presented. In addition, the chapter describes the main fiber propagation impairments limiting the IM/DD system for short and metro optical communication links.

In this thesis, a discussion on the linear and nonlinear limiting factors to MMT consideration for single channel wavelength over single mode fiber. Thus, for linear impairments, the topics chosen to be discussed are: Attenuation and Chromatic Dispersion (CD).

Attenuation is one of the significant impairment in each and every optical communication system, since it determines how far an optical signal can reach and can be detected by a receiver at an acceptable received optical power with a given system performance requirement. In addition, chromatic dispersion is a fundamental limitation in modern optical communication systems, due to the inherent dispersion nature of light wave pulses. Furthermore, CD influences the behavior and propagation of signals over fiber at a low power input transmission region and the interplay with the nonlinear fiber impairment at the high power region. This imposes a limitation on the maximum transmission reach of the system as discussed in chapter 5.

Intermodal dispersion is not discussed in this thesis since it is premeditated a major limitation and dominant factor over multimode fiber (considered for future work as discussed in chapter 7) and do not impose major influence on single mode fiber[55] .

For non-linear impairments, the topics chosen to be discussed related to single channel wavelength is related to intra-channel non-linearities, such that, Self-Phase Modulation (SPM), Intra-channel Four Wave Mixing (IFWM) and Intra-channel Cross Phase Modulation (IXPM). These topics have been selected due to its harmony with MMT proposal and validation of the practicality to be deployed in metro networks accompanied by dispersion compensation scheme (discussed in chapter 5).

Since MMT is considered in this thesis for the transmission of a single optical wavelength channel, hence, inter-channel non-linearities such as four-wave mixing and cross phase modulation is not examined, which will be considered for future works(as discussed in section 7.2).

Moreover, the other class of non-linear fiber impairments that is relevant for investigation; is the non-elastic scattering effects. Non-elastic scattering effects depend on the interaction between the optical pulses and the silica molecules of the optical fiber. The selected scattering effect that is relevant to single channel carrier transmission is Stimulated Brillouin Scattering (SBS). Stimulated Raman scattering is not discussed, as it has an influence with the transmission of multiple wavelength multiplexed systems[56].

2.2 Intensity-Modulated Direct-Detection (IM/DD) system

Intensity-Modulated Direct-Detection (IM/DD) system is a non-coherent method of transmission, where the information is conveyed in the optical intensity of the signal (or power) [57]–[60]. The non-variation in the phase is one of the main differences between non-coherent and coherent signaling formats. The high throughput and low cost features of IM/DD have driven it to be employed for a wide range of applications such as optical interconnects in data centers , short range communication links, Metropolitan Area Networks (MAN), Visible Light Communication (VLC) and infrared communication [61]–[66]. Also, the main advantage of employing IM/DD in a variety of applications is due to the availability of commercial optical low cost on the shelf [67]–[69].

2.2.1 Channel characteristics

Figure 2.1 shows a generic IM/DD system model. The intensity modulated signal is transmitted by modulating the power of the optical carrier $P(t)$. Thus, the opto-electronic component is responsible for the conversion of signal from the baseband frequency to the passband optical frequency generating an optical power signal $P(t)$ based upon the electrical signal $x(t)$, so that

$$P(t) = c\,x(t) \tag{2.1}$$

where c is the electro-optic conversion factor in Watt/Ampere. The electro-optical component can be a Laser Diode (LD), Light Emitting Diode (LED) or an External Modulator (EM)[67].

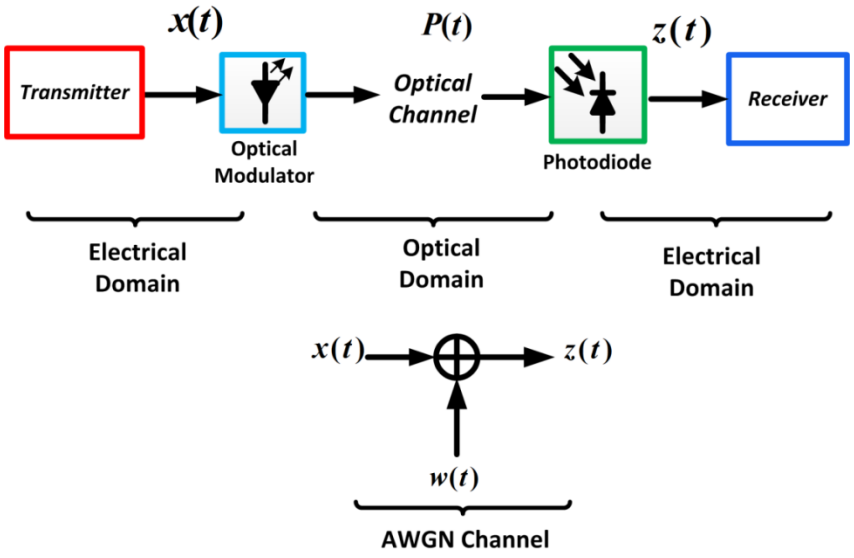

Figure 2.1 shows a general communication system.

In IM/DD, the optical channel can be modelled as an Additive White Gaussian Noise (AWGN) channel, which serves as a good model for all types of noise present [53], [57], [60], [70]. Hence, the received electrical signal can be expressed as

$$z(t) = R_r \ .x(t) + w(t) \tag{2.2}$$

where R_r is the photodiode responsivity in unit Ampere/Watt and $w(t)$ accounts for the Additive White Gaussian Noise.

Due to the physical structure of IM/DD channel, there are two main fundamental constraints on all transmitted modulation formats. Due to the power nature of the transmitted signal, thus, the transmitted signal should maintain a non-negativity constraint at all time instants, such that,

$$\min_{\forall\, t \in \Re} \quad P(t) \geq 0 \tag{2.3}$$

This constraint is taken in to consideration for design and analysis of IM/DD modulation formats[71]. Hence, system designers impose Direct Current (DC) bias for bipolar modulated formats in order to satisfy the non-negativity conditions.

From the safety perspective and since signal propagate in free space, thus, safety regulations must ensure that the emitted radiated power follows international bodies regulations for eye and skin safety precautions[53], [57], [72], [73]. A variety of international standards organizations, such as, the International Electro-technical Commission (IEC) (IEC60825-1), American National Standards Institute (ANSI) (ANSI Z136.1), European Committee for Electro-technical Standardization (CENELEC) have specified guidelines on the emitted power of IM/DD components[74]–[76].

Hence, in contrast to conventional channels, the second constraint is a limitation on the emitted peak and average signal power, so the maximum optical signal power signal should be less than or equal to the maximal power the eye can tolerate P_{eye}, such that,

$$\lim_{T\to\infty} \frac{1}{2T} \int_{-T}^{T} P(t) \leq P_{eye} \tag{2.4}$$

where T is linked to the signal time domain duration.

International bodies imposed safety precautions on both the average and peak power to guarantee eye and skin safety. For optical components sources emitting power at frequency greater than 55KHz, the average optical power is dominant over the peak power[77], [78]. Hence, a minimization for the average optical power of modulation formats is a desirable approach for IM/DD systems.

A numerous work have been carried to develop novel signaling formats and processing techniques in order to minimize the signal average power. Examples of these formats and techniques are constellation shaping, non-equiprobable signaling, multi-dimensional signaling, multilevel coding …etc [60], [79]–[85].

2.3 Signal Space Analysis

Apart from the time and frequency component of signals transmission formats, signal space analysis provide a convenient platform for representation and comparison between modulation formats[86]. This platform is based upon vector-domain analysis, which leads to a geometric representation of modulation formats. Thus, the ability to interpret the transmission formats behavior under different channel models.

Figure 2.2 shows a generic communication system. The system is composed of a number of input data bits k that form a vector symbol component x_k by the aid of a symbol vector mapping. The symbol x_k is composed of R-dimensions in a vector space S, where a condition $R \leq K$ is satisfied.

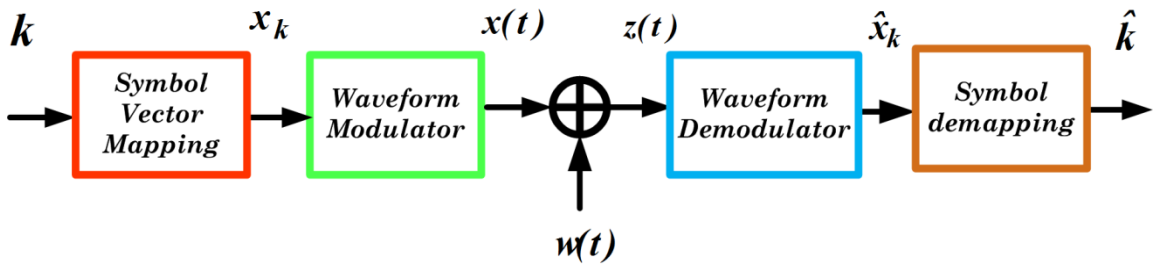

Figure 2.2 shows a general communication system.

Then, a waveform modulator is present which converts the symbol x_k to a time domain unique waveform $x_k(t)$ from a signaling set $x_k(t) = \{x_0(t), x_1(t), ..., x_{K-1}(t)\}$, where K is the total number of signaling waveforms to be transmitted through the channel and $w(t)$ accounts for the AWGN with zero mean and double sided power spectral density $\frac{N_0}{2}$.

Vector space S is considered as an Euclidean space spanned by a number of finite orthogonal R-dimensions. Let us define a number of orthonormal basis functions $\phi_j(t)$ where $j = 1,2, \dots, R$, which exhibit a unit length. These orthonormal basis function are characterized by being orthonormal, thus, can be expressed as

$$\langle \phi_l(t), \phi_m(t) \rangle = \int_{-\infty}^{\infty} \phi_l(t), \phi_m^*(t)\, dt = \begin{cases} 1 & l = m \\ 0 & l \neq m \end{cases} \tag{2.5}$$

$\phi_l(t), \phi_m(t)$ represent the orthonormal basis functions.

The signal $x_k(t)$ can be formed of the weighted linear combination of the basis function, such that,

$$x_k(t) = \sum_{k=1}^{R} x_{k,R}\ \phi_j(t) \tag{2.6}$$

The waveform $x_k(t)$ can be represented at the receiver by $z(t)$, such that,

$$z(t) = x_k(t) + w(t) \tag{2.7}$$

where $w(t)$ accounts for the AWGN in which the Probability Density Function (PDF) can be expressed as

$$PDF(w) = \frac{1}{\sqrt{2\pi\sigma_w{}^2}} e^{-w^2/2\sigma_w{}^2} \tag{2.8}$$

where $\sigma_w{}^2$ is equivalent to the noise variance. Assuming zero mean, the power spectral density in Watt/Hertz for all frequency spectrum is equivalent to

$$W(f) \overset{def}{=} \frac{N_o}{2} \qquad , -\infty \prec f \prec \infty \tag{2.9}$$

where $\frac{N_0}{2}$ is equivalent to the noise double sided power spectral density.

AWGN is a relevant channel model and extensively employed to model the IM/DD system environment[53], [57], [60], [70], [78], [87].

Hence, the noise variance can be expressed as

$$\begin{aligned} E\{w^2\} &= E\left\{\left(\int_{-\infty}^{\infty} w(t).\phi(t)\,dt\right)^2\right\} \\ &= E\left\{\int_{-\infty}^{\infty}\int_{-\infty}^{\infty} w(t).\phi(t).w(\tau).\phi(\tau)\,dt\,d\tau\right\} \\ &= \frac{N_0}{2} \end{aligned} \tag{2.10}$$

where $E\{.\}$ represents the expectation of the variable.

Without loss of generality, the vector representation of the continuous-time model of AWGN can be expressed by its corresponding discrete model as

$$z = x_k + w \tag{2.11}$$

The waveform demodulator extracts the transmitted vector from the received vector z by the aid of waveform demodulator which can be implemented utilizing a bank of matched filters or correlators , such that

$$z_j = \int_{-\infty}^{\infty} z(t)\phi_j(t)\,dt \tag{2.12}$$

The noise w can be expressed in the same form, i.e,

$$w_j = \int_{-\infty}^{\infty} w(t)\phi_j(t)\,dt \tag{2.13}$$

where $j = 1,2,..,R$. The matched filter receiver has an impulse response $h_j(t)$,i.e,

$$h_j(t) = \phi_j(-t) \tag{2.14}$$

By sampling the output of the matched filters, Signal To Noise Ratio (SNR) is maximized and statistics can provide an estimate for the most likely transmitted symbol. The probability conditional distribution of z can be expressed as

$$f_{z|X_k\,sent} = \frac{1}{\sqrt{2\pi\sigma^2}} e^{-\left(\frac{\|z-X_k\|^2}{2\sigma^2}\right)} \tag{2.15}$$

where σ is the variance.

Assuming an equiprobable signaling format, this methodology for symbol detection is based upon optimal detection, which is concerned with the detection employing maximum a posteriori (MAP) or Maximum likehood (ML) optimal detections.

Hence, utilizing the signal space methodology aided by the fact that the noise is AWGN, it can be deduced that this detector outputs the signal vector $\hat{x}_k$ that is calculated being the nearest Euclidean distance to the received signal vector z. Finally, by symbol de-mapping, it is converted to the most likely transmitted input bits $\hat{k}$.

2.4 Memoryless modulation or Non-coherent modulation

The thesis focuses in the area of memoryless multilevel transmission formats. Non-coherent modulation scheme is the least complex. Multilevel signaling allows for lower symbol rates at a fixed data rate, which is favorable in the presence of dispersive signal distortions, as well as for implementing digital electronic signal processing[88],[47].
In this section, an overview on ON-OFF Keying (OOK), Pulse Position Modulation (PPM) and Pulse Amplitude Modulation (PAM) modulation formats is presented. Although, this thesis focuses on multilevel modulation formats, some properties of OOK are reviewed since OOK is a relevant reference of comparison between MMT and other modulation formats as PAM as discussed in [53], [60].

2.4.1 ON-OFF Keying (OOK)

ON-OFF Keying (OOK) is the most widely employed modulation format in optical communication systems[89]. The terms OOK or 2-Pulse Amplitude Modulation are often employed synonymously for 2-PAM. Although, this thesis focuses on multilevel modulation formats, some properties of OOK are reviewed since OOK have been used as a reference of comparison between MMT and PAM as [53], [60]. Non Return to Zero (NRZ-OOK) refers to the fact that for binary high bit, the pulse signal does not return to zero during any instant of the symbol interval, while Return to Zero (RZ-OOK) return to zero at half of the symbol interval[90]. Figure 2.3 shows the symbol structure waveform of NRZ-OOK and RZ-OOK. RZ-OOK signal exhibit better receiver sensitivity compared to NRZ which has been employed for optically pre-amplified system with direct detection in [58] [59].

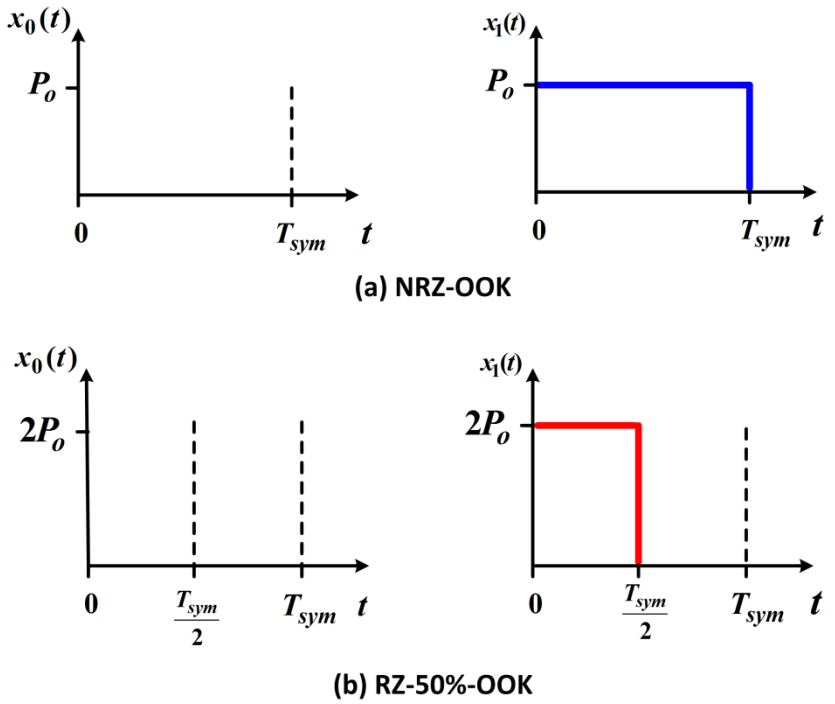

Figure 2.3 Symbol structure waveform of (a) NRZ-OOK and (b)RZ-OOK

RZ-OOK pulse has half the duty cycle (RZ-50%) compared to NRZ , thus, it exhibit an advantage having a higher peak signal at the receiver at the same optical power. However, RZ-OOK exhibit more spectral width compared with NRZ. The higher RZ signal bandwidth need to be taken in design consideration of Wavelength Division Multiplexing (WDM) transmission systems, where the frequency spacing between adjacent channels must be adjusted to the signal bandwidth in order to avoid inter-channel interference. Furthermore, the narrower spectral width of NRZ enables the denser packing of channels and therefore an increased capacity [91].

2.4.2 Pulse-Position Modulation (PPM)

Pulse-position modulation (PPM), is a method of encoding information over intensity modulated direct-detection channel [92], [93]. At the transmitter, the encoder maps blocks of *m* bits into a PPM symbol by dividing the symbol interval to $M_{ppm} = 2^m$ time slots. Figure 2.4 shows the symbol structure waveform of 4-PPM. The PPM is orthogonal where the pulses are time disjoint. The PPM receiver detects the PPM symbols by the aid of clock recovery and determines which of the M_{ppm} slots contains the laser pulse, and

performs the inverse mapping operation to recover the bit stream. The receiver bandwidth requirement is greater than the actual data rate affecting the detection operation.

For large *m*, the bandwidth requirement is exponentially increasing; which result in limiting the information throughput of the system due to electronics limitation on the sampling rate[94]. The optical power requirement can be expressed relative to OOK as [95]

$$P_{ppm} = \sqrt{\frac{2}{2^m}\frac{1}{\log_2(M_{ppm})}}\,P_{ook} \tag{2.16}$$

And the bandwidth requirement can be expressed as

$$B_{ppm} = \frac{2^m}{\log_2 M_{ppm}} B_{ook} \tag{2.17}$$

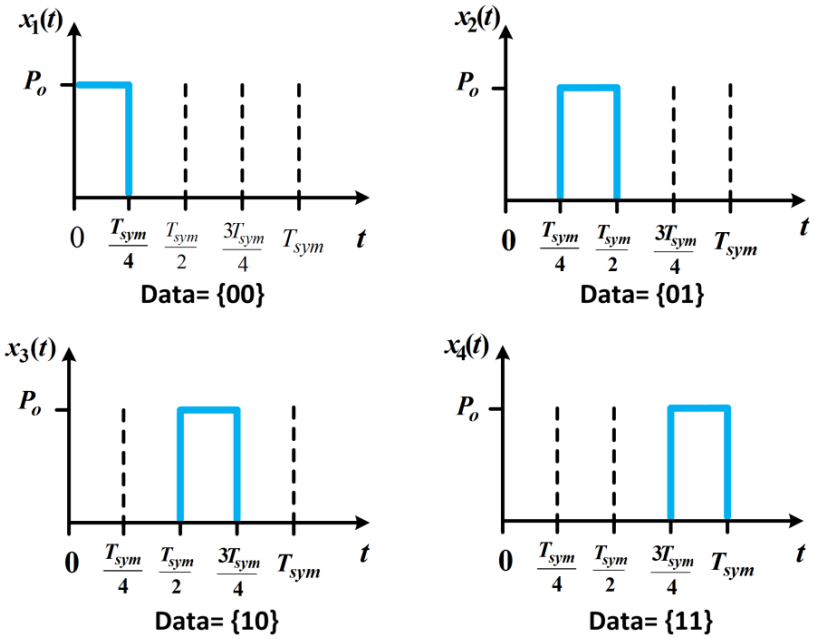

Figure 2.4 Symbol structure waveform of 4-PPM.

2.4.3 Pulse Amplitude Modulation (PAM)

Pulse Amplitude Modulation (PAM) is a classical modulation scheme which has gained a lot of research interest to be deployed in short and medium range IM/DD systems[30], [96]. In PAM, the transmitted signal $x(t)$ is mapped to a discrete digital amplitude waveform levels A_m which can occupy a value from a set of amplitudes values M. Electrical PAM have $A_{m,ele}$ signal amplitudes in which

$$A_{m,ele} = (2m - 1 - M)\, d \qquad \text{where } m = 1,2,...,M \tag{2.18}$$

where d is the minimum Euclidean distance between every pair of M-PAM symbols.

Due to the non-negativity constraint, the intensity modulated M-PAM is defined by $A_{m,in}$ signal amplitudes i.e

$$A_{m,in} = md \qquad \text{where } m = 1,2,...,M \tag{2.19}$$

Also, the M-PAM can be expressed with respect to the signal space analysis in terms of the basis function, i.e

$$x(t) = A_m \ \phi_{PAM}(t) \tag{2.20}$$

And the basis function for PAM shown in figure 2.5 can be expressed as

$$\phi_{PAM}(t) = \frac{1}{\sqrt{T_{sym}}} rect\left(\frac{t}{T_{sym}}\right) \tag{2.21}$$

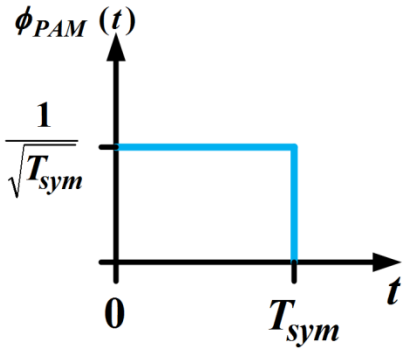

Figure 2.5 M-PAM basis function

where

$$rect(t) = \begin{cases} 1 & if\ 0 \le t < 1 \\ 0 & otherwise \end{cases}$$

The constellations of 4-PAM, 8-PAM and 16-PAM are shown in figure 2.6. The probability of bit error can be estimated based upon the M-PAM constellation as a function of the received optical power as The optical BER of M-PAM for IM/DD can be expressed as [59]

$$BER \approx \left(\frac{M-1}{M \ \log_2 M} \right) erfc \left(\frac{I_{pam}}{\sqrt{2}\,(M-1)\,\sigma_{pam}} \right) \tag{2.22}$$

where $I_{pam}$is the received M-PAM optical signal current $\sigma_{pam}$is the PAM noise variance. The BER behavior will be discussed in *section 4.2*.

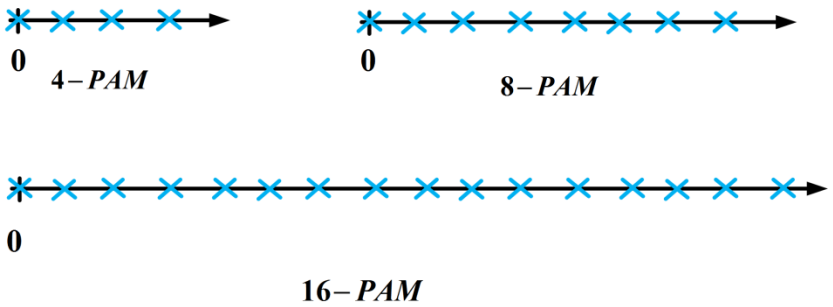

Figure 2.6 M-PAM signal constellation for 4-PAM, 8-PAM and 16- PAM.

Meanwhile, M-PAM is receiving much research interest in expanding the capacity of short and medium range optical links. Figure 1.6 and table 1.1 show some of the recent progress in the employment of M-PAM at varied distances and bitrates for optical short-haul and metro applications. It is clear that SMF is receiving increased interest due to its direct impact on a longer fiber reach and/or increased system capacity.

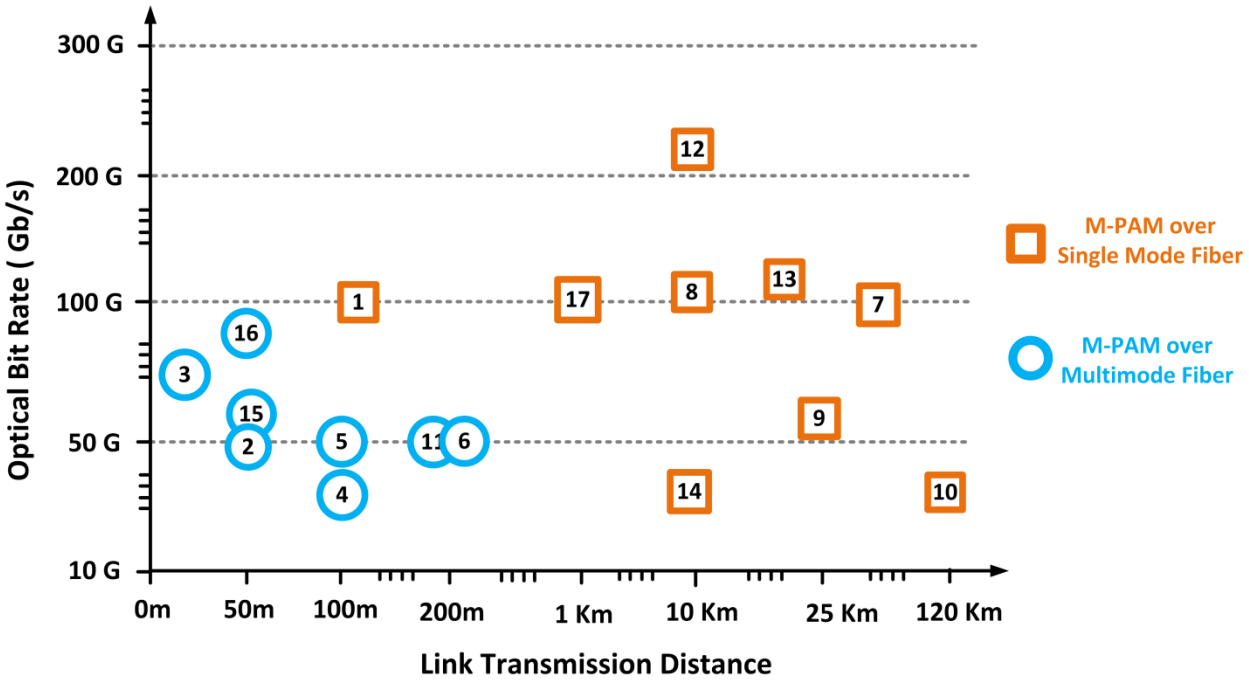

Figure 2.7 Research progress for employment of M-PAM with respect to variable link distances and bit rates highlighted in table 1.1.

Table 2.1 Recent experimental research progress employing M-PAM modulation format for short and medium range optical links.

Label	Year	Wavelength	Modulation Format	Bit Rate	Distance	Fiber Type	Reference
1	2012	1550nm	4-PAM	100Gb/s	100m	SMF	[97]
2	2013	850 nm	4-PAM	50 Gb/s	50m	MMF	[98]
3	2013	850nm	4-PAM	60 Gb/s	2m	MMF	[98]
4	2013	850nm	8-PAM	35.2 Gb/s	100m	MMF	[99]
5	2014	1060nm	4-PAM	50 Gb/s	100m	MMF	[100]
6	2014	1060nm	4-PAM	50 Gb/s	200m	MMF	[100]
7	2014	1550nm	4-PAM	100 Gb/s	30KM	SMF	[101]
8	2014	1310nm	4-PAM	107 Gb/s	10Km	SMF	[102]
9	2015	1550 nm	4-PAM	56 Gb/s	25Km	SMF	[103]
10	2015	1550nm	4-PAM	24 Gb/s	120Km	SMF	[40]
11	2015	850nm	4-PAM	50 Gb/s	200m	MMF	[104]
12	2015	1310nm	4-PAM	224 Gb/s	10Km	SMF	[43]
13	2015	1310nm	4-PAM	112 Gb/s	20km	SMF	[43]
14	2015	1550nm	4-PAM	21.4 Gb/s	10Km	SMF	[105]
15	2015	850nm	8-PAM	56 Gb/s	50m	MMF	[50]
16	2015	850nm	4-PAM	70 Gb/s	50m	MMF	[50]
17	2015	1550nm	4-PAM	100 Gb/s	1Km	SMF	[106]

2.5 Optical Modulation

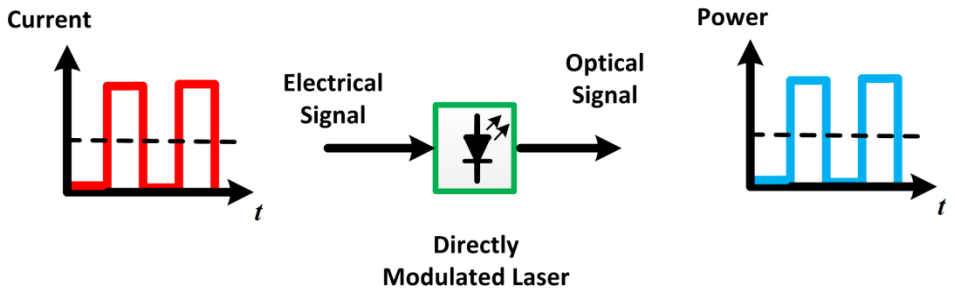

(a) Direct Modulation

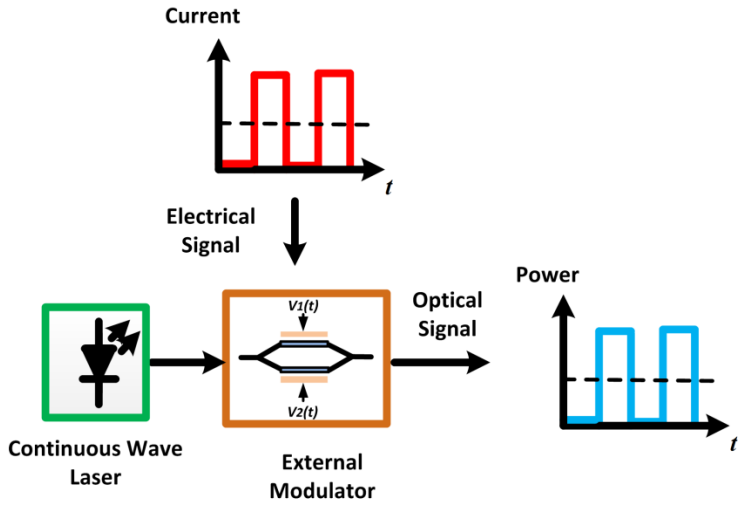

(b) External Modulation

Figure 2.8 Illustration of the operation methodology of direct (a) and (b) external modulation.

In IM/DD, the electrical data signal is intensity modulated on an optical carrier utilizing direct or external modulation. At high data rate, one significant and critical component in IM/DD system is the optical modulator.

Figure 2.8 shows an illustration of the operation methodology of direct and external modulation. *Direct Modulation* is a low complex way of optical modulation in which light is emitted according to an electrical data signal from a directly modulated laser only when a binary high signal is transmitted. In particular, the 100-Gb Ethernet is a standard both for very short-reach (less than 100 m) based on *vertical-cavity surface-emitting laser*

(VCSEL) sources in case of multi-mode fiber (MMF) propagation and for reach up to 10 km in case of single-mode fiber (SMF) propagation [1].

The bandwidth demand required in data-intensive environment as data centers is pushing the scientific community toward solutions guaranteeing Ethernet bitrates reaching 400G Ethernet [2], utilizing VCSEL lasers.

Another way is to modulate the light from a continuous wave laser by an *external modulator* as shown in figure 2.8(b). In IM/DD transmission systems with system aggregated bitrate larger than 10Gbaud/sec, external modulation turn to be a viable solution due to the impact of the laser source chirp on optical signal which can be highly reduced. The extinction ratio (*ER*) describes the modulation efficiency for both directly or externally optical modulated signal and is defined by the ratio of P_1 & P_0 as

$$ER = 10\log\left(\frac{P_1}{P_0}\right) \quad (dB) \tag{2.23}$$

2.5.1 Mach-Zehnder Modulator (MZM)

The MZM operational basics is originated on the principle of the electro-optic effect. The electro-optic effect is described by the difference in the applied electrical field resulting in the refractive index variation at both of the modular dual arms[107]. This variation in the refractive index imposes a change in the material propagation constant φ which leads to the presence of two phases at both arms of the modulator.

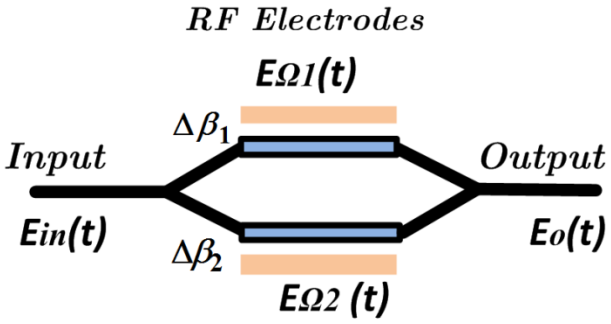

Figure 2.9 Mach-Zehnder Modulator structure.

As shown in figure 2.9, the MZM is composed of an input pair of waveguide arms (1 and 2) in a Y-branch architecture, in which light launched through one end, $E_{in}(t)$, is split to a two equal waveguide arms $E_{\Omega 1}$ and $E_{\Omega 2}$, which can be expressed as

$$E_{\Omega 1} = \frac{E_{in}(t)}{\sqrt{2}} e^{(j\omega t)} = E_{\Omega 2} \tag{2.24}$$

In case of non-applied electric field at the arms of the modulator, the signals arrive in phase and interfere constructively at the output of the modulator.

On the other hand, if an electric field is applied across the arms, thus, the output optical field takes the form

$$\begin{aligned} E_o &= \sqrt{\frac{1}{2}} \left(E_{\Omega 1}\ e^{\ j\Delta\beta_1} \right) + \sqrt{\frac{1}{2}} \left(E_{\Omega 2}\ e^{\ j\Delta\beta_2} \right) \\ &= E_{in}\ \cos\left(\frac{\Delta\beta}{2}\right) e^{\left(j\omega t - j\frac{\Delta o}{2} \right)} \end{aligned} \tag{2.25}$$

where $\Delta\beta_1$ and $\Delta\beta_2$ are the phase at the MZM modulator waveguides, $\Delta\beta = \Delta\beta_2 - \Delta\beta_1$ is the phase difference which is a measure of the constructive or destructive interference. The optical signal power of the MZM can be expressed as

$$P_o = \frac{P_{in}}{2} \left(1 + \cos\left(\Delta\beta\right)\right) \tag{2.26}$$

The MZM power transfer function can be shown in figure 2.10 in which the phase difference $\Delta\beta$ determine the operating point or bias point of the MZM. MZM operate by biasing the electrodes controlling the phase shift at a value equivalent to the quadrature point where the applied input voltage to the arms V_i is the voltage required to acquire a phase difference equivalent to $\Delta\beta = \frac{\pi}{2}$. On the other hand, biasing V_i at the zero point is can generate different modulation formats[108].

The relation between V_i and $\Delta\beta$ can be represented by

$$\Delta\beta = \frac{\pi V_i}{V_\pi} \tag{2.27}$$

where V_i is the applied voltage to the arms of the modulator and V_π is the required voltage to achieve a phase difference equivalent to $\Delta\beta = \pi$.

An internal chirp is a result of the amplitude modulation in the MZM which is due to the phase difference. This internal chirp can be expressed as

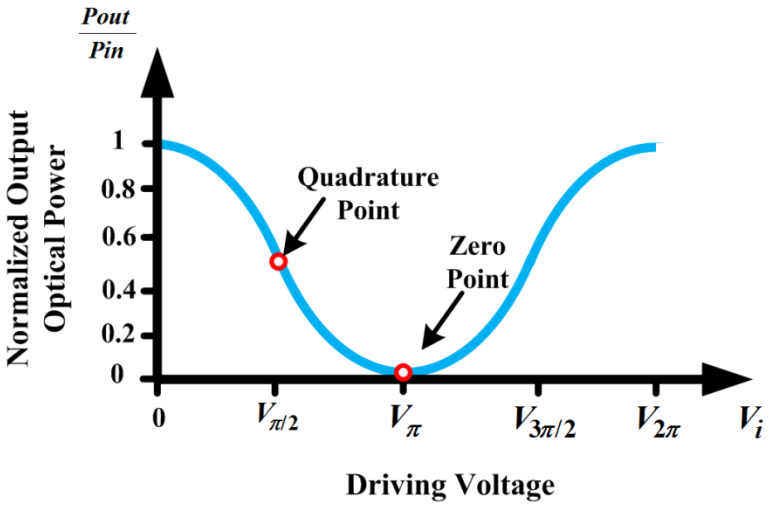

Figure 2.10 Mach-Zehnder Modulator power transmission function

$$\frac{do}{dt} = \frac{\alpha}{2P_o}\frac{dP_o}{dt} \tag{2.28}$$

where α is the frequency chirp parameter for the modulator which controls the modulator frequency chirping. This relation controls the chirp effect on the MZM transfer function. In case α is positive, thus a positive frequency chirp exists which causes a high frequency component at the leading edge or in other words, pulse said to be blue shifted. The relation can be elaborated more i.e,

$$\begin{aligned} \alpha &= \Theta.\cot\left(\frac{\Delta\beta}{2}\right) \\ &= \frac{\Delta n_1 + \Delta n_2}{\Delta n_1 - \Delta n_2}\cot\left(\frac{\pi V_i}{2V_\pi}\right) \end{aligned} \tag{2.29}$$

Where Θ represent the chirp factor which affect the internal symmetry of the modulator transfer function where Δn_1 and Δn_2 is the index change per input voltage across the MZM modulator arms.

2.6 Pre-Amplified Optical Receiver

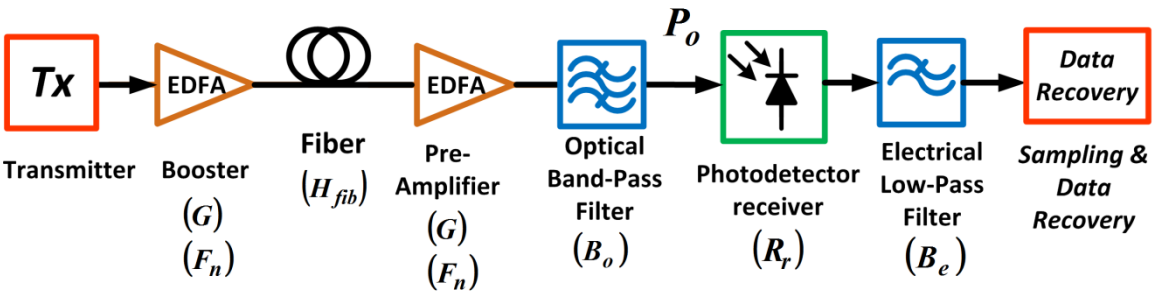

Figure 2.11 Pre-amplified system model.

Figure 2.11 shows the pre-amplified based receiver that is employed in MMT investigation for metro networks presented in chapter 5. It is composed of an optical link with an Erbium Doped Fiber Amplifier (EDFA) pre-amplifier accompanied by an optical band pass filter, a semiconductor photodetector and an electrical low pass filter. The optical filter with a bandwidth B_0 reduces ASE-noise impact on the optical signal.

The received power P_0 by the photodiode generates a photocurrent equivalent to

$$I = R_r . P_o \tag{2.30}$$

where R_r is the responsibility of the photodiode, which can be expressed as

$$R_r = \frac{\eta e}{h\nu} \tag{2.31}$$

where η is the quantum efficiency, e is the electron charge and $h\nu$ is the photon energy. Typical values for the responsivity of photodiodes are equivalent to 0.4-0.8 A/W[109], [110].

The fiber is modelled using a low pass equivalent representation of a linear bandpass system in which the fiber dispersion is accounted through the quadratic (nonlinear) phase response of the fibers transfer function, given by[111]

$$H_{fib} \approx \exp\left(j\frac{\Pi D L \lambda^2 f^2}{c} - \alpha_{dB}\frac{L}{2}\right) \tag{2.32}$$

where c is the free-space speed of light, λ is the wavelength of operation, L is the trans mission distance, D is the dispersion parameter in (ps/km .nm) . After the photodiode, a low pass filter exist with bandwidth B_e to filter the noise out of the detected electrical signal spectral width.

In the link design, there exit a different number of amplifiers with booster, inline and pre-amplifiers configurations. This results in the addition of amplified spontaneous emission (ASE) noise components to the noise received by the photodetector. The added noise components can be classified in to: signal-ASE beat noise σ^2_{s-ASE}, ASE-ASE beat noise $\sigma^2_{ASE-ASE}$, ASE-shot noise σ^2_{ASE-sh} and signal-shot noise σ^2_{s-sh} .

According to [111] ,the ASE-ASE beat noise $\sigma^2_{ASE-ASE}$ component can be expressed as

$$\begin{aligned}\sigma^2_{ASE-ASE} &= 4R_r^2\, P^2_{ASE}\, B_o\, B_e \\ &= \left(G\, F_n\, e\eta\right)^2 B_o\, B_e\end{aligned} \tag{2.33}$$

Where G is the amplifier gain, F_n is the amplifier noise figure , P_{ASE} is the optical noise power density , B_e is the low pass filter electrical bandwidth, B_o is the optical filter bandwidth . While, the ASE-shot beat noise $\sigma^2_{ASE-shot}$ is represented by

$$\begin{aligned}\sigma^2_{ASE-shot} &= 4R_r\, eP_{ASE}\, B_o\, B_e \\ &= 2G\, F_n\, e^2\, \eta\, B_o\, B_e\end{aligned} \tag{2.34}$$

The signal-ASE noise σ^2_{s-ASE} can be expressed as

$$\sigma^2_{s-ASE} = 4R_r^2\, G\, P_{ASE}\, P_o\ B_e \tag{2.35}$$

while, the signal-shot noise σ^2_{s-Shot}

$$\sigma^2_{s-shot} = 2R_r\, G\, P_{ASE}\ B_e \tag{2.36}$$

Another source of noise is thermal noise σ^2_T, which can be expressed as

$$\sigma_T^2 = \frac{4k_B T F_n B_e}{R_L} \tag{2.35}$$

where T is the temperature (in Kelvin), R_L is the load resistance, k_B is the Boltzmann constant. The electrical filer transfer function can be expressed in terms of the noise bandwidth B_e as

$$B_e = \int_{-\infty}^{\infty} \left| H_e(f)^2 \right| df \tag{2.37}$$

where $H_e(f)$ is the transfer function of the electrical signal. The role of the electrical filter is the equalization of the detected signal and reduction of noise imposed on the received waveform.

The ASE-ASE beat noise $\sigma_{ASE-ASE}^2$ spectrum can be calculated as the auto-correlation of the ASE optical spectrum. Taking the transfer function frequency response into account, the noise bandwidth of the ASE–ASE beat noise $\sigma_{ASE-ASE}^2$ is calculated as

$$\sigma_{ASE-ASE}^2 = \int_{-\infty}^{\infty} \left| H_e(f)^2 \right| \left| H_o(f)^2 \right| * \left| H_o(f)^2 \right| df \tag{2.38}$$

where $H_o(f)$ is the transfer function of the optical signal. The photodiode dark current of the detector is very small compared to the photocurrent and therefore is ignored.

2.7 Linear fiber Impairments

The linear fiber characteristics can be classified in to three main parameters: fiber attenuation and Chromatic Dispersion (CD) or Group Velocity Dispersion (GVD). These parameters influence the behavior and propagation of signals in fiber at a low power input transmission region and the interplay with the nonlinear fiber impairment at the high power region, which impose a limitation on the maximum transmission reach of the system as discussed in section.

2.7.1 Fiber Attenuation

The propagation of a light signal in optical fiber is influenced by total internal reflections in the fiber core medium surrounded by the cladding. These reflections are caused by the fiber design in which refractive indices of the core and cladding are varied acquiring total internal reflections. Fiber attenuation is the main limiting factor for signal transmission across large distance reach. The relation between attenuation and transmission distance can be expressed in terms of the signal power after propagating inside the fiber with length z as

$$P(z,t) = P_{in}(t)\, e^{(-\alpha z)} \tag{2.39}$$

where α representing attenuation factor in Neper/meter, $P_{in}(t)$ is the input optical intensity or power. It can be determined by measuring the input and output power through the relation

$$\alpha = \frac{1}{z} \ln\left(\frac{P_{in}(t)}{P(z,t)} \right) \tag{2.40}$$

There is another relation which better describe α_{dB} as an attenuation coefficient in terms of dB/KM as

$$\alpha_{dB} = \frac{1}{z}\, 10 \log\left(\frac{P(0,t)}{P(z,t)} \right) \tag{2.41}$$

The relation between both parameters α and α_{dB} can be expressed from eq.2.40 and eq.2.41 as

$$\frac{\alpha_{dB}}{\alpha} = 4.343 \tag{2.42}$$

The α parameter is dependent on the operating optical signal wavelength λ. A typical model for the attenuation with respect to the operating wavelength can be shown in figure 2.12. The dotted line shows the attenuation of old fibers that were made before the 1980s. In addition to strong water absorption peaks, the attenuation is generally higher than new fibers due to material impurity and waveguide scattering. The impurities

impose an increased absorption in a certain wavelength regions. The vibrational resonances of OH-ions occur near 2.73μm with higher harmonics at 1.39μm and 0.95 μm as shown in figure 2.12. Three wavelength windows have been utilized for optical communications in 850 nm, 1310 nm, and 1550 nm where fiber attenuation exhibits minimum losses. Table2.1 show the wavelength range of optical communications bands.

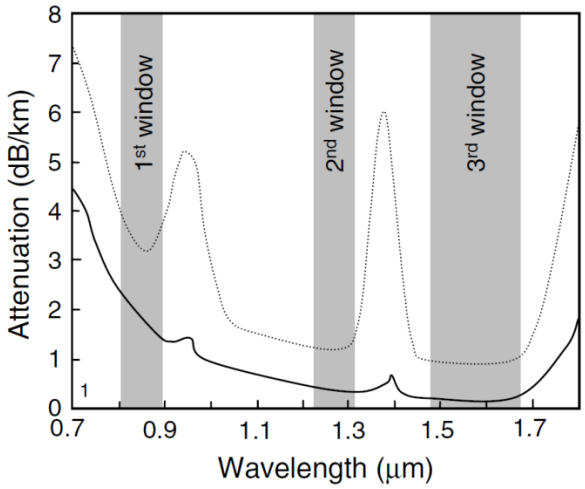

Figure 2.7 Attenuation of old (dotted line) and new (solid line) silica fibers. The shaded regions indicate the three telecommunication wavelength windows
[112].

Table 2.2Wavelength range of optical communications bands

Band	Wavelength (nm)
O Band	1260 nm - 1360 nm
E Band	1360 nm - 1460 nm
S Band	1460 nm - 1530 nm
C Band	1530 nm - 1565 nm
L Band	1565 nm - 1625 nm
U Band	1625 nm - 1675 nm

2.7.2 Dispersion

Dispersion is responsible for the propagation of different signal components travelling in fiber at different velocities resulting on pulse delay when arrived at the photodiode. There are two main dispersion types, First, intermodal dispersion which is the major limitation in multimode fiber due to the pulse propagation with different velocities at different fiber modes which result in inter-symbol interference.

The second is intramodal dispersion, which occurs within a mode of fiber transmission and has two contributions, waveguide dispersion and material or chromatic dispersion. As for waveguide dispersion, it is due to the propagation of a portion of light in the fiber cladding which have a relatively lower refractive index compared to the core. The waveguide dispersion can be mitigated by proper system design consideration. Dispersion Shifted Fiber (DSF) or Nonzero Dispersion Fiber (NZDF) can be employed to counteract the partial effects of chromatic dispersion.

The second fundamental contribution is chromatic dispersion, which takes place significantly in single mode fiber. Since the thesis proposes MMT to be deployed across single mode fiber, thus, chromatic dispersion is elaborated in details.

2.7.2.1 Chromatic Dispersion

One of the significant characteristics of optical fiber communication is the pulse broadening during travelling at various spectral components in SMF. The modulated field may be described as an infinite sum of different frequency components (i.e. a Fourier transform). For such a field, the effect of a dispersive medium will result in different frequency components traveling at different velocities. This can be reasoned to the frequency dependence nature of the fiber medium refractive mode index, which causes different spectral components to propagate at different group velocities. Thus, chromatic dispersion is known also as Group Velocity Dispersion (GVD). Hence, CD results in the broadening of the propagating signal and the existence of interference between adjacent pulses known as Inter-symbol-interference (ISI). Figure 2.13 shows the implication of the chromatic dispersion. The group velocity v_g can be expressed as

$$v_g = \left(\frac{d\beta_p}{df}\right)^{-1} \tag{2.43}$$

$$= \frac{c}{n_g}$$

where β_p is the propagation constant and $\beta_p = \frac{n\,f}{c}$, n_g is the group index parameter. if we want to express the different arrival times of the spectral components of the signal through fiber. we can develop the time delay equation to be

$$\Delta T = \frac{dT}{df} \quad f$$

$$= L\,\Delta f \left(\frac{d^2\beta_p}{d\omega^2}\right) \tag{2.44}$$

$$= L\,\Delta f\,\beta_{p_2}$$

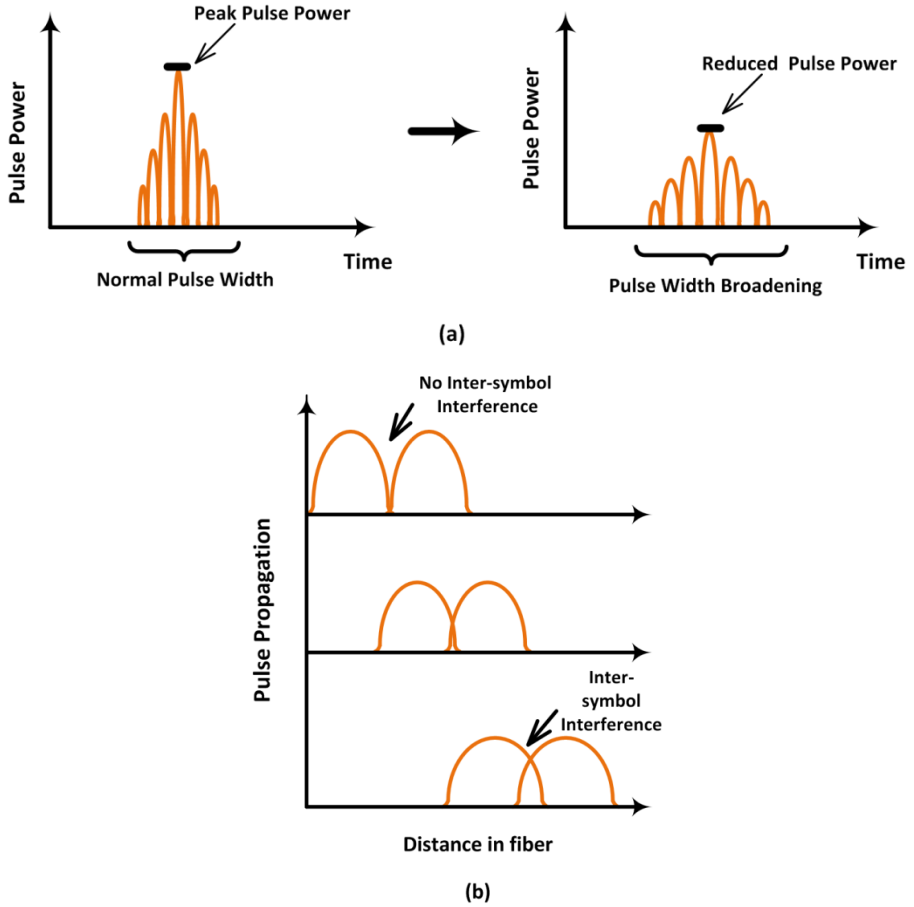

Figure 2.8 Chromatic dispersion effects (a) Pulse broadening (b) Inter-symbol interference.

with Δf representing the spectral bandwidth of the pulse and β_{p_2} defined as group velocity parameter and $f = \frac{2\pi c}{\lambda}$. Also, the time delay can be expressed as

$$\Delta T = D\ L\ \Delta\lambda \tag{2.45}$$

where D is the dispersion parameter in (ps/nm.km) and can be expressed as

$$D = \frac{d}{d\lambda}\left(\frac{1}{v_g}\right) = -\frac{2\pi c}{\lambda^2}\ \beta_{p_2} \tag{2.46}$$

The total fiber dispersion for a conventional single mode fiber (SMF) in the 1.55μm region varies between 16 to 19 ps/nm·km[55], [113].

2.8 Non-Linear Fiber impairments

The intra-channel non-linearity is one of the main fiber non linearities that affects fiber transmission between the signals on itself at a single wavelength. The propagation of pulses with bitrates in the order > 10G in fiber is not only limited by the linear fiber impairments, however, it has strong proportionality with fiber intra-channel non-linearity. Thus, it is significant to investigate the non-linear interplay between adjacent pulses in the presence of dispersion which cause pulse broadening at high aggregated channel bitrates. Fundamentally, there are three types of intra-channel non linearities: SPM, Intra-IXPM and IFWM [69].

2.8.1 Self-Phase Modulation

For fiber non-linearity being investigated, an inclusion of fiber Kerr effect in the fiber channel model is necessary[114]. Kerr occurs due to the dependence of the refractive index on the launched fiber optical intensity. For single channels, this leads the optical field amplitude to have a self-induced phase modulation by the signal self-power, in which this phenomenon is called Self Phase Modulation (SPM)[115], [116].

As the need for high power pulses for maximum reach and error free fiber optic link systems, their performances are eventually limited by SPM effect [117]. Since, the dominant non-linear effect in transmission systems is self-phase modulation (SPM).

SPM appears due to the dependence of the refractive index on the signal intensity, which leads to an induced phase change for the pulse propagating in the fiber [3]. The different parts of the pulse undergo different phase shifts, which give rise to chirping of the pulses. Pulse chirping in turn enhances the pulse broadening effect caused by CD. This chirping effect is proportional to the transmitted power, which in turn SPM effects to be more pronounced in the systems employing high transmitted powers. At the high power levels, SMF has a large anomalous dispersion due to the GVD of 16.75 ps/nm/km. Therefore, necessities emerge to compensate the envelope time domain pulse broadening, which leads to a chirp at the end of the propagation distance.

Methods that utilize the employment of SPM effect in the compensation for the second and almost the third order dispersion parameters have been previously proved effective by using Dispersion Compensation Fiber (DCF) in pre and post compensation scenarios [6-8].

Dispersion and SPM effects can be mathematically modeled in our transmission links referring to Non-linear Schrodinger (NLS) equation. Simulation was performed for MMT in both dispersion post-compensated and combination of pre- and post-compensated transmission links. The optimum value of dispersion pre-compensation is reported in order to enhance the performance of MMT system in terms of SPM tolerance as discussed in *section 5.3*.

2.8.1.1 SPM Mathematical Modal

The mathematical model which best describes the propagation of the pulses in SMF, were taken to account for the effect of SPM and GVD in the NLS as [56]

$$\frac{\partial A(\tau,z)}{\partial z} = -\frac{\alpha}{2}A(\tau,z) - \frac{j}{2}\beta_2(z)\frac{\partial A(\tau,z)}{\partial \tau^2} + j\gamma\left|A(\tau,z)\right|^2 A(\tau,z) \tag{2.47}$$

where z is the longitudinal propagation distance, $U(z,\tau)$ is the normalized amplitude for a Gaussian pulse and the amplitude for a complex electric field pulse envelope is equal to

$$A(z,\tau) = \sqrt{P_o}\exp(-\alpha z/2)U(z,\tau) \tag{2.48}$$

where $\tau = (t - z/\nu_g)/T_o$ denotes the retarded time framework for the GVD (ν_g), T_o is the pulse width, α represent the attenuation coefficient, β_2 and γ represent the GVD parameter and the fiber nonlinearity parameter, respectively. The non-linear factor is described by the dominant parameter, which is the dispersion length (L_D):

$$L_D = T_o^2/|\beta_2| \tag{2.49}$$

And the non-linear length (L_{NL}) as

$$L_{NL} = 1/\gamma P_o \tag{2.50}$$

Where γ the non-linearity parameter is dependent on the operating wavelength, the non-linear index of refraction n_2 and the effective core area A_{eff} by

$$\gamma = \frac{w_o\, n_2}{c\, A_{eff}} = \frac{2\pi\, n_2}{\lambda\, A_{eff}} \tag{2.51}$$

Both the GVD and SPM phenomenon will be considered in our system as $L >> L_{NL}$ and $L >> L_D$ where L is the fiber length.

2.8.2 Intra-channel Cross-Phase Modulation (IXPM) and Intra-channel Four-Wave Mixing (IFWM) Non-linearities

At high system baud rates, the impact of the intra channel non-linearity becomes dominant. This can be shown in figure 2.14 highlighting the impact of non-linearity with respect to channel bitrate, fiber local dispersion and format spectral efficiency[108], [118]. For high capacity time division systems reaching higher than 10 G baud per channel, the dominant nonlinear effects are due to IXPM and IFWM[88]. IXPM and IFWM are considered an interactions among neighboring bits (pulses) that are a result of fiber intra-channel nonlinearities. Considering three propagating signals P_1, P_2 and P_3, the interplay effect between them can be expressed by [119]

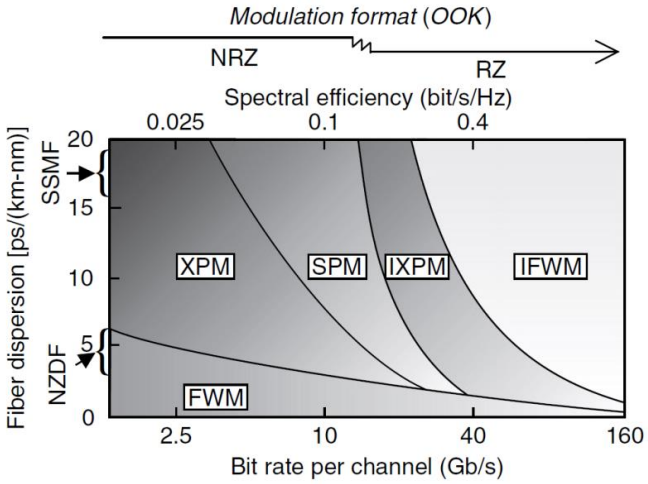

Figure 2. 9 Impact of fiber non-linearity with respect to channel bitrate, fiber local dispersion and spectral efficiency[108], [118]

$$j\frac{\partial P_1}{\partial z}-\frac{\beta_2}{2}\frac{\partial^2 P_1}{\partial t^2}=-\gamma\left\{\left(\overbrace{|P_1|^2}^{SPM}+\overbrace{2|P_2|^2+2|P_3|^2}^{IXPM}\right)P_1+\overbrace{2P_1P_2P_3^*}^{IFWM}\right\} \tag{2.52}$$

where the first component represents the SPM effect, the second component represents the IXPM effect with its interplay with consecutive neighboring signals and the third term represents the IFWM and its interplay between neighboring signals.

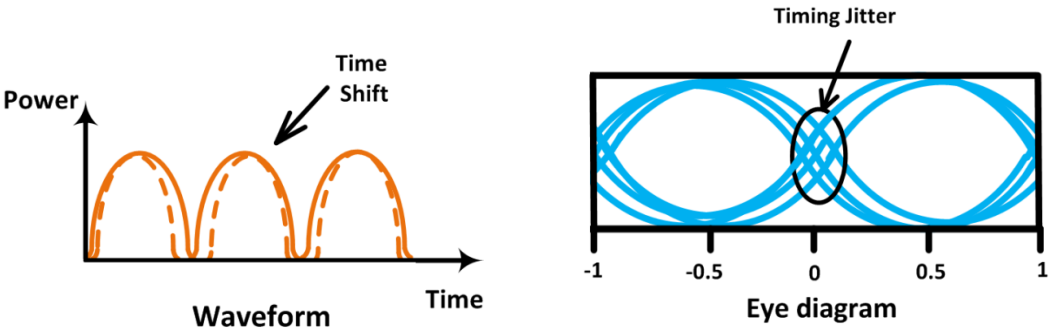

(a) (b)

Figure 2.10 IXPM effect on signal: a) Time shift occurrence in waveform. b) Timing jitter occurrence in eye diagram.

.

IXPM impose phase modulation between consecutive neighboring signals[56]. Figure 2.15 shows the impact of IXPM on signal waveform and eye diagram. A frequency chirp occur as a result of the time dependency of the signal phase modulation which is translated to a timing jitter[87]. Although the signal energy remains constant, the IXPM lead to fluctuations in the symbol period and the symbol amplitude which causes an amplitude-jitter and closure of the eye diagram as shown in figure2.14 [120]. IXPM impact can be reduced or controlled by proper design of dispersion management map [121]. Some forms PPM have been investigated capable of suppressing IXPM and IFWM by adding guard interval to transmitted pulse sequence[122].

At high bit rate, the signal suffer a frequency shift which is translated to a time delay, thereby resulting in the formation of ghost pulses or shadow pulses. If there is a vacant slot as RZ-OOK format, a small pulse fluctuation appears (ghost pulse). However, if the signal structure occupy 100% duty cycle, thus, the time delay will lead neighboring slots to beat together creating variations in main pulse amplitude or an amplitude jitter. Figure 2.16 shows the impact of IFWM on signal waveform and eye diagram. A lot of research have been carried on mitigating the effect of IFWM by destructive interference utilizing bitwise phase changes coding techniques and other techniques for Time Division Multiplexed (TDM) systems[123]–[126].

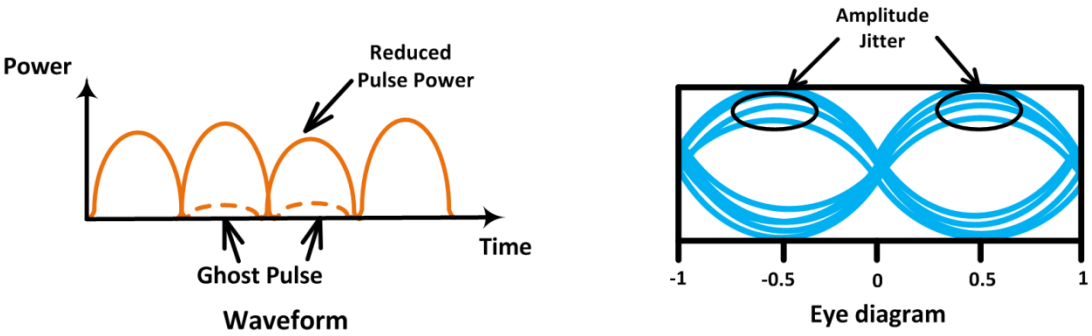

Figure 2.11 IFWM effect on signal: a) Ghost pulse occurrence in waveform.
b) Amplitude jitter occurrence in eye diagram.

2.8.3 Stimulated Brillouin Scattering (SBS)

In contrast to the Kerr-non linearity effects, there is another non linearity which is based on inelastic scattering process where a photon of the propagating signal interacts with the fiber medium and during this process a new photon with less energy is launched. At high power levels, the nonlinear phenomena Stimulated Brillouin Scattering (SBS) associated lead to the presence of optical amplification in the backward direction. The SBS can cause signal attenuation if the launched power is higher than a certain threshold[110]. SBS have been studied theoretically and numerically over different fiber modes[127]–[129]. The effect of SBS optical threshold power P_{SBS} can be calculated as [55]

$$P_{SBS} \approx \frac{21b\,A_e}{g_B\,L_{eff}} \tag{2.52}$$

where A_e is the effective area of fiber, g_B is the Brillouin gain coefficient which equal to 5×10^{-11} m/W and b take value between 1 and 2 depending on the relative polarizations of the pump and Stokes waves and L_{eff} is the effective fiber length and can be expressed as

$$L_{eff} = \frac{1-e^{-\alpha_{dB}L}}{\alpha_{dB}} \tag{2.53}$$

One way of mitigating the effect of SBS is to modulate the laser pump current at a frequency region in the upper KHz regime[130].

2.9 Concluding Remarks

This chapter presented an overview for the fundamentals of modulation formats, optical components, fiber linear and non-linear impairment. In addition, the chapter described the constraints and channel characteristics that exist in intensity modulated direct detection channels.

Modulation Formats which are relevant for comparison with MMT has been discussed. Also, the modulation formats that are employed and relevant for comparison with the proposed technique, is presented and discussed. The chapter concluded by a description for the main fiber propagation impairments limiting the IM/DD system for short and metro optical communication links. The chapter discussed the linear fiber impairments such as attenuation and chromatic dispersion. In addition, non linear impairments such as self phase modulation and intra-channel non linearities have been discussed. Also, the nonlinear phenomena Stimulated Brillouin Scattering (SBS) which lead to the presence of optical amplification in the backward direction has been explained.

The topics have been chosen based upon their relevance to the intensity modulated directed detection systems, discussed and presented in the thesis.

3. Chapter 3 - MMT System Model and Performance Metrics

3.1 The Methodology behind MMT Structural Design

The pioneer Claude Shannon put the foundation for digital communication through his classical paper [131], which has paved the way for the huge advances in communication and information theory. The paper puts a limitation on the maximal rate for reliable transmission over a noisy channel (equivalent to low bit error probability). It stated that the transmission of data under a noisy channel can be achieved with a specified signal power at an arbitrarily low bit error probability as long as the coding rate is not exceeding a certain factor, which is the channel capacity (in bits/sec). Shannon has formulated his theory in an equation which has been expressed as [131]

$$C = B\log_2(1+\frac{S}{N}) = B\log_2(1+\frac{P}{N_o.B}) \tag{3.1}$$

where C is the channel capacity in (bits/sec), B is the bandwidth of the channel in (Hz), S or P is the average received signal power in (Watts), N is the total received signal noise power in (Watts) and equivalent to $N = N_o B$, N_o is the one-sided power spectral density and S/N represents the Signal To Noise Ratio (SNR). The method or approach to achieve this channel capacity have been left by Shannon as an open question for researchers all over the world and through many years, to develop the practical methodologies and design procedures to achieve this capacity boundary or Shannon limit[132], [133].

To answer this question, system designers have considered the three pivotal trade-off design resources that govern any data transmission format proposed by Shannon capacity formula. The three-tradeoff key factors are power, bandwidth and complexity.

The formula in other words states that, the ultimate goal of the design of any transmission format is to reach an impactful trade-off between design parameters to overcome the challenges and meet the requirements of a particular desired application.

According to Shannon equation, the capacity (in b/s) is directly proportional to the SNR. Aided by the fact, that SNR and Bit Error Rate (BER) have an inverse exponential relationship in which as the BER decrease (enhance) as the SNR requirement increase. Thus, one solution to increase the capacity was to employ higher order modulation formats offering an expansion in system information capacity (in bits/symbol). Higher order modulation formats features scaling system baud rate at a fraction of the aggregated bit rate.

Recently, M-PAM has been proposed as a higher order modulation format for short-haul and metro networks [30], [41], [134]. M-PAM is a multiple-level bandwidth-limited transmission format offering a high spectral efficiency on the cost of high power penalty[86]. As such, 8-PAM with 3 bits/symbol and 16-PAM with 4 bits/symbol have imposed large SNR requirement to achieve an acceptable BER at a fixed baud rate. This high SNR requirement is reasoned to the higher number of levels penalties that are associated with increasing the number of levels. A solution has been proposed to 8-PAM format, is to apply error correction techniques, as block coding and Forward Error Correction (FEC) codes to enhance the SNR, but again this implicates a rise in the system complexity [41], [48], [50].

According to our problem statement, the thesis aims to design a power efficient and high capacity transmission format for reducing the power consumption of data intensive applications (as discussed in *chapter 1*). Thus, as our research motivation combined with avoiding the high power penalty imposed on higher order M-PAM modulation format, MMT design has taken in to account other trade-off parameters to increase the capacity without significant power penalty cost. The other signal dimension considered was dividing the symbol duration into two slots (as discussed in *section 3.3.1*).

Although, dividing the MMT slots induce an increased bandwidth penalty. However, increasing the bandwidth, has two major effects on the capacity. First, it raises the

available link degrees of freedom since as $S/N = \frac{P}{N_o.B}$, thus at fixed SNR, the dependency is clear on limiting the power P. In other words, at fixed power P and by increasing the bandwidth B, the SNR requirement is decreased. The second effect is comprised on the SNR requirement per dimension, which will be spread among the dimensions or degree of freedoms with the bandwidth increase.

Although, increasing the bandwidth had a positive impact on increasing the capacity and reducing the SNR requirement, however, we cannot neglect the fact that increasing the bandwidth above a certain value, will entangle a weaker impact on the capacity. This can be verified by Shannon capacity equation assuming high bandwidth, the equation can be approximated by [135]

$$\begin{aligned} C &= B\log_2(1+\frac{P}{N_o.B}) \\ &\approx B(\frac{P}{N_o.B}).\log_2 e = \frac{P}{N_o}\log_2 e \end{aligned} \tag{3.2}$$

As such, it is clear that in this case, the capacity is directly proportional to the average received power and increasing the bandwidth further has a very limited effectiveness. At this point, the channel capacity is power limited in which the capacity does not increase further with increasing the bandwidth; however, it increases with increasing the power.

As such argument, MMT structure has been designed utilizing two slots only, in which increasing the number of MMT slots more than two will impose more bandwidth penalty with non-significant trade-off advantage for desired application.

As above-mentioned consideration, MMT structural design has considered reaching an impactful intermediate compromise between power and bandwidth. Hence, MMT has been designed as a joint multiplexing and modulation format, which can be viewed as a hybrid combination between M-PPM and M-PAM modulation formats. The joint design in MMT causes more degree of freedom in optimizing the performance, which can be viewed as a power efficient alternative and bandwidth efficient alternative compared to M-PAM and M-PPM, respectively.

3.2 Channel Characteristics

Due to the huge demand for both low-complex and low-cost modulation formats featuring low power consumption for metropolitan and short range optical fiber systems[25], [53], [60], [136], [137], hence, N-channel MMT is presented as a power efficient alternative transmission format for non-coherent applications. Although, N-channel MMT is a modulation format that is applicable for wired and wireless communication links, however, it is the interest of this thesis to present N-channel MMT for Intensity-Modulated Direct-Detection (IM/DD) links. The reason behind choosing the IM/DD channel was driven by the trade-off advantage between cost and power efficiency fulfilling the thesis objectives, compared with coherent systems.

In IM/DD, the information is conveyed in the form of optical power intensity signal $P(t)$, where the input is an electrical signal $X_K(t)$. The direct detection is a linear process where the photodiode is responsible for the opto-electrical conversion.

IM/DD channel characteristics have two fundamental constraints on all implemented transmission formats. Since information is conveyed by modulating the instantaneous optical power signal $P(t)$, thus, no negative amplitudes can be used [53], [73], [78], [138]. Hence, N-channel MMT has been designed to fulfill the non-negativity constraint at all time instants, i.e

$$\min_{\forall\, t \in \Re} \quad P(t) \geq 0 \tag{3.3}$$

Since N-channel MMT is designed to cope with IM/DD for both fiber and wireless optical links (where the signal propagate in free space), thus, eye safety is an important metric. Eye safety is one of the most vital restrictions for IM/DD systems operating in the infrared, ultraviolet, visible communication frequency band. Safety regulations must ensure that the emitted radiated power follows international bodies regulations for eye and skin safety precautions[53], [57], [72], [73].

Hence, in contrast to conventional channels, the second constraint is a limitation on the emitted peak and average signal power, so the maximum optical signal power should be less than or equal the maximal power the eye can tolerate P_{eye} as

$$\lim_{T_{sym}\to\infty} \int_{-T_{sym}}^{T_{sym}} P(t) \leq P_{eye} \tag{3.4}$$

The maximum allowable power the eye can tolerate is dependent upon the intensity modulated system application. In addition, it is strongly dependent on the wavelength of operation. At 1550nm wavelength, the maximum allowable power for safe operation is less than 10 mW. While, at 1310nm, the maximum allowable power is less than 8.8 mW [138].

In this thesis, N-channel MMT design is focused mainly for optical fiber links while the discussion on wireless optical links will be considered for future works (as discussed in *section 7.2*).

Figure 3.1 shows a generic free space model for N-channel MMT IM/DD system. The optical intensity modulator is responsible for generating an optical power signal, so that

$$P(t) = c\, X_k(t) \tag{3.5}$$

where c is the electro-optic conversion factor in Watt/Ampere. Note that the optical power is proportional to $X_k(t)$ and not to $X_k^2(t)$ due to the fact that in a system based on IM/DD, the SNR is proportional to the square of the received optical power (due to square law detector) [53], [60]. In IM/DD optical communication with non-optical amplification, the optical channel can be modelled as an Additive White Gaussian Noise (AWGN) channel which serve as a good model for all types of noise present [53], [57], [60], [70]. Hence, the received electrical signal can be expressed as

$$z(t) = R_r \,.c\,. X_k(t) + w(t) \tag{3.6}$$

where R_r is the photodiode responsivity and $w(t)$ accounts for the AWGN with zero mean and double sided power spectral density $\frac{N_0}{2}$, which is equivalent to the thermal noise at the system receiver environment.

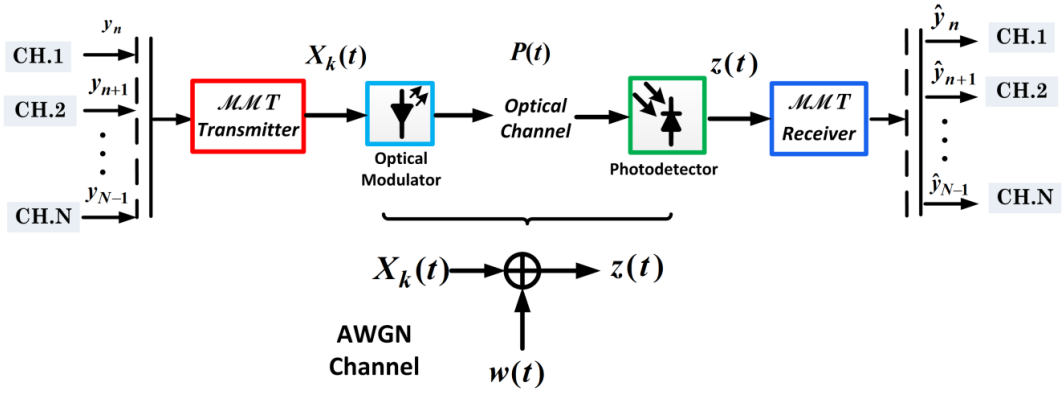

Figure 3.1 N-channel MMT free space channel model for IM/DD systems.

3.2 Signal Space Model

Signal space model is a benchmark assessment methodology for investigating modulation formats in general and especially for IM/DD systems. Signal space have been first proposed by Kotelnikov [139] two years earlier before it was proposed by Shannon in 1949 [140], then afterwards it has been developed widely by Wozencraft and Jacobs[141]. The signal space analysis approach has been employed widely to provide an in-depth evaluation of various modulations and coding techniques [82], [142]–[144]. The concept of portraying different modulation formats as constellation points in Euclidean space lead to more consistent and efficient approach for mandatory design tradeoff analysis and discussions. Moreover, the advantage of signal space comprised in the ability of conveying signal sets and noise as vector space components in a geometric representation where probabilities of these components can be derived [86], [90], [145].

3.2.1 N-channel MMT Signal Model

Since MMT signals are dependent upon two orthogonal time slots, the signal calculations can be interpreted from the vector space component by the construction of orthogonal basis functions. Signals can be represented by defining a set of orthonormal basis function $\phi_j(t)$ for $j = 1, 2, \ldots, R$ where R is equivalent to the number of signal dimensions or slots (S) as in [58], [82], [86] , which satisfy $R \leq K$. Therefore, each of the signals can be expressed as

$$X_k(t) = \sum_{j=1}^{S} x_{k,j}\ \phi_j(t) \tag{3.7}$$

where $k = 0, \ldots, K-1$ and $x_k = x_{k,1}, x_{k,2}, \ldots, x_{k,R}$ is the vector component representation of $x_k(t)$ with respect to the defined basis functions. The basis function per slot is represented by

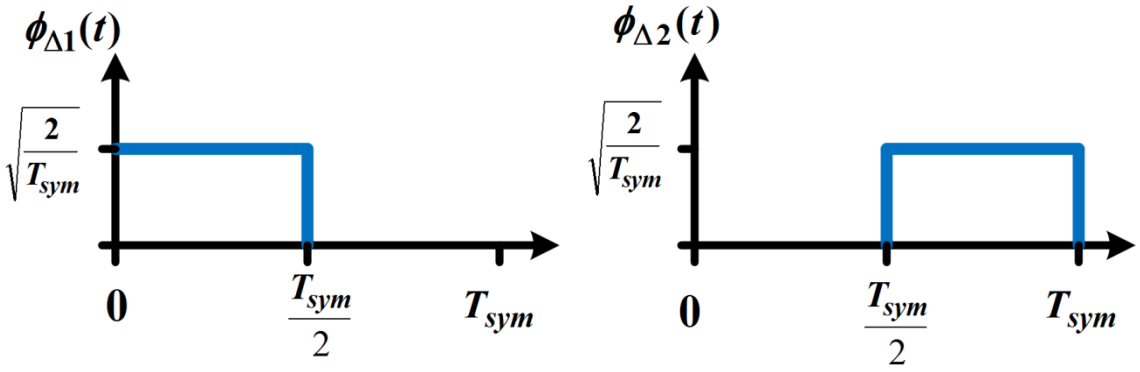

Figure 3.2 N-channel MMT format generated orthonormal basis functions.

$$\phi_{\Delta S}(t) = \sqrt{\frac{2}{T_{sym}}}\ rect(t - \frac{S-1}{2}) \quad for\ \ (S-1)\frac{T_{sym}}{2} \leq t \leq \frac{S.T_{sym}}{2} \tag{3.8}$$

where

$$rect(t) = \begin{cases} 1 & if\ 0 \leq t < 1 \\ 0 & otherwise \end{cases}$$

Figure 3.2 Shows the N-channel MMT developed basis function following the IM/DD channel constraint. It is clear that each of the time slots is non-overlapping in the time domain. The N-channel MMT symbols can be expressed as a linear combination of its basis functions. Thus, the MMT symbol can be translated to the weighted sum of two orthogonal basis functions corresponding to two consecutive one-dimensional signal constellations. The signal $x_{k,\Delta S}(t)$ is defined with respect to the basis function as

$$x_{k,\Delta S}(t) = A_{m,\Delta S}\sqrt{\frac{T_{sym}}{2}}\ \phi_{\Delta S}(t) \tag{3.9}$$

Each of the N-channel MMT symbol is defined by multiplying an amplitude $A_{m,\Delta S}$ by the corresponding basis function. While the entire MMT signal can be represented based on the basis functions as

$$X_k(t) = \sum_{S=1}^{\Delta S} A_{m,\Delta S}\sqrt{\frac{T_{sym}}{2}}\ \phi_{\Delta S}(t)\ = A_{m,\Delta 1}\sqrt{\frac{T_{sym}}{2}}\ \phi_{\Delta 1}(t) + A_{m,\Delta 2}\sqrt{\frac{T_{sym}}{2}}\ \phi_{\Delta 2}(t) \tag{3.10}$$

and each $x_{k,\Delta S}(t)$ is defined to guarantee the non-negativity constraint as

$$\min_{t}\ x_{k,\Delta S}(t) \geq 0 \tag{3.11}$$

Figure 3.3 shows the sixteen different signals for 4-Channel MMT with respect to the defined MMT basis function in eq(3.10).

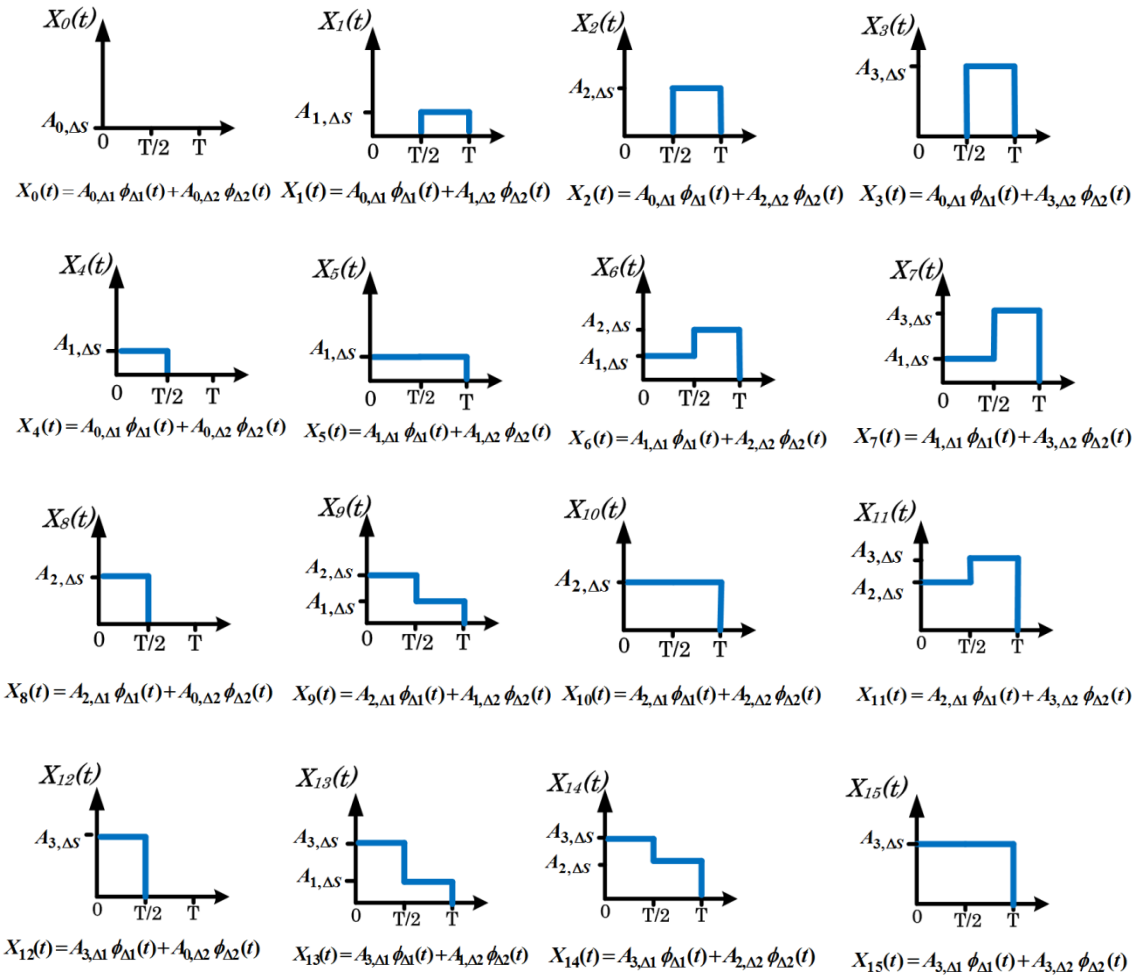

Figure 3.3 4-Channel MMT generated symbols in terms of the basis functions.

3.2.2 Geometric Representation of N-channel MMT

The N-channel MMT signal can be viewed as a vector space component in a geometric representation[86], [146]. By employing vector representation, the Euclidean distance between any pair of signal vectors can be expressed as $d = \sqrt{\left\| x_i - x_j \right\|^2}$. This can be translated to compute the Euclidean distance between the two MMT signals slots as

$$\begin{aligned} d_{MMT} &= \sqrt{\left\| x_{k,\Delta 1} - x_{k,\Delta 2} \right\|^2} \\ &= \sqrt{\frac{T_{sym}}{2}[(x_{i,\Delta 1} - x_{j,\Delta 1})^2 + (x_{i,\Delta 2} - x_{j,\Delta 2})^2]} \end{aligned} \tag{3.12}$$

where $i, j = 0,1,2,...,M_{\Delta S}$ and each MMT signal is represented in vectors in terms of each constellation dimension as $X_k = (x_{k,\Delta 1}, x_{k,\Delta 2})$ which is equivalent to it waveform representation $X_k(t)$.

For IM/DD systems, the constellation diagram for N-channel MMT symbol structure is shown in figure 3.4, compared to its counterpart of M-PAM in figure 3.5.

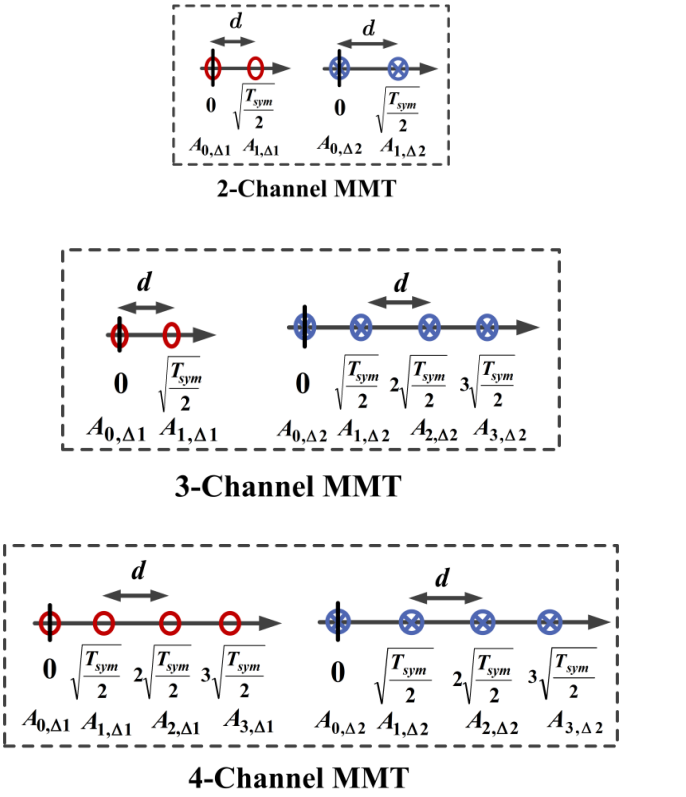

Figure 3.4 Signal space constellation geometry 2, 3, and 4-channel MMT for IM/DD systems.

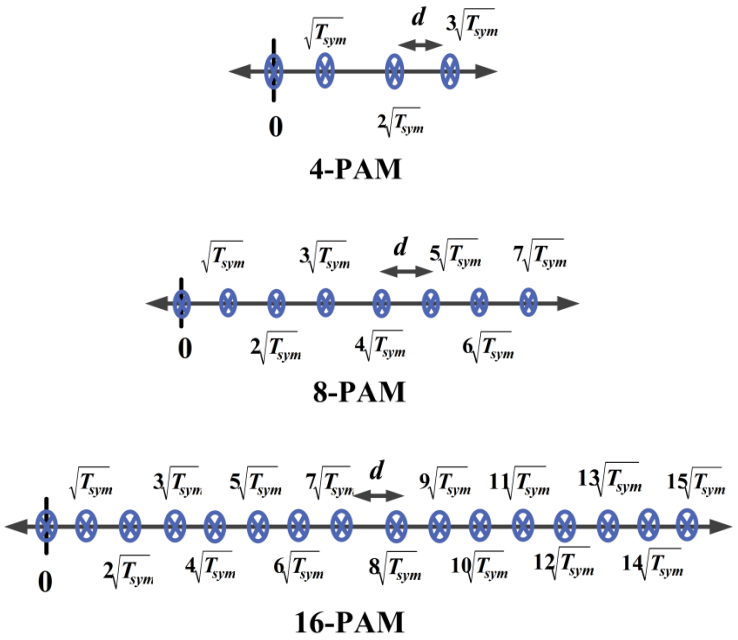

Figure 3.5 Signal space constellation 4-, 8- and 16-PAM for IM/DD systems.

3.3 MMT Transceiver Model

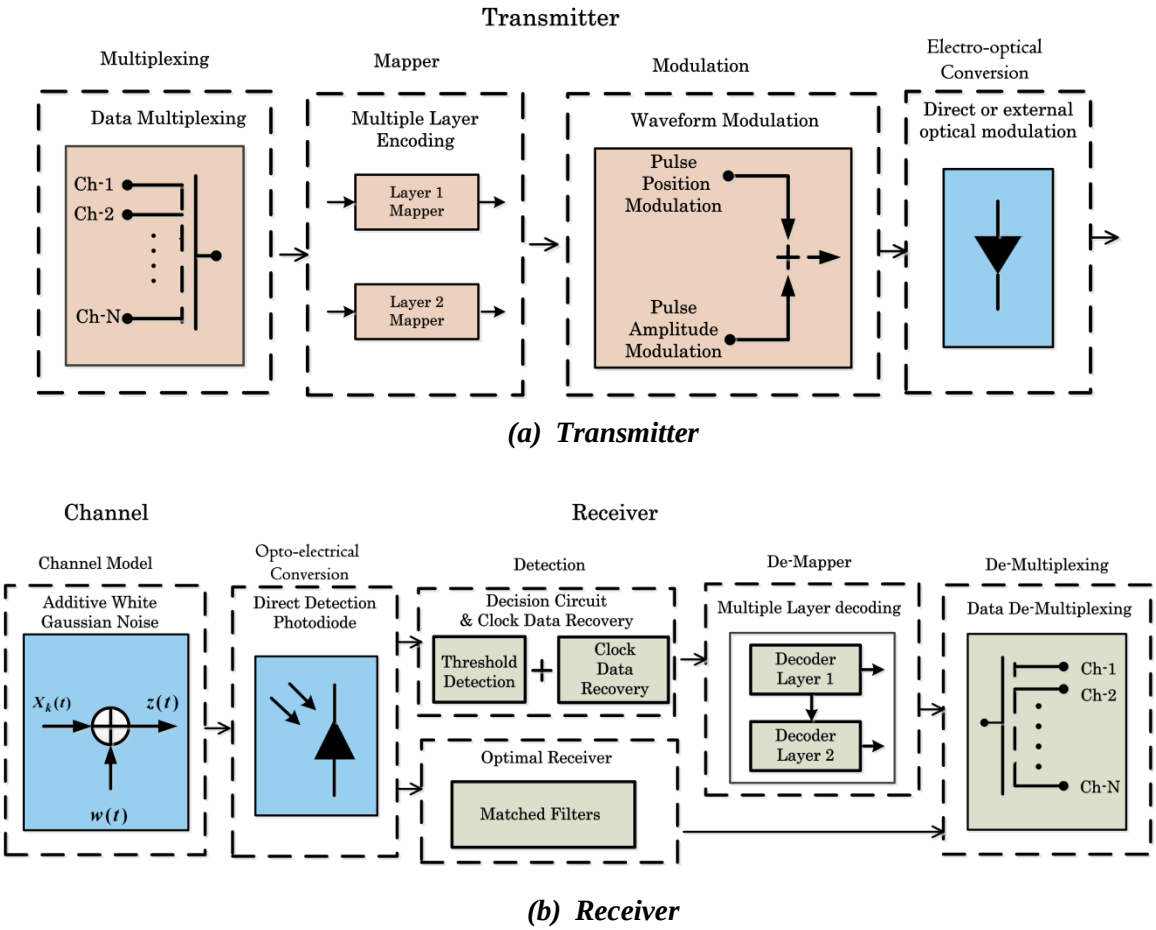

Figure 3.6 MMT generic transceiver model, (a) Transmitter and (b) Receiver.

Figure 3.6 shows a general model for both MMT transmitter 3.6(a) and receiver 3.6(b). The input data from different channels are multiplexed and divided into a set of data clusters. Then, MMT mapper exploits a multiple layer mapping algorithm to encode the subset partitioned multiplexed channels data under mapping rules. The main function of the MMT mapper unit is to transform the received data array from different channels (users) into a sequence of symbols according to a predefined algorithm, which is based upon a defined mapping rules. Afterwards, the data are modulated considering a hybrid combination between Pulse Amplitude Modulation (PAM) and Pulse Position Modulation (PPM). The symbol duration is divided in to two slots and each slot is composed of multiple amplitude levels dependent upon the number of channels or information capacity (in bits/symbol).

The N-channel MMT is classified under memoryless multilevel modulation scheme with multi-dimensional constellation diagram. N-channel MMT is based upon two consecutive one-dimensional constellation, designed for IM/DD systems. In IM/DD, Electro-Optical conversion is present by the responsibility of Directly Modulated Laser (DML) or an external optical modulator, which produce an intensity (power) signal proportional to the input electrical replica.

In MMT receiver design, two symbol detection methodologies have been considered to provide the detection techniques for the MMT symbols. First, detection based upon an optimal receiver with a bank of matched filter, where an abstract analytical performance evaluation for N-channel MMT technique can be performed. This analytical model can be considered later for comparison with other modulation formats. The optimal receiver involves a decoding process based upon Maximum Likehood Sequence Detection (MLSD) for the received message, searching among the set of N-channel MMT constellation points for the nearest Euclidean distance to the received message. The MLSD enable attaining the lowest probability of error. Thus, it can be employed as a performance measure to evaluate and compare MMT performance with other modulation formats.

The second method is a threshold detection receiver, which is based upon a dual threshold detection among the two symbol slots, in addition to a clock data recovery for synchronization with the transmitter. Before the threshold detection, an electrical filter is present in order to reshape signals and remove noise. Then, MMT de-mapper is present where a multiple stage decoding process takes place according to preset de-mapping rules defined later in *section 3.3.3.1*. In the end, the data is de-multiplexed back to the channels or users.

3.3.1 Basic Properties and Waveform Synthesis

The number of MMT symbol waveform alphabet (K) is equivalent to the number of different possible input channels combinations $K = 2^N$. The MMT method to convey information is not only based on dividing the symbol duration in to two sub interval slots, but also dependent on a varied number of levels per slot. The number of levels per slot ($M_{\Delta S}$) is related to the code length $\ell_{\Delta S}$ per cluster $Y_{\Delta S}$ for the multiplexed channels by

$$M_{\Delta S} = 2^{\ell_{\Delta S}} \tag{3.13}$$

i.e $M_{\Delta S} = \{2^1, 2^2, ..., 2^{\ell_{\Delta S}}\}$. The MMT signaling symbol set K is equivalent to the product of the number of levels for the two slots

$$K = M_{\Delta 1} \,.\, M_{\Delta 2} \tag{13.14}$$

where $M_{\Delta 1}, M_{\Delta 2}$ denote number of levels for slot $\Delta 1$ and slot $\Delta 2$, respectively. Moreover, the number of multiplexed bits N is related to the code length $\ell_{\Delta S}$ per cluster by

$$N = \sum_{i=1}^{\Delta S} \log_2(M_i) = \sum_{i=1}^{\Delta S} (\ell_{\Delta i}) \tag{3.15}$$

Figure 3.7 depicts the generic MMT symbol format that employs a varied number of slot amplitude levels ($A_{m,\Delta S}$) (dependent on the cluster code length $\ell_{\Delta S}$), and two slots (ΔS), for " N " number of users. The time duration of each slot interval (T_{slot}) is given by $T_{slot} = \frac{T_{sym}}{2}$, where T_{sym}, is the MMT symbol duration (1/ bitrate).

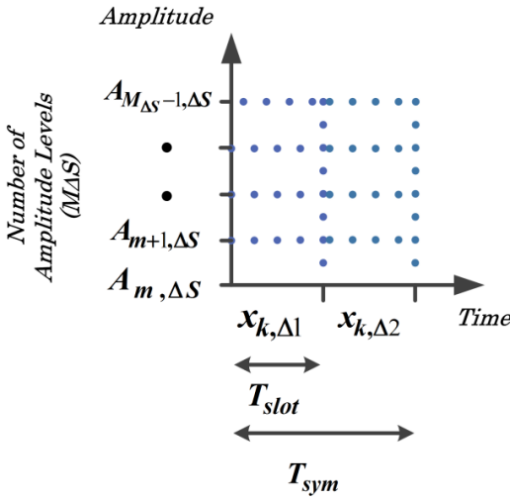

Figure 3.7 MMT symbol format.

N-Channel MMT has been designed for multiplexing and modulation of multiple different data channels (or users) bit streams. Two, three and four bits/symbol information capacities have been represented by 2-, 3- and 4-channel MMT, respectively. The N-channel waveform structure for 2-, 3- and 4-channel MMT are shown in figure 3.8.

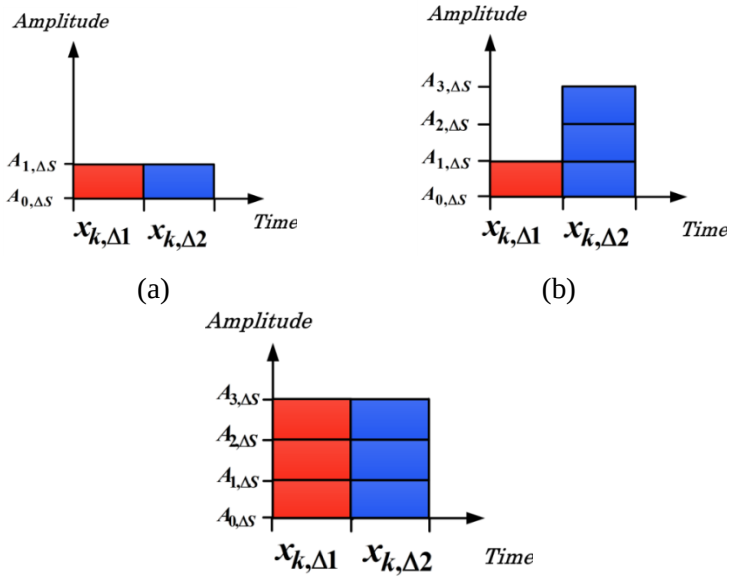

Figure 3.8 N-channel waveform structure for (a)2-Channel MMT , (b)3-Channel MMT and (c) 4-channel MMT.

3.3.2 N-channel MMT Transmitter Model

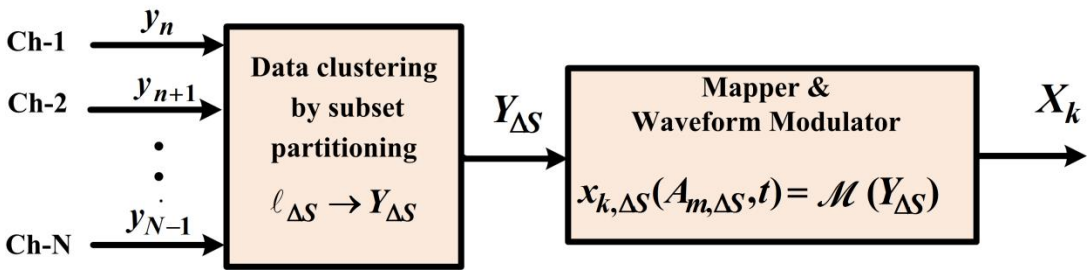

Figure 3.9 MMT transmitter proposed model.

MMT transmitter model is depicted in figure 3.9. The MMT mapper on the transmission side is built with an input array of parallel channels $N = [y_n, y_{n+1}, ..., y_{N-1}]$ where $n = 0,1,2,..,N-1$, with an array size of $N > 1$. Each channel (user) data is represented by y_n, where $y_n \in \{0,1\}$.

The mapper maps the parallel input channels data to MMT different unique symbols. The serially converted input data array is split in to two clusters (subsets) $Y_{\Delta S}$, where each cluster address is denoted by a subscript index ΔS where $\Delta S = \{\Delta 1, \Delta 2\}$. The code length ($\ell_{\Delta S}$) per cluster $Y_{\Delta S}$ in principle is dependent upon the number of input channels and is equal to

For odd number of channels *For even number of channels*

$$\overbrace{\ell_{\Delta 1} = \frac{N-1}{2} bits \qquad \ell_{\Delta 2} = \frac{N+1}{2} bits} \qquad \overbrace{\ell_{\Delta 1}, \ell_{\Delta 2} = \frac{N}{2} bits} \qquad (3.16)$$

A mapper and waveform modulator unit performs bijective-mapping operation to map the input multiplexed cluster $Y_{\Delta S}$ to a distinct MMT symbol. The basic idea behind MMT mapper is to exploit a multiple layer mapping algorithm to encode an input multiplexed data channels to a subset partitioned data cluster following MMT mapping rules. MMT mapper and waveform generator is composed of a subdivided dual slot amplitude modulator. The MMT symbol is composed of a waveform that belongs to a set of signal waveform alphabet $X_K = \{X_0(t), X_1(t)...., X_{K-1}(t)\}$ where K is the size of the

MMT signaling set. The message sent during a symbol interval is chosen as one of the waveform alphabets X_K, which are sent independently of each other. The N-channel MMT signal are equiporbable with an equal probability of $1/K$. Note that the waveform symbol pattern is divided in to two slots $\Delta S = \Delta 1, \Delta 2$ in which amplitude modulated waveform per slot represented by $x_{k,\Delta 1}(t)$ and $x_{k,\Delta 2}(t)$ where subscript k, ΔS denote the alphabet index and the slot index, respectively.

At an instant *t*, the MMT mapper maps the input data cluster $Y_{\Delta S}$ to an amplitude-modulated waveform following the mapping table 3.1, which can be expressed as

$$x_{k,\Delta S}(A_{m,\Delta S}, t) = \{ A_{m,\Delta S} = \mathbf{M}_{Map}(Y_{\Delta S}) \mid Y_{\Delta S} = [y_0, y_1, .., y_{N-1}] \} \tag{3.17}$$

where $x_{k,\Delta S}(A_{m,\Delta S}, t)$ denotes the amplitude modulated waveform corresponding to slot ΔS and $Y_{\Delta S}$ is the data cluster mapped to an amplitude level $A_{m,\Delta S}$. The mapper modulator unit generates two consecutive slot waveforms $X_K = [x_{k,\Delta 1}(t_i), x_{k,\Delta 2}(t_{i+1})]$.

For more illustration of the MMT technique, the MMT data encoding system is based on two layer mapping for a two-consecutive one-dimensional system where each layer represent single dimension. The first layer comprises mapping the data subset $Y_{\Delta 1}$ to the first slot for synthetization to the first constellation dimension by modulation and denoting it $x_{k,1}(A_{m,slot1})$ where $A_{m,slot1}$ represent the amplitude modulation for the first slot ,i.e

$$\mathrm{M}_{\mathrm{slot1}}(Y_{\Delta 1}) \mapsto x_{k,1}(A_{m,slot1}) \tag{3.18}$$

In the same manner, the second layer encompass mapping the data subset $Y_{\Delta 2}$ to the second slot for synthetization to the second MMT constellation dimension and denoting it $x_{k,2}(A_{m,slot2})$ where $A_{m,slot2}$ denote the amplitude modulation for the second slot, i.e

$$\boldsymbol{M}_{\text{slot2}}(Y_{\Delta 2}) \mapsto x_{k,2}(A_{m,slot2}) \tag{3.19}$$

The symbol alphabet is transmitted upon the mapping of both data clusters each to its correspondent slot to form an MMT symbol generated by the waveform modulator, i.e

$$\boldsymbol{M}_{\text{MMT}}(Y_{\Delta 1}, Y_{\Delta 2}) \mapsto x_{k,1}(A_{m,slot1}), x_{k,2}(A_{m,slot2}) \tag{3.20}$$

Table 3.1 shows a 4-channel MMT two layer symbol mapping operation. In time domain, the MMT mapper waveform unit is capable of generating the MMT symbols following a formulated expression, i.e

$$x_{k,\Delta S}(A_{m,\Delta S}, t) = \begin{cases} A_{m,\Delta S} W_{T_{sym}}(t - \dfrac{(S-1)}{2}) & \text{for } (S-1)\dfrac{T_{sym}}{2} \le t \le \dfrac{S.T_{sym}}{2} \\ 0 & \text{otherwise} \end{cases} \tag{3.21}$$

where each k represents an MMT symbol from a total of $X_{K-1}(t)$ symbols, $W_{T_{sym}}$ is the waveform corresponding to MMT symbol duration T_{sym} and ΔS is the slot index where $\Delta S = \{\Delta 1, \Delta 2\}$.

The waveform dependent variables are amplitude and time; the amplitude is based upon the mapping rule in (3.17) and table 3.1, while the time interval depends upon the slot number ($S = 1$ or $S = 2$) which corresponds to the slot index

Table 3.1 4-Channel MMT SYMBOL MAPPER.

First Mapping Layer	Second Mapping Layer
$\mathcal{M}_{\text{slot1}}(Y_{\Delta 1}) \mapsto x_{k,\Delta 1}(A_{m,\Delta 1})$	$\mathcal{M}_{\text{slot2}}(Y_{\Delta 2}) \mapsto x_{k,\Delta 2}(A_{m,\Delta 2})$
$\mathcal{M}_{s=1}(00) \mapsto x_{k,\Delta 1}(A_{0,\Delta 1})$	$\mathcal{M}_{s=2}(00) \mapsto x_{k,\Delta 2}(A_{0,\Delta 2})$
$\mathcal{M}_{s=1}(01) \mapsto x_{k,\Delta 1}(A_{1,\Delta 1})$	$\mathcal{M}_{s=2}(01) \mapsto x_{k,\Delta 2}(A_{1,\Delta 2})$
$\mathcal{M}_{s=1}(11) \mapsto x_{k,\Delta 1}(A_{2,\Delta 1})$	$\mathcal{M}_{s=2}(10) \mapsto x_{k,\Delta 2}(A_{2,\Delta 2})$
$\mathcal{M}_{s=1}(10) \mapsto x_{k,\Delta 1}(A_{3,\Delta 1})$	$\mathcal{M}_{s=2}(11) \mapsto x_{k,\Delta 2}(A_{3,\Delta 2})$

$$\mathcal{M}_{\text{MMT}}(Y_{\Delta 1}, Y_{\Delta 2}) \mapsto [x_{k,\Delta 1}(A_{m,\Delta 1}), x_{k,\Delta 2}(A_{m,\Delta 2})] \equiv X_K$$

$$\mathcal{M}(00,00) \mapsto [x_{0,\Delta 1}(A_{0,\Delta 1}), x_{0,\Delta 2}(A_{0,\Delta 2})] \equiv X_0$$

$$\mathcal{M}(00,01) \mapsto [x_{1,\Delta 1}(A_{0,\Delta 1}), x_{1,\Delta 2}(A_{1,\Delta 2})] \equiv X_1$$

$$\mathcal{M}(00,10) \mapsto [x_{2,\Delta 1}(A_{0,\Delta 1}), x_{2,\Delta 2}(A_{2,\Delta 2})] \equiv X_2$$

$$\mathcal{M}(00,11) \mapsto [x_{3,\Delta 1}(A_{0,\Delta 1}), x_{3,\Delta 2}(A_{3,\Delta 2})] \equiv X_3$$

$$\mathcal{M}(01,00) \mapsto [x_{4,\Delta 1}(A_{1,\Delta 1}), x_{4,\Delta 2}(A_{0,\Delta 2})] \equiv X_4$$

$$\mathcal{M}(01,01) \mapsto [x_{5,\Delta 1}(A_{1,\Delta 1}), x_{5,\Delta 2}(A_{1,\Delta 2})] \equiv X_5$$

$$\mathcal{M}(01,10) \mapsto [x_{6,\Delta 1}(A_{1,\Delta 1}), x_{6,\Delta 2}(A_{2,\Delta 2})] \equiv X_6$$

$$\mathcal{M}(01,11) \mapsto [x_{7,\Delta 1}(A_{1,\Delta 1}), x_{7,\Delta 2}(A_{3,\Delta 2})] \equiv X_7$$

$$\mathcal{M}(10,00) \mapsto [x_{8,\Delta 1}(A_{2,\Delta 1}), x_{8,\Delta 2}(A_{0,\Delta 2})] \equiv X_8$$

$$\mathcal{M}(10,01) \mapsto [x_{9,\Delta 1}(A_{2,\Delta 1}), x_{9,\Delta 2}(A_{1,\Delta 2})] \equiv X_9$$

$$\mathcal{M}(10,10) \mapsto [x_{10,\Delta 1}(A_{2,\Delta 1}), x_{10,\Delta 2}(A_{2,\Delta 2})] \equiv X_{10}$$

$$\mathcal{M}(10,11) \mapsto [x_{11,\Delta 1}(A_{2,\Delta 1}), x_{11,\Delta 2}(A_{3,\Delta 2})] \equiv X_{11}$$

$$\mathcal{M}(11,00) \mapsto [x_{12,\Delta 1}(A_{3,\Delta 1}), x_{12,\Delta 2}(A_{0,\Delta 2})] \equiv X_{12}$$

$$\mathcal{M}(11,01) \mapsto [x_{13,\Delta 1}(A_{3,\Delta 1}), x_{13,\Delta 2}(A_{1,\Delta 2})] \equiv X_{13}$$

$$\mathcal{M}(11,10) \mapsto [x_{14,\Delta 1}(A_{3,\Delta 1}), x_{14,\Delta 2}(A_{2,\Delta 2})] \equiv X_{14}$$

$$\mathcal{M}(11,11) \mapsto [x_{15,\Delta 1}(A_{3,\Delta 1}), x_{15,\Delta 2}(A_{3,\Delta 2})] \equiv X_{15}$$

3.3.2.1 N-channel MMT Symbol Rate

One of the main advantages that features MMT compared with other modulation formats, is the system symbol rate reduction. N-channel MMT data capacity multiplexing feature enhances the eligibility for scaling the baud rate with the limitations that exists in electronic and optical components operating at a fraction of the aggregated data rate.Therefore, N-channel MMT has the capability of reducing the baud rate to $1/\log_2(M_{\Delta 1} M_{\Delta 2})$ of the the aggregated bit rate.

As such, 2-channel MMT features a baud rate equivalent to 1/2 of its aggregated bitrate compared with OOK. While, 3-channel MMT has a baud rate equivalent to 1/3 of its aggregated bitrate compared with OOK. Also, 4-channel MMT is capable of decreasing the electronic requirement of its components to a baud rate equivalent to 1/4 of the aggregated bit rate compared with OOK.

3.3.3 Receiver Model

The receiver is one of the crucial components in the transceiver design due to their responsibility in recovering the transmitted data. The receiver function is to decide upon a certain observation the transmitter sent message. This decision is determined based upon a pre-set a particular criteria.

As mentioned earlier, two receiver detection designs have been proposed for N-Channel MMT, which can be classified as follows :-

1. **Threshold detection receiver for the numerical model.**

2. **Optimal detection receiver for the analytical Model.**

3.3.3.1 Threshold Detection Receiver

The N-channel MMT threshold detection methodology employs a reduced complexity algorithm, which is based upon dividing detection process to two stages in correspondence with the two consecutive one-dimensional constellation nature of MMT. Conventionally, the processing de-mapping unit should searches for the transmitted message among all possible combinations of the lattice constellation points that is equal to $\mathbf{2}^{N}$ symbols. However, in MMT design, the detection process is divided in to two stages; in which the first stage is searching for the transmitted first cluster message over the lattice of the first dimension that are equivalent to $\frac{K}{M_{\Delta S}}$ of the total MMT symbols. Afterwards, the second stage in turn searches for the second cluster message over the second dimensional constellation lattice points that are equivalent to $\frac{K}{M_{\Delta S}}$ of the total MMT symbols. This method can reduce the number of the search processing hardware device to a number proportional to a total number of processing searches equivalent to

$$I_{tot} = I_{st1} + I_{st2} \tag{3.22}$$

,the number of processing searches for each stage $I_{st,\Delta S}$ is equivalent to

$$I_{st,\Delta S} = \frac{K}{M_{\Delta S}} \tag{3.24}$$

where K is the number of MMT symbols and $M_{\Delta S}$ is the number of levels per slot. The reduction in number of constellation search lattice points is equivalent to ($K - I_{tot}$). The multistage decision and de-mapping operation is shown with respect to constellation points in figure 3.10 (a-c) for 2-channel, 3-channel and 4-channel MMT, respectively.

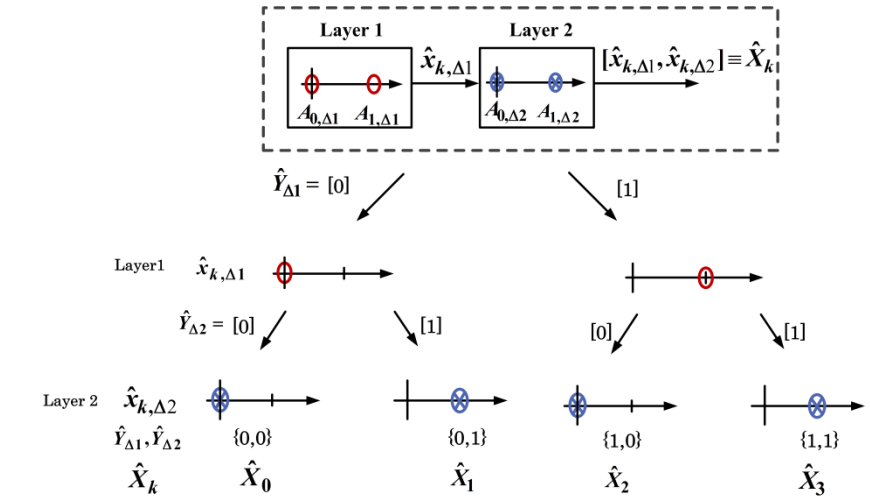

(a)2-channel MMT

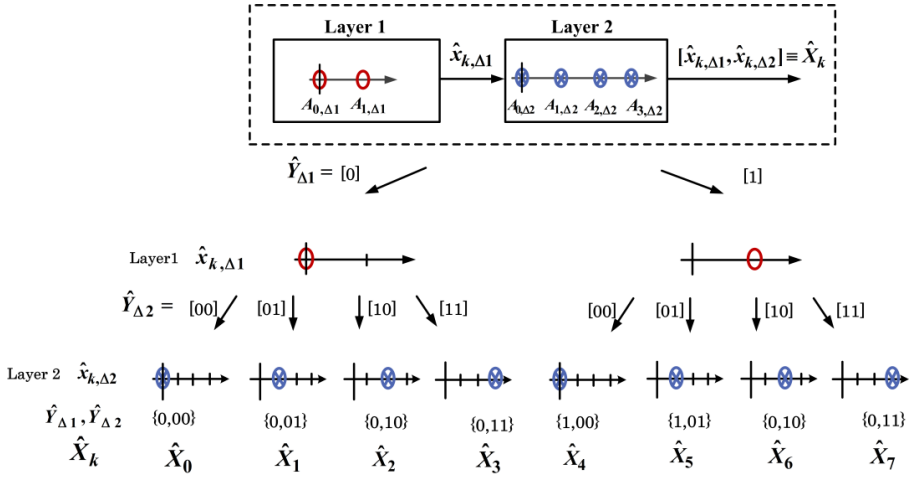

(b) 3-channel MMT

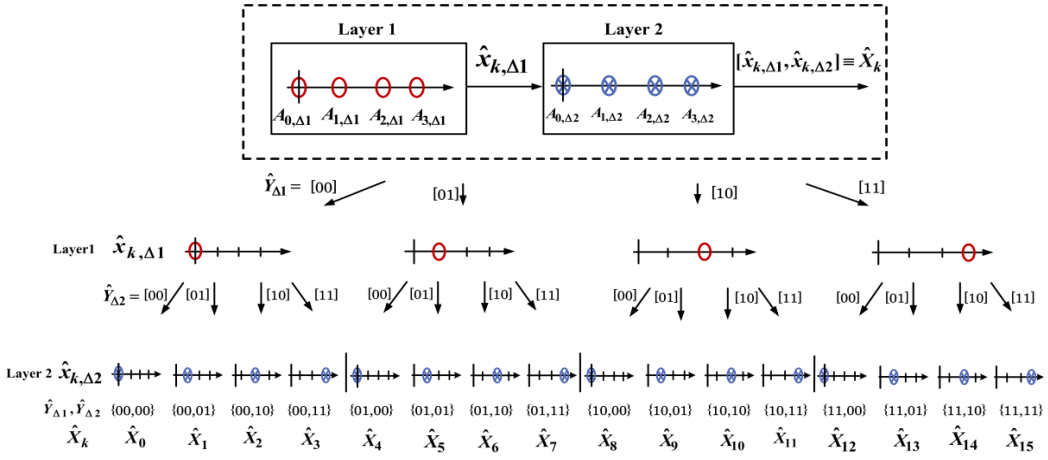

(c) 4-Channel MMT

Figure 3.10 De-mapping multistage decision methodology for (a) 2-Channel MMT, (b) 3-Channel MMT, and (c) 4-Channel MMT.

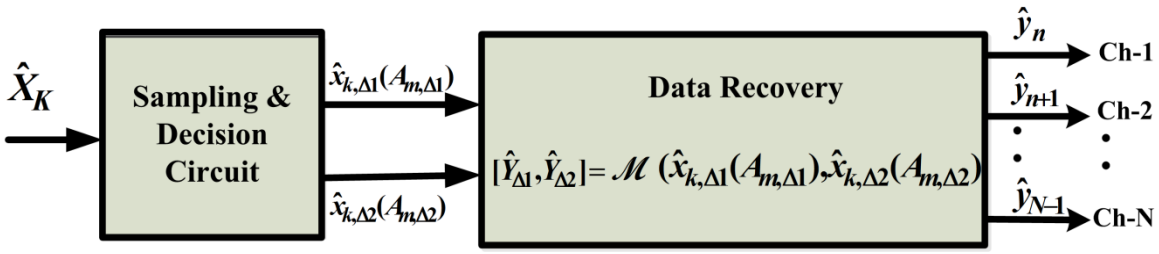

Figure 3.11 MMT De-Mapping receiver structure.

The MMT receiver model is shown in figure 3.11. MMT threshold detection receiver employs a low complexity decision circuit and data recovery algorithm. At the receiver side, the received signal is fed into sampling and decision circuit. The samples are taken at two sampling points $SP_{\Delta S}$ (one sampling point per slot ΔS). The outputs of the sampling circuit are fed into a decision and de-mapping unit. In this unit, the sampled values are compared against a number of threshold values.

$$\delta_{i,\Delta S} = \{\delta_{i,\Delta S}, \delta_{i+1,\Delta S}, ..., \delta_{M_{\Delta S}-1,\Delta S}\} \tag{3.25}$$

where $M_{\Delta S}$ corresponds to the number of levels for a slot ΔS.

Sampling circuit outputs are driven to a decision and regeneration unit for the data recovery that is according to preset defined de-mapping rules shown in table 3.2. The de-mapping operation is based upon two layers multistage detection operation as shown in figure 3.8 to map the received slot waveforms $\hat{x}_{k,\Delta1}(A_{m,\Delta1}), \hat{x}_{k,\Delta2}(A_{m,\Delta2})$ to a distinct constellation point .The two stages de-mapping operation can be expressed as

$$[\hat{Y}_{\Delta1}, \hat{Y}_{\Delta2}] = \boldsymbol{M}_{De\text{-}Map}\ (\hat{x}_{k,\Delta1}(A_{m,\Delta1}), \hat{x}_{k,\Delta2}(A_{m,\Delta2})) \tag{3.26}$$

Table 3.2 4-Channel MMT SYMBOL De-Mapper.

4-Ch. MMT De-Mapping Detection Rules				***Symbol Decision*** $\hat{X}_K$
1st Cluster Rule Slot 1 Ch1 - Ch2	***1st Stage Decision***	***2nd Cluster Rule Slot 2 Ch3 - Ch4***	***2nd Stage Decision***	
if $SP_{\Delta 1} \le \delta_{1,\Delta 1}$	$\hat{x}_{0,1}(A_{0,\Delta 1})$	*if* $SP_{\Delta 1} \le \delta_{1,\Delta 2}$	$\hat{x}_{0,2}(A_{0,\Delta 2})$	$[\hat{x}_{0,1}(A_{0,\Delta 1}), \hat{x}_{0,2}(A_{0,\Delta 2})] \equiv \hat{X}_0$
	$\hat{x}_{1,1}(A_{0,\Delta 1})$	*if* $\delta_{2,\Delta 2} \ge SP_{\Delta 1} \succ \delta_{1,\Delta 2}$	$\hat{x}_{1,2}(A_{1,\Delta 2})$	$[\hat{x}_{1,1}(A_{0,\Delta 1}), \hat{x}_{1,2}(A_{1,\Delta 2})] \equiv \hat{X}_1$
	$\hat{x}_{2,1}(A_{0,\Delta 1})$	*if* $\delta_{3,\Delta 2} \ge SP_{\Delta 1} \succ \delta_{2,\Delta 2}$	$\hat{x}_{2,2}(A_{2,\Delta 2})$	$[\hat{x}_{2,1}(A_{0,\Delta 1}), \hat{x}_{2,2}(A_{2,\Delta 2})] \equiv \hat{X}_2$
	$\hat{x}_{3,1}(A_{0,\Delta 1})$	*if* $SP_{\Delta 1} \succ \delta_{3,\Delta 2}$	$\hat{x}_{3,2}(A_{3,\Delta 2})$	$[\hat{x}_{3,1}(A_{0,\Delta 1}), \hat{x}_{3,2}(A_{3,\Delta 2})] \equiv \hat{X}_3$
if $\delta_{2,\Delta 1} \ge SP_{\Delta 1} \succ \delta_{1,\Delta 1}$	$\hat{x}_{4,1}(A_{1,\Delta 1})$	*if* $SP_{\Delta 1} \le \delta_{1,\Delta 2}$	$\hat{x}_{4,2}(A_{0,\Delta 2})$	$[\hat{x}_{4,1}(A_{1,\Delta 1}), \hat{x}_{4,2}(A_{0,\Delta 2})] \equiv \hat{X}_4$
	$\hat{x}_{5,1}(A_{1,\Delta 1})$	*if* $\delta_{2,\Delta 2} \ge SP_{\Delta 1} \succ \delta_{1,\Delta 2}$	$\hat{x}_{5,2}(A_{1,\Delta 2})$	$[\hat{x}_{5,1}(A_{1,\Delta 1}), \hat{x}_{5,2}(A_{1,\Delta 2})] \equiv \hat{X}_5$
	$\hat{x}_{6,1}(A_{1,\Delta 1})$	*if* $\delta_{3,\Delta 2} \ge SP_{\Delta 1} \succ \delta_{2,\Delta 2}$	$\hat{x}_{6,2}(A_{2,\Delta 2})$	$[\hat{x}_{6,1}(A_{1,\Delta 1}), \hat{x}_{6,2}(A_{2,\Delta 2})] \equiv \hat{X}_6$
	$\hat{x}_{7,1}(A_{1,\Delta 1})$	*if* $SP_{\Delta 1} \succ \delta_{3,\Delta 2}$	$\hat{x}_{7,2}(A_{3,\Delta 2})$	$[\hat{x}_{7,1}(A_{1,\Delta 1}), \hat{x}_{7,2}(A_{3,\Delta 2})] \equiv \hat{X}_7$
if $\delta_{3,\Delta 1} \ge SP_{\Delta 1} \succ \delta_{2,\Delta 1}$	$\hat{x}_{8,1}(A_{2,\Delta 1})$	*if* $SP_{\Delta 1} \le \delta_{1,\Delta 2}$	$\hat{x}_{8,2}(A_{0,\Delta 2})$	$[\hat{x}_{8,1}(A_{2,\Delta 1}), \hat{x}_{8,2}(A_{0,\Delta 2})] \equiv \hat{X}_8$
	$\hat{x}_{9,1}(A_{2,\Delta 1})$	*if* $\delta_{2,\Delta 2} \ge SP_{\Delta 1} \succ \delta_{1,\Delta 2}$	$\hat{x}_{9,2}(A_{1,\Delta 2})$	$[\hat{x}_{9,1}(A_{2,\Delta 1}), \hat{x}_{9,2}(A_{1,\Delta 2})] \equiv \hat{X}_9$
	$\hat{x}_{10,1}(A_{2,\Delta 1})$	*if* $\delta_{3,\Delta 2} \ge SP_{\Delta 1} \succ \delta_{2,\Delta 2}$	$\hat{x}_{10,2}(A_{2,\Delta 2})$	$[\hat{x}_{10,1}(A_{2,\Delta 1}), \hat{x}_{10,2}(A_{2,\Delta 2})] \equiv \hat{X}_{10}$
	$\hat{x}_{11,1}(A_{2,\Delta 1})$	*if* $SP_{\Delta 1} \succ \delta_{3,\Delta 2}$	$\hat{x}_{11,2}(A_{3,\Delta 2})$	$[\hat{x}_{11,1}(A_{2,\Delta 1}), \hat{x}_{11,2}(A_{3,\Delta 2})] \equiv \hat{X}_{11}$
if $SP_{\Delta 1} \succ \delta_{3,\Delta 1}$	$\hat{x}_{12,1}(A_{3,\Delta 1})$	*if* $SP_{\Delta 1} \le \delta_{1,\Delta 2}$	$\hat{x}_{12,2}(A_{0,\Delta 2})$	$[\hat{x}_{12,1}(A_{3,\Delta 1}), \hat{x}_{12,2}(A_{0,\Delta 2})] \equiv \hat{X}_{12}$
	$\hat{x}_{13,1}(A_{3,\Delta 1})$	*if* $\delta_{2,\Delta 2} \ge SP_{\Delta 1} \succ \delta_{1,\Delta 2}$	$\hat{x}_{13,2}(A_{1,\Delta 2})$	$[\hat{x}_{13,1}(A_{3,\Delta 1}), \hat{x}_{13,2}(A_{1,\Delta 2})] \equiv \hat{X}_{13}$
	$\hat{x}_{14,1}(A_{3,\Delta 1})$	*if* $\delta_{3,\Delta 2} \ge SP_{\Delta 1} \succ \delta_{2,\Delta 2}$	$\hat{x}_{14,2}(A_{2,\Delta 2})$	$[\hat{x}_{14,1}(A_{3,\Delta 1}), \hat{x}_{14,2}(A_{2,\Delta 2})] \equiv \hat{X}_{14}$
	$\hat{x}_{15,1}(A_{3,\Delta 1})$	*if* $SP_{\Delta 1} \succ \delta_{3,\Delta 2}$	$\hat{x}_{15,2}(A_{3,\Delta 2})$	$[\hat{x}_{15,1}(A_{3,\Delta 1}), \hat{x}_{15,2}(A_{3,\Delta 2})] \equiv \hat{X}_{15}$

Based on the regeneration rules, the decision circuit detects the received samples and estimates the corresponding transmitted amplitude waveform per slot $\hat{x}_{k,\Delta S}(A_{m,\Delta S})$. Consequently, the decision is fed to the data recovery unit to extract the sent data clusters based on the defined algorithm.

Figure 3.12 shows the calculated eye diagram structure for 2, 3, and 4-channel MMT system composed of multiple fragmented eye diagrams with different threshold levels.

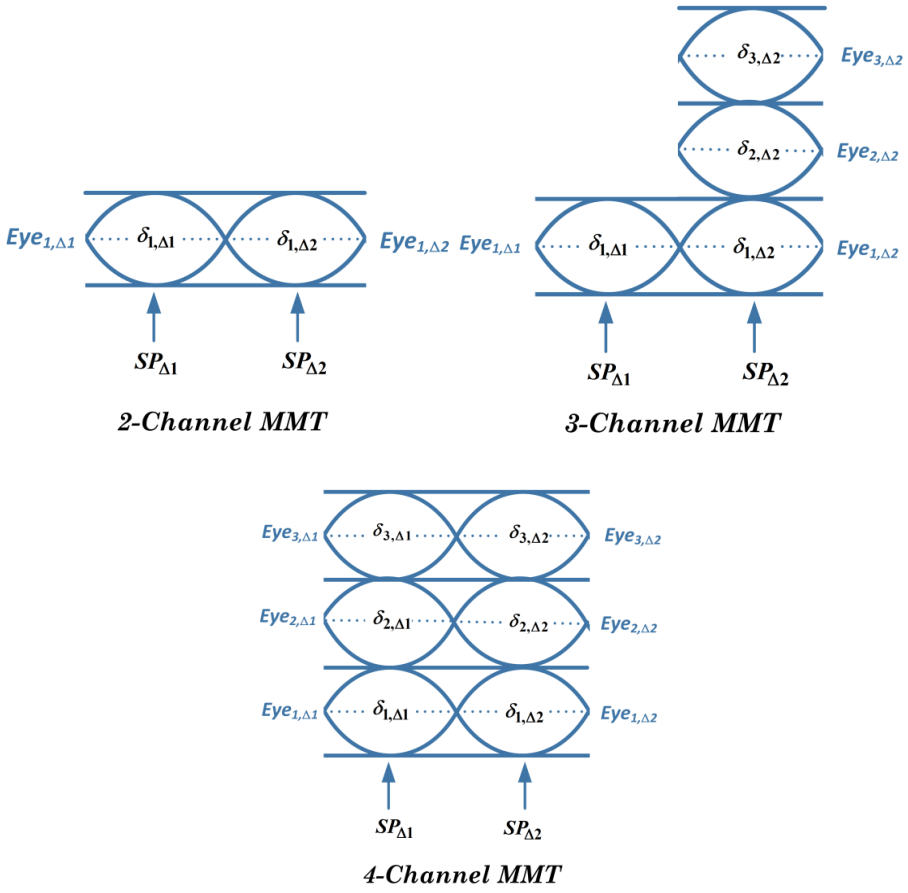

Figure 3.12 2-, 3- and 4-Channel MMT eye diagrams

3.3.3.2 Optimal Detection Receiver

Signal space analysis discussed in section 3.2 aimed to analyze N-channel MMT with respect to an abstraction level by representing it in N-dimensional signal constellation. This kind of representation necessitates unambiguous evaluation criteria to be a platform for comparison with other modulation formats. Hence, an optimal receiver detection receiver has been assumed for the detection of the MMT symbols where a precise computation of the bit error probability of a set of pairwise signals can be realized. Optimal receiver has been extensively employed for the optimal detection of modulation formats[53], [86], [90], [138], [147]–[149]. Since, a signal space analysis is employed, thus, it is more convenient to express the MMT system in terms of its vector component assuming additive Gaussian channel as

$$z = X_k + w \tag{3.27}$$

where w is the vector noise component, X_k is the transmitted MMT signal vector and z is the received signal vector. At the receiver, the received message $\hat{X}_k$ can be estimated upon the detection of z. The receiver detection process is based upon Maximum likehood sequence detection (MLSD) following[86], [126], [145], [150]–[155].

Assuming equiprobable MMT signals, the optimal receiver involves a detection process for the received message, searching among the set of N-channel MMT constellation points for the nearest Euclidean distance to the received message. This maximization of the correct decision of the sent MMT symbol can be expressed as

$$\hat{X}_k = \underset{0 \le k \le K}{\arg\max}\ P_{X_k} P(z | X_k \ \textit{is sent}) \tag{3.28}$$

where P_{X_k} is the priori probability of the transmission of MMT symbols and is equivalent to $P_{X_k} = \dfrac{1}{M_{\Delta 1} M_{\Delta 2}}$.

The signal space point nearest to the received message is output as an estimate to the received N-channel symbol. Assuming Gaussian random variables, the received vector z is dependent upon the conditional probability density function, which can be expressed as

$$f_{z|X_k\ sent} = \frac{1}{\sqrt{2\pi\sigma^2}} e^{(-\frac{\|z-X_k\|^2}{2\sigma^2})} \tag{3.29}$$

where σ^2 is the variance equivalent to $\frac{N_o}{2}$. Hence, by substitution from (4.27) in (4.26). Assuming a MLSD, $\hat{X}_k$ can be derived as [86]

$$\hat{X}_k = \arg\max_{0\le k\le K} P_{X_k} \frac{1}{\sqrt{2\pi\sigma^2}} e^{(-\frac{\|z-X_k\|^2}{2\sigma^2})} \tag{3.30}$$

Since $\frac{1}{\sqrt{2\pi\sigma^2}}$ is a constant, thus, neglecting it will not affect the result, where

$$\hat{X}_k = \arg\max_{0\le k\le K} \ln \frac{1}{M_{\Delta 1} M_{\Delta 2}} - \frac{\|z-X_k\|^2}{2\sigma^2} \tag{3.31}$$

By substitution with $\sigma^2 = \frac{N_o}{2}$ and multiplying the equation with $\frac{N_o}{2}$,

$$\hat{X}_k = \arg\max_{0\le k\le K} \frac{N_o}{2} \ln\left(\frac{1}{M_{\Delta 1} M_{\Delta 2}} - \frac{\|z-X_k\|^2}{2} \right) \tag{3.32}$$

Since the natural logarithm ln (.) is a monotonically increasing function and by neglecting the constants, hence, the optimal $\hat{X}_k$ is equivalent to

$$\hat{X}_k = \arg\max_{0\le k\le K} [-\|z-X_k\|^2] \tag{3.33}$$

Eq. (3.33) which looks in to maximizing the negative correct decision of the received MMT symbol is equivalent to minimizing it square root positive counterpart to be

$$\hat{X}_k = \arg\min_{0 \le k \le K} \left\| z - X_k \right\| \tag{3.34}$$

Assuming an equiprobable MMT signals, eq.(3.26)-(3.33) show that the MMT optimum receiver have maximized the correct decision of MMT symbol (which is equivalent to minimizing the bit error probability). The detection process involves searching among the set of N-channel MMT constellation points for the one with minimum Euclidean distance to the received message. The optimal receiver includes a continuous time matched filter where its impulse response is the same as the transmitted MMT symbols pulse shape[86], [89], [156].

The matched filter maximizes the SNR of the MMT signal at the detection instant. Since the MMT signals are represented in terms of their basis functions, thus, the impulse response of the employed matched filter can be expressed as

$$h_{\Delta S}(t) = \phi_{\Delta S}(T_m - t) = \sqrt{\frac{2}{T_{sym}}}\, rect(t - \frac{S-1}{2}) \quad for \;\; (S-1)\frac{T_{sym}}{2} \le t \le \frac{S.T_{sym}}{2} \tag{3.34}$$

where T_m is a filter design specification aspect and sampling occurs in an instant $t = T_m$ of the output of the matched filter. Figure 3.13 shows the MMT optimal receiver structure. It consists of two continuous time matched filter with an equivalent impulse response to the two MMT basis functions. The output of the matched filter is sampled at time instance equivalent to MMT defined dual slot duration. The output of the matched filter is denoted by the convolution of the received message and the filter impulse response to be

$$y_m(t) = z(t) * h_{\Delta S}(t) = \int_{-\infty}^{\infty} z(t)\,\phi_{\Delta S}(T_m - t)dt \tag{3.35}$$

Then, a correlator is present where a multiplying operation for the output of the filter with each signal $x_{k,\Delta S}(t)$ coefficient and integrate the result to find all the inner products of the received message $z(t)$. Afterwards, a constant term is added which is equivalent to each signal coefficient C_m . Then, a selector is present where the largest value is chosen as a decision to be the most probable estimated transmitted message $\hat{x}_{k,\Delta S}(t)$ per slot. Finally, a de-mapping unit exists in the final stage to determine the final overall message and then maps data to the corresponding channels. A lot of practical MLSD have been implemented using state of the art CMOS technology[157], [158]. Also, MLSD have been employed extensively to mitigate fiber impairments [151], [154], [159].

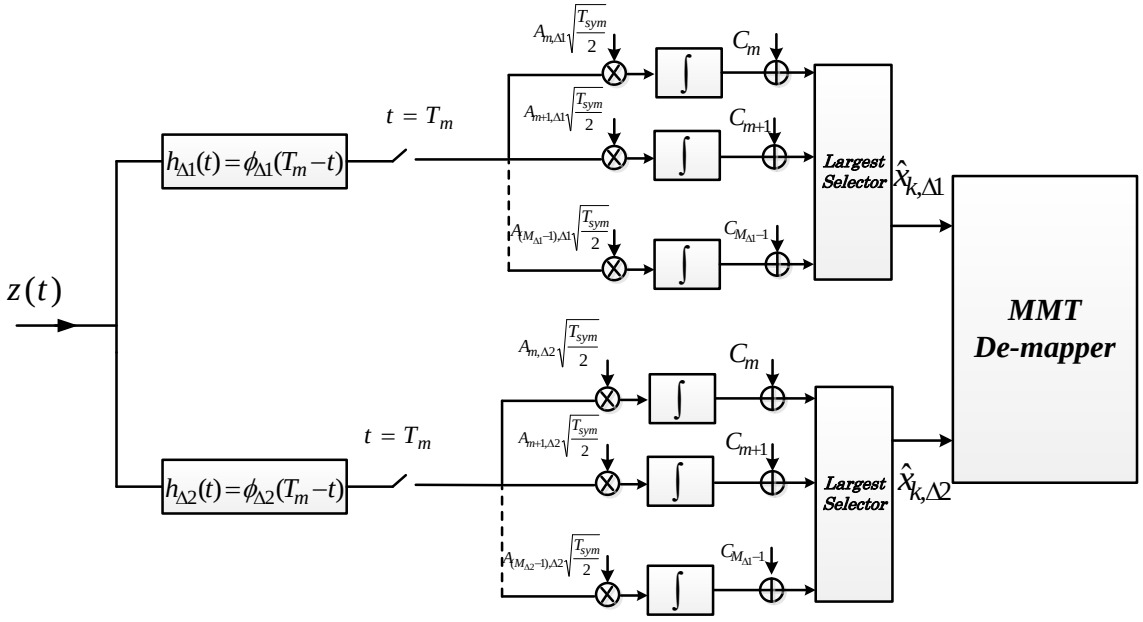

Figure 3.13 N-channel MMT optimal matched filter receiver.

3.4 Performance Evaluation Criterion

The proper choice of the performance assessment methodology is a crucial part in evaluating the effectivity of MMT novel transmission format. These parameters consider the interaction between signal characteristics and noise components existing in optical fiber communication systems.

Thus, for MMT evaluation the thesis has considered as highlighted in *chapter 1*, two major approaches: analytical evaluation model and numerical investigation model.

3.4.1 Analytical Evaluation Model

Since, MMT is proposed as a novel power efficient transmission format for high speed short range optical networks. Hence, it is the interest of the thesis to provide an efficient benchmark assessment method for evaluating the power efficiency of MMT compared with other similar multilevel modulation formats i.e M-PAM. The analytical evaluation is based upon the signal space analysis presented in (section 3.2) and the optimal detection receiver presented in (section 3.3.3.2).

Although, the MMT analytical evaluation criterion has been discussed in details in *chapter 4*, however, it can be summarized in the main following assessment approaches:-

- ✓ Bit Error Rate (BER) model to calculate the N-channel MMT BER with respect to the received optical power and comparing it with M-PAM; in order to assess the receiver optical sensitivity for both formats.
- ✓ Asymptotic power efficiency evaluation based upon signal space analysis in order to assess the power penalties of MMT and M-PAM transmission formats relative to OOK, at fixed bit rate and fixed baud rate. This evaluation criterion is an elegant validation methodology for MMT derived BER model.
- ✓ Investigation for the N-channel MMT performance characteristics at different noise levels in the presence of the dominant sources of noise for short-haul optical transmission applications.

- ✓ Comparison between N-channel MMT and M-PAM with respect to power penalty, spectral efficiency and receiver sensitivity at an aggregated bit rates of 10G, 40G and 100Gb/s.

3.4.2 Numerical Evaluation Model

MMT is designed for deployment not only for short-haul optical links, but also as a potential practical format for metropolitan area networks for application related, but not limited to, data center to data center metro links, Metro-Ethernet, enterprise/campus Ethernet links etc.. Hence, it is the interest of the thesis to expand the analysis by investigation of the performance of MMT in the presence of pre-amplified receiver noise model.

This investigation comprises a consideration of numerous number of characteristics for both, the electrical and optical system components (i.e, modulators, filters, amplifiers, fibers, receivers, etc..) combined with fiber medium linear and non-linear impairments. The interaction of these components characteristics with each other and with medium impairments affect the overall system performance. Hence, an optimization for system design parameters is crucial for setting a design environment with certain specific boundaries in order to fulfill the system objectives.

As such mentioned reasons, numerical simulation analysis has been carried out for the design and testing of MMT system employing a hybrid co-simulation environment between MATLAB® (version 12.1) and OptiSystem® (version 12) [114], [160]. In this simulation analysis, we have been able to build, define and optimize our own MMT custom design, and measurement techniques using a numerical semi-analytical model.

3.4.2.1 Thesis Simulation Software

The significance of the employment for computer aided software has been recommended by top researchers and industry professionals in the optical communication field [89], [114]. *OptiSystem*® is a worldwide verified simulation software enabling the design, customization, testing of modulation formats over optical links[161]. The software has been validated through numerous comparisons between analytical, experimental and simulation works[160]. It comprises a wide variety of active and passive photonic and electrical components. Furthermore, the software leverages an interface for an integrated module between *OptiSystem*® and *MATLAB*® programming language. This feature has enabled us to evaluate the MMT format according to our developed unique BER model adequate with MMT structure via *MATLAB*®.

3.4.2.2 BER based upon threshold detection receiver

The BER computation is considered the key figure of merit evaluation metric in receiver systems[114], [162], [163]. The BER is dependent mainly upon the data transmission structure and the receiver detection methodology. In this section, a customized BER model based upon MMT *Threshold detection receiver* is developed.

Conventionally, Gaussian and chi-squared distributions are assumed to estimate the signaling formats Probability Density Functions (PDF). The Gaussian distribution has been extensively employed in BER estimation of multilevel data transmission formats utilizing threshold detection receiver[59], [60], [87], [138], [164], [165]. The MMT symbol BER can be estimated based upon the approximation of the probability density function (PDF) following the Gaussian distribution.

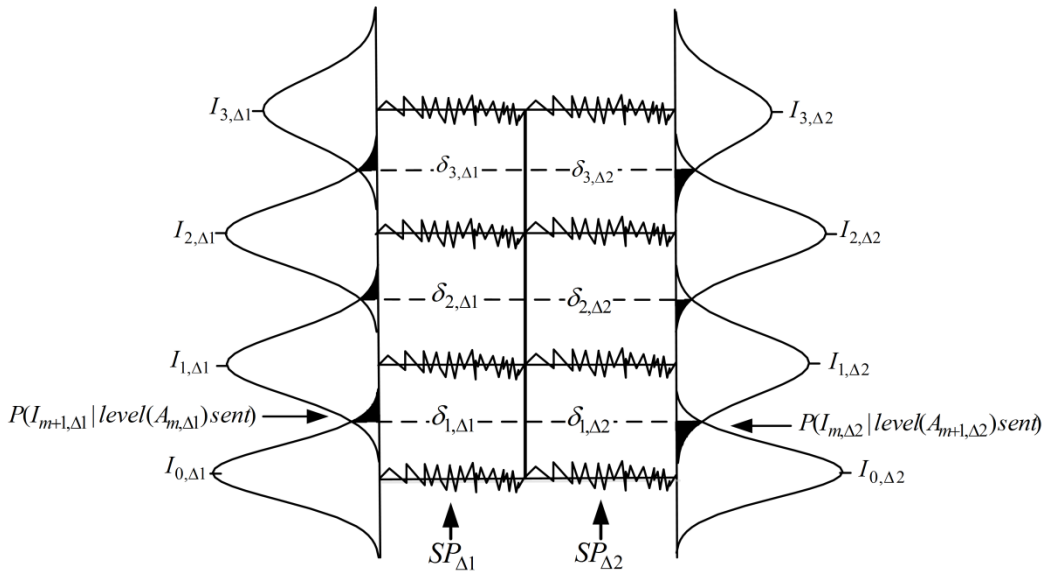

Figure 3.14 4-Channel MMT conditional Gaussian PDF.

Since the MMT symbol is composed of multiple levels, thus the bit error probability for a multilevel format is based upon the PDF of the upper and lower levels. This can be expressed as

$$BER = \sum_{m=0}^{M_{\Delta S}-1}\left(p(A_{m,\Delta1}).P(I_{m+1,\Delta1}\,|\,level\ (A_{m,\Delta1})\,sent) + p(A_{m+1,\Delta1}).P(I_{m,\Delta1}\,|\,level\ (A_{m+1,\Delta1})\,sent)\right) \tag{3.36}$$

where $p(A_{m,\Delta1}) = 1/2$ is the priori probability of transmitting level $A_{m,\Delta1}$, $P(I_{m+1,\Delta1}\,|\,level\ (A_{m,\Delta1})\,sent)$ is the probability of wrong decision of the received random variable $I_{m+1,\Delta1}$ while $A_{m,\Delta1}$ level have been sent.

Figure 3.14 shows the 4-channel MMT conditional Gaussian PDF. In the development of the BER formula, it is assumed that the receiver is comparing the sampled current or voltage to a reference threshold value δ for each eye. For 4-channel MMT, the BER can be computed for eye 1 as

$$BER_{1,\Delta S} = \frac{1}{2}\left(P(I_{0,\Delta S}\,|\,level\ (A_{1,\Delta S})\,sent) + P(I_{1,\Delta S}\,|\,level\ (A_{0,\Delta1})\,sent)\right) \tag{3.37}$$

which is equivalent to the PDF as

$$BER_{1,\Delta S} = \frac{1}{2}[\int_{-\infty}^{\delta_{1,\Delta s}} f_{I_1}(x_1)\,dx_1 + \int_{\delta_{1,\Delta s}}^{I_{1,\Delta S}} f_{I_0}(x_0)\,dx_0] \quad (3.38)$$

where $f_I(x)$ is the pdf of continuous random variable with Gaussian distribution and equivalent to

$$f_I(x) = \frac{1}{\sqrt{2\pi}\sigma_I} e^{-\frac{(x-I)^2}{2\sigma_I{}^2}} \quad (3.39)$$

, for the second eye equivalent BER can be expressed in a similar manner as

$$BER_{2,\Delta S} = \frac{1}{2}\left(P(I_{1,\Delta S} \mid level\ (A_{2,\Delta S})\ sent) + P(I_{2,\Delta S} \mid level\ (A_{1,\Delta S})\ sent)\right) \quad (3.40)$$

which is equivalent to the PDF as

$$BER_{2,\Delta S} = \frac{1}{2}[\int_{I_{1,\Delta S}}^{\delta_{1,\Delta s}} f_{I_2}(x_2)\,dx_2 + \int_{\delta_{1,\Delta s}}^{I_{2,\Delta S}} f_{I_1}(x_1)\,dx_1] \quad (3.41)$$

And for the third eye equivalent BER as

$$BER_{3,\Delta S} = \frac{1}{2}\left(P(I_{2,\Delta 1} \mid level\ (A_{3,\Delta 1})\ sent) + P(I_{3,\Delta 1} \mid level\ (A_{2,\Delta 1})\ sent)\right) \quad (3.42)$$

which is equivalent to the corresponding third level PDF as

$$BER_{3,\Delta S} = \frac{1}{2}[\int_{\delta_{3,\Delta s}}^{\infty} f_{I_2}(x_2)\,dx_2 + \int_{I_{2,\Delta S}}^{\delta_{3,\Delta s}} f_{I_1}(x_1)\,dx_1] \quad (3.43)$$

In the development of the BER formula, it is assumed that the receiver is comparing the sampled current or voltage to a reference threshold value δ for each eye. It is essential to define the optimal threshold δ for each eye. This can be deduced by assuming a Gaussian distribution and substituting in the relation

$$\frac{\delta_{m+1,\Delta S} - I_{m,\Delta S}}{\sigma_{m,\Delta S}} = \frac{I_{m+1,\Delta S} - \delta_{m+1,\Delta S}}{\sigma_{m+1,\Delta S}} \tag{3.44}$$

where $m \in \{0,1,2,.....,M_{\Delta S} - 1\}$. Therefore, the threshold value can be expressed as

$$\delta_{m+1,\Delta S} = \frac{I_{m,\Delta S}\,\sigma_{m+1,\Delta S} + I_{m+1,\Delta S}\,\sigma_{m,\Delta S}}{\sigma_{m,\Delta S} + \sigma_{m+1,\Delta S}} \tag{3.45}$$

The threshold levels have been optimized by signal processing for equal spacing between amplitude levels.

The overall BER per slot can be expressed as

$$BER_{\Delta S} = \frac{1}{4}[Q(\frac{I_{1,\Delta S} - I_{0,\Delta S}}{\sigma_{0,\Delta S} + \sigma_{1,\Delta S}}) + Q(\frac{I_{2,\Delta S} - I_{1,\Delta S}}{\sigma_{1,\Delta S} + \sigma_{2,\Delta S}}) + Q(\frac{I_{3,\Delta S} - I_{2,\Delta S}}{\sigma_{2,\Delta S} + \sigma_{3,\Delta S}})] \tag{3.46}$$

where Q-factor can be defined as

$$Q(y) = \frac{1}{\sqrt{2\pi}} \int_{y}^{\infty} e^{-x^2}\, dx \tag{3.47}$$

The MMT overall symbol BER can be expressed in terms of the average of the two slot BER as

$$BER_{N-channel} = \frac{1}{S} \sum_{i=1}^{\Delta S} BER_{\Delta i} \tag{3.48}$$

where *S* denotes the number of slots.

3.4.2.3 BER based on Eye Diagram Q-factor

Q-factor evaluation is considered as a fast and accurate method of choice for evaluation of system BER performance[110], [166]–[170]. The Q-factor has been standardized in accordance with ITU-TG.976 and OFSTP-9 TIA/EIA-526-9[171]–[174]. The BER can be calculated based upon the eye diagram Q-factor by analyzing the mean μ and the noise standard deviation σ as shown in figure 3.15. The accumulated noise can be analyzed analytically with the eye opening in the waveform by

$$Q_{eye} = \frac{\left|\mu_{A_m,\Delta S} + \mu_{A_{m+1},\Delta S}\right|}{\sigma_{A_m,\Delta S} + \sigma_{A_{m+1},\Delta S}} \tag{3.49}$$

where $\mu_{A_m,\Delta S}$ is the mean value of level A_m for slot ΔS in the eye diagram and $\sigma_{A_m,\Delta S}$ is the noise standard deviation at the sampling time $SP_{\Delta S}$ for level A_m and slot ΔS, as shown in figure 3.15. In Q-factor measurement, the threshold and sampling point are chosen on the basis maximizing the Q-factor. The Gaussian approximation for the received signal after the photodetector, is considered the most widely employed technique since it attain an accurate approximated results compared with experimental ones[175], [176].

Using this technique for eye diagram evaluation, a BER relation with Q-factor can be employed[117]. The BER can be expressed as

$$BER_{eye} = \frac{1}{2} erfc\left(\frac{Q_{eye}}{\sqrt{2}}\right) \tag{3.50}$$

where *erfc* is the complementary error function, defined as

$$erfc(x) = \frac{2}{\sqrt{\pi}} \int_{x}^{\infty} e^{-t^2}\, dt \tag{3.51}$$

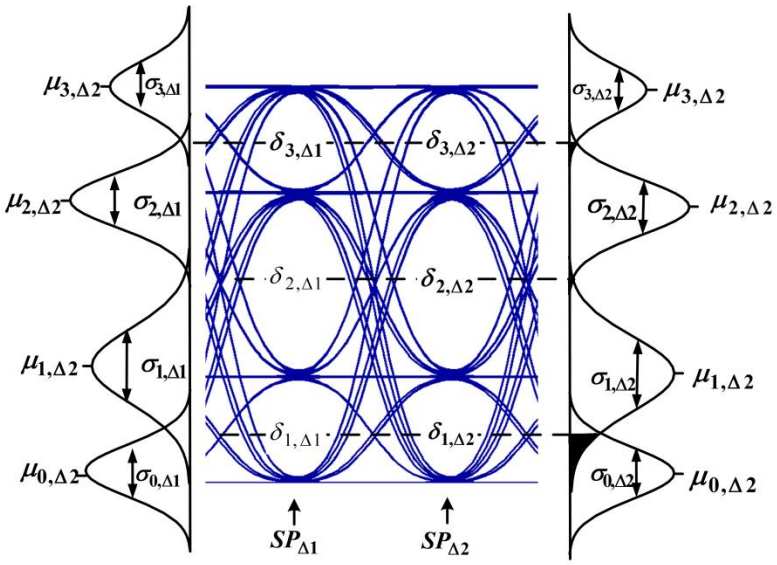

Figure 3.15 4-channel MMT Eye diagram with Probability Density Functions (PDF).

3.4.2.4 Receiver Sensitivity

Receiver sensitivity is considered a widely standardized approach for BER quantification and system performance assessment for numerical and experimental works[55], [177], [178]. The receiver sensitivity is calculated at an acceptable BER value in a back-to-back system configuration. The sensitivity is based upon measuring the minimum required received optical power to the receiver in order to acquire a certain BER performance. The receiver sensitivity is dependent upon many of transmission system characteristics and component settings (i.e amplifier gain, extinction ratio, modulator type, filter bandwidth…etc.). Accordingly, the optimization of component characteristics and system settings is required. As for metro networks, a BER value $=10^{-9}$ is considered a standardized acceptable BER for reliable data system transmission, while for short haul optical networks, a BER value $=10^{-12}$ is considered[110].

3.4 Concluding Remarks

The methodology behind the development of N-channel MMT format structure has been presented and discussed. Accordingly, the MMT structural design has considered dividing its symbol duration into two slots with a variable number of levels per slot which is dependent upon the input channel count. As such, N-channel MMT has considered the impactful trade-off between system parameters to satisfy the requirement and offer a solution to the thesis problem statement in realizing a high capacity transmission format accompanied by a reduced power budget.

A benchmark classical procedure for defining novel modulation formats with respect to a signal space model has been performed. The N-channel MMT signal space analysis has included a definition for its orthonormal basis function. Then, a derivation for the N-channel MMT symbols with respect to its basis function has been derived. Afterwards, a construction diagram for N-channel signal space constellation was shown.

In addition to the signal space analysis, a development of the rules and theory governing the transmission and reception of N-channel MMT signaling format, have been addressed. Two receiver detection methodologies have been proposed for the detection and recovery of MMT transmission format. The first is based upon threshold detection, while the second is based upon optimal detection.

Finally, the criteria for the performance evaluation of N-channel MMT has been presented. Two performance approaches are employed to investigate and analyze the performance of N-channel MMT; the first is analytical evaluation, while, the second is numerical evaluation.

4. Analytical Performance Evaluation

4.1 Power Performance Metrics

In order to assess the performance of MMT power efficiency, the average electrical power and optical power expressions are developed. These metrics will be the framework for assessing N-channel MMT compared with other IM/DD transmission formats. The average electrical and optical power, are derived based upon the basis functions and the constellation geometry in the electrical and optical domain following [58], [82], [179].

4.1.1 Electrical Domain

The first evaluation metric is the average electrical power which is defined as

$$P_{elect} = \lim_{T\to\infty} \frac{1}{2T} \int_{-T}^{T} X_k{}^2(t)\ dt \tag{4.1}$$

which, can be simplified to

$$P_{elect} = \frac{E_{avg,e}}{T_s} \tag{4.2}$$

where T_s is the total signal duration, $E_{avg,e}$ is the average electrical energy per signal constellation in the electrical domain and equivalent to

$$E_{avg,e} = \frac{1}{K} \sum_{k=1}^{K} \| X_k \|^2 \tag{4.3}$$

For MMT, the energy in signal $x_{k,\Delta S}(t)$ can be expressed by

$$E_e = \|X_k\|^2 = \left\|{x_{k,\Delta S}}^2\right\| + \left\|{x_{k,\Delta S}}^2\right\|) \\ = \frac{T_{sym}}{2}({A_{m,\Delta 1}}^2 + {A_{m,\Delta 2}}^2) \tag{4.4}$$

,the average electrical energy for $x_{k,\Delta S}$ per slot ΔS can be expressed by

$$E_{avg,e_{\Delta S}} = \frac{T_{sym}}{4M_{\Delta S}} \sum_{i=0}^{M_{\Delta S}-1} {A^2}_{i,\Delta S} \\ = \frac{T_{sym}}{24}(M_{\Delta S}-1)(2M_{\Delta S}-1) \tag{4.5}$$

where $M_{\Delta S}$, ($M_{\Delta S} = \{2^1, 2^2, ..., 2^{\ell_{\Delta S}}\}$) represents the number of levels per slot. While, the total average electrical energy per MMT symbol will be

$$E_{avg,e} = \frac{T_{sym}}{2M_{\Delta 1}M_{\Delta 2}} \sum_{i=0}^{M_{\Delta 1}-1} \sum_{j=0}^{M_{\Delta 2}-1} ({A^2}_{i,\Delta 1} + {A^2}_{j,\Delta 2}) \\ = \frac{T_{sym}}{12}[(M_{\Delta 1}-1)(2M_{\Delta 1}-1) + (M_{\Delta 2}-1)(2M_{\Delta 2}-1)] \tag{4.6}$$

for an equivalent number of levels per slot where ($M_{\Delta 1} = M_{\Delta 2} = M_{\Delta}$), $E_{avg,e}$ is

$$E_{avg,e} = \frac{T_{sym}}{6}(M_{\Delta}-1)(2M_{\Delta}-1) \tag{4.7}$$

4.1.2 Optical Domain

The second evaluation metric is the average optical power, which is defined as

$$P_{avg,o} = \lim_{T\to\infty} \frac{\nu}{2T} \int_{-T}^{T} x_k(t)\ dt \tag{4.8}$$

where ν is the electro-optic conversion factor in watts/Ampere, and $P_{avg,o}$ can be simplified to

$$P_{avg,o} = \frac{E_{avg,o}}{\sqrt{T_s}} \tag{4.9}$$

where $E_{avg,o}$ is the average optical energy per signal constellation in the optical domain and $\nu = 1$ has been assumed where the average optical energy per signal can be simplified to

$$E_o = \frac{1}{K} \sum_{k=1}^{K} \| x_k \| \tag{4.10}$$

In a similar manner as the energy electrical domain, the average optical energy per slot ΔS for $x_{k,\Delta S}$ can be expressed by

$$E_{avg,o_{\Delta S}} = \frac{\sqrt{T_{sym}}}{2\sqrt{2}M_{\Delta S}} \sum_{i=0}^{M_{\Delta S}-1} A_{i,\Delta S} \tag{4.11}$$

while the total average optical energy per MMT symbol will be

$$\begin{aligned} E_{avg,o} &= \frac{\sqrt{T_{sym}}}{\sqrt{2}M_{\Delta 1}M_{\Delta 2}} \sum_{i=0}^{M_{\Delta 1}-1} \sum_{j=0}^{M_{\Delta 2}-1} (A_{i,\Delta 1} + A_{j,\Delta 2}) \\ &= \frac{\sqrt{T_{sym}}}{2\sqrt{2}} [(M_{\Delta 1} - 1) + (M_{\Delta 2} - 1)] \end{aligned} \tag{4.12}$$

This parameter includes the D.C bias which satisfies the non-negativity constraint highlighted earlier and discussed in [53], [58], [73], [82].

4.2 Performance Analysis Utilizing Direct Modulation

4.2.1 Bit Error Rate Analytical Model

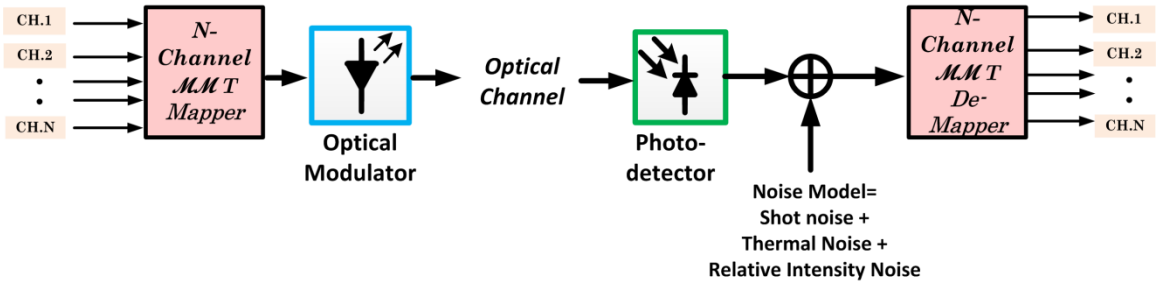

(a) MMT transceiver

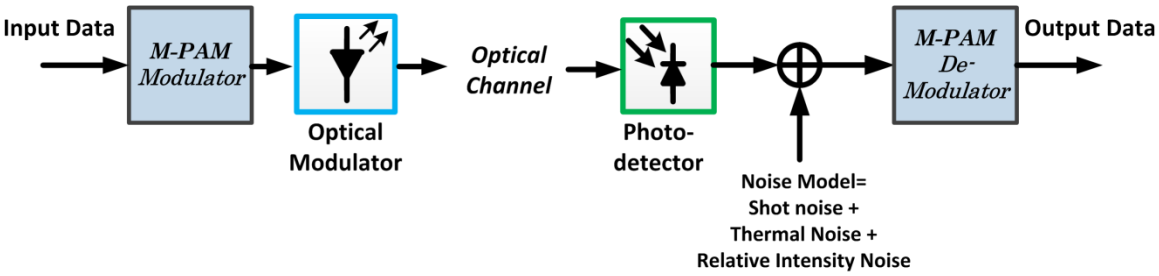

(b) PAM transceiver

Figure 4.1 system model for direct modulation light-wave system. (a) MMT transceiver, (b) PAM transceiver.

IM/DD systems for short-haul high speed optical transceivers can employ both Directly Modulated Laser (DML) and Externally Modulated Laser (EML). However, the state of the art for short range links prefer DML, due to its cost effectiveness and low power consumption, besides being applicable for integration in CMOS chips with limited non linearity[12], [42], [50], [59], [97], [180], [181].

Hence, the thesis considers the direct modulation noise model for our MMT and M-PAM BER comparison. Figure 4.1 shows the lightwave system model considered for MMT in figure 4.1(a) and M-PAM in figure 4.1(b) direct modulation noise model.

The development of an explicit BER expression for the N-channel MMT transmission formats in terms of the receiver optical power is essential [50], [59], [86], [90], [96]. The generic SER can be expressed as

$$SER = \sum_{x=0}^{M-1} P_m \, P_{y|x} \tag{4.13}$$

where P_m is the priori probability of the transmission of symbols, $P_{y|x}$ is the probability of receiving a symbol y given that symbol x is transmitted and can be expressed as

$$P_{y|x} == \frac{1}{2} \sum_{j=0}^{M-1} erfc\left(\frac{\left| I_{th,j} - I_i \right|}{\sqrt{2}\,\sigma_i} \right) \tag{4.14}$$

where M denotes number of levels I_i is the current associated with the optical electric field transmission on the PIN photodiode at symbol i; $I_{th,j}$ is the threshold current and σ_i is the root mean square of the noise variance current for a symbol i.

The BER formula is dependent upon the type of mapping the binary bit cluster to the symbols, where Gray mapping has an expected slightly improved performance compared with natural mapping[182]–[184]. This is because of less number of bit transitions per symbol. The mapping type is influenced by the average hamming distance, which corresponds to a BER expression variation. Assuming the thermal noise as the dominant noise source, the BER for N-channel MMT can be expressed as:

$$BER_{MMT} \cong \frac{d_H}{\log_2(M_{\Delta 1}.M_{\Delta 2})} \left(\frac{M_{\Delta 1} - 1}{M_{\Delta 1}} + \frac{M_{\Delta 2} - 1}{M_{\Delta 2}} \right) erfc\left[\frac{I_{avg}}{\sigma} \left(\frac{1}{M_{\Delta 1} - 1} + \frac{1}{M_{\Delta 2} - 1} \right) \right] \tag{4.15}$$

where d_H is the average hamming distance, σ is the Root-Mean-Square (RMS) of the

current noise and I_{avg} is the average photodiode current and dependent upon the received optical power P_{opt} by $I_{avg} = R_r P_{opt}$ where R_r is the photodiode responsivity[155]. The average hamming distance for N-channel MMT can be estimated for N-channel MMT as

$$d_H = 2 - \frac{\log_2(M_{\Delta 1} M_{\Delta 2})}{M_{\Delta 1} M_{\Delta 2} - 1} \tag{4.16}$$

where for gray mapping, the average hamming distance d_H is equal to 1 .

Assuming directly modulated optical link, there are three fundamental noise components, shot noise σ_S, thermal noise σ_T and relative intensity noise σ_I. The total current variance noise σ_{TT}^2 can be expressed as

$$\sigma_{TT}^2 = \sigma_S + \sigma_T + \sigma_I \tag{4.17}$$

$$\sigma_{TT}^2 = 2q I_{avg} \Delta f + \frac{4 k_B T F_n \Delta f}{R_L} + I_{avg}^2 N_{RIN} \Delta f \tag{4.18}$$

where σ_S is the shot noise, σ_T is the thermal noise and σ_I is the relative intensity noise, q is the electron charge, Δf is the receiver spectral width, k_B is Boltzmann constant, T is the temperature (in Kelvin), R_L is the load resistance, F_n is the electrical amplifier noise figure and N_{RIN} is the relative intensity noise. For simplicity, the dark current has been neglected as its effect is much less than the detected photodiode current. Also, a set of values has been assumed where noise figure $F_n = 5\,dB$, Temperature $T = 298\,K$, Load resistance $R_L = 50\Omega$, Relative Intensity Noise $N_{RIN} = -155\,dB/Hz$ and photodiode responsivity $R_r = 0.8\,A/W$.

4.2.2 Bit Error Rate Results

In this section, the thesis present a fully analytical comparison between MMT and M-PAM for single wavelength transmission at aggregated bit rates of 10Gb/s, 40Gb/s and 100Gb/s. The investigation have been developed at these bit rates, since, there are a current ongoing groups working to standardize 40Gb/s and 100Gb/s Ethernet considering multilevel modulation format (M-PAM) for short range optical networks.

4.2.2.1 BER Comparison between 2-channel MMT and M-PAM at bit rates of 10Gb/s, 40Gb/s and 100Gb/s

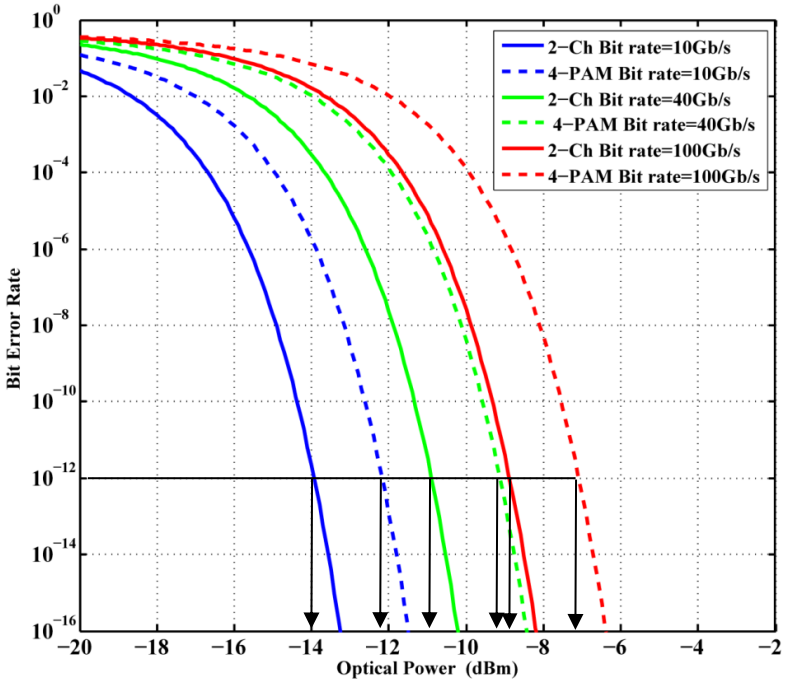

Figure 4.2 Optical sensitivity versus BER for 2-channel MMT and 4-PAM at 10Gb/s, 40Gb/s and 100Gb/s.

At information capacity of 2 bits/ symbol, figure 4.2 shows the optical sensitivity of 2-channel MMT and 4-PAM at fixed aggregated bit rate of 10Gb/s, 40Gb/s and 100Gb/s. At bit rate 10 Gb/s and BER=10^{-12}, 2-channel MMT has an optical sensitivity = –14 dBm and 4-PAM exhibit a sensitivity= –12.2 dBm. While, at bit rate 40 Gb/s and BER= 10^{-12}, 2-channel MMT and 4-PAM exhibit an optical sensitivity= –10.9 dBm and –9.1

dBm, respectively. Additionally, at the same BER=10^{-12} and bit rate 100Gb/s, 2-channel MMT and 4-PAM exhibit an optical sensitivity= –8.9 dBm and –7.1 dBm, respectively. The optical gain of 2-channel over 4-PAM is equivalent to 1.8 dB. This superiority of 2-channel MMT over 4-PAM can be justified by the power penalty that is induced due to the signal constellation of both formats and the inherent number of levels difference between 2-channel MMT and 4-PAM (as verified in *section 4.3*).

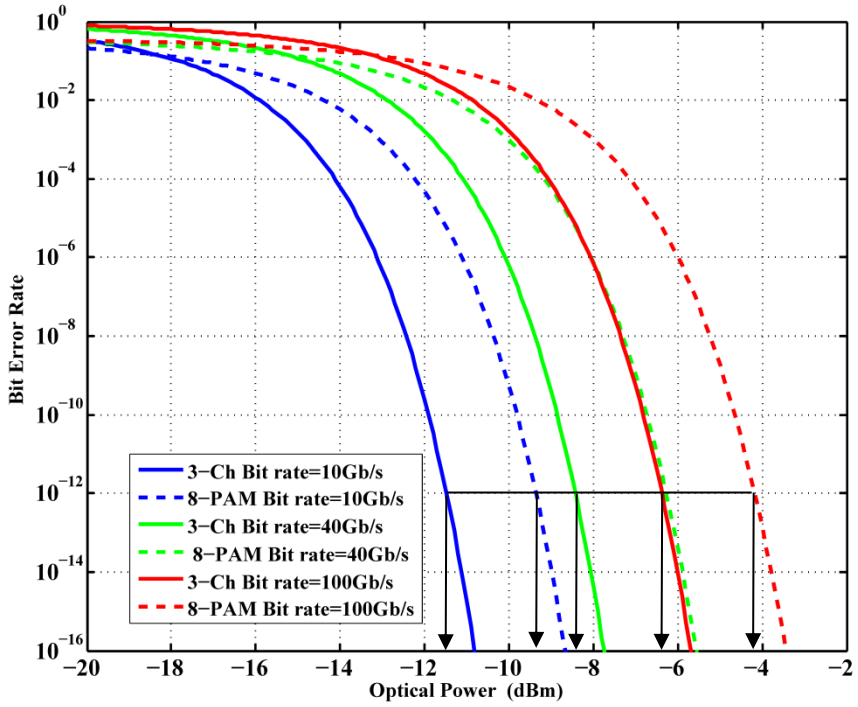

Figure 4.3 Optical sensitivity versus BER for 3-channel MMT and 4-PAM at 10Gb/s, 40Gb/s and 100Gb/s.

At information capacity= 3bits/Symbol, figure 4.3 shows the optical receiver sensitivity of 3-channel MMT and 8-PAM at fixed aggregated bit rate of 10Gb/s , 40Gb/s and 100Gb/s. At bit rate 10Gb/s and BER=10^{-12}, 3-channel MMT has an optical sensitivity $=-11.5\,dBm$ and 8-PAM exhibit a sensitivity $=-9.3\,dBm$. While, at bit rate 40Gb/s and BER=10^{-12}, 3-channel MMT and 8-PAM exhibit an optical sensitivity= –8.5 dBm and –6.3 dBm, respectively. Moreover, at BER=10^{-12} and bit rate 100Gb/s, 3-channel MMT and 8-PAM exhibit an optical sensitivity= –6.4 dBm and –4.2 dBm,

respectively. The optical penalty of 8-PAM over 3-channel is equivalent to approximately 2.2 dB. This is justified by the constellation size difference between 3-channel MMT with four amplitude levels spread among two slots and 8-PAM with eight amplitude levels exhibiting one slot.

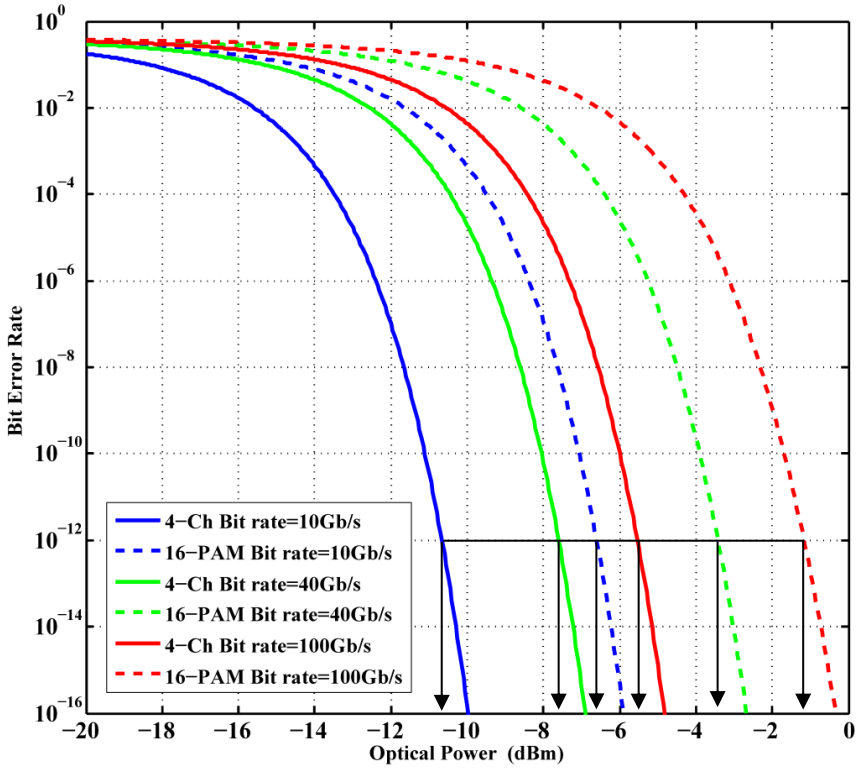

Figure 4.4 Optical sensitivity versus BER for 4-channel MMT and 4-PAM at 10Gb/s, 40Gb/s and 100Gb/s.

At information capacity= 4 bits/symbol, figure 4.4 denote the optical receiver sensitivity of 4-channel MMT and 16-PAM at fixed aggregated bit rate of 10 Gb/s , 40Gb/s and 100Gb/s. At bit rate 10Gb/s and BER=10^{-12}, 4-channel MMT has an optical sensitivity = –10.7 dBm and 16-PAM exhibit a sensitivity= –6.7 dBm. While, at bit rate 40Gb/s and BER=10^{-12}, 4-channel MMT and 16-PAM exhibit an optical sensitivity= –8.3 dBm and –4.3 dBm, respectively. Additionally, at the same BER=10^{-12} and bit rate 100 Gb/s, 4-channel MMT and 16-PAM exhibit an optical sensitivity= –5.5 dBm and –1.5 dBm, respectively. In the case of 4 bits/symbol, 4-channel outperforms 16-PAM by around 4 dB, which is mainly due to the double slot design advantage of MMT that leads to the reduction in the number of levels from sixteen in PAM to four in MMT.

4.2.2.2 Overall Comparison between N-channel MMT and M-PAM Relative to OOK

At asymptotically high SNR, the performance difference between various modulation formats approach constant values. Hence, a classical approach to assess novel transmission formats is to evaluate and compare between the performances of modulation formats with respect to On-Off Keying as a benchmark modulation format. On-Off keying have been employed as a platform for comparison with other modulation formats in [53], [60], [185]. By the development of an explicit BER expression for N-channel MMT derived in (4.15), a comparison between MMT and M-PAM with respect to common relative factor, represented by OOK format is a considered a significant persuasive evaluation metric [86].

At fixed Bitrate of 40 Gb/s, figure 4.5 shows the received optical power versus theoretical BER assessment for both N-channel MMT and M-PAM with respect to OOK. The M-PAM modulation formats have been analyzed following the M-PAM BER expression in [13]. The receivers spectral widths were set as Δf_{OOK}=40 GHz $\Delta f_{2-ch.MMT}$=40 GHz, $\Delta f_{3-ch.MMT}$=26.6 GHz , $\Delta f_{4-ch.MMT}$=20 GHz, Δf_{4-PAM}=20 GHz , Δf_{8-PAM} =13.3 GHz, Δf_{16-PAM}=10 GHz for OOK, 2-channel MMT, 3-channel MMT, 4-channel MMT, 4-PAM, 8-PAM, 16-PAM, respectively.

At BER of 10^{-12}, the received optical powers sensitivities are –10.9 dBm, –9.1 dBm, –8.5 dBm, –6.3 dBm , –8.3 dBm and –4.3 dBm for 2-channel MMT, 4-PAM, 3-channel MMT, 8-PAM, 4-channel MMT and 16-PAM, respectively.

Therefore the optical power penalty relative to OOK are, 1.55 dB, 3.3 dB, 3.85 dB, 6.05 dB, 4.85 dB and 8.85 dB for 2-channel MMT, 4-PAM, 3-channel MMT, 8-PAM, 4-channel MMT and 16-PAM, respectively. These results are verified by our asymptotic power efficiency results discussed in section 4.3.

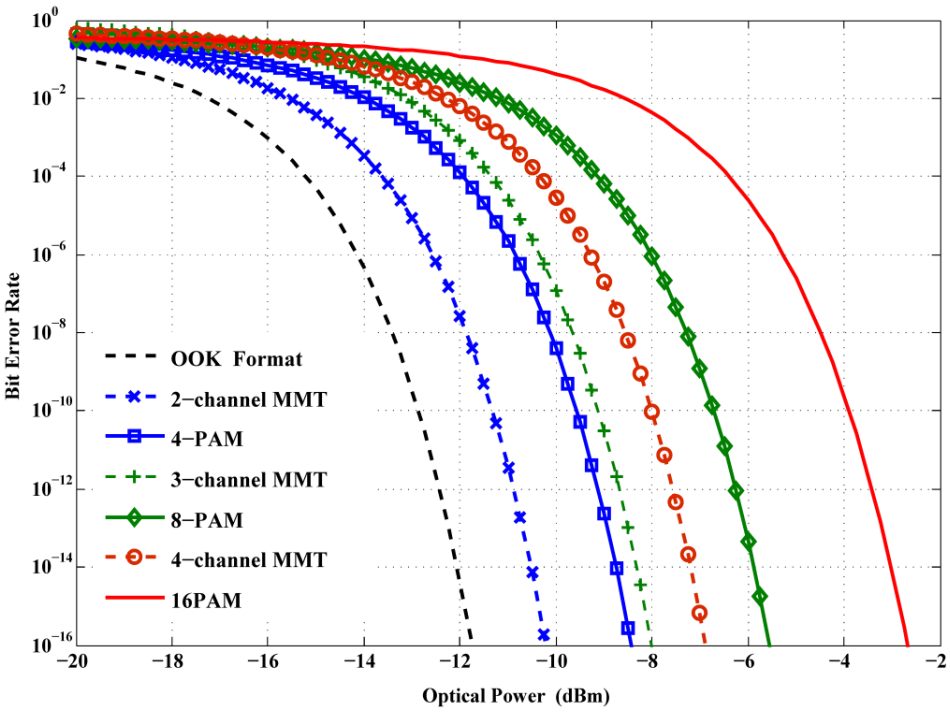

Figure 4.5 Theoretical optical receiver sensitivities of N-channel MMT, M-PAM and OOK transmission formats..

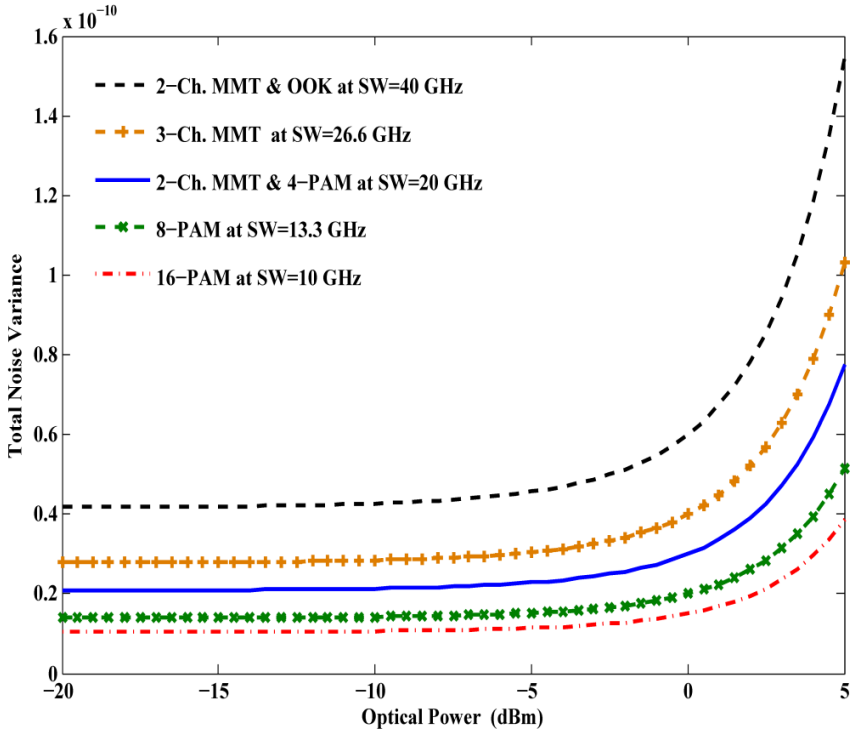

Figure 4.6 Total noise variance in [A^2] versus the received optical power at various spectral width.

The impact of noise on MMT and M-PAM modulation formats with respect to a varied optical power at a fixed aggregated bit rate of 40Gb/s is explored. Figure 4.6 shows the effect of varying the spectral width and optical power on the total noise variance for N-Channel MMT and M-PAM transmission format. An optimal equidistant MMT and M-PAM signals have been assumed as shown in figures 3.4 and 3.5 in order to yield an optimal performance difference.

For information capacity= 2 bits/symbol, the power gain advantage of 2-channel MMT symbol over 4-PAM is equivalent to 1.75 dB. Moreover, 3-channel MMT outperforms 8-PAM (with 8-levels) by 2.2 dB. On the other hand, for information capacity of 4 bits/symbol, 4-channel MMT need 4 dB less power requirement when compared with 16-PAM, that's beside the non-linear effects of increasing the number of levels to sixteen[30].

4.2.3 Noise Model Analysis

In this section, the effect of various levels of channel noise on N-channel MMT and M-PAM are investigated.

4.2.3.1 Thermal Noise

At a finite temperature, the random motion of electrons at the receiver circuitry side leads to the generation of the thermal noise[117]. Thermal noise can be represented as a fluctuating current, which is added to the photodiode receiver produced current. There are two main factors controlling the thermal noise. Although, a high receiver load resistance R_L needed to be employed in order to minimize the thermal noise, however, the photodiode bandwidth is inversely proportional to the load resistance [110], [178]. Hence, a trade-off compromise need to be considered for such relation. In optical communication, a front-end preamplifier component is necessary to be attached in a combined package with the photodiode receiver. In silicon photonic optical interconnects, a Trans-Impedance Amplifier (TIA) is employed where it is positioned after the photodetector in order to convert weak current signals produced by the low responsivity photodetectors to an appropriate voltage signal to drive subsequent blocks (in our case

the decision circuit)[186], [187]. Hence, the amplifier noise contribution is presented as the Noise Figure (NF) which influences the SNR and consequently the thermal noise. Thermal noise can be modeled as IId stationary Gaussian random process[110], [188].

Figure 4.7 shows the influence of various noise figure values on thermal noise variance at different receiver bandwidth range. At fixed $\Delta f = 10GHz$ and NF=3 dB, 4dB, 5dB and 6dB the thermal noise variance is equal to $6.5\,pA^2$, $8.2\,pA^2$, $10.4\,pA^2$ and $13.1\,pA^2$, respectively. Front end amplifier design specification can limit the impact of thermal noise at the input and output of the amplifier[117], [188], [189]. Moreover, it is clear that the noise variance is proportional to the frequency range. At low cutoff frequency range $\Delta f \le 10GHz$, the impact of increasing the frequency on the thermal noise is large. However, on receiver bandwidth $\Delta f > 10GHz$, the increase in thermal noise is much less than at low frequency range. Nowadays commercial receiver VCSEL components are available on market with cut of frequencies reaching 37GHz[50].

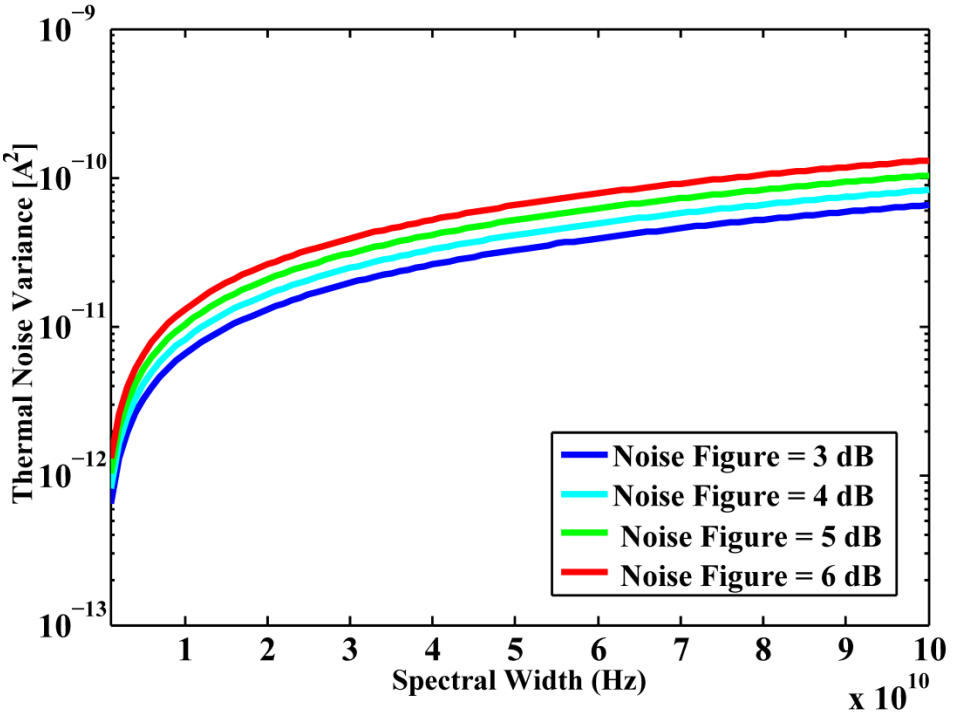

Figure 4.7 Thermal noise variance versus spectral width at different noise figure values.

4.2.3.2 Shot Noise

Shot noise is a natural process that occurs due to the random fluctuation distribution of electrons generated during the quantum photo-detection process[55], [89].

since for direct detection PIN receivers, shot noise is not the prevailing noise component, but the thermal noise. However, since shot noise scales linearly with the signal power, thus, optical sensitivity enhancement can play a role to keep low levels of shot noise [110].

It can be deduced from (4.18) that the amount of shot noise introduced to any modulation format is dependent linearly on both the spectral component and the received optical power to acquire a certain BER value. For the model discussed, the shot noise is not the dominant source of noise.

4.2.3.3 Effects of Relative Intensity Noise (RIN)

Relative intensity noise can be one of the major elements that degrade the system SNR[114], [190]. Although the RIN noise is associated with the transmitter source, however, the intensity fluctuations of the laser are transformed to the receiver in the form of electrical noise. Thus, thermal noise at the photodiode may not be the dominant noise source. High levels of random intensity fluctuation in the output of a laser may cause a higher RIN noise effect[55], [191], [192]. Relative intensity noise has a Gaussian response distribution with a noise variance dependent upon the laser optical power. Hence, increasing the emitted optical power to an extent may not lead to better BER system performance since the noise power at the receiver is increased likewise. Fiber optical communication designers take in to account the RIN element and be certain that its effect is limited to a pre-defined extent. Most link budget analysis carried out by IEEE standards industry groups, set a maximum penalty for the RIN noise factor[193].

Thus, investigation of BER floors at different optical power affected by various RIN noise values is essential.

Figure 4.8(a-c) depicts the effect of a series number of RIN noise levels range from -120 dB/Hz to -150 dB/Hz on 2-channel, 3-channel and 4-channel MMT BER at an

aggregate bit rate 40 Gb/s. The results show a non-linear relationship between the BER and the optical power that is dependent upon the component RIN noise. At low RIN noise level -150 dB/Hz, a low BER can be observed with the increase in the optical power. However, at high RIN noise component = -120 dB/Hz accompanied by an increase in the optical power, the curve results in an error floor where BER cannot exceed that level. Furthermore, it is clear that the number of MMT channels increase is inversely proportional to BER floor that can be attained. This is due to the number of levels increment, which leads to more impact of intersymbol interference, which leads to more BER floor.

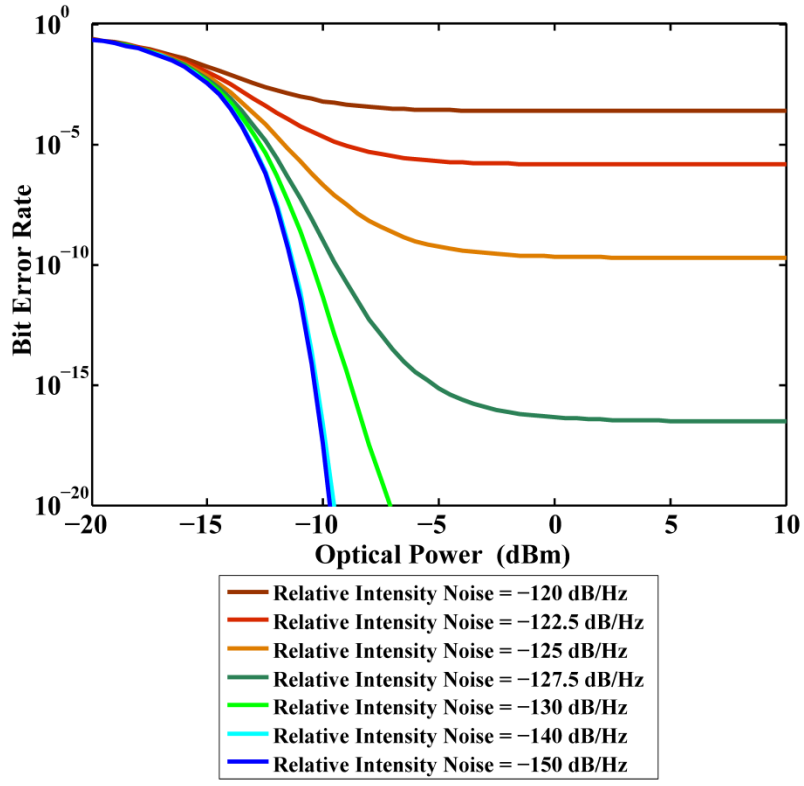

(a) 2-Channel MMT

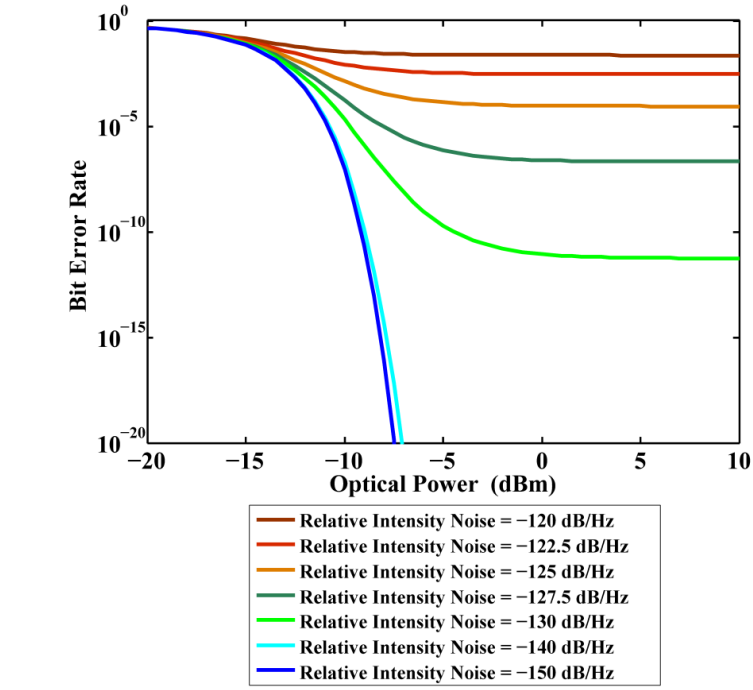

(b) 3-channel MMT

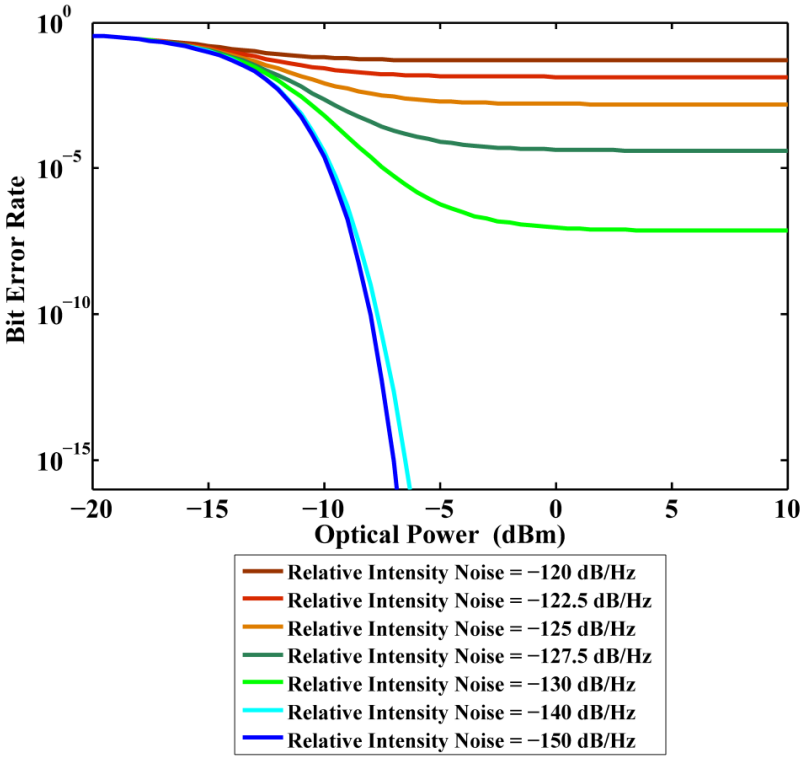

(c) 4-Channel MMT

Figure 4.8 The BER curves at various effects of RIN noise, (a) for 2-channel MMT, (b) for 3-channel MMT, and (c) for 4-channel MMT.

Figure 4.9(a-c) depicts the effect of the RIN noise levels on 4-PAM, 8-PAM and 16-PAM BER at the same aggregate bit rate 40 Gb/s. Comparing the results of N-channel MMT and M-PAM, the dependency of the number of amplitude levels on the BER floor is clear. For information capacity of 2 bits/symbol and -120dB/Hz , 2-channel MMT and 4-PAM show an approximately equivalent BER floor at $\cong 5\times10^{-4}$, while at relatively lower RIN noise level 2-channel MMT shows more robustness to noise compared to M-PAM whereas at -127.5 dB/Hz, the BER floor for 2-channel MMT and 4-PAM are $\cong 1\times10^{-17}$ and $\cong 5\times10^{-15}$, respectively.

At information capacity= 3 bits/symbol and127.5 dB/Hz, 8-PAM are more influenced by RIN noise compared with 3-channel MMT, where the BER floors are $\cong 5\times10^{-7}$ and $\cong 1\times10^{-5}$ for 3-channel MMT and 8-PAM, respectively.

At information capacity= 4 bits/symbol and 127.5 dB/Hz, as shown in figure 4.8(c), 4-channel MMT has a BER floor $\cong 5\times10^{-5}$ where the 16-PAM has a BER floor of $\cong 1\times10^{-2}$. It is worth to note that even at relatively lower RIN noise components, N-Channel MMT shows more tolerance to RIN noise and acquires better BER floor in contrast to M-PAM transmission format at the same aggregate bit rate.

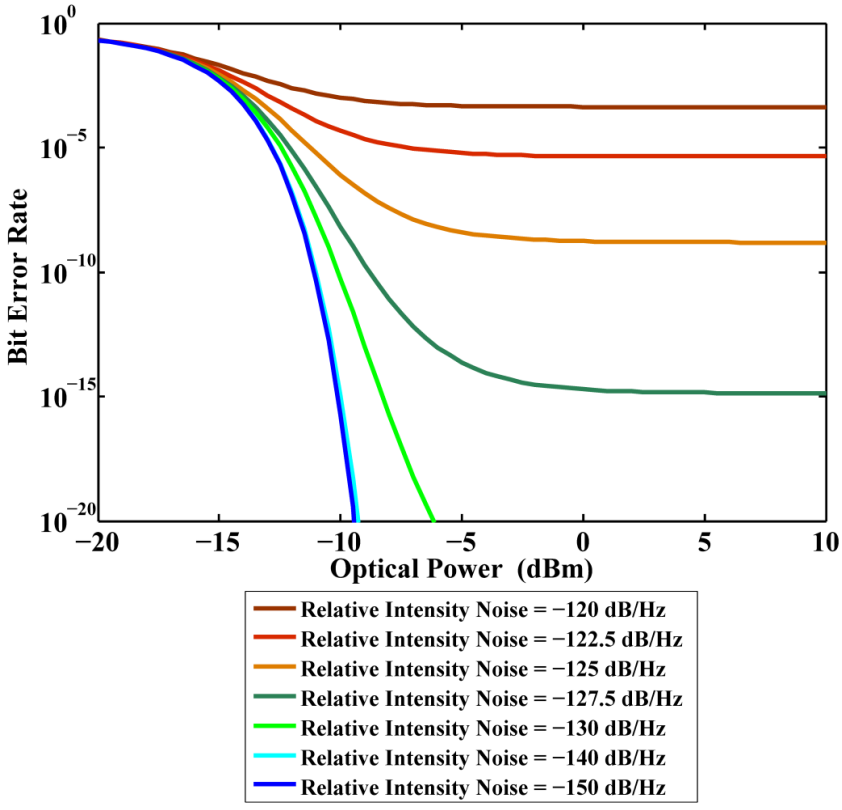
Bit Error Rate
Optical Power (dBm)
Relative Intensity Noise = −120 dB/Hz
Relative Intensity Noise = −122.5 dB/Hz
Relative Intensity Noise = −125 dB/Hz
Relative Intensity Noise = −127.5 dB/Hz
Relative Intensity Noise = −130 dB/Hz
Relative Intensity Noise = −140 dB/Hz
Relative Intensity Noise = −150 dB/Hz

(a) 4-PAM

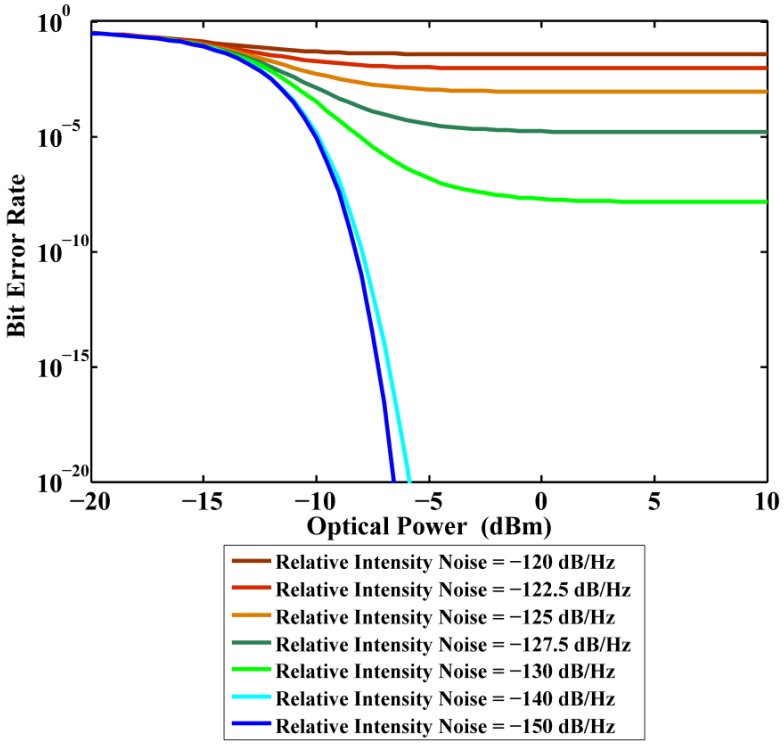
Bit Error Rate
Optical Power (dBm)
Relative Intensity Noise = −120 dB/Hz
Relative Intensity Noise = −122.5 dB/Hz
Relative Intensity Noise = −125 dB/Hz
Relative Intensity Noise = −127.5 dB/Hz
Relative Intensity Noise = −130 dB/Hz
Relative Intensity Noise = −140 dB/Hz
Relative Intensity Noise = −150 dB/Hz

(b) 8-PAM

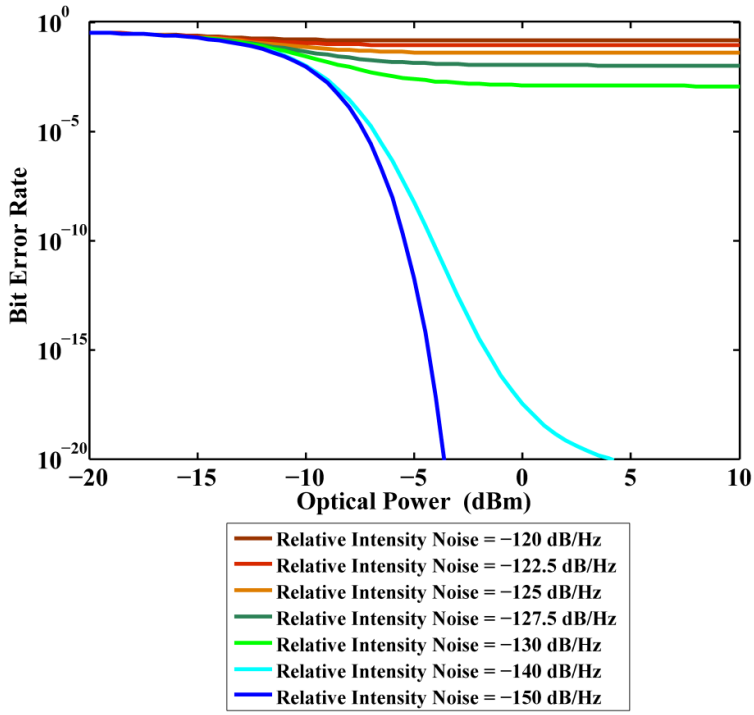

(c) 16-PAM

Figure 4.9 The BER curves at various effects of RIN noise, (a) for 4-PAM, (b) for 8-PAM and (c) for 16-PAM.

4.2.3.4 RIN Power penalty

Most link budget design analysis that are performed during setting of IEEE standards specify the maximum allowable penalty as a result of each noise component[41], [194]–[196]. The power penalty can be assessed based upon computation of the required optical power needed to attain a specific BER. For error free transmission BER of 1×10^{-12} is required. Hence, for clearer picture of the effects of RIN on M-PAM and N-channel MMT, power penalty as a function of RIN noise is explored.

At BER $=1\times10^{-12}$ and assuming a maximum allowable power penalty of 0.5 dB due to RIN, figure 4.10 (a-c) shows the N-channel MMT power penalty as a function of the RIN at various spectral width.

At spectral widths of 10 GHz, 20GHz, 30GHz and 50GHz which correspond to different bit rates, 2-channel MMT, shows a maximum acceptable RIN spectral density to be $\leq -133 dB/Hz$, $\leq -132 dB/Hz$, $\leq -130 dB/Hz$ and $\leq -127 dB/Hz$, respectively.

At spectral widths of 10 GHz, 20GHz, 30GHz and 50GHz, 3-channel MMT, shows a maximum acceptable RIN spectral density to be $\leq -140\,dB/Hz$, $\leq -138\,dB/Hz$, $\leq -136\,dB/Hz$ and $\leq -133\,dB/Hz$, respectively. While, at spectral width of 10 GHz, 20GHz, 30GHz and 50GHz, 3-channel MMT, shows a maximum acceptable RIN spectral density to be $\leq -143\,dB/Hz, \leq -141\,dB/Hz, \leq -139\,dB/Hz$ and $\leq -136.5\,dB/Hz$, respectively.

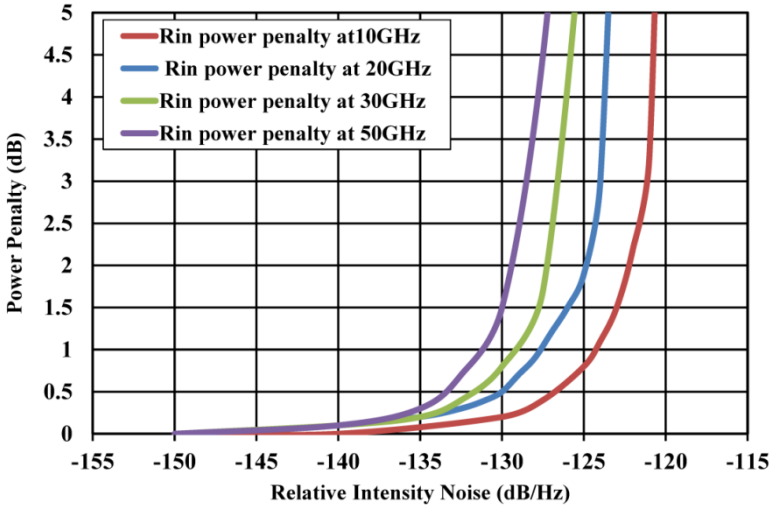

(a) 2-channel MMT

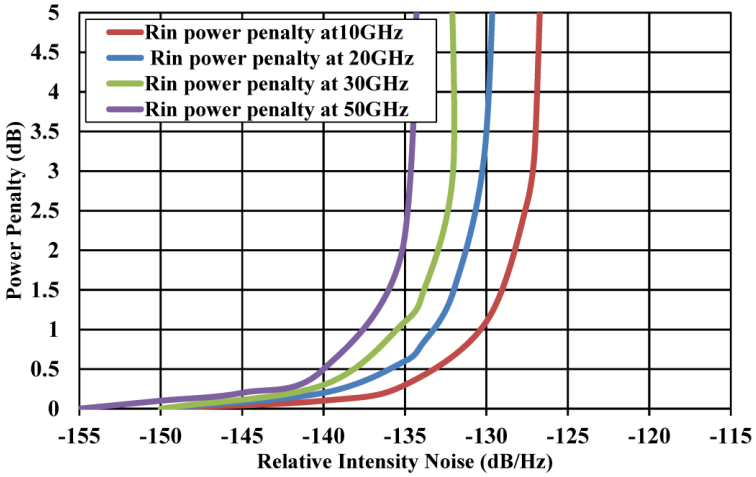

(b) 3-channel MMT

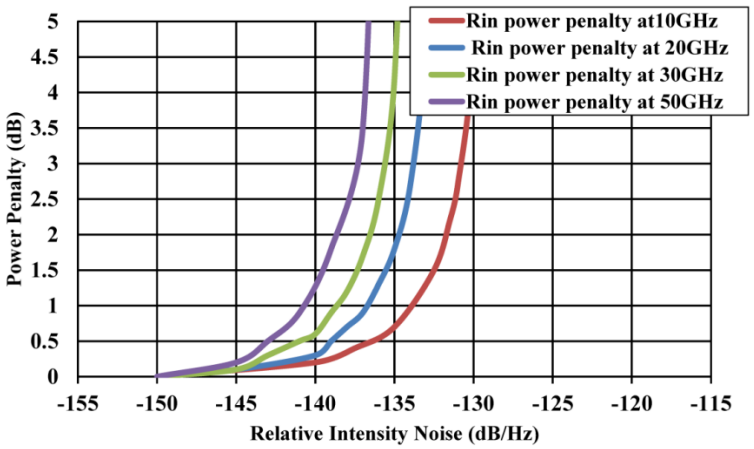

(c) 4-Channel MMT

Figure 4.10 N-channel MMT power penalty as a function of relative intensity noise at various spectral width.

At spectral widths of 10 GHz, 20GHz, 30GHz and 50GHz which correspond to different bit rates, 4-PAM, shows a maximum acceptable RIN spectral density to be $\leq -137 dB/Hz$, $\leq -134 dB/Hz$, $\leq -136 dB/Hz$ and $\leq -130 dB/Hz$, respectively. At spectral widths of 10 GHz, 20GHz, 30GHz and 50GHz, 8-PAM, shows a maximum acceptable RIN spectral density to be $\leq -145 dB/Hz$, $\leq -142.5 dB/Hz$, $\leq -140 dB/Hz$ and $\leq -137.5 dB/Hz$, respectively.

While, at spectral widths of 10 GHz, 20 GHz, 30 GHz and 50 GHz, 16-PAM, shows a maximum acceptable RIN spectral density to be $\leq -150 dB/Hz$, $\leq -147 dB/Hz$, $\leq -146 dB/Hz$ and $\leq -143 dB/Hz$, respectively.

To conclude, the maximum RIN for N-channel MMT and M-PAM have been specified. The calculation were based upon an allowable power penalty equivelant to 0.5 dB (according to IEEE standard) for varied spectral widths.

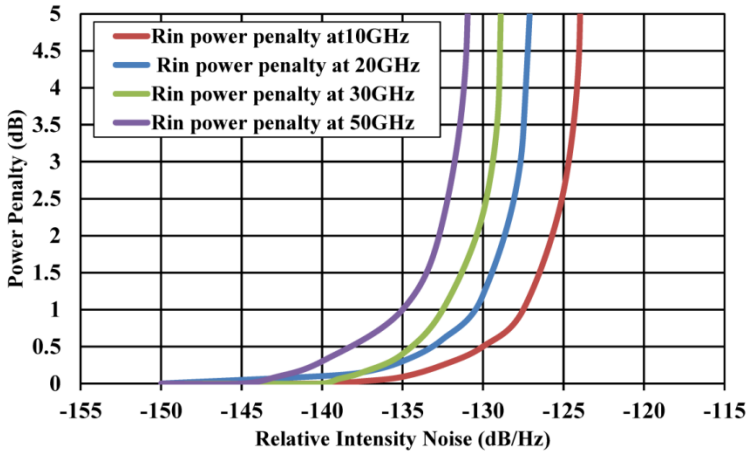

(a) 4-PAM

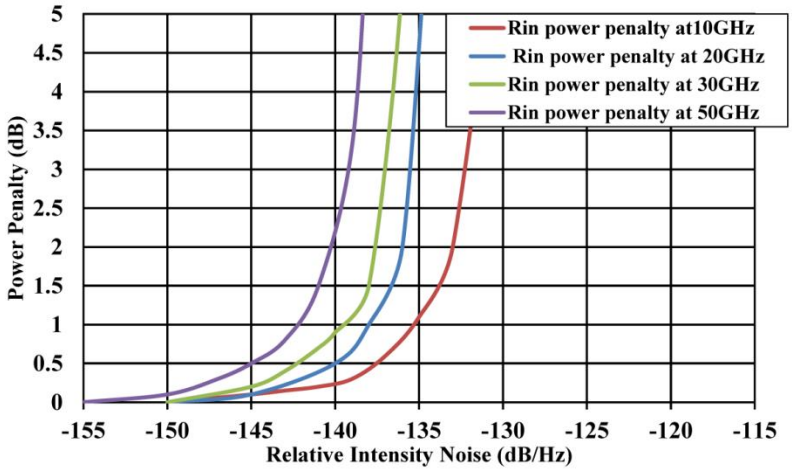

(b) 8-PAM

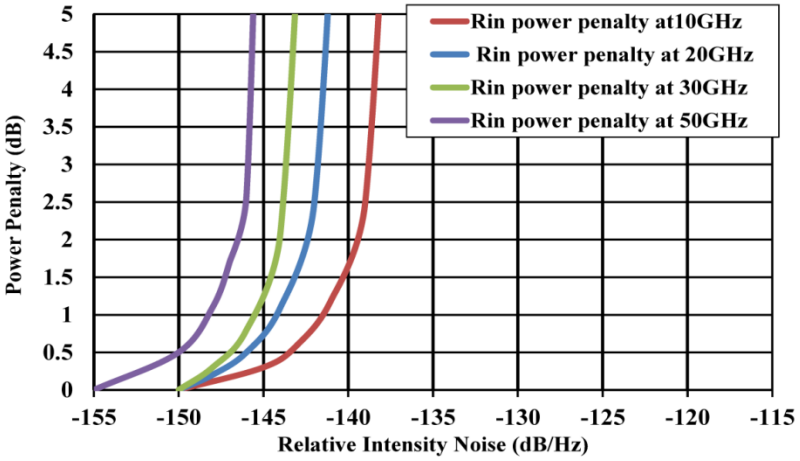

(b) 16-PAM

Figure 4.11 Power penalty of M-PAM as a function of relative intensity noise at various spectral.

4.3 Asymptotic Power Efficiency Analysis and Results

At asymptotically high SNR, the performance difference in dB between the different modulation formats approaches constant values .One classical approach to assess novel transmission formats, is to evaluate and compare between schemes with respect to OOK as a benchmark for power efficiency[53], [58], [60] .

4.3.1 Power Penalty at Fixed Baud Rate

For Intensity Modulated (IM) non-coherent transmission formats, the basic element for power penalty is directly related to the number of amplitude levels. Assuming stationary noise only with AWGN spectral density, at fixed baud rate, the M-PAM power penalty is equivalent to [165]

$$P_{p,PAM} = 10\,Log(M-1) \quad \text{[dB]} \tag{4.19}$$

A theoretical power penalty expression with respect to OOK has been derived for N-channel MMT modulation. At fixed baud rate, the N-Channel MMT optical power penalty with respect to OOK can be represented by

$$\begin{aligned} P_{p,MMT} &= 10Log\left(\frac{P_{avg,o_{MMT}}}{P_{avg,o_{OOK}}}\right) = \\ &= 10\,Log\left(\frac{(M_{\Delta 1}-1)+(M_{\Delta 2}-1)}{\sqrt{2}}\right) \end{aligned} \quad \text{[dB]} \tag{4.20}$$

Where $P_{avg,o_{OOK}}$, $P_{avg,o_{MMT}}$ are the average optical powers for OOK and MMT signaling, respectively. The MMT has been derived based upon signal constellation by substitution from (4.12) in (4.9).

Figure 4.12 shows the power penalty of M-PAM modulation format with respect to the number of levels at fixed baud rate. Relative to On Off Shift Keying (OOK), 4-PAM, 8-PAM, 16-PAM and 32-PAM depicts an inherent power penalties due to their number of levels augmentation, equivalent to $4.77\,dB$, $8.45\,dB$, $11.76\,dB$ and $14.91\,dB$, respectively.

Figure 4.13 shows the power penalty of N-Channel MMT with respect to the maximum number of levels over its two slots at fixed baud rate. Relative to OOK, 2-Channel 3-Channel, 4-Channel, 5-Channel and 6-Channel MMT has power penalties equivalent to $1.5dB$, $4.51dB$, $6.27\,dB$, $8.5dB$ and $14.91dB$, respectively.

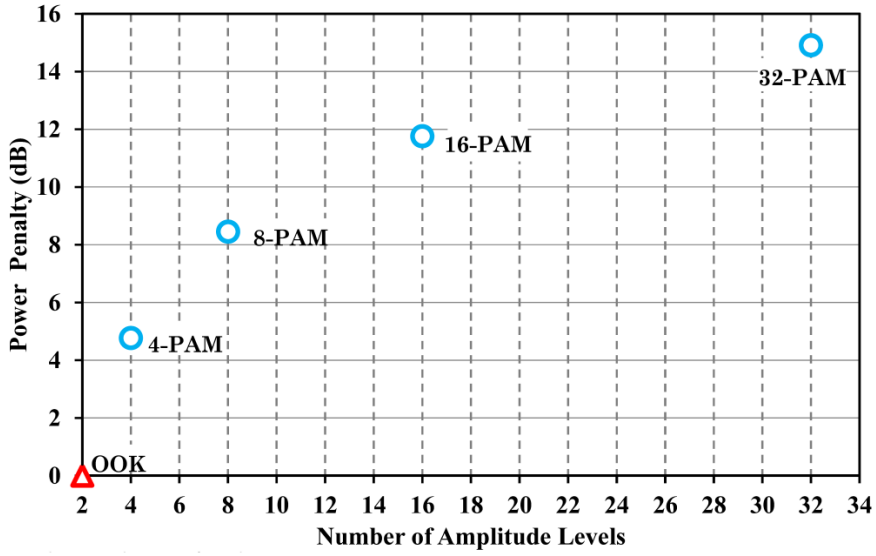

Figure 4.12 M-PAM power penalty with respect to number of amplitude levels at fixed baud rate.

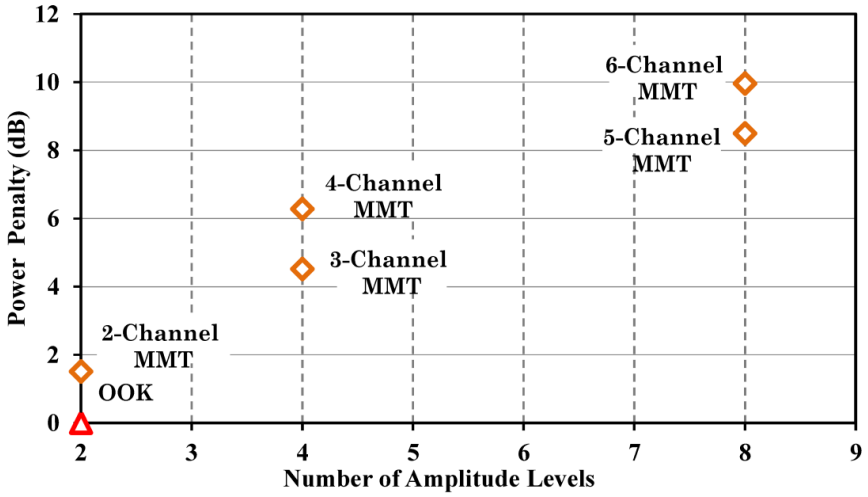

Figure 4.13 N-channel MMT power penalty with respect to the maximum number of amplitude levels of its two slots at fixed baud rate.

4.3.2 Power Penalty at Fixed Bit Rate

Assuming stationary noise only with AWGN spectral density, at fixed bit rate, the M-PAM power penalty is equivalent to

$$P_{pb,PAM} = 10\,Log\left(\frac{(M-1)}{\sqrt{\log_2 M}}\right) \quad \text{[dB]} \tag{4.21}$$

On the other side, at fixed bitrate an expression to calculate the theoretical inherent power penalty for N-channel MMT modulation format has been derived. At fixed bitrate, the N-Channel MMT optical power penalty with respect to OOK can be represented by

$$P_{pb,MMT} = 10\log\left[\sqrt{\frac{2}{\log_2(M_{\Delta 1}.M_{\Delta 2})}}\left(\frac{(M_{\Delta 1}-1)+(M_{\Delta 2}-1)}{\sqrt{2}}\right)\right] \quad \text{[dB]} \tag{4.22}$$

by taking into consideration the relative proportionality of the noise power to the noise voltage.

Figure 4.14 shows the power penalty of M-PAM modulation format with respect to the number of levels at fixed bitrate. Relative to on-off-shift-keying format, 4-PAM, 8-PAM, 16-PAM and 32-PAM have an inherent power penalties due to its number of levels augmentation which are equivalent to $3.26\,dB$, $6.06\,dB$, $8.75\,dB$ and $11.42\,dB$, respectively.

Figure 4.15 shows the power penalty of N-Channel MMT with respect to the maximum number of levels over its two slots at fixed bitrate. Relative to OOK, 2-Channel MMT, 3-Channel MMT, 4-Channel MMT, 5-Channel MMT and 6-Channel MMT exhibit power penalties equivalent to $1.5\,dB$, $3.6\,dB$, $4.77\,dB$, $4.47\ dB$ and $5.7\,dB$, respectively.

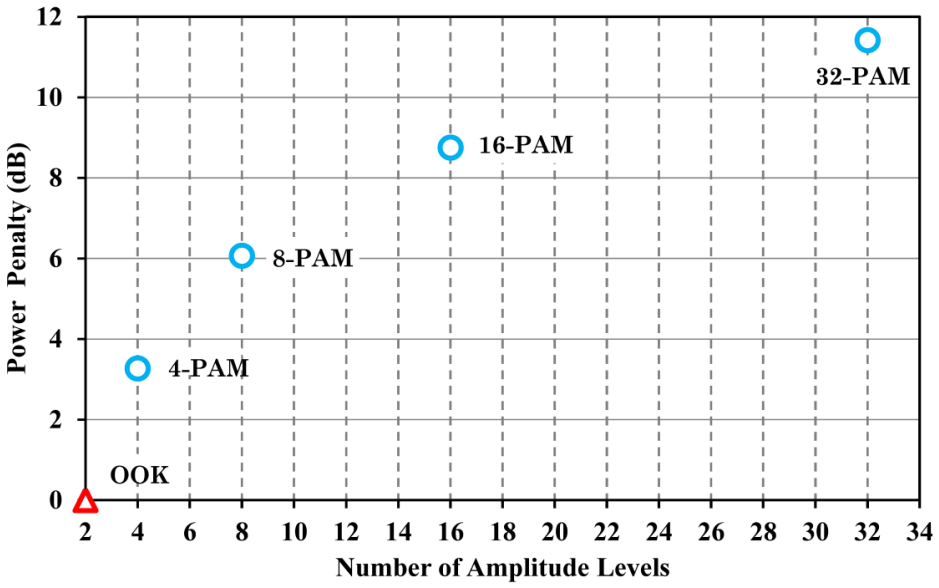

Figure 4.14 M-PAM power penalty with respect to number of amplitude levels at fixed bit rate.

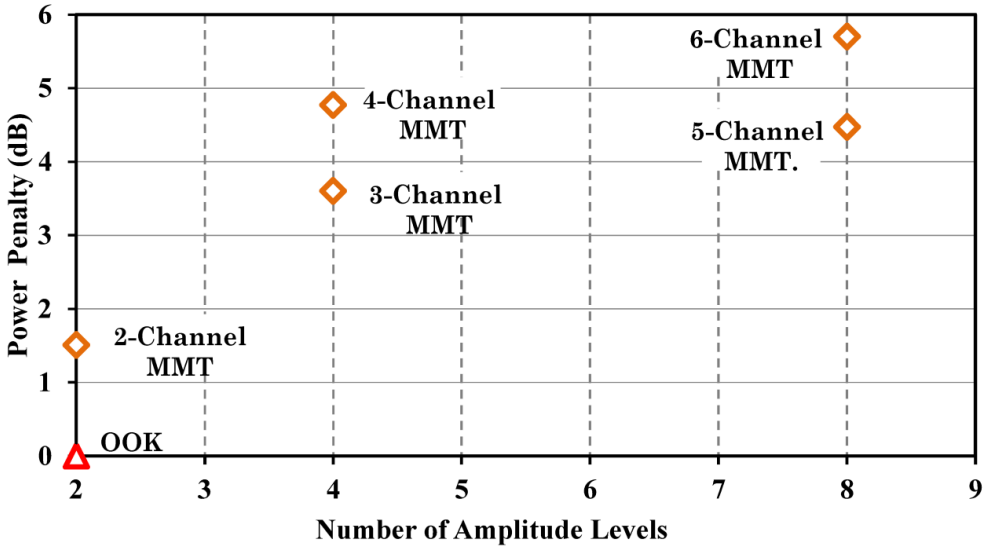

Figure 4.15 N-channel MMT power penalty with respect to the maximum number of amplitude levels of its two slots at fixed bit rate.

4.3.3 Power penalty with respect to OOK at Fixed information capacity

Since N-channel MMT is designed for a practical interest to expand the capacity of optical communication networks, thus, investigating the performance of N-Channel and M-PAM with respect to information capacity is essential. To calculate the differences in power efficiency with respect to the information capacity, the asymptotic power penalty relative to OOK, is provided.

At fixed bandwidth, figure 4.16 shows the asymptotic power penalty of N-Channel MMT and M-PAM modulation format relative to OOK to achieve an equivalent BER performance at asymptotically high SNR. For information capacity of 2 bits/symbol, 2-channel MMT has a power gain of 3.27 dB over 4-PAM compared to OOK at a fixed baud rate. For information capacity=3 bits/symbol, 8-PAM need 3.94 dB more required optical power compared to 3-channel MMT, both with respect to OOK. For information capacity=4 bits/symbol, 16-PAM has an optical power penalty of 5.5 dB worse than 4-channel MMT at the same BER performance.

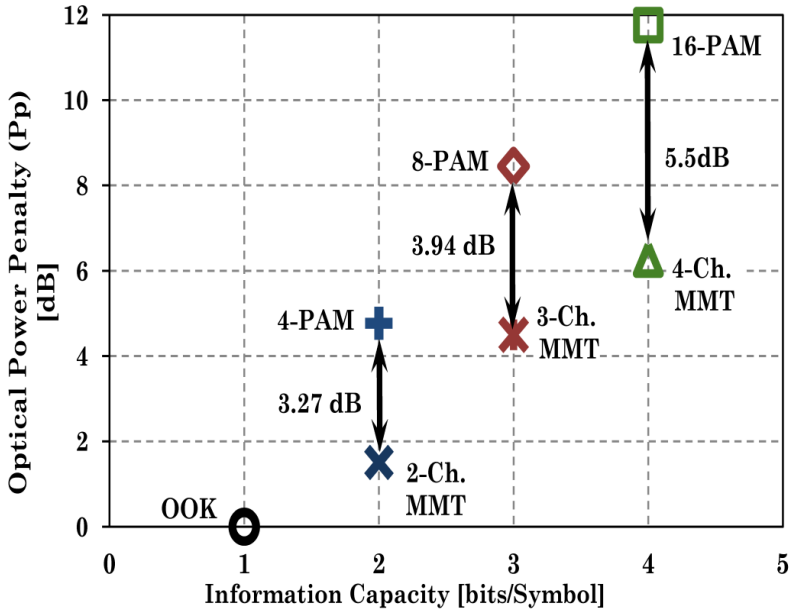

Figure 4.16 The average optical power penalty for M-PAM and N-channel MMT with respect to the information capacity relative to OOK at a fixed bandwidth.

In order to have a meaningful assessment, in figure 4.17 the N-Channel MMT is compared with M-PAM at a constant bit rate constraint with respect to the information capacity. At fixed bit rate, Fig. 5(b) depicts the asymptotic power penalty of N-Channel MMT and M-PAM modulation format proportional to OOK as in eq. (33) to achieve a proportional BER performance at asymptotically high SNR. For information capacity= 2 bits/symbol, 2-channel MMT has an incremental gain of 1.76 dB over 4-PAM relative to OOK at fixed aggregated data rate. For information capacity= 3 bits/symbol, 3-channel MMT require 2.2 dB reduced optical power against 8-PAM at a BER figure $\leq 10^{-6}$. For information capacity= 4 bits/symbol, 4-channel MMT has an optical power gain of 4 dB more than 16-PAM, relative to OOK.

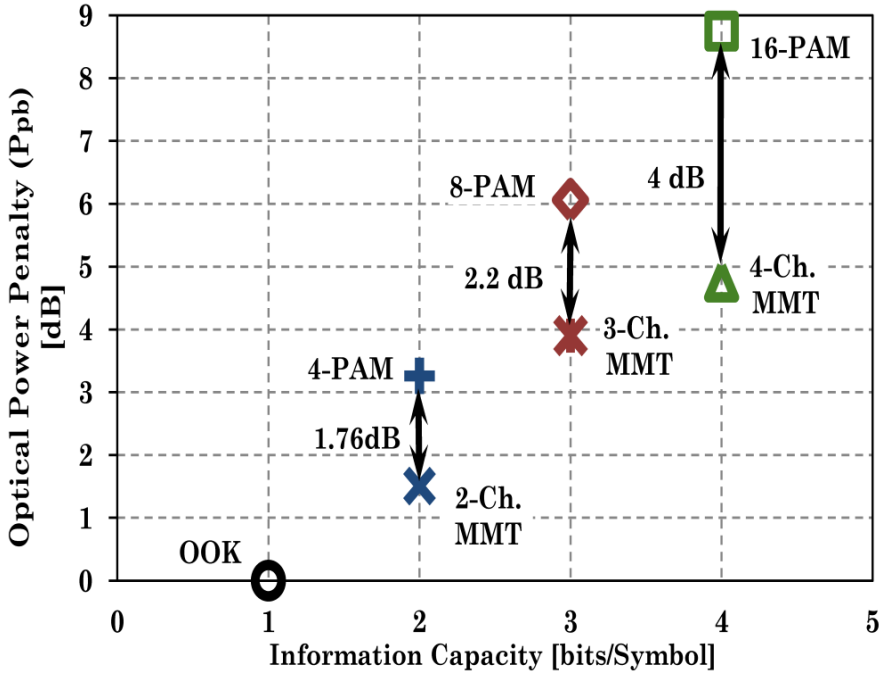

Figure 4.17 The average optical power penalty for M-PAM and N-channel MMT with respect to the information capacity relative to OOK at a fixed bitrate.

4.4 Concluding Remarks

It is worth noting that the asymptotic optical power efficiency of the calculated data formats has an agreement and verify our theoretical results obtained in fig.4.2 – fig. 4.5 at BER $=10^{-12}$ since the results are compared in both cases relative to OOK. Also, the M-PAM penalties matches the verified experimentally results discussed in [59].

Electrical bandwidth is one of the important trade-off metrics for modulation formats. The spectral width of N-channel MMT modulation format relative to OOK can be expressed as

$$SW_{MMT} = \frac{number\ of\ slots\ (S) \times SW_{OOK}}{number\ of\ MMT\ channels\ \ (N)} = \frac{2}{\log_2 (M_{\Delta 1}.M_{\Delta 2})} SW_{OOK} \quad [\text{Hz}] \qquad (4.23)$$

where SW_{OOK} is the spectral width of OOK for IM/DD system.

Table 4.1 summarizes the performance of MMT and PAM formats in terms of spectral efficiency, number of levels and receiver sensitivity for transmission of 2, 3 and 4 bits/symbol. Although the transmission of 4 bits/symbol using 16-PAM system has a spectral efficiency advantage over 4-channel MMT system, but it suffers from a significant power penalty due to the division of its eye diagram to 15 narrow eyes which has not proven practical for implementation [4]. As illustrated in Table 4.1, 4-channel MMT with the spectral efficiency of $2\ b/s/Hz$ can be considered as an effective and desirable practical compromise between power efficiency advantage and an appropriate spectral efficiency for 4 bits/symbol transmission systems.

These results published in [197] verify our proposed signal design advantage on the power efficiency of N-channel MMT system compared to M-PAM, which justify our consideration for N-Channel MMT transmission format as a potential practical candidate for deployment in high capacity power limited systems.

Table 4.1 Overall comparison between N-channel MMT and M-PAM at 40Gb/s.

Setup at 40 Gb/s	***Information Capacity in bits/symbol***	***Spectral Efficiency (b/s/Hz)***	***Spectral Width (Hz) at a given Bit Rate "R"***	***Number of levels***	***Receiver Sensitivity*** **BER=10^{-9}** ***(dBm)***
2-channel MMT	**2**	**1**	**R**	**2**	**–11.6**
3-channel MMT	**3**	**1.5**	**2 R / 3**	**3**	**–9.3**
4-channel MMT	**4**	**2**	**R / 2**	**4**	**–8.3**
4-PAM Format	**2**	**2**	**R / 2**	**4**	**–9.85**
8-PAM Format	**3**	**3**	**R / 3**	**8**	**–7.1**
16-PAM Format	**4**	**4**	**R / 4**	**16**	**–4.3**

5. Chapter 5: Numerical Performance Analysis

5.1 Introduction

Nowadays, the variety of services and internet application in data centers, enterprises, organizations and campuses have led to more capacity demand in metropolitan area networks[12]. N-channel MMT is designed not only for optical interconnects, but also a potential applicable and feasible solution for medium range high-speed optical links. Beside the conventional analytical performance evaluation parameters of modulation formats that is dependent upon signal characteristics such as Euclidean distance in signal space, signal shape, power efficiency, spectral efficiency…etc. It is the substantial to investigate N-channel MMT system reach in an optically amplified transport configuration for Metropolitan Area Networks (MAN).

Optical links are classified based upon the reach and capacity[110]. Access networks exhibit a maximum reach of 50 Km and dominated by Ethernet and optical transport networks technology (OTN). Metro networks are designed for metropolitan areas with a typical ring topology and a reach of less than 300 km with an Erbium Doped Fiber Amplifier (EDFA) amplifier placed every 80Km. Regional networks are responsible for inter-city links with a maximum reach of 600 Km. In the end, long-haul links, which is considered the core of the internet network with transmission reach that extend between 600 km to 10,000 km.

5.2 N-Channel MMT for Metro Networks

In this section, an expansion for the performance investigation analysis for MMT in the presence of pre-amplifier receiver has been adopted. In metropolitan area networks, EDFA amplifiers are employed in a booster and pre-amplifier configurations. The dominant noise source in these optically amplified links is due to the Amplified Spontaneous Emission Noise (ASE) [110].

In this section, an investigation for the back-to-back receiver sensitivity of 2-ch, 3-ch and 4-ch MMT at an aggregated bit rate of 40Gb/s and 100Gb/s utilizing single wavelength carrier is manifested. The sensitivity is based upon measuring the minimum required received optical power to the receiver in order to acquire a certain BER performance. For metro networks, a BER value $=10^{-9}$ is considered a good BER platform for reliable data transmission system.

The forthcoming evaluation for the receiver sensitivity includes two types of Mach-Zehnder Modulators (MZM); the first is based upon the MZM analytical model and the second is single drive Multiple-Quantum-Well Mach-Zehnder Modulator (MQW-MZM), which is based upon pre-defined measurement model defined in Appendix A. The receiver employed in these analyses, is the MMT threshold detection receiver discussed in section 3.3.3. The BER for MMT is estimated according to the BER and Q-factor models demonstrated in section 3.4.2.

5.2.1 2-Channel MMT with 2 bits/symbol

Performance evaluation for the receiver sensitivity of 2-channel MMT with 2 bits/symbol at 40 and 100Gb/s system aggregate bit rate in the presence of dominant ASE noise source, is presented.

5.2.1.1 System setup Utilizing MZM Analytical Model

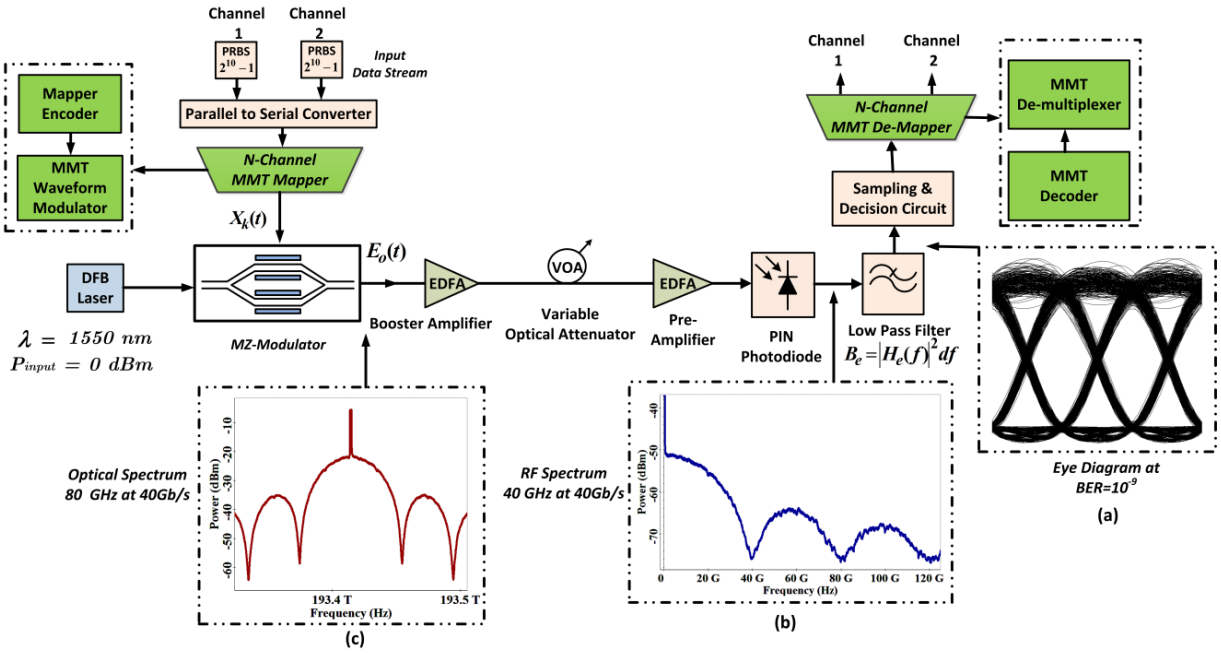

Figure 5.1 2-Channel MMT system setup at aggregated bit rate 40Gb/s, (a) Eye diagram at BER=10^{-9} ,(b) RF Spectrum and (c) Optical Spectrum.

Figure 5.1 shows the system setup of 2-channel MMT employing an MZM analytical model at aggregated system bit rate of 40 Gb/s with baud rate 20 G baud/sec. In the electrical domain, the MMT transmitter multiplexes the data from 2 data channels (or users) using MMT mapping algorithm (as discussed in section 3.3). The two channels of data are modeled using a Pseudo Random Bit Sequence (PRBS) generator of the order $2^{10}-1$ following [198]. A PRBS generator (AGILENT-Keysight-N4974A) is commercially available with data rate 40Gb/s and maximum pattern sequence reaching $2^{31}-1$[199].

Afterwards, the electrical MMT signal is converted to an optical MMT signal by the aid of Mach-Zhender Modulator (MZM). The MZM is composed of two 3 dB couplers connected by dual waveguides with an equivalent length, which acts as an intensity

modulator based upon the inferometric principle. The MZM analytical behavior can be expressed by an optical signal E_{out} as [161], [200]

$$E_{out} = E_{in}(t).\cos(\theta(t)).e^{j\theta(t)} \tag{5.1}$$

where $E_{in}(t)$ is the electrical field input to the modulator, $\theta(t)$ is the phase difference between the two arms of the MZM and can be defined as

$$\theta(t) = \frac{\pi}{2}(\frac{1}{2} - ER.(X(t) - \frac{1}{2})) \tag{5.2}$$

where ER is the extinction ratio and $X(t)$ is the input electrical modulated signal. A Variable optical attenuator (VOA) exists to vary the optical power in order to measure the receiver sensitivity at an acceptable BER value. The eye diagram of 2-channel MMT system with 2×20 Gbit/s is shown in figure 5.1(a). In figure 4.19 (b), RF spectrum analyzer is employed enabling a calculation for the Power Spectral Density (PSD) of MMT signal relative to the frequency in the electrical domain. The RF bandwidth of 2-channel MMT is shown equivalent to $\Delta f_{RF} = 40GHz$ with a spectral efficiency of 1 b/s/Hz and an optical spectrum resolution filtered bandwidth of 1 GHz[112]. Furthermore, figure 5.1 (c) depicts the optical spectrum of 2-channel MMT employing optical spectrum analyzer, which enables a calculation for the Power Spectral Density (PSD) of MMT signal relative to the frequency in the optical domain. The optical spectral width is equivalent to $\Delta f_o = 80GHz$ (twice the RF spectral bandwidth) acquiring a spectral efficiency of 0.5 b/s/Hz at an optical spectrum resolution filtered bandwidth of 0.01nm. An optical spectrum analyzer (OSA) (AGILENT-71452B) is commercially available with resolution bandwidth accuracy 0.5 nm [201].

5.2.1.2 2-channel MMT Receiver Sensitivity utilizing MZM Analytical Model

Figure 5.2 depicts and compares the receiver sensitivities of 2-channel MMT system at 40Gbs/ and 100Gb/s. The system settings has been optimized to maintain the minimum sensitivity at BER $=10^{-9}$. For 2-channel MMT at 40Gb/s, the optical sensitivity is equivalent to $=-30.7\,dBm$, while at 100 Gb/s, the sensitivity corresponds to $-26.7\,dBm$. The power penalty for increasing the throughput from $40G \rightarrow 100G$ is 4 dB for an equivalent BER performance.

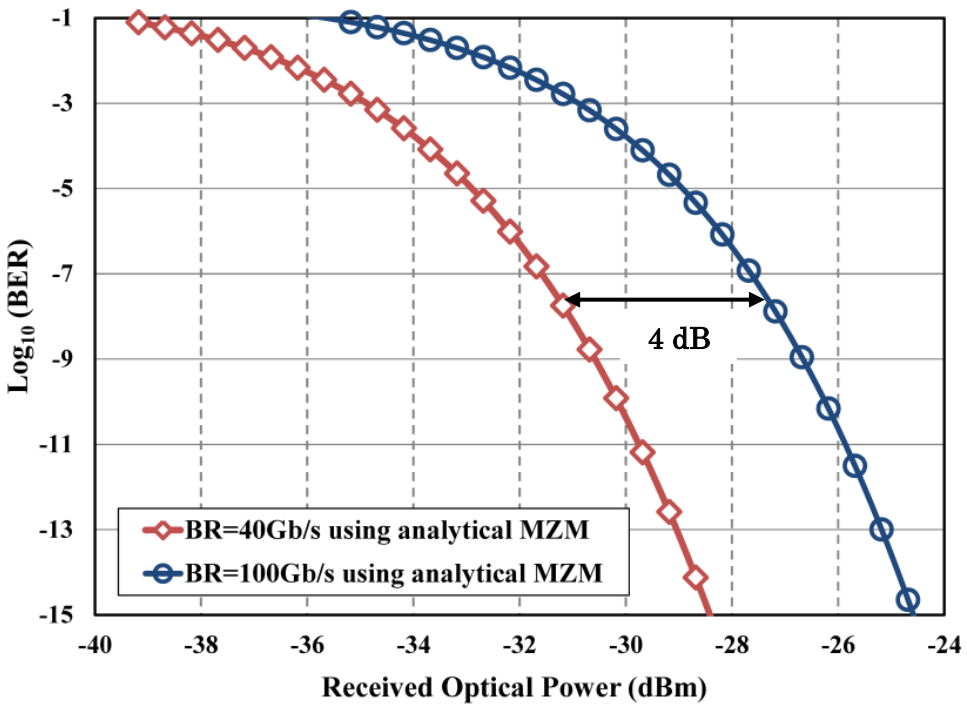

Figure 5.2 2-channel MMT receiver sensitivity versus BER employing analytical MZM model at bit rates 40Gb/s and 100Gb/s.

5.2.1.3 System setup using Single Drive Multiple-Quantum-Well Mach-Zehnder (MQW-MZM)

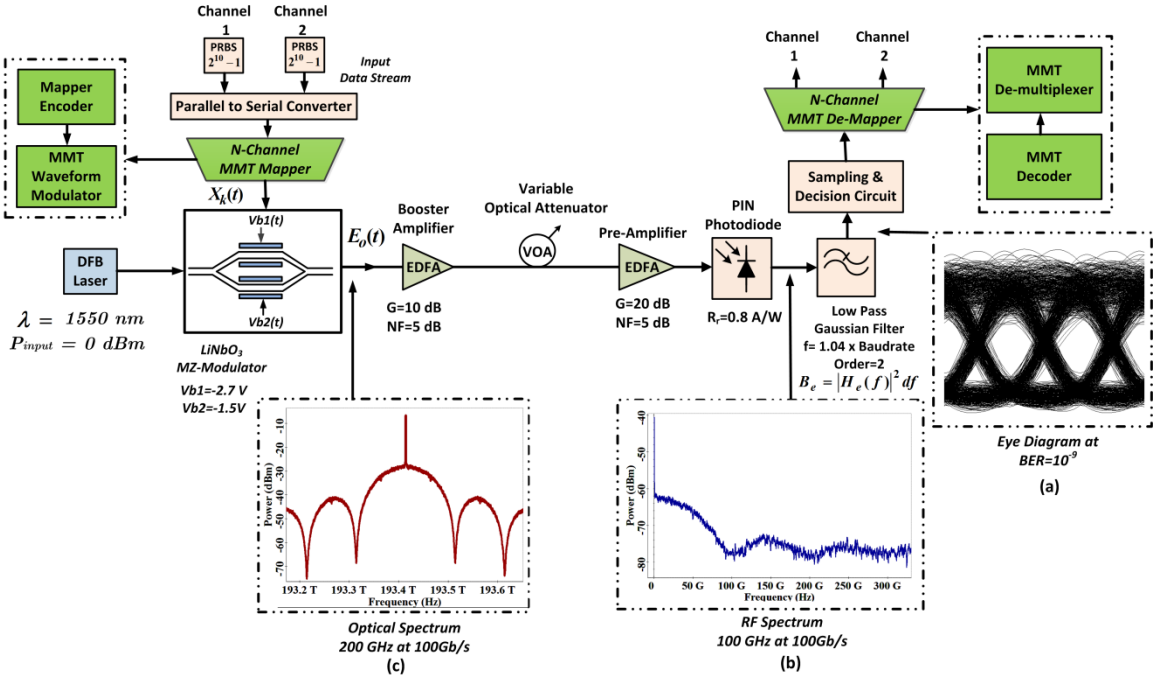

Figure 5.3 2-Channel MMT system setup employing single drive MQW-MZM modulator at aggregated bitrate 100Gb/s, (a)Eye diagram at BER=10^{-9} ,(b)RF Spectrum, and (c)Optical Spectrum.

Figure 5.3 depicts 2-channel MMT system setup utilizing MQW-MZM at aggregated system bit rate of 100 Gb/s with baud rate 50 Gbaud/sec. The booster EDFA amplifier has a gain= 10dB with 5 dB noise figure, while the pre-amplifier has a gain of 20 dB with a 5 dB noise figure. An EDFA (Optilab-EDFA) optical component is commercially available with maximum gain=25dB and noise figure=4.5dB[202]. The photodiode responsivity is equal to 0.8 A/W. A commercially available pin photodiode (THORLABS-D400FC InGaAs PIN) with responsivity reaching 0.95A/W[203]. A second order low pass Gaussian filter has been adopted with a cutoff frequency $\Delta f = 1.05 \times baudrate$, which corresponds to $52.5 GHz$.

5.2.1.4 Pre-Amplifier Gain Optimization

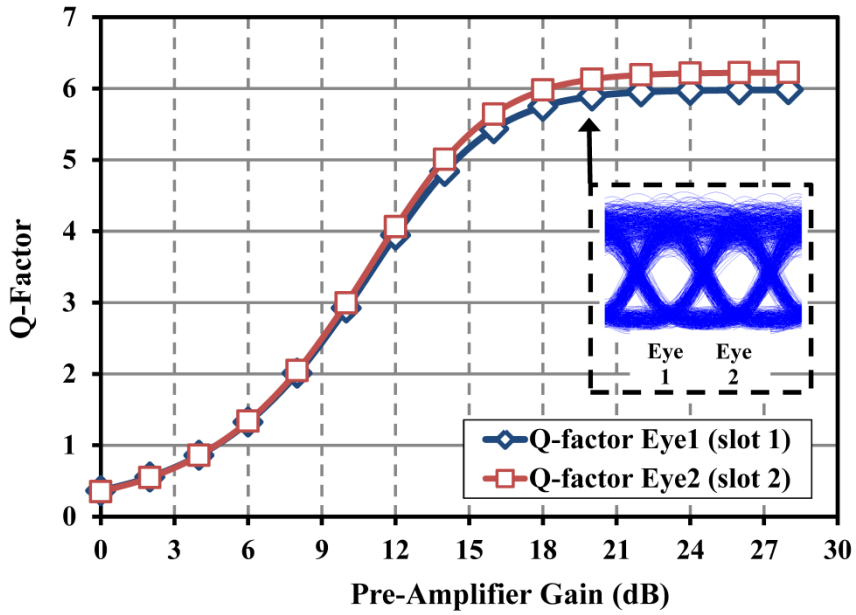

Figure 5.4 2-channel MMT system pre-amplifier gain optimization.

A pre-amplifier is a crucial component that is placed at the optical link receiving end to enhance the receiver sensitivity. Since, 2-channel MMT system evaluation is dependent upon the calculated eye diagram, which is split into two slots eye diagram. Hence, it is desirable to optimize the pre-amplifier gain in order to obtain the maximum allowable Q-factor for both slots.

Figure 5.4 shows the Q-factor of eye 1 (slot 1) and eye 2 (slot2) relative to the launched pre-amplifier gain. With a pre-amplifier gain G=20 dB, the 2-channel MMT acquire an acceptable Q-factor values 5.9 and 6.1 for eye 1 and eye 2, respectively. These Q-factors are equivalent to an acceptable metro link BER $\leq 10^{-9}$. Figure 5.4 depicts the eye diagram observing non major degradation between the two slots Q-factors, except for penalty equivalent to 0.1 dB on eye 2 relative to eye 1. We conjecture that this penalty is due to to the inter-symbol interference between the two slots.

5.2.1.5 2-channel MMT Receiver Sensitivity comparison

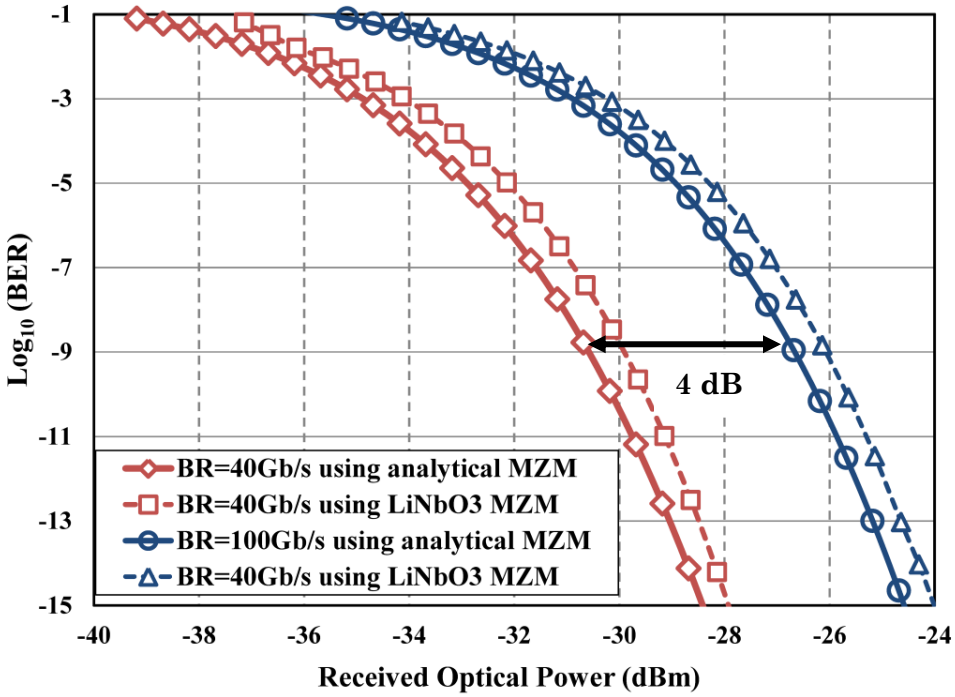

Figure 5.5 2-channel MMT receiver sensitivity versus BER employing analytical MZM model and MQW-MZM at 40Gb/s and 100Gb/s.

Figure 5.5 depicts a comparison between the employment of single drive MQW-MZM and analytical MZM model on 2-channel MMT system with respect to the receiver sensitivity at bit rates 40Gbs/ and 100Gb/s. For single drive MQW-MZM model at BER = 10^{-9}, the receiver sensitivity is equivalent to $=-30.1\ dBm$ for 40Gb/s system, while it is equivalent to $-26.1\ dBm$ for 100Gb/s. The corresponding eye diagrams with each slot Q-factor are shown in figure 5.6. The results agree well with the 2-channel MMT utilizing MZM analytical model discussed in figure 5.2 with a 4dB penalty of increasing the bit rate from 40G to 100G. Furthermore, a power penalty of 0.6 dB is observed with the utilization of single drive MQW-MZM compared with the MZM analytical model.

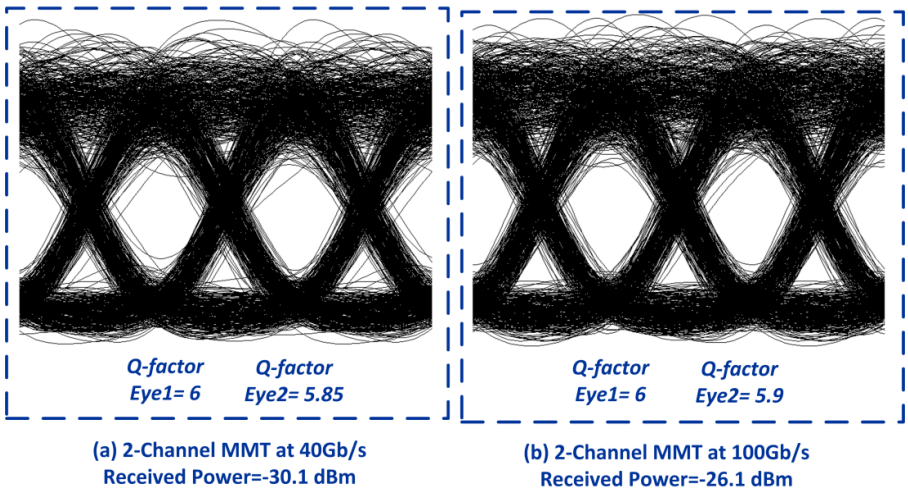

Figure 5.6 2-channel MMT Eye diagram at BER $=10^{-9}$:- (a) At 40Gb/s using single drive MQW-MZM model, and (b) At 100Gb/s using single drive MQW-MZM model.

5.2.2 3-channel MMT with 3 bits/symbol

In this section, performance assessment on realizing the transmission of 3bits/symbol employing 3-channel MMT at 40Gb/s and 100Gb/s system aggregate bit rates, in the presence of pre-amplified receiver model.

5.2.2.1 System setup using Analytical MZM

In the same manner as 2-channel MMT , figure 5.7 shows the system setup of 3-channel MMT utilizing MZM analytical model at an aggregated bit rate 40Gb/s equivalent to 13.3 G baud/sec. In the electrical domain, the MMT transmitter multiplexes the data from 3 data channels using MMT mapping algorithm. The three channels of data are presented by an input pseudo random bit sequence (PRBS) of $2^{10}-1$. The booster amplifier has a gain G=10dB with noise figure NF=5dB, whereas the pre-amplifier has a gain G=20dB with noise figure NF=5dB. Eye diagram for the 3-channel MMT electrical signal at the sampling and decision device is shown in figure 5.7(a). The received optical signal corrupted mainly by ASE noise is filtered by a 2nd order low pass Gaussian filter. The electrical low pass filter cutoff frequencies are optimized to acquire $\Delta f = 1.05 \times baudrate$ which corresponds to $\approx 14 GHz$.

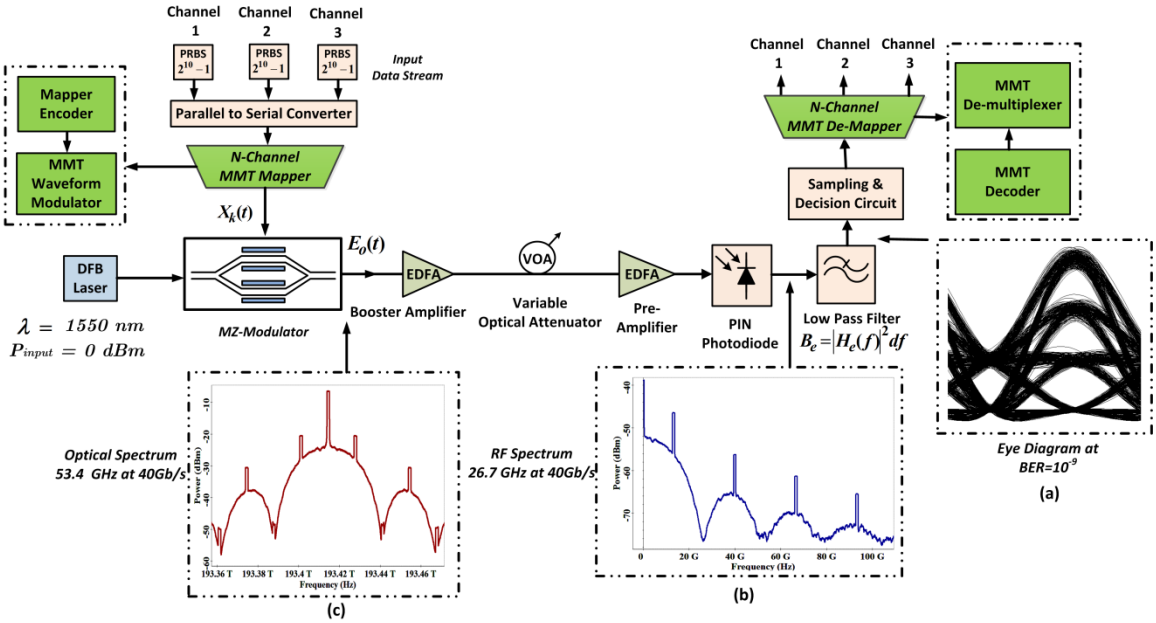

Figure 5.7 3-Channel MMT system setup at aggregated bit rate 40Gb/s, (a) Eye diagram at BER= 10^{-9} ,(b) RF Spectrum and (c) Optical Spectrum.

As shown in figure 5.7(b), by the inspection of the RF optical spectrum $f_{RF} = 26.7\,GHz$ with a spectral efficiency of 1.5 b/s/Hz. Moreover, the optical spectral width exhibit $f_o = 53.4GHz$ as figure 5.7 (c) depicts. This spectral width is equivalent to a spectral efficiency of 0.75 b/s/Hz. By the inspection of the optical spectrum, 3-channel MMT spectrum is shaped as continuous samples in the frequency domain, and a high power discrete tone at the carrier center frequency corresponding to a 1550 nm wavelength. Other weaker residual tones exist at multiples of the bit rate. 3-channel MMT frequency spectrum exhibits a strong spectral content at line rate. This feature is beneficial in simplifying the clock recovery.

5.2.2.2 Receiver sensitivity Utilizing Analytical MZM and single drive MQW-MZM

In the same manner as section 5.2.1, figure 5.8 depicts a receiver sensitivity comparison between single drive MQW-MZM and the analytical MZM model for 3-channel MMT system at 40Gbs/ and 100Gb/s. Table 5.1 shows the optimized modulator device parameters for both setup configurations. For single drive MQW-MZM, the receiver sensitivity at BER $=10^{-9}$ is equivalent to $=-26\,dBm$ with OSNR=24.9 at 40Gb/s system. While, for 100Gb/s, it is equivalent to $-22.1\,dBm$ with OSNR=27.6dB at 100Gb/s. On the other hand, using analytical MZM model, the receiver sensitivity at BER $=10^{-9}$ is equivalent to $=-23.9\,dBm$ with OSNR=28.1 at 40Gb/s system. While, for 100Gb/s, it is equivalent to $-20\,dBm$ with OSNR=31.5dB. The power penalty due to the increase in the aggregated bit rate from 40G to 100G is equivalent to 3.9 dB. Furthermore, it can be deduced that there is a penalty of 2.1 dB due to the use of single drive MQW-MZM compared with the analytical MZM model.

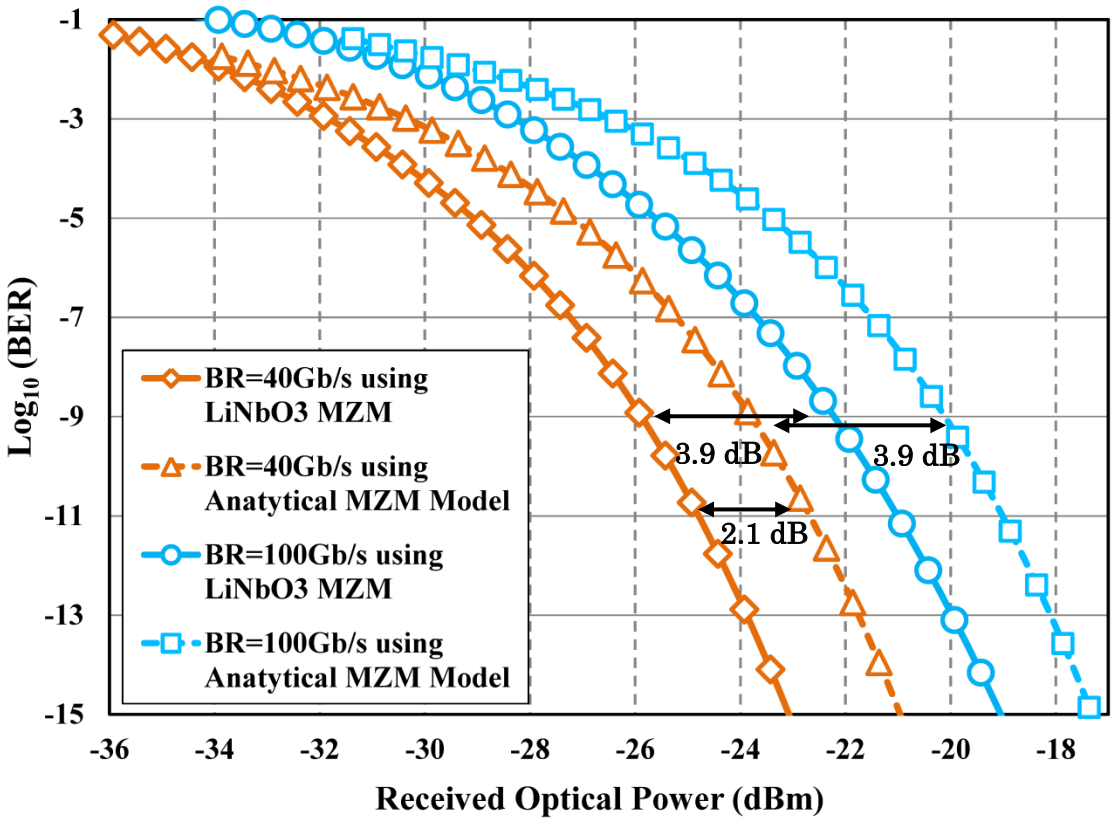

Figure 5.8 3-channel MMT receiver sensitivity versus BER employing analytical MZM model and single drive MQW-MZM at 40Gb/s and 100Gb/s.

Table 5. 1 3-channel MMT system setup optical modulators specifications

MZM Parameters	***Analytical MZM Model At 40Gb/s***	***Single drive MQW-MZM Model At 40Gb/s***	***Analytical MZM Model At 100Gb/s***	***Single drive MQW-MZM Model At 100Gb/s***
Bias Voltages	*Not Applicable*	*Vb_1= -1.8V Vb_2= -1.1V*	*Not Applicable*	*Vb_1= -1.8V Vb_2= -1.1V*
Extinction Ratio	*=18 dB*	*Not Applicable*	*16 dB*	*Not Applicable*
Modulation Voltage	*Not Applicable*	*1.5 V*	*Not Applicable*	*1.5 V*

Figure 5.9 shows the eye diagram for the receiver sensitivity results presented earlier at BER=10^{-9}. The calculated eye diagram for 3-channel MMT is composed of multiple levels with a fragmentation of main eyes to four smaller eyes with four different Q-factors. Hence, an equal spacing between levels is essential. For analytical MZM with sensitivity -23.9 dBm at 40Gb/s, The Q-factor (Q_eye1_s1, Q_eye1_s2, Q_eye2_s2, Q_eye3_s2) is equivalent to 10.35, 11.8, 7 and 5.7, respectively. However, as shown in figure 5.9, for single drive MQW-MZM at 40Gb/s, the Q-factor (Q_eye1_s1, Q_eye1_s2, Q_eye2_s2, Q_eye3_s2) is equivalent to 7.5, 8.1, 5.7 and 9, respectively. It is clear that due to the optical optimization of the bias voltages in single drive MQW-MZM, the levels are more distributed equally, as a result the noise is more evenly distributed on each level. In a similar manner, 100Gb/s system exhibited better performance.

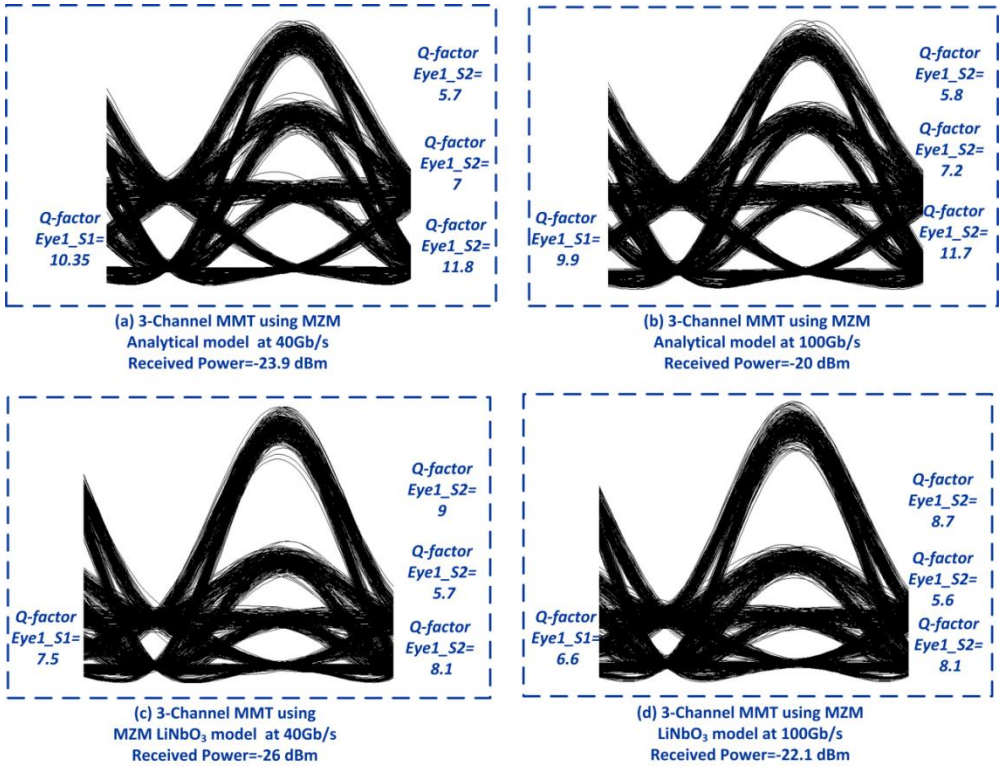

Figure 5.9 3-channel MMT Eye diagram at BER =10^{-9} (a) at 40Gb/s using analytical MZM model, (b) at 100Gb/s using analytical MZM model, (c) At 40Gb/s using single drive MQW-MZM, and (d) At 100Gb/s using single drive MQW-MZM model

5.2.3 4-channel MMT with 4 bits/symbol

In this section, performance assessment on realizing the transmission of 3bits/symbol employing 4-channel MMT at 40Gb/s and 100Gb/s system aggregate bit rate, in the presence of pre-amplified receiver.

5.2.3.1 System setup using Analytical MZM

In the same manner as section 5.2.2.3, figure 5.10 shows the system setup of 4-channel MMT using MZM analytical model at an aggregated bit rate 40Gb/s equivalent to 10G baud/sec. In the electrical domain, the MMT transmitter multiplexes the data from 4 data channels using MMT mapping algorithm. The four channels of data are modelled by an input pseudo random bit sequence (PRBS) of $2^{10}-1$. The booster amplifier has a gain G=10dB with noise figure NF=5dB, whereas the pre-amplifier has a gain G=20dB with noise figure NF=5dB. Eye diagram for the 4-channel MMT electrical signal at the sampling and decision device are given in figure 5.10(a). The received optical signal corrupted mainly by ASE noise is filtered by a 2nd order low pass Gaussian filter.

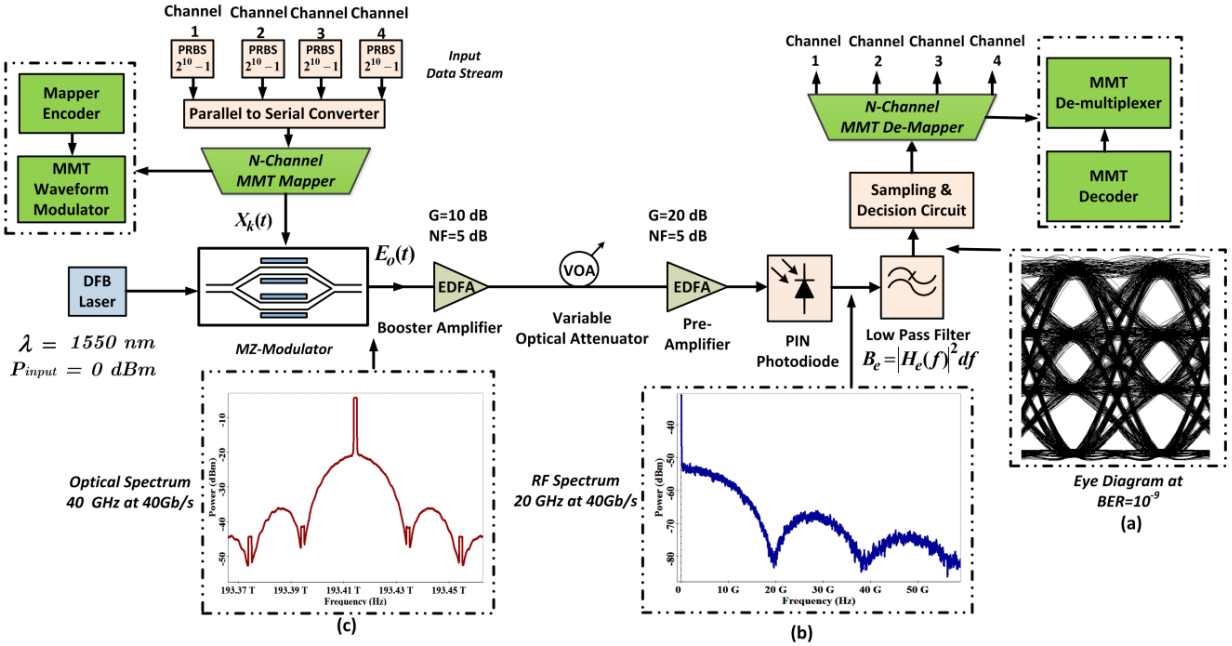

Figure 5.10 4-Channel MMT system setup at aggregated bit rate 40Gb/s, (a) Eye diagram at BER=10^{-9} ,(b) RF Spectrum, and (c) Optical Spectrum

The electrical low pass filter cut-off frequencies are optimized to be $\Delta f = 1.2 \times baudrate$ which corresponds to $\approx 12\ GHz$. As shown in figure 5.10(b), by the inspection of the RF optical spectrum $f_{RF} = 20GHz$ with a spectral efficiency of 2 b/s/Hz. Moreover, the optical spectral width exhibit spectral bandwidth equivalent to $f_o = 40GHz$ acquiring a spectral efficiency of 1 b/s/Hz as shown in figure 5.10(c) with a resolution filtered bandwidth 0.01nm.

5.2.3.2 Receiver sensitivity using Analytical MZM and single drive MQW-MZM

In the same manner as section 5.4.2.2, figure 5.11 depicts a comparison between the employment of single drive MQW-MZM and the analytical MZM model on 4-channel MMT system with respect to the receiver sensitivity at 40Gbs/ and 100Gb/s. Table 5.2 shows the modulator device parameters for both setup configurations, using analytical MZM model and single drive MQW-MZM. For single drive MQW-MZM, the receiver sensitivity at BER $= 10^{-9}$ is equivalent to $= -22.8\ dBm$ for 40Gb/s system, while it is equivalent to $-18.8\,dBm$ at 100Gb/s. On the other hand, using analytical MZM model, the receiver sensitivity at BER $= 10^{-9}$ is equivalent to $-23.6\,dBm$ with OSNR=28.1 for 40Gb/s system, whereas it is equivalent to $-19.6dBm$ at 100Gb/s. The power penalty due to increasing the aggregated bit rate from 40G to 100G is equivalent to 4 dB.

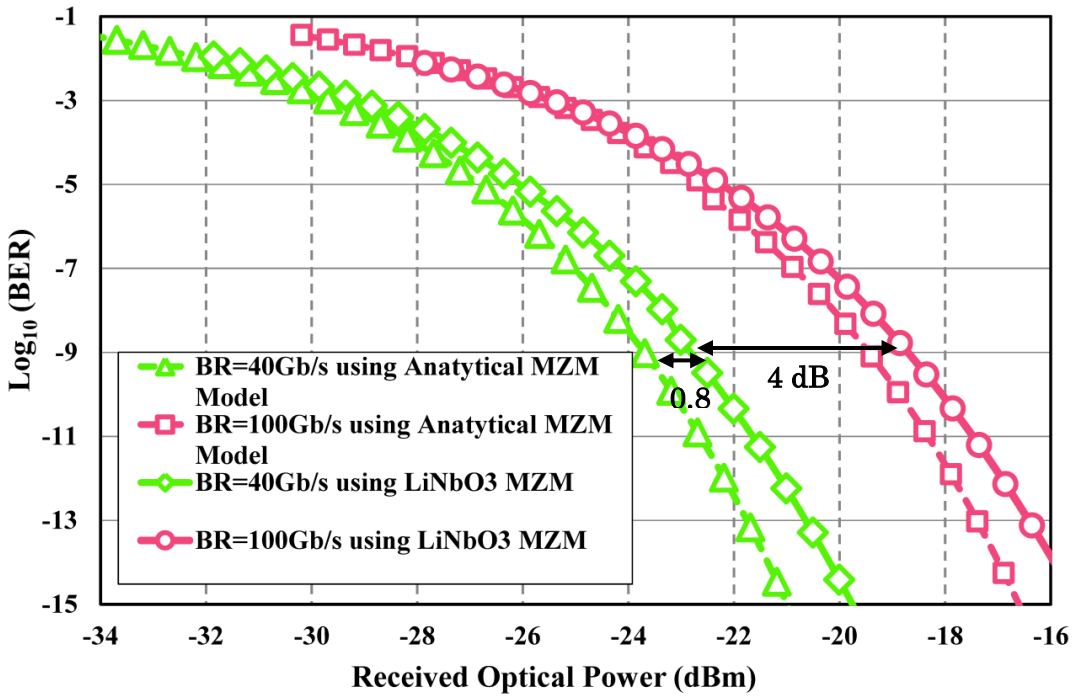

Figure 5.11 4-channel MMT receiver sensitivity versus BER employing analytical MZM model and single drive MQW-MZM at 40Gb/s and 100Gb/s.

Table 5. 2 4-channel MMT system setup optical modulators specifications.

MZM parameters	***Analytical MZM Model At 40Gb/s***	***Single drive MQW-MZM Model At 40Gb/s***	***Analytical MZM Model At 100Gb/s***	***Single drive MQW-MZM Model At 100Gb/s***
Bias Voltages	*Not Applicable*	*Vb_1= -2.8V Vb_2= -1.8V*	*Not Applicable*	*Vb_1= -2.8V Vb_2= -1.8V*
Extinction Ratio	*29 dB*	*Not Applicable*	*29 dB*	*Not Applicable*
Modulation Voltage	*Not Applicable*	*1.5 V*	*Not Applicable*	*1.5 V*

Furthermore, it can be deduced that there is a penalty of $\approx 0.8dB$ due to the use of single drive MQW-MZM compared with the analytical MZM model. Figure 5.12 depicts the calculated eye diagram for 4-channel MMT in which it is composed of multiple levels with a fragmentation of main eyes to four smaller eyes with eight different Q-factors. For analytical MZM with sensitivity -23.6 dBm at 40Gb/s, The Q-factor (Q_eye1_s1, Q_eye2_s1, Q_eye3_s1, Q_eye1_s2, Q_eye2_s2, Q_eye3_s2) is equivalent to 10.8, 6, 5.9, 11.1, 6.4 and 5.8, respectively. However, as shown in figure 5.12, for single drive MQW-MZM at 40Gb/s, the Q-factor (Q_eye1_s1, Q_eye2_s1, Q_eye3_s1, Q_eye1_s2, Q_eye2_s2, Q_eye3_s2) is equivalent to 10.9, 5.6, 7.6, 10.5, 5.9 and 7.9, respectively.

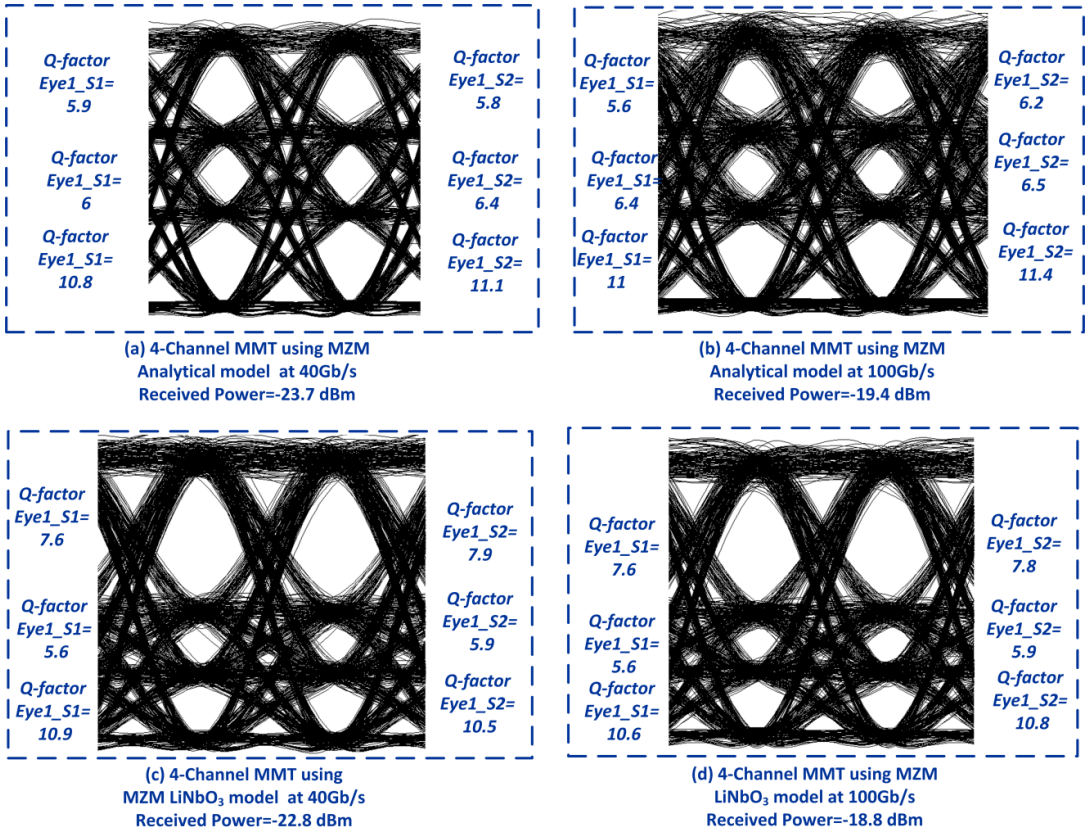

Figure 5.12 4-channel MMT Eye diagram at BER $=10^{-9}$, (a) at 40Gb/s using analytical MZM model, (b) at 100Gb/s using analytical MZM model, (c) At 40Gb/s using single drive MQW-MZM model, and (d)) At 100Gb/s using single drive MQW-MZM model

5.2.4 Receiver Sensitivity Comparison between MMT and M-PAM

In the presence of EDFA amplifiers, the information capacity effect in terms of number of bits/symbol (2, 3, and 4) on receiver sensitivity of MMT and PAM systems at an aggregate bit rate of 40 Gb/s are shown in figure 5.13. In comparison with M-PAM system, the transmission of 2, 3 and 4 bits/symbol using MMT system can improve the receiver sensitivity by 7.4 dB, 11.3 dB, and 17.5 dB, respectively. This power penalty in M-PAM is due to the higher number of levels in comparison to the MMT system, with the fragmentation consequences of main eyes to the smaller eyes as shown in the eye diagram in figure 5.13. It is worth noting that the difference in power penalty with respect to the theoretical results is due to the employment of an EDFA booster and preamplifier where the signal dependence on spontaneous beat noise dominates, which leads to an additional power penalty to reach 8 dB. Furthermore, the penalty increase is reasoned to the non-equal spacing that lead to increase the penalty, especially in higher order PAM formats utilizing 8 and 16 levels [108], [204], [205].

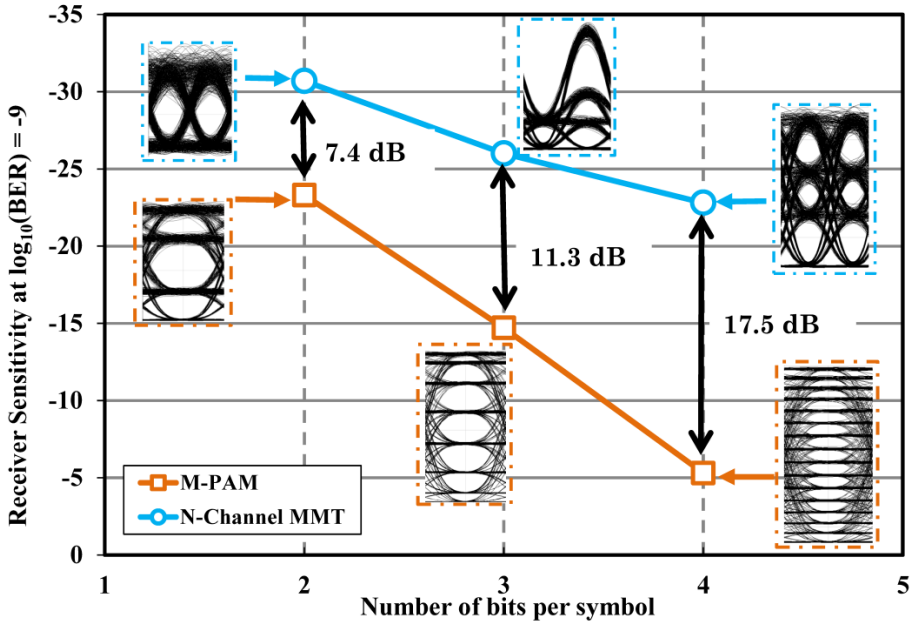

Figure 5.13 Receiver sensitivities comparison between 2, 3, and 4 bits/symbol transmission, using M-PAM and MMT systems at an aggregated bitrate of 40 Gb/s .

5.3 N-channel MMT evaluation in the presence of Fiber linear and non-linear impairments

Optical amplifiers existence introduces a certain level of ASE noise, which is dependent upon the gain[110], [206], [207]. The need for amplifier gain depends on the transmission distance in which long fiber transmission links necessitate an increase in the amplifier gain, which is translated to an more impact from the ASE noise. Also, due to the attenuation characteristics in the fiber, the longer the fiber reach presuppose more input power requirement. However, we cannot neglect the fact that increasing the input power will stimulate the non-linear effects, thus leading to distortion of the propagating signal. Furthermore, other practical deployment considerations that include the optimization of components settings and the interplay between the signal characteristics and fiber impairments must be taken into account.

Hence, a study and quantification for the impact of fiber non-linear impairments in which the interaction between Group Velocity Dispersion (GVD), Self-Phase Modulation (SPM) and intra-channel non-linearities, is crucial. Accordingly, there is a necessity in choosing an adequate dispersion compensation scheme to compensate for the accumulated residual dispersion in fiber transmission spans. Furthermore, the N-channel MMT maximum system reach will be discussed for metro networks.

As such, in this section the exploration of N-channel MMT transmission format behavior against fiber linear and non-linear impairments are essential to satisfy the thesis objective (in section 1.3, objective number 4).

5.3.1 Chromatic Dispersion Tolerance

The main system linear limitation for high rate optical systems on SMF is mainly due to chromatic dispersion. Chromatic dispersion can be the dominant reason for signal ISI and it occurs due to the dependence relation between the operating wavelength and the optical fiber index of refraction[208]–[210]. This leads to a pulse broadening in the time domain envelope because of the change in the propagation speed of different spectral component of the pulse. This broadening results in the signal distortions at the end of the fiber with length L. The relation between the maximum dispersion length L_D and the spectral width Δf is given by[110]

$$L_D = \frac{c}{RD\lambda^2\Delta f} \tag{5.3}$$

where 'c' is the speed of light in vacuum, 'R' is the bit rate, 'D' is the dispersion parameter, and 'λ' is the signal wavelength. It is clear that the pulse spectral width is inversely proportional to both the dispersion parameter and the transmission length which correspond to the pulse width. Hence, the signal with narrower spectral width exhibit better chromatic dispersion tolerance than other higher spectral width schemes. Also, it can be deduced the inverse proportionality relation between the link length and the bit rate .For systems with higher order modulation formats, the bit rate in eq. (5.3) turn to be the system baud rate. Accordingly, the less the baud rate will procure longer signal propagation reach.

5.3.1.1Comparison between N-channel MMT and M-PAM

As discussed in section 5.3.1, beside dispersion dependent variables that control the amount of dispersion tolerance; also, optimization of component characteristics and system configuration settings has an influence. Accordingly, dispersion tolerance may vary due to the interaction of different components with each other.

The chromatic dispersion tolerance of 2-, 3-, and 4-channel MMT have been investigated in a back-to-back configuration allowing an abstract quantification for MMT system tolerance to chromatic dispersion. An analytical Mach-zehnder modulator model has been employed in order to investigate the maximum optimized chromatic dispersion tolerance for the schemes under study.

Figure 5.14 depicts the chromatic dispersion tolerance of 2-channel MMT, 3-channel MMT and 4-channel MMT at 40 Gb/s and 100 Gb/s. At BER=10^{-9}, 2-channel, 3-channel and 4-channel MMT exhibit a dispersion tolerance of $\pm 158\, ps/nm$, $\pm 246\, ps/nm$ and $\pm 460\, ps/nm$ at 40 Gb/s, respectively. While, at 100Gb/s, 2-channel, 3-channel and 4-channel MMT shows a dispersion tolerance of $\pm 28\, ps/nm$, $\pm 40\, ps/nm$ and $\pm 76\, ps/nm$, respectively.

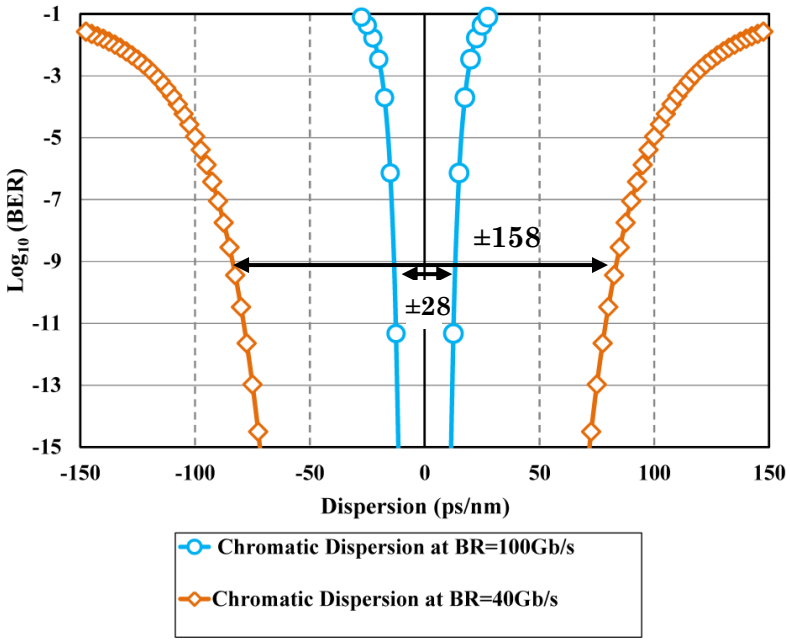

(a) 2-channel MMT

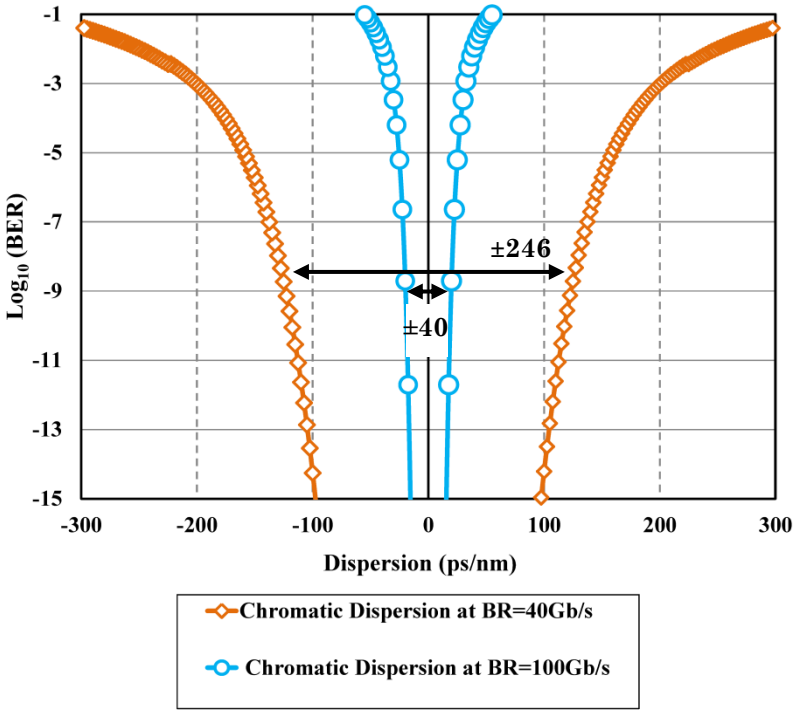

(b) 3-channel MMT

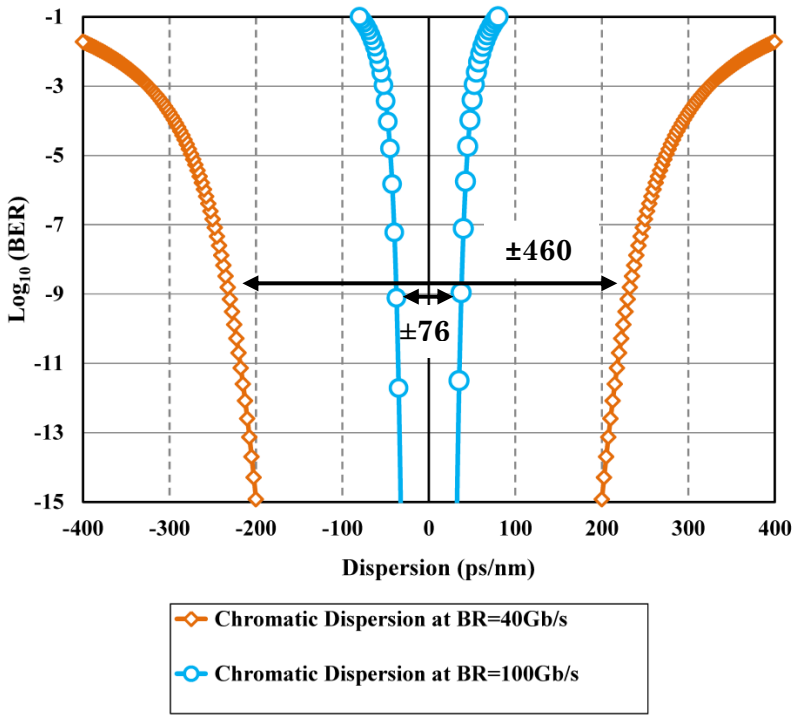

(c) 4-channel MMT

Figure 5.14. Dispersion tolerances in a back to back configuration for (a) 2-channel MMT, (b)3-channel MMT and (c)4-channel MMT.

Figure 5.15 shows a comparison for the optical spectral width between 2-ch, 3-ch and 4-ch MMT systems at the same aggregate bit rate of 40 Gb/s. The optical spectral width is equivalent to 80 GHz, 53.4 GHz and 40 GHz for 2-ch MMT, 3-ch-MMT and 4-ch MMT, respectively. As (5.3) the narrower the optical spectrum, the more tolerance is the modulation format to chromatic dispersion. Hence, it can be expected that 4-MMT exhibit a superior chromatic dispersion tolerance when compared with 2-channel MMT and 3-channel MMT. Moreover, for 100Gb/s, N-channel MMT observe less tolerance since the signal pulse width is much less than its counterpart which lead to more ISI effect. Furthermore, higher information capacity MMT channels leads to a reduction in the symbol rate, which reflects more tolerance to chromatic dispersion.

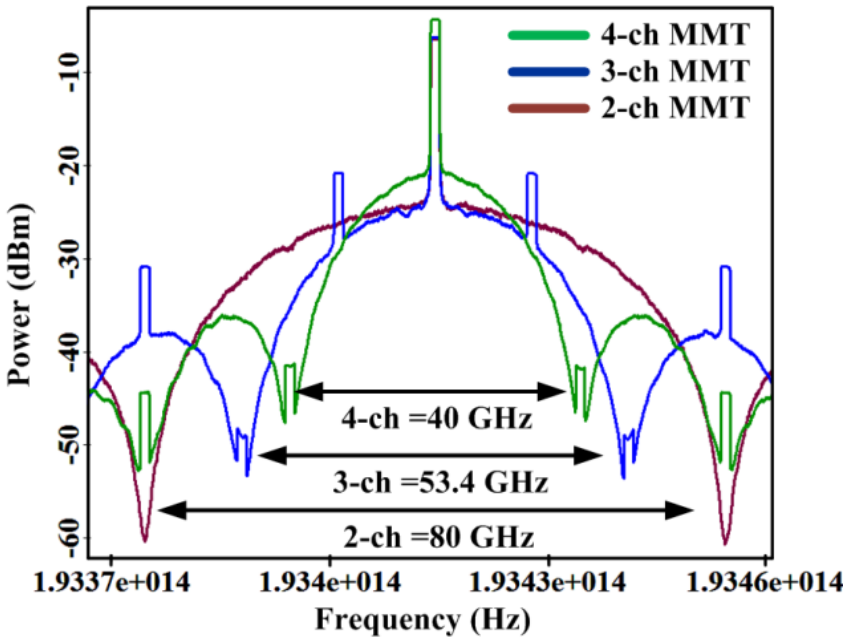

Figure 5.15 Optical spectrum of N-channel MMT formats at 40Gb/s.

Figure 5.16 depicts the chromatic dispersion tolerance of 4-PAM, 8-PAM and 16-PAM at 40Gb/s and 100Gb/s. System settings have been optimized to acquire the maximum performance which is equivalent to a minimum BER. At an acceptable BER= 10^{-9}, 4-PAM exhibits a dispersion tolerance of $\pm 224\,ps/nm$ and $\pm 36\,ps/nm$, for 40Gb/s and 100Gb/s, respectively. While, at 40Gb/s, 8-PAM shows a dispersion tolerance equivalent to $\pm 40\,ps/nm$. However, 8-PAM observes a BER floor of $6x10^{-6}$ at 0 ps/nm dispersion for 100Gb/s system aggregated bit rate. In addition, 16-PAM also shows a BER floor of $6x10^{-3}$ and $5x10^{-2}$ at 0 ps/nm dispersion for 40Gb/s and 100Gb/s, respectively. The chromatic dispersion tolerance degradation for 8-PAM and 16-PAM is due to the exhibition of multiple amplitude of levels, which imposes an inherent penalty as discussed in section 4.3. Thus, leads to a difficulty in acquiring an equidistant spacing between levels as shown in the eye diagrams shown in figure 5.16(b) and figure 5.16(c) at a dispersion tolerance of ±5 ps/nm.

The 4-PAM results can be validated by comparing it to the analytical investigation utilizing optimal electrical and optical receiver bandwidth settings combined with equal level spacing utilizing more complex signal PDF approximation models as Karhunen-

Leove expansion and saddle point approximation, in which 4-PAM have acquired 400ps/nm[204]. The superior tolerance for 4-PAM is due to the optimality assumptions for electrical and optical receiver settings combined with the equal spacing between M-PAM levels.

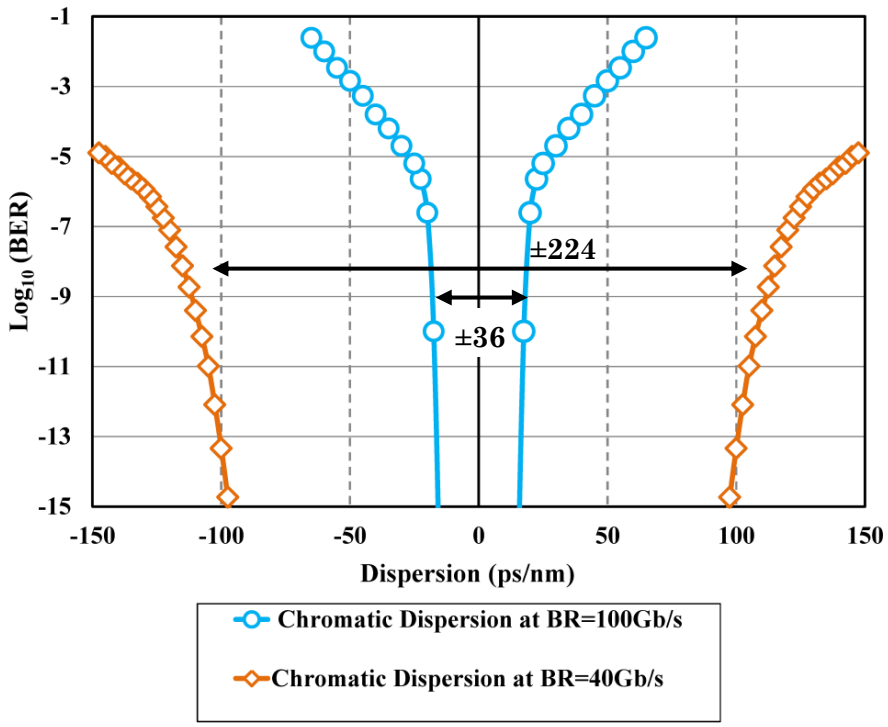

(a) 4-PAM

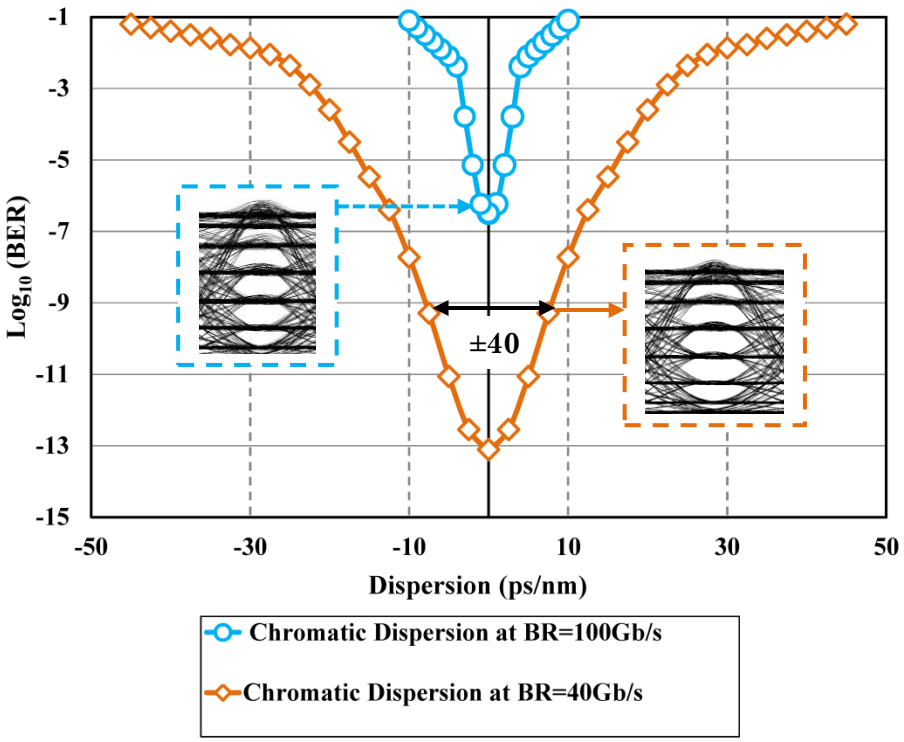

(b) 8-PAM

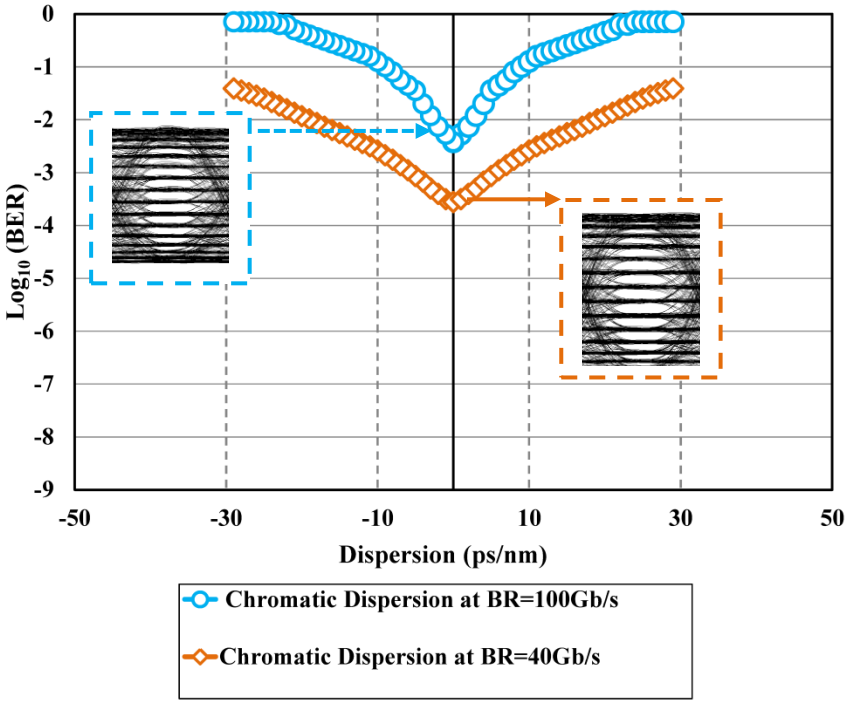

(c) 16-PAM

Figure 5.16 Dispersion tolerances in a back to back configuration for (a) 4-PAM, (b) 8-PAM and (c) 16-PAM.

5.3.2 System Tolerance to fiber Non-linearity

5.3.2.1 Introduction

For fiber non-linearity investigation, an inclusion for the fiber Kerr effect in the fiber channel model is necessary. Kerr occurs due to the dependence of the refractive index on the launched fiber optical intensity[110]. For single channels, this leads the optical field amplitude to have a self-induced phase modulation by the signal self-power, in which this phenomenon is called Self Phase Modulation (SPM).

As the need for high power pulses for maximum reach and error free fiber optic link systems, their performances are eventually limited by SPM effect . Since, the dominant non-linear effect in transmission systems is self-phase modulation (SPM). Thus, in this section, the effect of self-phase modulation is investigated over N-channel MMT optical fiber links.

5.3.2.2 Self Phase Modulation

SPM appears due to the dependence of the refractive index on the signal intensity, which leads to an induced phase change for the pulse propagating in the fiber [122], [211]–[213]. The different parts of the pulse undergo different phase shifts, which give rise to chirping of the pulses. Pulse chirping in turn enhances the pulse broadening effect caused by CD. This chirping effect is proportional to the transmitted power, which turns SPM effects to be more pronounced in systems employing high transmitted powers [214]. At the high power levels, Standard Single Mode Fiber (SSMF) has a large anomalous dispersion due to the Group Velocity Dispersion (GVD) of ~ 16.75 ps/nm/km. Therefore, necessities emerge to compensate the envelope time domain pulse broadening, which leads to a chirp after propagation.

Methods which exploit the use of SPM effect in the compensation for the second and almost the third order dispersion parameters have been previously proved effective by using Dispersion Compensation Fiber (DCF) in pre and post compensation scenarios [6-8].

In this section, the dispersion balance and SPM effects in our transmission link referring to non-linear Schrodinger (NLS) equation is modelled. Simulation is performed in both dispersion post-compensated and combination of pre- and post-compensated transmission links. The optimum value of dispersion pre-compensation is reported in order to enhance the performance of MMT system in terms of SPM tolerance.

For SMF with operating wavelength $\lambda = 1550\,nm$, $\beta_2 = -20\ ps^2/km$ and $D = 16.75\ ps/kmnm$. At 40Gb/s with symbol duration $T_{sym} = 100\ ps$ (baudrate=10G). The MMT signal can be considered as a Gaussian pulse with an incident pulse field in the form [56]

$$E(0,t) = \sqrt{P_o}\exp(\frac{-t^2}{2T_o^2}) \tag{5.4}$$

where T_o is the pulse width. The relation between the pulse width and the full width at half maximum (T_{FWHM}) can be expressed as

$$T_o \cong \frac{T_{FWHM}}{1.665} \tag{5.6}$$

Hence, by employing a default value for the Gaussian pulse for T_{FWHM} corresponds to 0.5 of the pulse width. Hence, 4-ch MMT pulse width at 40Gb/s (10Gbaud) corresponds to a dispersion length $L_D = 45Km$, while for 100Gb/s(25Gbaud) 4-ch MMT system, corresponds to a dispersion length $L_D = 7.2Km$. As such values, a dispersion compensation technique need to be employed in MMT to compensate for the residual dispersion in medium range metro networks.

5.3.2.3 Post Compensation System Setup

In this study, a simulation system involving two software, MATLAB® and OptiSystem® were employed to model the N-channel MMT system performance in both electrical and optical domains. System BER performance has been evaluated using the BER model described in section 3.4.2.

System setup is shown in figure 5.17 for N-channel MMT where N corresponds to 2-, 3-, 4-channel MMT multiplexed and modulated using mapping algorithm discussed earlier. System have been modelled for 40G/s and 100Gb/s, each channel is represented by a PRBS= $2^{10}-1$. The MMT symbol is used to modulate a Continuous Wave (CW) laser, operating at 1550nm wavelength by the aid of Mach-zehnder modulator. The modulator is biased by varying the bias voltages applied to the MZM arms. An optimized extinction ratio hs been set in the modulator to operate at the linear region with a high peak to average power ratio.

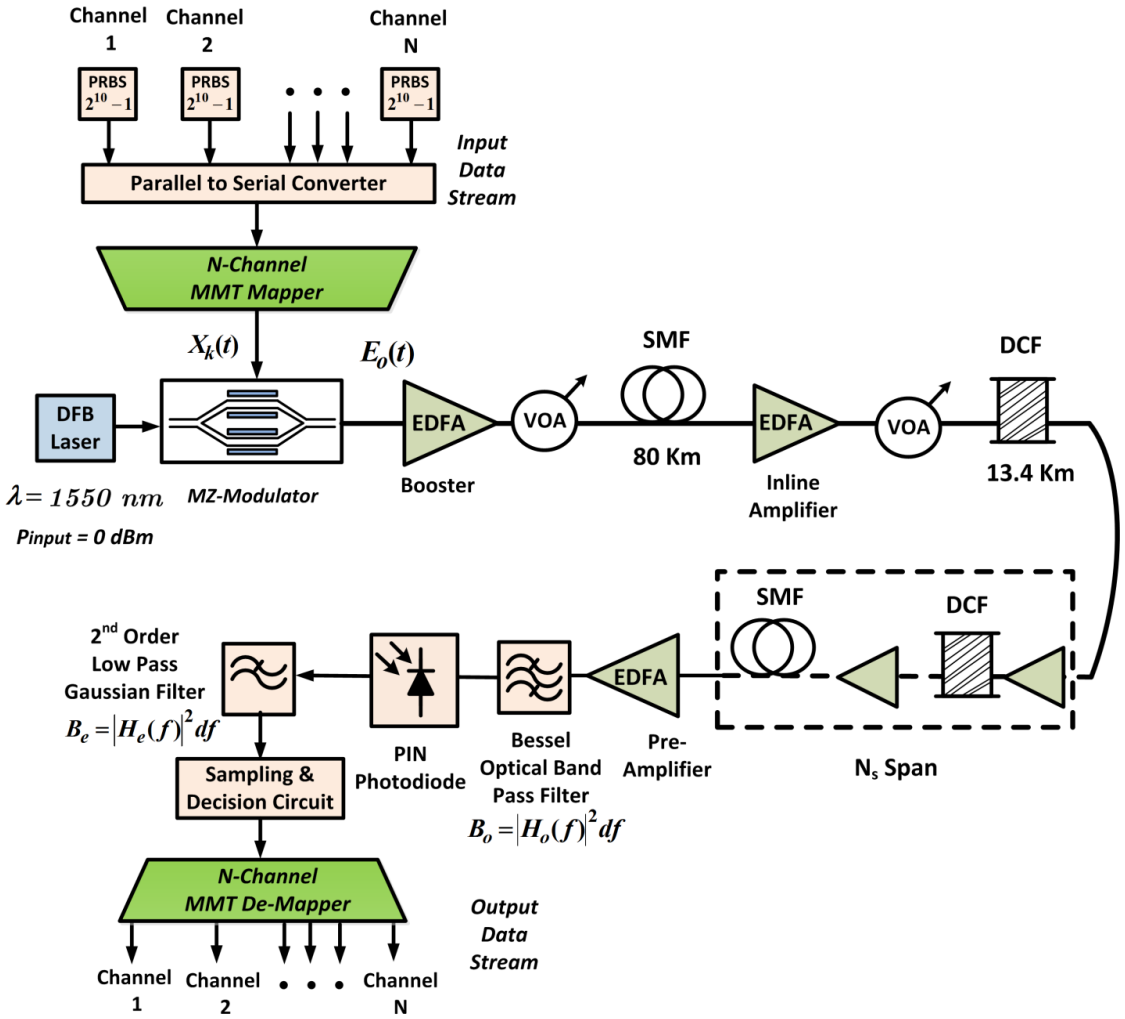

Figure 5.17 Transmission setup in post compensation configuration used for the investigations of maximum fiber reach and optimized power settings.

The link is composed of N_s number of spans of SMF transmission fiber each 80Km correspond to a loss of 16dB and a 13.4Km DCF fiber module with loss 6.7dB. A commercially available DCF and SMF modules with the designated specification[113], [215]. The noise figure in all of the amplifiers, including the optical pre-amp have a typical noise figure =6 dB. In line amplifiers have been employed to compensate for the link length attenuation and components coupling loss factors. It is worth noting that due to the existence of EDFA amplifiers, thus, ASE noise have been considered with other non-linear noise factors. Table 5.3 defines the SMF and DCF parameters specifications.

TABLE 5. 3 FIBER DESIGN PARAMETERS

SINGLE MODE FIBER (SMF) SPECIFICATION

Symbol	Parameter	Value
D	Dispersion	$16.75\ ps/km.nm$
S	Dispersion Slope	$0.075\ ps/nm^2.km$
α	Attenuation Coefficient	$0.2\ dB/Km$
A_{eff}	Effective Area	$80\ um^2$
β_2	GVD parameter	$-20\ ps^2/km$
n_2	Non Linear Index of Refraction	$26\times10^{-21}\ m^2/W$
L	SMF Length	80 Km

DISPERSION COMPENSATED FIBER (DCF) SPECIFICATION

D	Dispersion	$-100\ ps/km.nm$
A_{eff}	Effective Area	$12\ um^2$
α	Attenuation Coefficient	$0.5\ dB/Km$

The length ratio has been designed to compensate for the normal and anomalous dispersion regimes where the overall second-order dispersion is calculated to be zero. Since, SMF operating in the wavelength region $\lambda = 1550nm$, thus, an anomalous dispersion equivalent to $D = 16.75\ ps/km.nm$ is observed. Hence, adjustment in the DCF link length is employed in order for both fibers to compensate each other. The DCF exhibit dispersion equivalent to $D \geq 100\ ps/km.nm$. Figure 5.18 shows the system dispersion map employing post compensation on a span-by-span basis with an accumulated dispersion equivalent to 1340 ps/nm.

For 2-channel MMT, MZM extinction ratio have been optimized to 22dB, with a Bessel 1st order optical bandpass filter with cutoff frequency of= $2.1 \times Bitrate$ and 2nd order electrical low pass Gaussian filter with cutoff frequency= $1.2 \times Baudrate$. For 3-channel MMT, MZM extinction ratio has been optimized to 20 dB with a Bessel 2nd order optical band pass filter= $3 \times Baudrate$ and 2nd order electrical low pass Gaussian filter with cutoff frequency= $1.2 \times Baudrate$. For 4-channel MMT, MZM extinction ratio have been optimized to 22dB , with a Bessel 1st order optical bandpass filter= $2.1 \times Baudrate$ and 2nd order electrical low pass Gaussian filter with cutoff frequency= $1.2 \times Baudrate$.

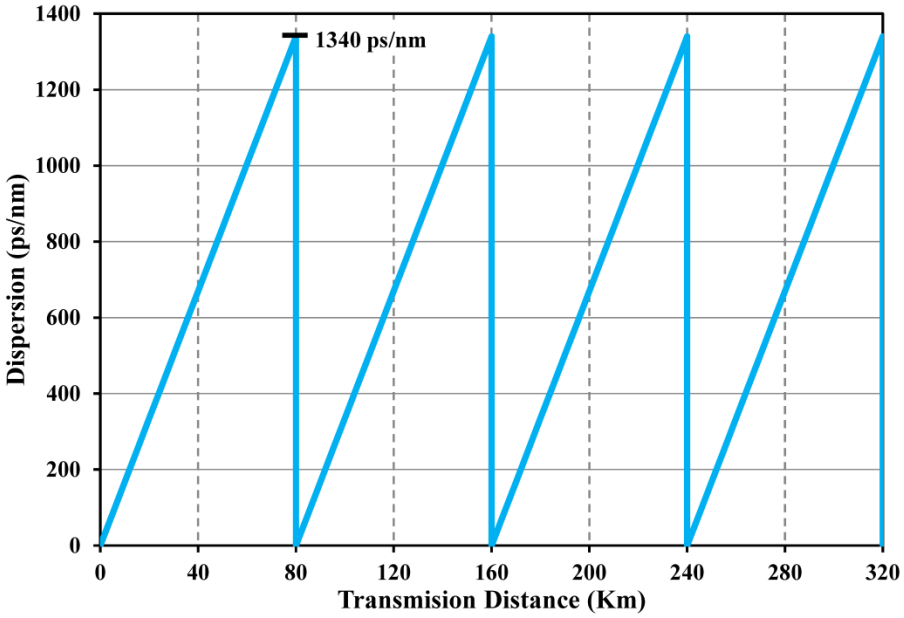

Figure 5.18 Dispersion map of post compensation configuration.

5.3.2.4 Post compensation Results

In order to quantify the system non-linear tolerance, the link launched optical power is increased continuously up till the non-linearity consequences are significant. This is apparent by noticing a degradation in the performance due to Kerr non-linear effect. A contour plot is a meaningful graphical representation for the relationship between three variable in two dimensions[216], [217]. In order to define the system best performance regions, a contour plot investigating the maximum Q-factor at an optimized fiber power region. The system Q-factor is calculated with the variation of both the input launched power to the SMF span ($P_{in,SMF}$) and the input propagated power in to the DCF ($P_{in,DCF}$). The horizontal and vertical axis correspond to variation in the launched power to the SMF ($P_{in,SMF}$) and DCF ($P_{in,SMF}$), respectively. In order to secure a reliable communication link, the transmission distance has been investigated over a maximum number of fiber spans in which the system attains a Q-factor ≥ 6 which corresponds to a system BER $\leq 10^{-9}$ [218].

Figure 5.19 shows the contour plot for 2-channel MMT at 40Gb/s over a transmission distance of 11x80Km equivalent to 880KM. 2-channel MMT exhibit a wide input power region in to the SMF for a Q-value of 6 where the input SMF power range from ~ -5 dBm to ~ 5 dBm. Also, contour plot shows two maximum Q-factor power regions. The first at $P_{in,SMF} = -3dBm$ and $P_{in,DCF} = -6dBm$. The maximum input SMF power have achieved a $P_{in,SMF} = 1dBm$ with $P_{in,DCF} = -7dBm$. Since the DCF fiber is designed to work in the normal dispersion region where the DCF is manufactured with an effective core area $\leq 20 \times 10^{-6} m^2$, while on the other hand the typical SMF effective area is in the range between $50 \times 10^{-6} m^2$ to $80 \times 10^{-6} m^2$ [110]. Hence, the impact of Kerr non-linearity effect on DCF will be larger than its counterpart in SMF, which is reflected on larger non-linear tolerance due to increasing the power on SMF $P_{in,SMF}$ compared with $P_{in,DCF}$.

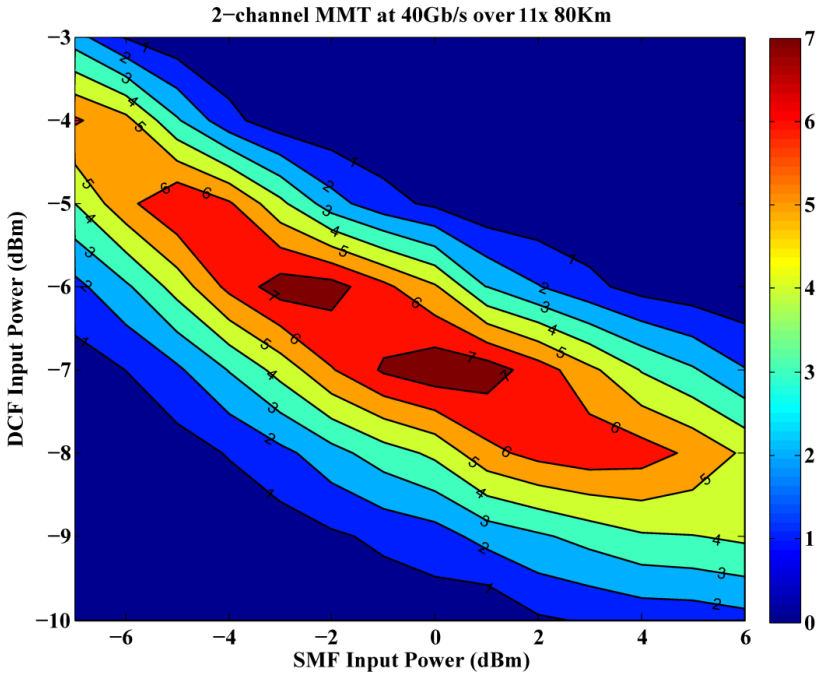

Figure 5.19 Contour plot at variable input power $P_{in,SMF}$ and $P_{in,DCF}$ for 2-channel MMT at 40Gb/s over 720 Km in a post compensation configuration

Figure 5.20 shows the contour plot for 3-channel MMT at 40Gb/s over a transmission distance of 3x80KM. At metro link equivalent to 240Km SMF transmission distance, 3-channel MMT system exhibits a wide power region for a Q-value of 6 where the input SMF power range from $-3dBm$ to $\approx 5.5dBm$. The system shows one tiny maximum Q-factor region at Q-factor=7, where $P_{in,SMF}$ is between $1dBm$ and $2dBm$ with $P_{in,DCF} = -8dBm$.

The reduced transmission distance compared to 2-channel MMT is mainly due to the nonlinear characteristics effects on signal format that governs its SPM nonlinear impact. This is aided by the fact of increasing the interplay between SPM and GVD in fiber with the already existing ASE noise. Also, the multilevel power penalty and the division of the main eye diagram into 4 small eye diagrams have induced different noise standard of deviation on each level eye.

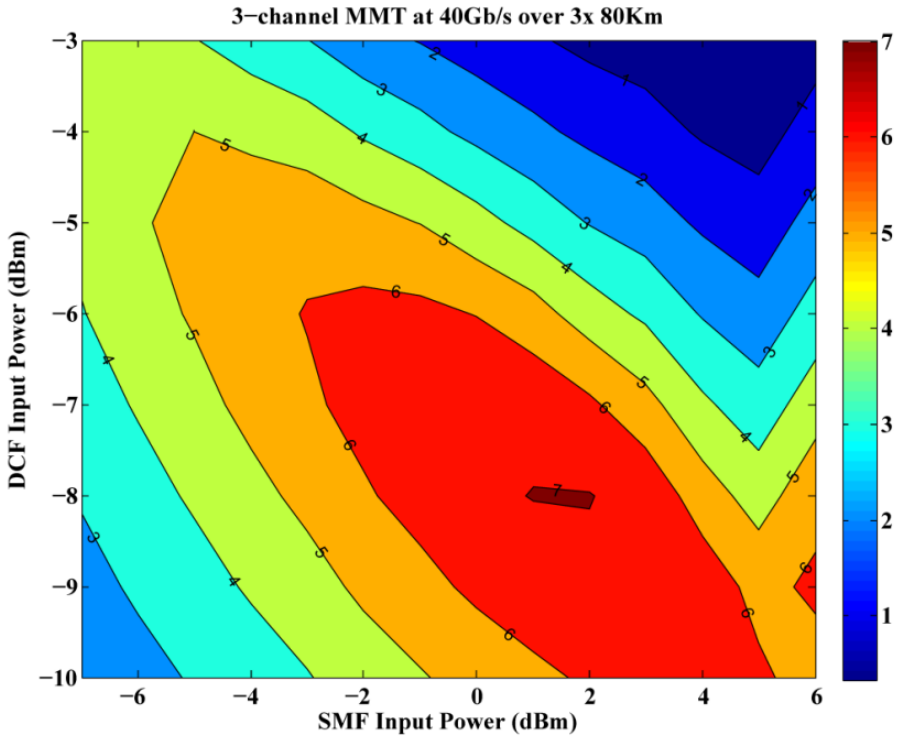

Figure 5.20 Contour plot at variable input power $P_{in,SMF}$ and $P_{in,DCF}$ for 3-channel MMT at 40Gb/s over 240 Km in a post compensation configuration.

Figure 5.21 shows the contour plot for 4-channel MMT at 40Gb/s over a transmission distance of 3x80Km. At metro link equivalent to 240Km SMF transmission distance, 4-channel MMT system exhibits a relatively less wide power region compared with 2-ch and 3-ch MMT for a Q-value of 6 where the input SMF power range from $-1dBm$ to $\approx 4dBm$. The system shows one tiny maximum Q-factor region at Q-factor=6.4 where $P_{in,SMF}$ is between $\approx 1dBm$ and $2dBm$ with $P_{in,DCF} = -7dBm$.

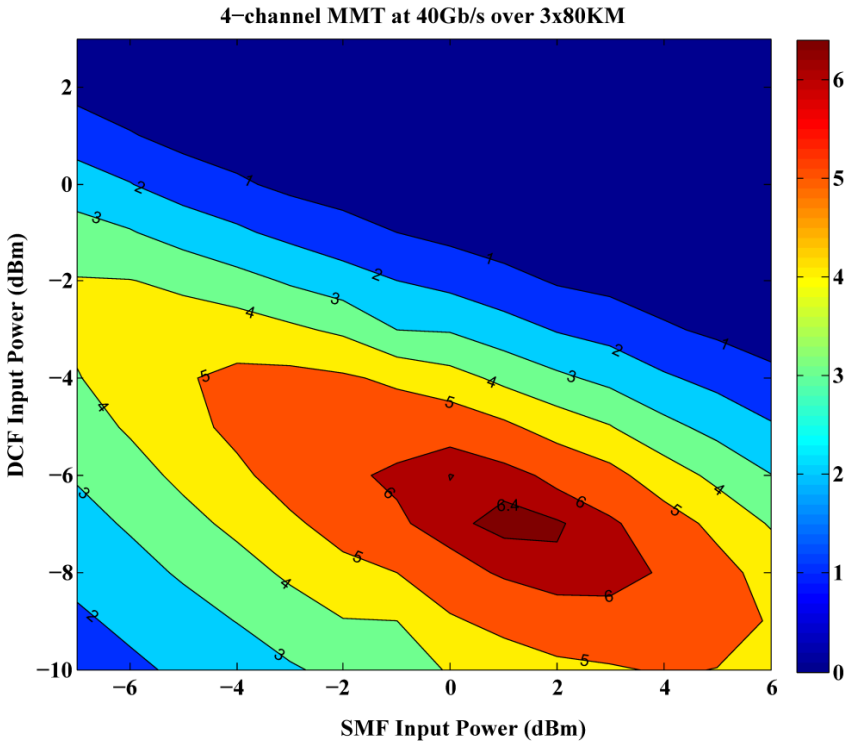

Figure 5.21 Contour plot at variable input power $P_{in,SMF}$ and $P_{in,DCF}$ for 4-channel MMT at 40Gb/s over 240 Km in a post compensation configuration.

Figure 5.22 shows the contour plot for 4-channel MMT at 100Gb/s over a transmission distance of 80Km. As shown, 4-channel MMT system exhibits a wide operating power region for both input power to SMF and DCF where for a Q-value of 7, the input SMF power range from $\approx 0 dBm$ to $\approx 4.5 dBm$ and the input DCF power range from $\approx -10 dBm$ to $\approx -1.5 dBm$. While, at Q-factor=6, the $P_{in,SMF}$ range between $\approx -2 dBm$ and $\approx 6.5 dBm$. However, this large dynamic range region of operation is on a tradeoff cost of limited transmission distance of 80Km. The higher the bit rate the smaller the pulse width which are more susceptible to inter symbol interference. 4-channel MMT system exhibits a relatively less wide power region compared with 2-ch and 3-ch MMT for a Q-value of 6 where the input SMF power range from $-1 dBm$ to $\approx 4 dBm$. The system shows one tiny maximum Q-factor region at Q-factor=6.4 where $P_{in,SMF}$ is between $\approx 1 dBm$ and $2 dBm$ with $P_{in,DCF} = -7 dBm$.

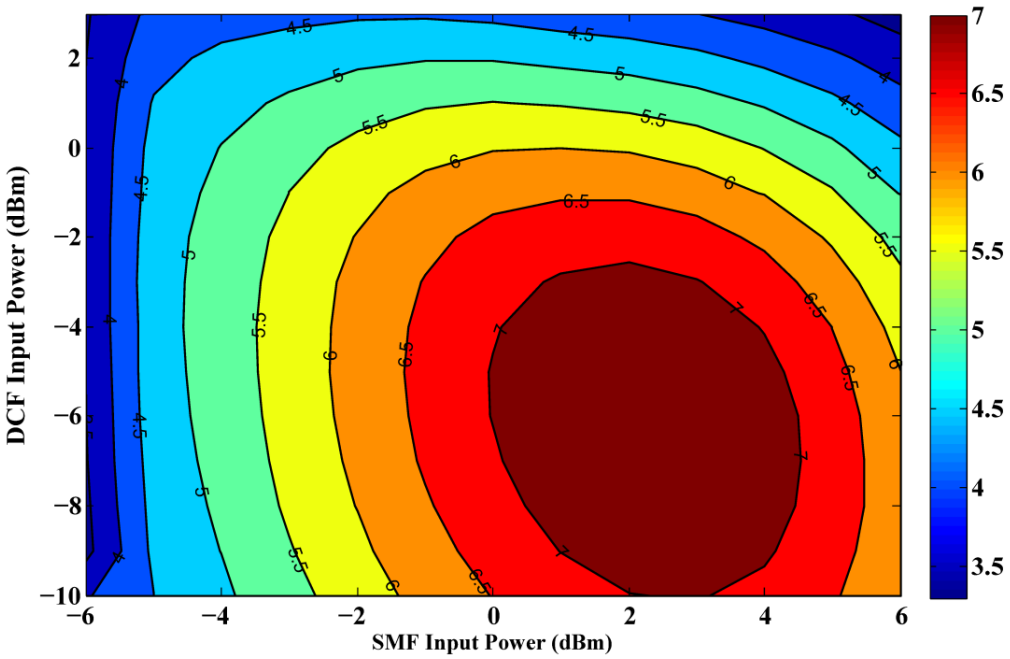

Figure 5.22 Contour plot at variable input power $P_{in,SMF}$ and $P_{in,DCF}$ for 4-channel MMT at 100Gb/s over 80 Km in a post compensation configuration.

Figure 5.23 shows the contour plot for 4-PAM contour plot at 40Gb/s over a transmission distance of 2x80Km. At metro link equivalent to 240Km SMF transmission distance, 4-PAM system exhibits a less maximum transmission compared with 4-ch MMT at the same spectral efficiency for a Q-value of 6 with power region ranging from an input SMF power between $\approx -1dBm$ to $\approx 4dBm$. The contour plot shows a maximum Q-factor region at Q-factor=6.5 where $P_{in,SMF}$ is between $\approx 0dBm$ and $3dBm$ with $P_{in,DCF}$ ranging between $\approx -7.6dBm$ to $\approx -5dBm$.

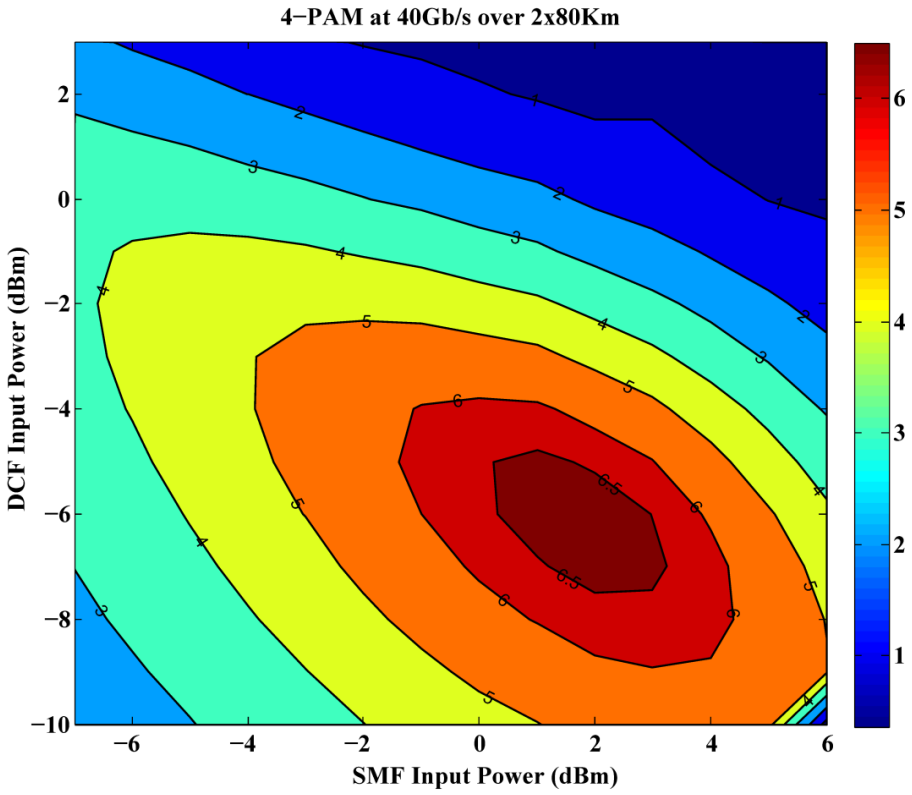

Figure 5.23 Contour plot at variable input power $P_{in,SMF}$ and $P_{in,DCF}$ for 4-PAM at 40Gb/s over 160 Km in a post compensation configuration.

5.3.2.5 Pre-Post Compensation System Setup

In this section, an investigation for the employment of pre-post dispersion compensation is presented. The employment of pre-post compensation scheme aims to enhance the transmission characteristics of modulation formats under study. Instead of compensating for all accumulated dispersion in a 100% post setup, pre-post configuration involves applying pre- and post-compensation modules before and after the SMF transmission on a span by span basis.

System setup of pre-post compensation have been shown in figure 5.24 with the same settings as figure 5.17 except with an optimized pre-post compensation settings of 2.4Km dispersion pre compensation DCF module and 11 Km dispersion post compensation DCF module. The pre- and post-dispersion distances have been selected based upon an optimization process for the lowest BER. The effect of SPM is neglected in the DCF as the input power into the DCF is fixed to -7dBm. Figure 5.25 shows the system pre-post dispersion map. The dispersion pre-compensation module accounts for -240 ps/nm, while the dispersion post compensation module for 1100 ps/nm, in which both are equivalent to the total dispersion of 1340 ps/nm.

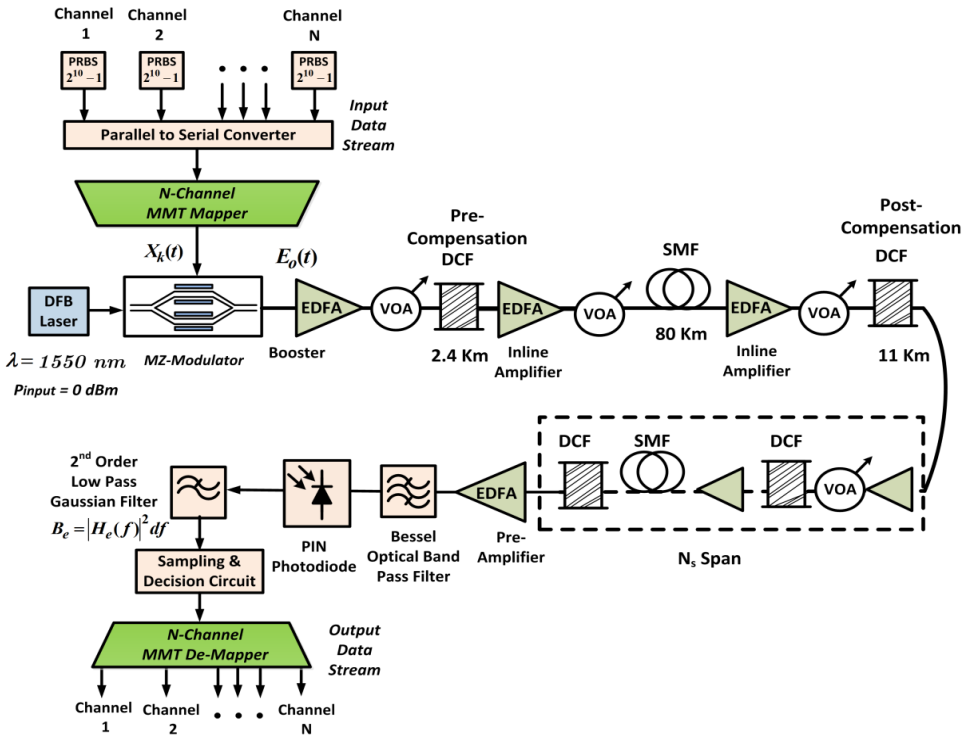

Figure 5.24 Transmission setup in pre-post compensation configuration used for the investigations of maximum fiber reach and optimized power settings at fixed $P_{in,DCF}$.

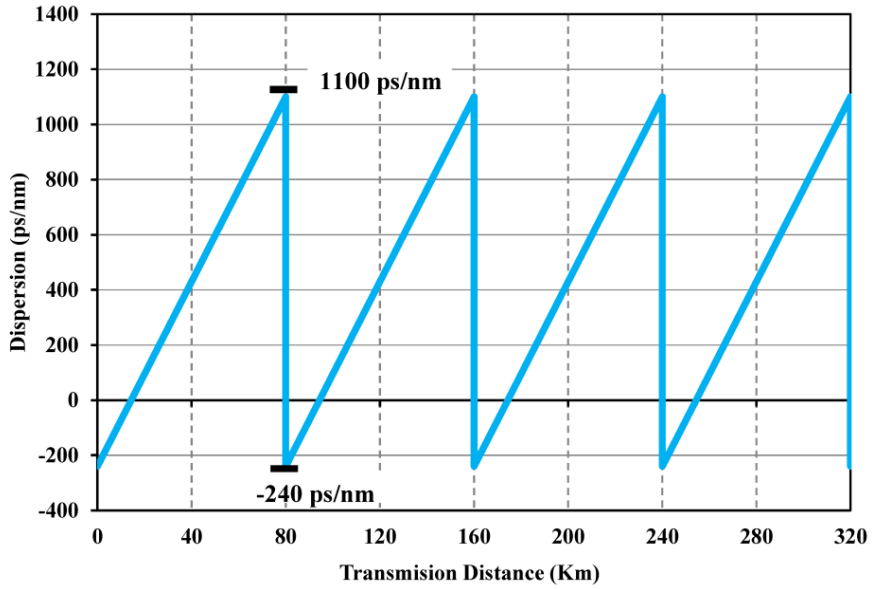

Figure 5.25 Dispersion map of pre-post compensation configuration.

5.3.2.6 Performance comparison between Post and Pre-post Compensation Results

In this section, performance evaluation comparison has been carried between N-channel MMT and 4-PAM, in the presence of a post and pre-post dispersion compensation techniques. The investigation has been carried by examining the maximum performance input power to the SMF that enables a better characterization for the transmission behavior, thus, enable increased system tolerance to nonlinear impairments. The tolerance can be translated to a longer fiber in the presence of non-linear impairments added to it linear impairments.

Although, the system performance has been investigated over multiple N_s spans at an acceptable reliable transmission equivalent to $\mathrm{BER} \leq 10^{-9}$. However, the transmission reach exhibit longer distance by considering the addition of a Forward Error Correction (FEC) module in which the FEC BER limit is $=10^{-3}$ [219].

5.3.2.6.1 2-Channel MMT at 40Gb/s and 100Gb/s

For 2-channel MMT, figure 5.26 shows the BER dependence on launched power at variable transmission distances in a post compensation and pre-post compensation design configuration at 40Gb/s and 100Gb/s. The SPM in the DCF can be neglected since the launched power has been optimized, fixing it to -7 dBm.

At 40 Gb/s, 2-channel MMT system has been investigated over 880Km, 960 Km, 1040Km, 1200Km, 1280Km and 1360Km transmission distances in a post compensation configuration. Figure 5.26(a) shows 2-channel MMT exhibiting a maximum transmission distance equivalent to 960 Km (12x80Km) with an input SMF power $P_{in,SMF}$=0 dBm at acceptable BER data transmission.

On the other hand, by having a pre-post compensation configuration, with transmission distances of 1040Km, 1200 Km, 1360Km, 1520Km, 1680Km and 1840Km, the maximum performance has been shifted to be +1 dBm with an increased reach of 1200Km (15x80Km) at an acceptable BER data transmission.

At 100 Gb/s, 2-channel MMT system has been investigated over 480Km, 560 Km, 640Km, 720Km and 800Km transmission distances in a post compensation configuration. Figure 5.26(b) shows 2-channel MMT exhibits a maximum transmission distance equivalent to 480 Km (6x80Km) with an input SMF power $P_{in,SMF}$=1 dBm at error free transmission ($BER \leq 10^{-9}$). At 100 Gb/s, pre-post compensation does not observe an enhancement in performance except for shifting the maximum input power to +2dBm (this result is discussed in *section 5.3.2.7.1*).

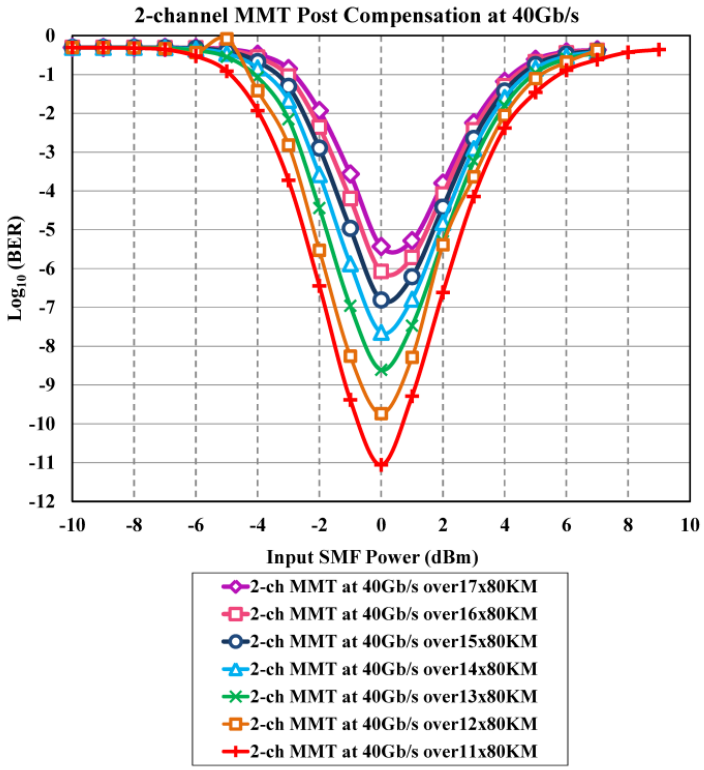

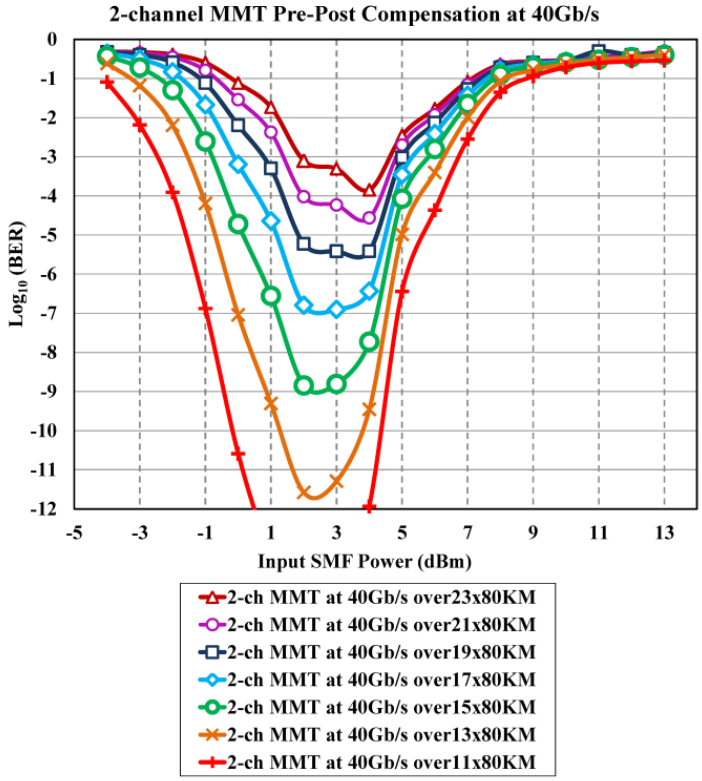

(a)2-channel MMT at 40Gb/s Post-compensation and Pre-Post Compensation

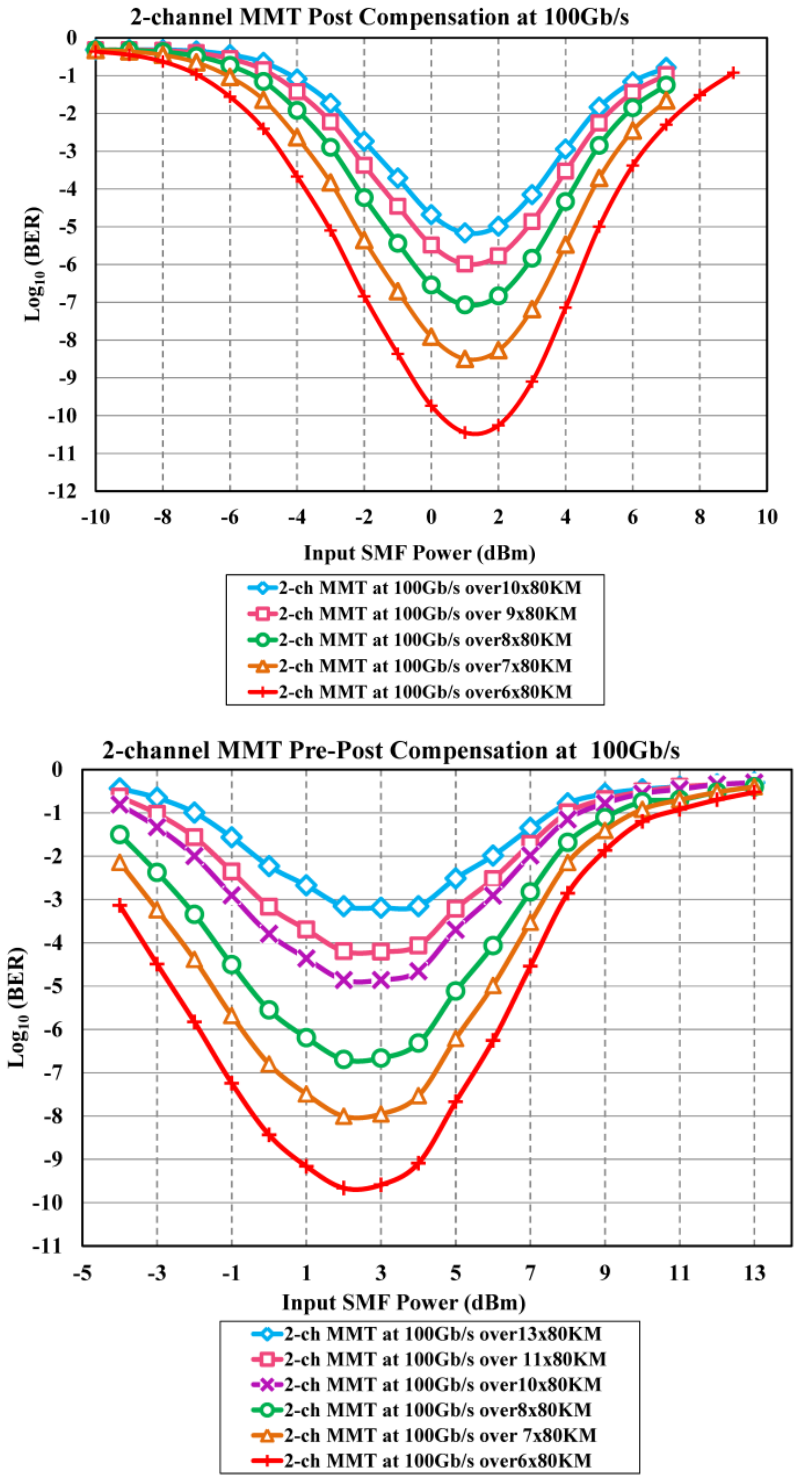

(b) 2-ch MMT at 100Gb/s Post-compensation and Pre-Post Compensation

Figure 5.26 BER as a function of the launch power for 2-channel MMT over multiple span distances in both post and pre-post compensation configurations at (a)40 Gb/s and (b) 100Gb/s.

5.3.2.6.2 3-Channel MMT at 40Gb/s and 100Gb/s

For 3-channel MMT, figure 5.27 shows the BER dependence on launched power at variable transmission distances in a post compensation and pre-post compensation design configuration at 40Gb/s and 100Gb/s. The SPM in the DCF can be neglected since the launched power has been optimized, fixing it to -6.8 dBm.

At 40 Gb/s, 3-channel MMT system has been investigated over 240KM, 320KM, and 400KM transmission distances in a post compensation configuration. Figure 5.27(a) shows 3-channel MMT exhibiting a maximum transmission distance equivalent to 240 Km (3x80Km) with an input SMF power $P_{in,SMF}$=0 dBm at acceptable reliable transmission of ($BER \leq 10^{-9}$). On the other hand, by having a pre-post compensation configuration, with transmission distances of 240Km, 320Km, 400Km, and 480Km, the maximum performance has been shifted to be +1 dBm with an increased reach of 320Km (4x80Km) at an acceptable reliable transmission of ($BER \leq 10^{-9}$).

At 100 Gb/s, 3-channel MMT system has been investigated over 160Km, 240Km and 320Km transmission distances in a post compensation configuration. Figure 5.27(b) shows 2-channel MMT exhibiting a maximum transmission distance equivalent to 160 Km (2x80Km) with an input SMF power $P_{in,SMF}$=2 dBm at acceptable reliable transmission of ($BER \leq 10^{-9}$). At 100 Gb/s, pre-post compensation does not exhibit an enhancement in performance except for shifting the maximum input power to +3dBm.

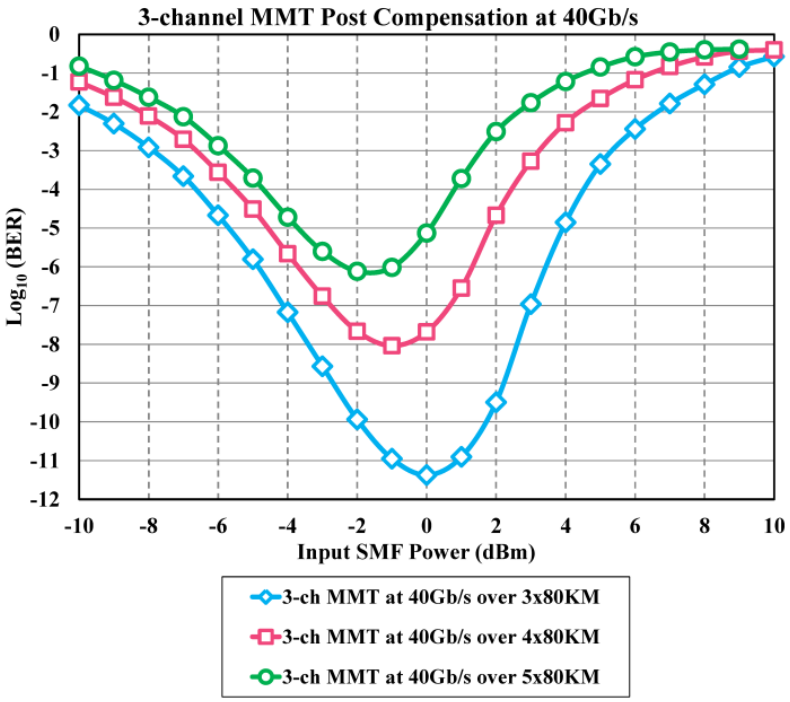

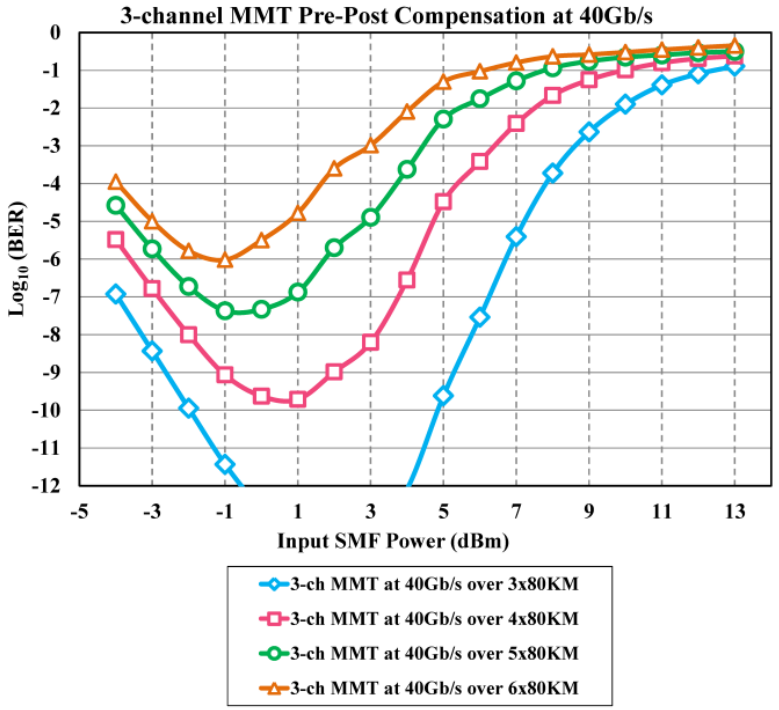

(a)3-channel MMT at 40Gb/s Post-compensation and Pre-Post Compensation

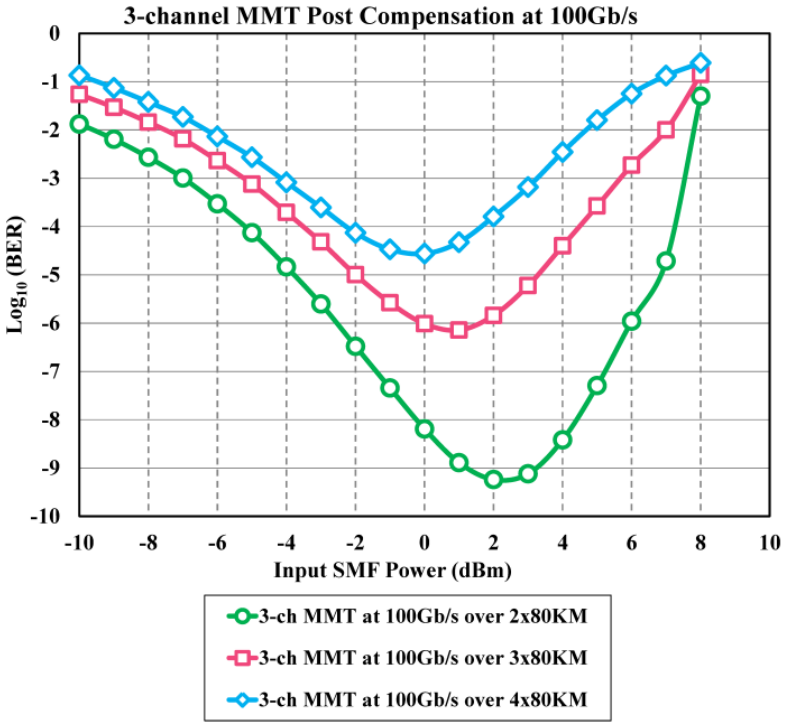

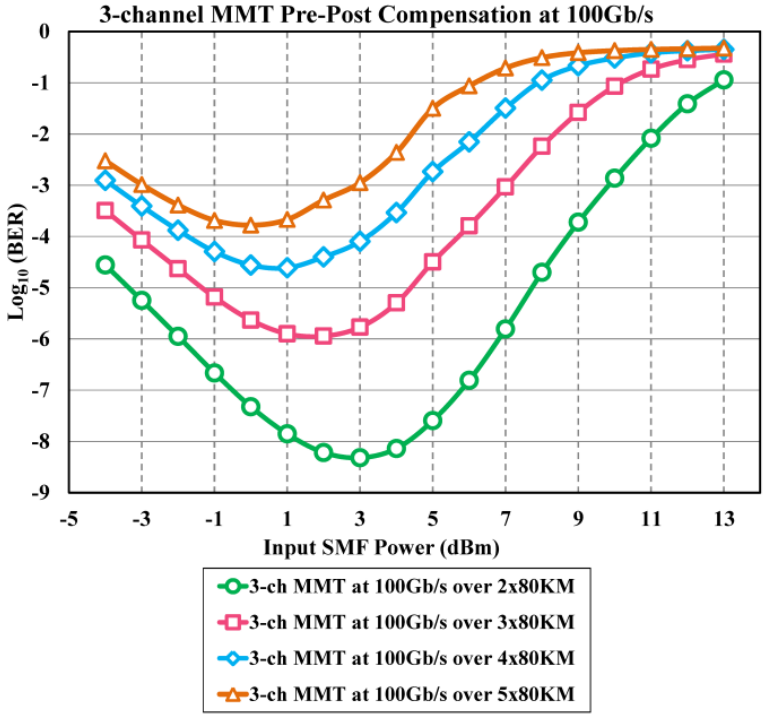

(b)3-ch MMT at 100Gb/s Post-compensation and Pre-Post Compensation

Figure 5.27 BER as a function of the launched power for 3-channel MMT over multiple span distances in both post and pre-post compensation configurations at (a)40 Gb/s and (b) 100Gb/s.

5.3.2.6.3 4-Channel MMT at 40Gb/s and 100Gb/s

For 4-channel MMT, figure 5.28 shows the BER dependence on launched power at variable transmission distances in a post compensation and pre-post compensation design configuration at 40Gb/s and 100Gb/s. The SPM in the DCF can be neglected since the launched power has been optimized, fixing it to -7 dBm.

At 40 Gb/s, 4-channel MMT system has been investigated over 160Km, 240Km, 320 Km, 400Km and 480Km transmission distances in a post compensation configuration. Figure 5.28(a) shows 4-channel MMT exhibiting a maximum transmission distance equivalent to 240 Km (3x80Km) with an input SMF power $P_{in,SMF}$=1 dBm at at acceptable reliable transmission ($BER \leq 10^{-9}$). On the other hand, by having a pre-post compensation configuration, with transmission distances of 240Km, 320Km, 400 Km, 480Km, 560Km and 640Km, the maximum performance has been shifted 3dB to be +4 dBm with an increased reach of error free transmission to 320Km (4x80Km).

At 100 Gb/s, 4-channel MMT system has been investigated over 80Km, 160 Km, 240Km, 320Km and 400Km transmission distances in a post compensation configuration. Figure 5.28(b) shows 4-channel MMT exhibiting a maximum transmission distance equivalent to 80 Km (1x80Km) with an input SMF power $P_{in,SMF}$=2 dBm at acceptable reliable transmission of($BER \leq 10^{-9}$). While, pre-post compensation at 100Gb/s with transmission distances of 160 Km, 240Km 320Km and 400Km show a relatively better performance with a maximum performance shifted 2dB to be $P_{in,SMF}$=+4dBm with an increased reach equivalent to 160Km (2x80Km).

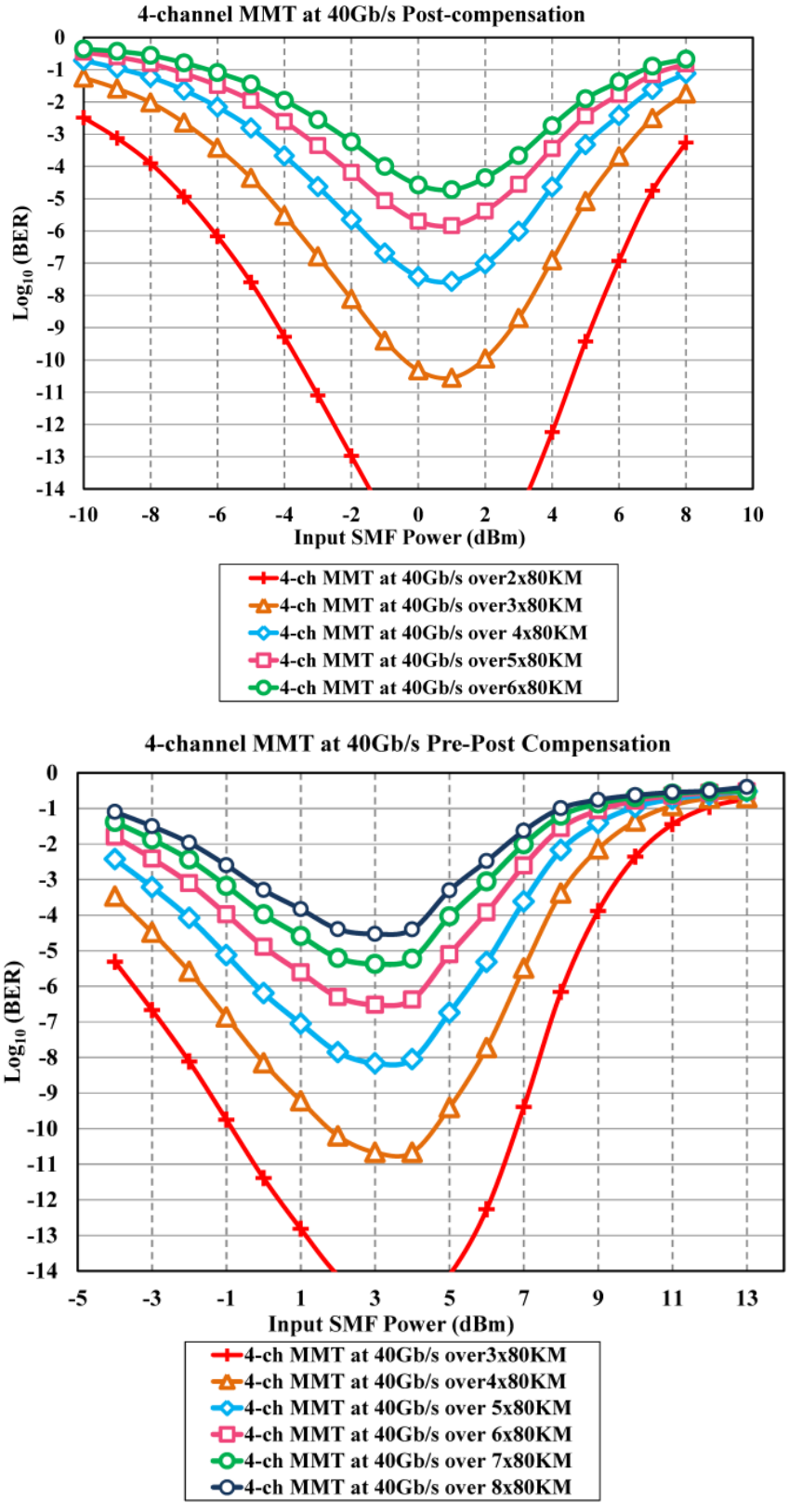

(a)4-channel MMT at 40Gb/s Post-compensation and Pre-Post Compensation

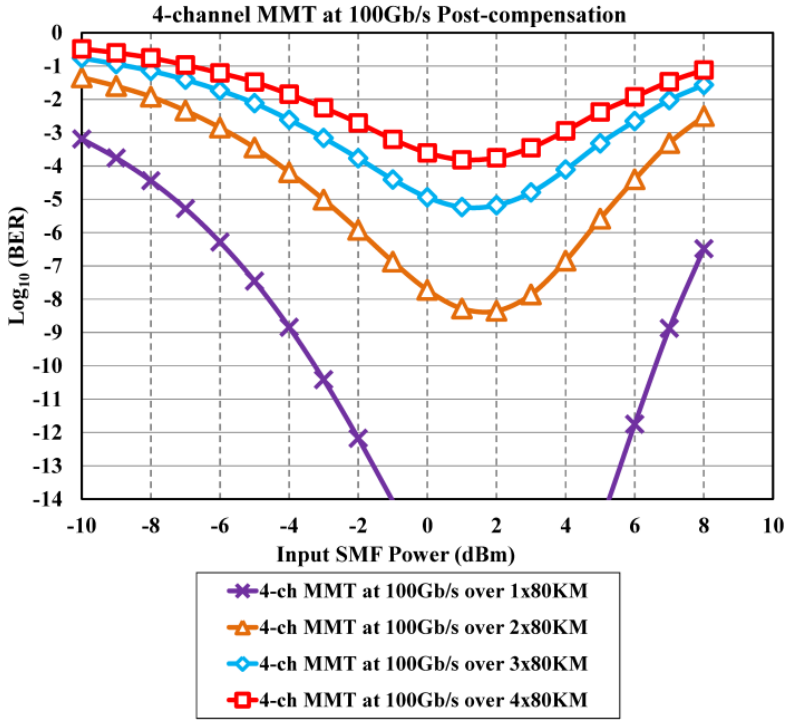

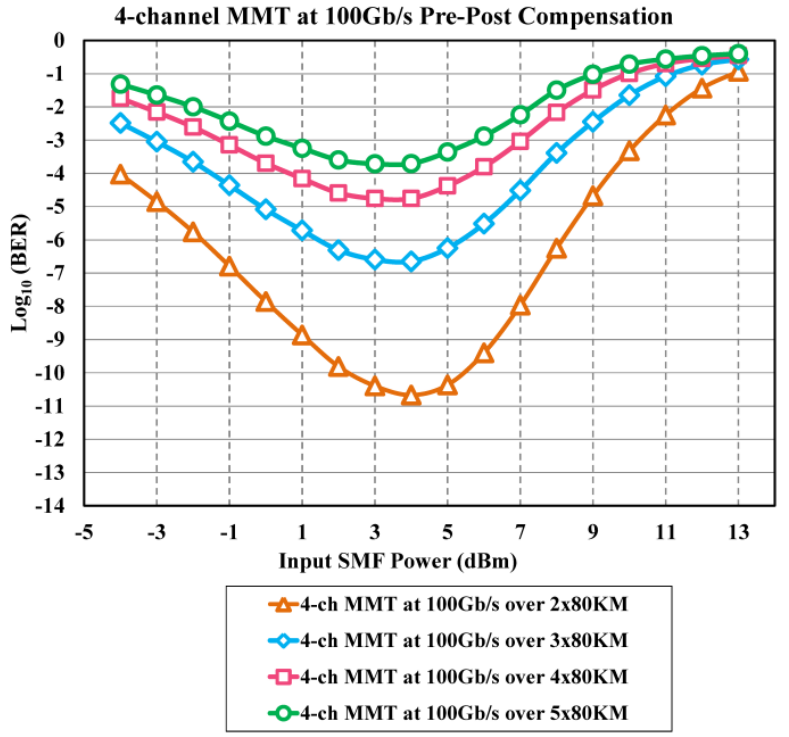

(b) 4-ch MMT at 100Gb/s Post-compensation and Pre-Post Compensation

Figure 5.28 BER as a function of the launched power for 4-channel MMT over multiple span distances in both post and pre-post compensation configurations at (a)40 Gb/s and (b) 100Gb/s.

5.3.2.6.4 4-PAM at 40Gb/s and 100Gb/s

For 4-PAM, figure 5.29 shows the BER dependence on launched power at variable transmission distances in a post compensation and pre-post compensation design configuration at 40Gb/s and 100Gb/s. The SPM in the DCF can be neglected since the launched power has been optimized, fixing it to -7 dBm.

At 40 Gb/s, 4-PAM system has been investigated over 80Km, 160Km, 240Km, 320 Km, 400Km and 480Km transmission distances in a post compensation configuration. Figure 5.29(a) shows 4-channel MMT exhibiting a maximum transmission distance equivalent to 160 Km (2x80Km) with an input SMF power $P_{in,SMF}$=1 dBm at acceptable reliable transmission of ($BER \leq 10^{-9}$). On the other hand, by having a pre-post compensation configuration, with transmission distances of 240Km, 320Km, 400 Km, 480Km and 560Km, the maximum performance has been shifted 3dB to be +4 dBm with an increased reach equivalent to 240Km (3x80Km).

At 100 Gb/s, 4-PAM system has been investigated over 80Km, 160 Km, 240Km, and 320Km transmission distances in a post compensation configuration. Figure 5.29(b) shows 4-PAM exhibiting a maximum transmission distance equivalent to 80 Km (1x80Km) with an input SMF power $P_{in,SMF}$=4 dBm at acceptable reliable transmission of ($BER \leq 10^{-9}$). At 100 Gb/s, pre-post compensation does not exhibit an enhancement in performance.

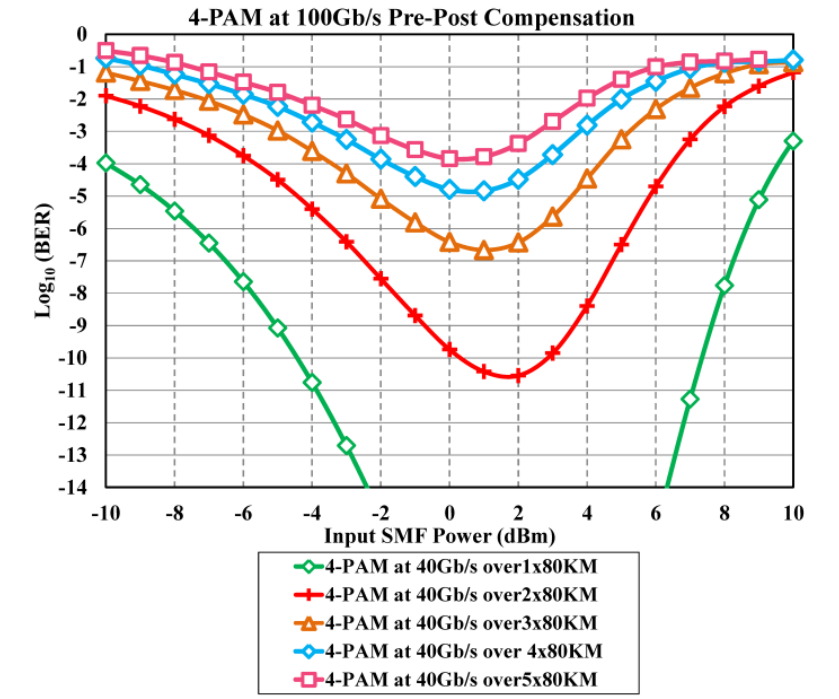

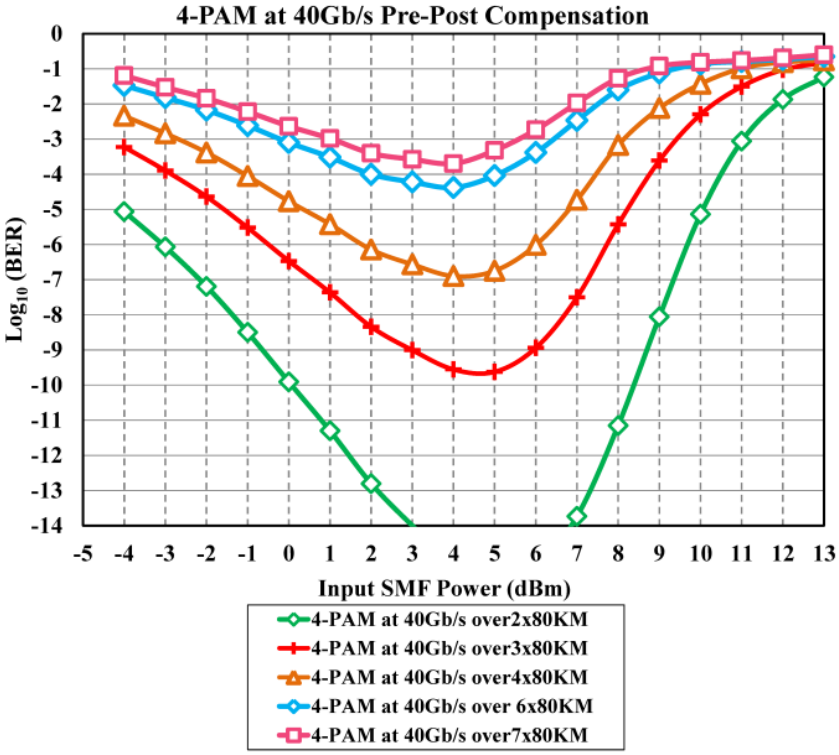

(a) 4-PAM at 40Gb/s Post-compensation and Pre-Post Compensation

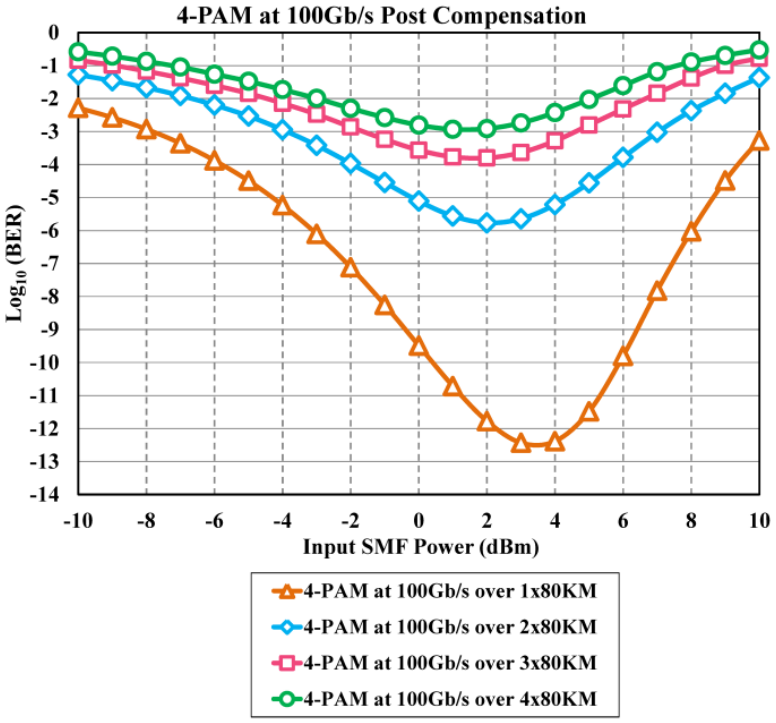

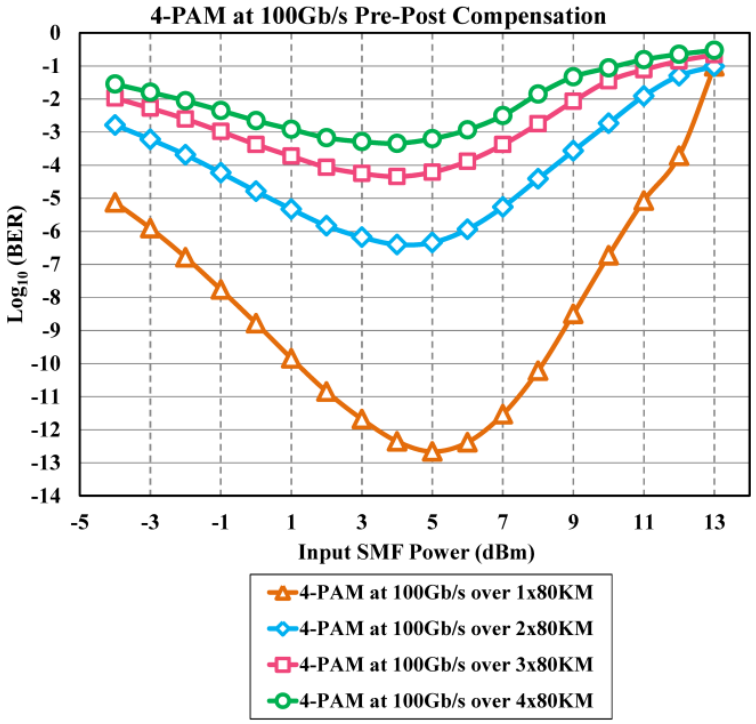

(b)4-PAM at 100Gb/s Post-compensation and Pre-Post Compensation

Figure 5.29 BER as a function of the launched power for 4-PAM over multiple span distances in both post and pre-post compensation configurations at (a)40 Gb/s and (b) 100Gb/s.

5.3.2.6.5 Discussion on Results

From the results of N-channel MMT and 4-PAM modulation format non-linear tolerance to SPM in addition to ASE and GVD. The curves are symmetrical around the optimal maximum performance input power over various distances in which the system nonlinear tolerance is defined. With the increase in the input power to the SMF, the non-linear effects of SPM accumulate and degradation in the system BER is observed.

For 40Gb/s systems, N-channel MMT and 4-PAM pre-post compensation setup have exhibited better tolerance when compared with 100% fully post compensation in which the performance of the maximum input power is increased and shifted to higher levels. This is reflected in increasing the error free fiber reach. The result was expected and the reason is due to the existence of a combination between chromatic dispersion and SPM, in anomalous dispersion regime where $\beta_2 \prec 0$, SPM induced chirp produce new frequency component, which is red shifted in the leading edge and blue shifted in the tailing pulse edges. Since red frequency components have a higher velocity than the blue components. Thus, the effect of GVD and SPM accumulate, leading to fasten the rate of pulse broadening when compared with the effect of GVD pulse broadening only; which is the case when full post compensation is employed. However, in normal dispersion region where $\beta_2 \succ 0$, the GVD chirp is negative while the SPM induced chirp is positive. This leads to pulse compression and thus leading to less pulse broadening; which is the case when the pre-compensation DCF module has been employed.

For 100Gb/s aggregated bit rate systems, although the systems are operating in a baud rates of 20G, 33.3G, 25G and 50G baud/sec for 2-channel MMT, 3-channel MMT, 4-channel MMT and 4-PAM, respectively, however, this high speed rates impose more dominance of intra-channel non-linearity factors. This lead the pulse to be influenced by nonlinear pulse inter-symbol-interference, timing jitter and amplitude jitter[89], [220], [221].

The impact of intra-channel non-linearity is strongly dependent on the system bitrate[55]. Accordingly, pre-post compensation of 100Gb/s systems has not depicted a performance enhancement, except for a relatively better BER result for 4-channel MMT as shown in figure 5.28(b). Intra-channel non-linearities are divided in to Intra-channel Cross Phase Modulation (IXPM) and Intra-channel Four Wave Mixing (IFWM), which interplay with SPM degrading the system performance.

5.3.2.7 IFWM and IXPM Investigation

In order to elaborate more on the IFWM and IXPM phenomenon, figures 5.30-5.38 show eye diagram comparison at different increasing input power values between two configurations, first in which GVD and ASE noise exist but with disabled SPM effect. The second is a system with SPM enabled coupled with all other linear impairments (GVD and ASE). It is clear from the eye diagram that with increasing the input power from 0 dBm to 6 dBm, the eye diagram performance degrades suffering from a clear timing jitter between the dual N-channel slots. The input power to the DCF has been chosen according to the defined contour plot power regions in figure 5.22 and figure 5.23. This is due to the impact of IXPM combined with SPM. Also, it is evident that at the same power regions, eye diagrams showed a degradation in performance for systems in which SPM is enabled, this degradation is noticeable with amplitude ghost fluctuations, which can be reasoned to the impact of IFWM effect.

IFWM and IXPM have direct proportionality with increasing the system baud rate. This is due to the reduction in pulse width, which induces a rise in waveform amplitude jitter. Moreover, multiple level formats suffer from amplitude fluctuations in all levels, which cause more eye closure, thus, reducing the Q-factor. This can be verified by observing the eye diagrams at 40Gb/s and 100Gb/s. Although, at 40Gb/s the implication discussed for the IFWM and IXPM exists, however, it is not dominant as its counterpart at aggregated bit rate of 100Gb/s.

It is worth noting that by comparison between 4-channel MMT and 4-PAM at both the same spectral efficiency and aggregated bit rate, 4-channel MMT shows a better non-linear tolerance. This can be justified by 4-channel MMT baud rate advantage, where 4-channel MMT operate at half the baud rate compared with 4-PAM. At 40Gb/s and 100 Gb/s aggregated system bit rates, 4-channel MMT exhibit 10Gbaud/sec and 25Gbaud/sec, while 4-PAM operate with 20Gbaud/sec and 50Gbaud/sec, respectively.

Since the nonlinear Kerr effect, which occurs due to increasing the input power, is polarization dependent. Hence, a solution is proposed to suppress Kerr non-linearity effect and thus, reducing the impact of IXPM and IFWM. The method is based upon the transmission of adjacent bits in alternate polarizations [222]. This technique has been reported enhancing the eye diagram by reducing the amplitude fluctuations and timing jitter.

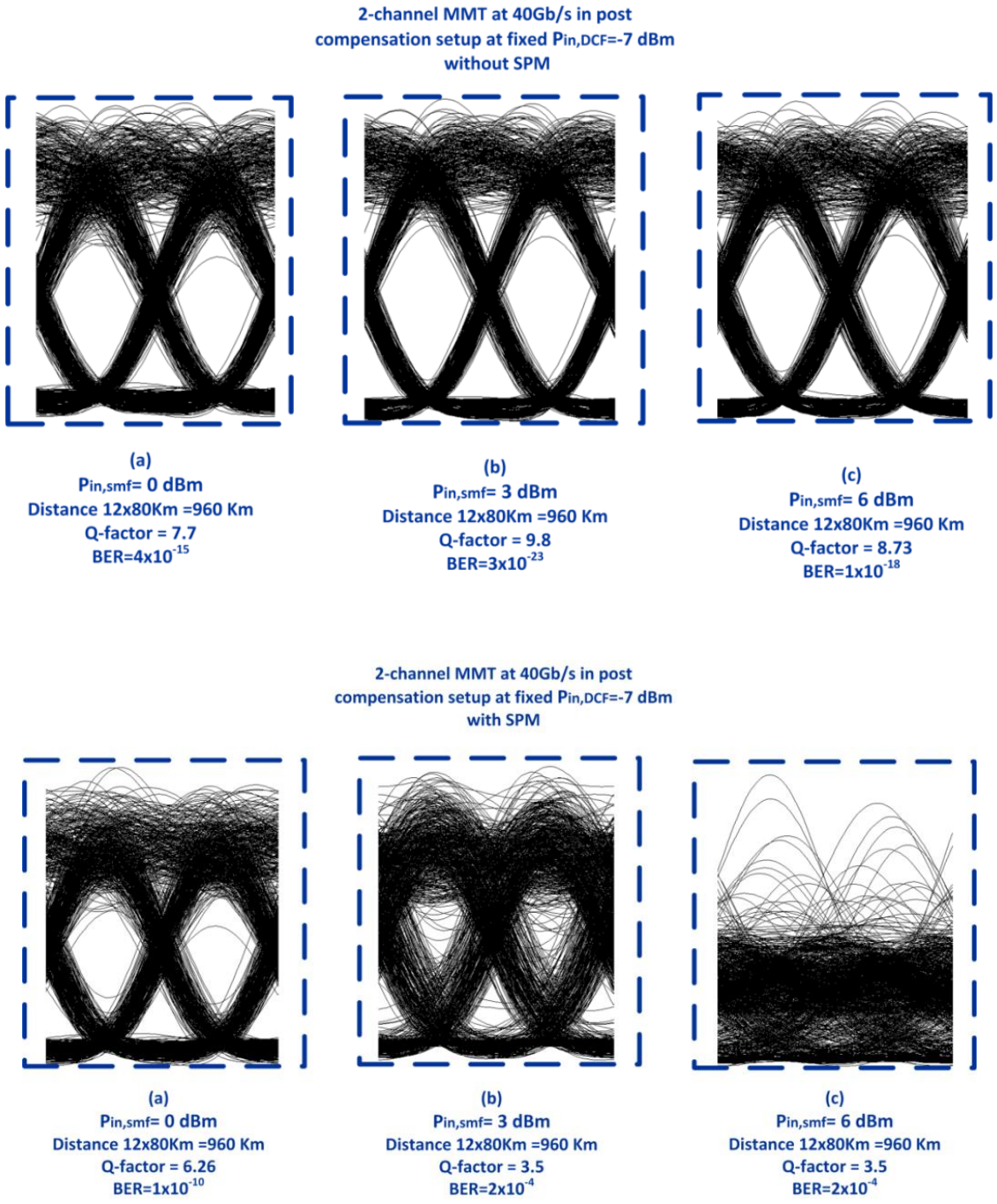

Figure 5.30 Eye diagrams comparison at 40Gb/s between 2-channel MMT in a configuration without enabling the SPM effect and with SPM enabled at various input SMF power at fixed (a) $P_{in,SMF} = 0dBm$, (b) $P_{in,SMF} = 3dBm$ and (c) $P_{in,SMF} = 6dBm$.

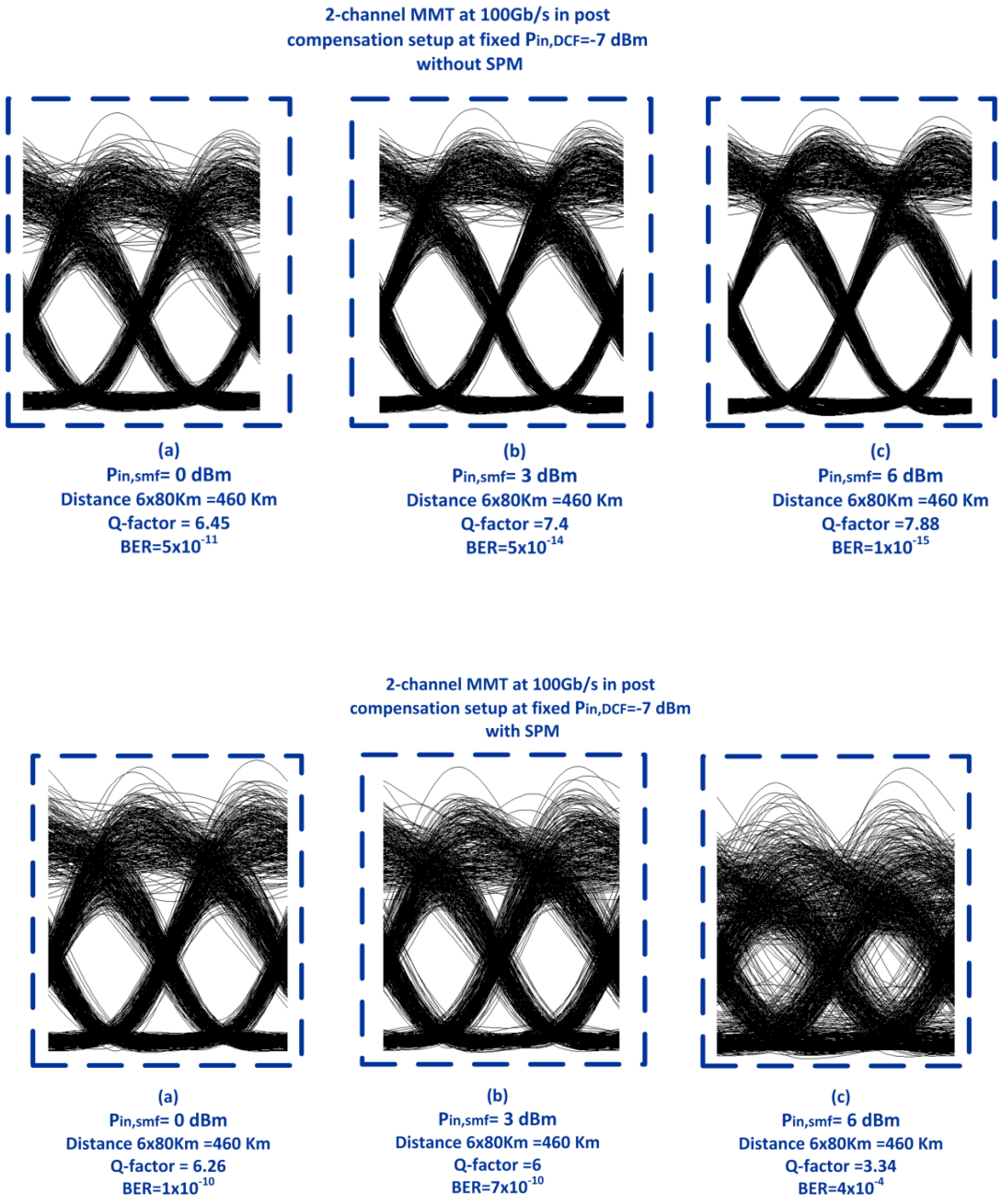

Figure 5.31 Eye diagrams comparison at 100Gb/s between 2-channel MMT in a configuration without enabling the SPM effect and with SPM enabled at various input SMF power at fixed (a) $P_{in,SMF} = 0dBm$, (b) $P_{in,SMF} = 3dBm$ and (c) $P_{in,SMF} = 6dBm$.

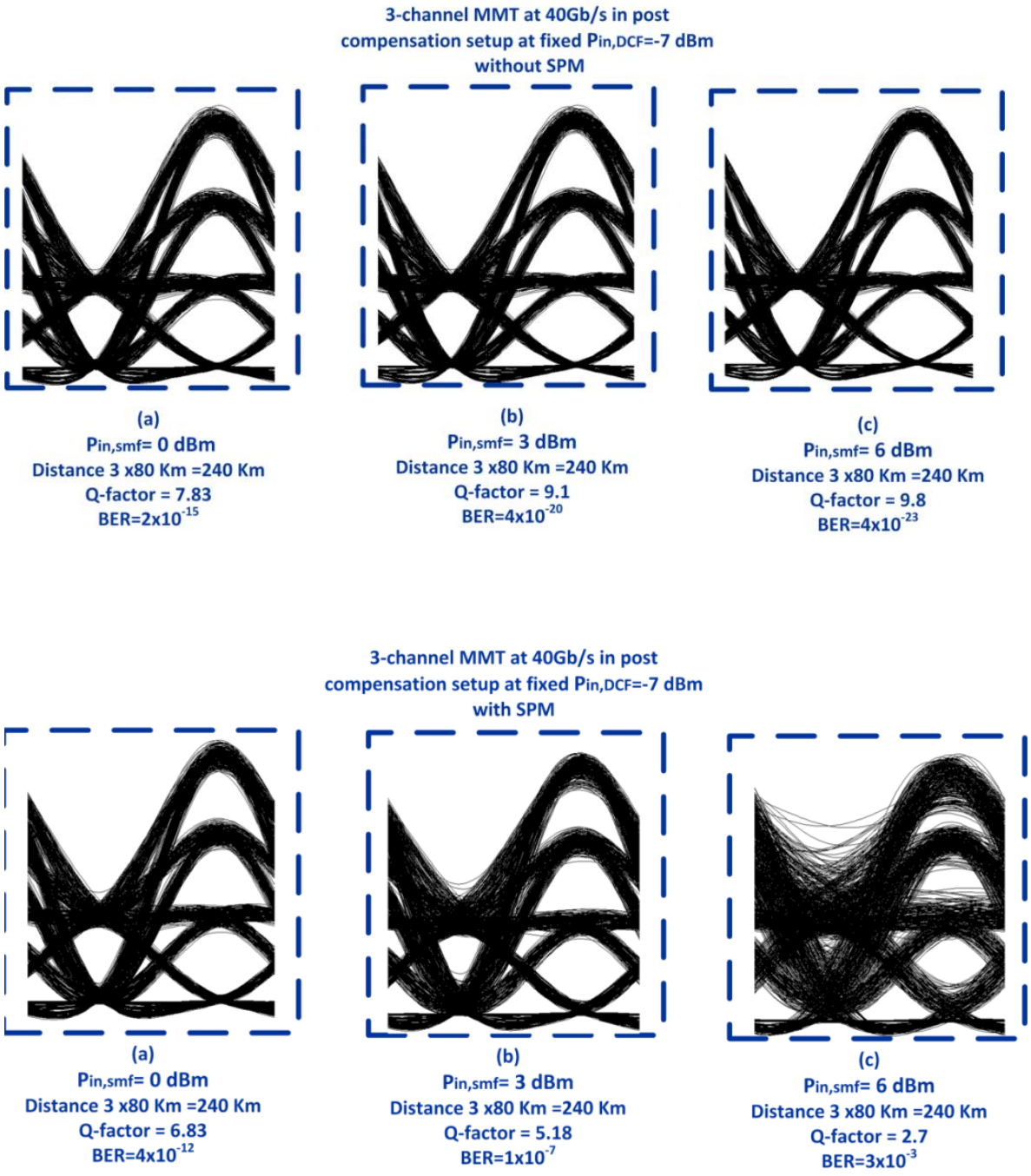

Figure 5.32 Eye diagrams comparison at 40Gb/s between 3-channel MMT in a configuration without enabling the SPM effect and with SPM enabled at various input SMF power at fixed (a) $P_{in,SMF} = 0dBm$, (b) $P_{in,SMF} = 3dBm$ and (c) $P_{in,SMF} = 6dBm$.

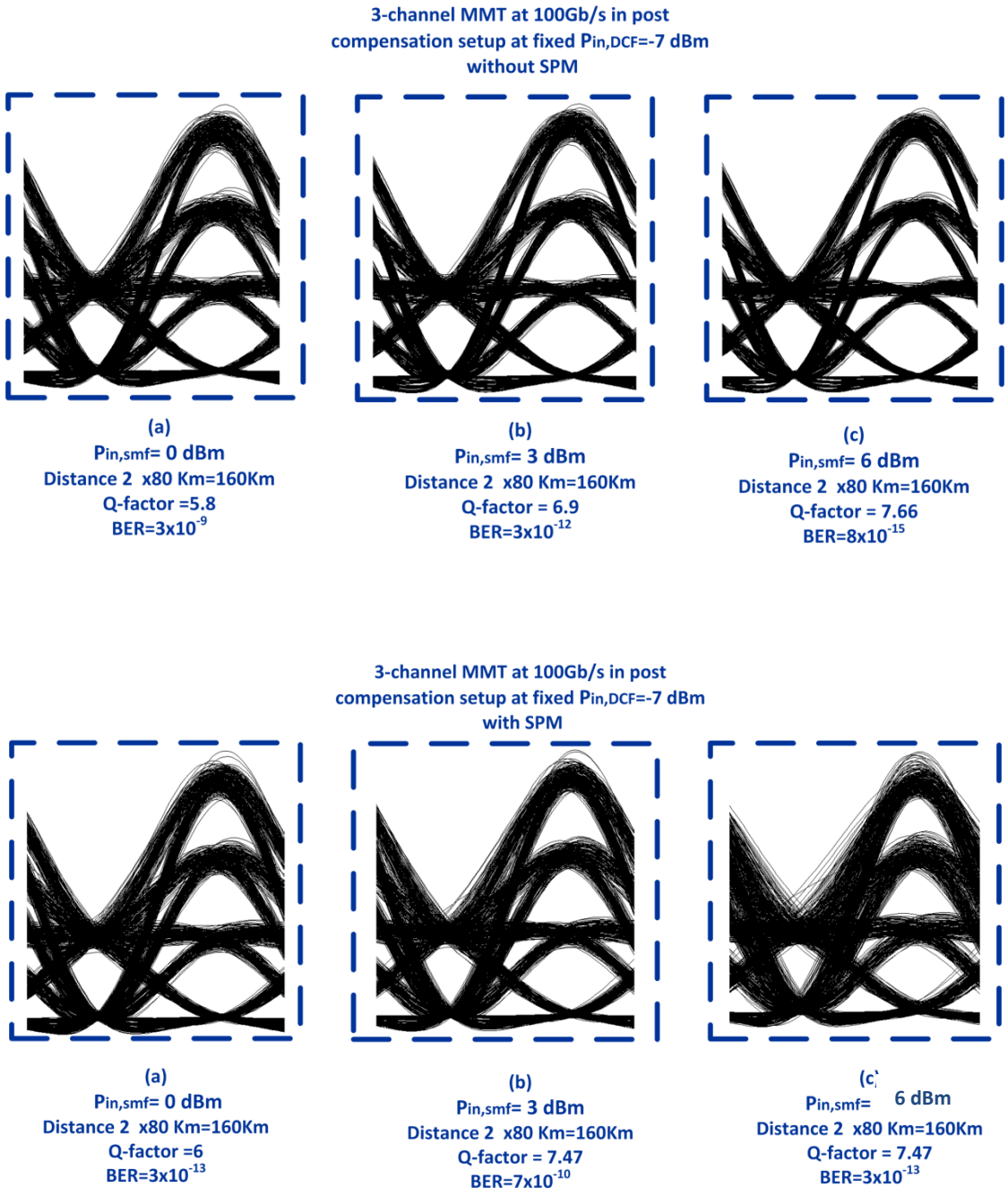

Figure 5.33 Eye diagrams comparison at 100Gb/s between 3-channel MMT in a configuration without enabling the SPM effect and with SPM enabled at various input SMF power at fixed(a) $P_{in,SMF} = 0dBm$, (b) $P_{in,SMF} = 3dBm$ and (c) $P_{in,SMF} = 6dBm$.

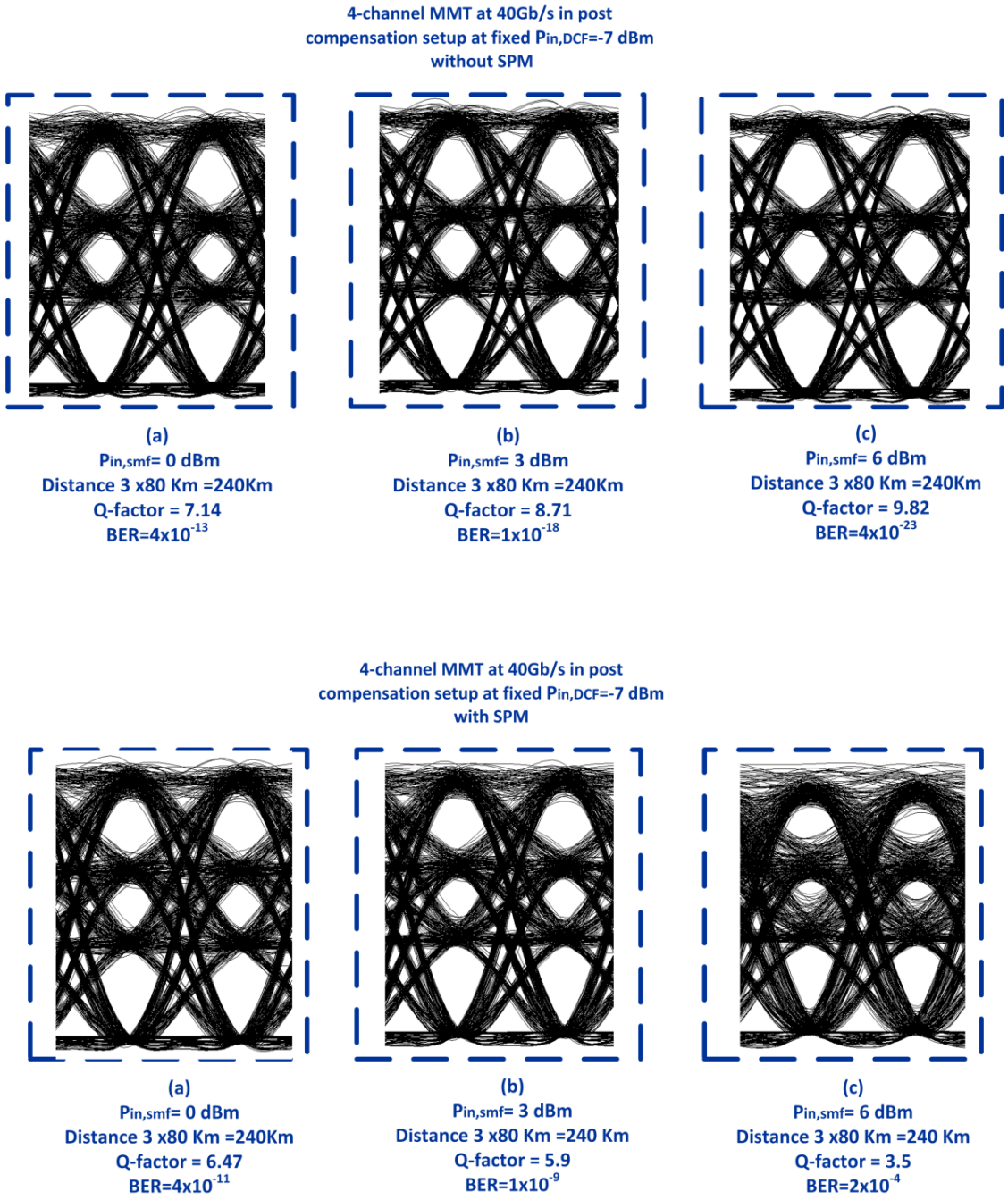

Figure 5.34 Eye diagrams comparison at 40Gb/s between 4-channel MMT in a configuration without enabling the SPM effect and with SPM enabled at various input SMF power at fixed (a) $P_{in,SMF} = 0dBm$, (b) $P_{in,SMF} = 3dBm$ and (c) $P_{in,SMF} = 6dBm$.

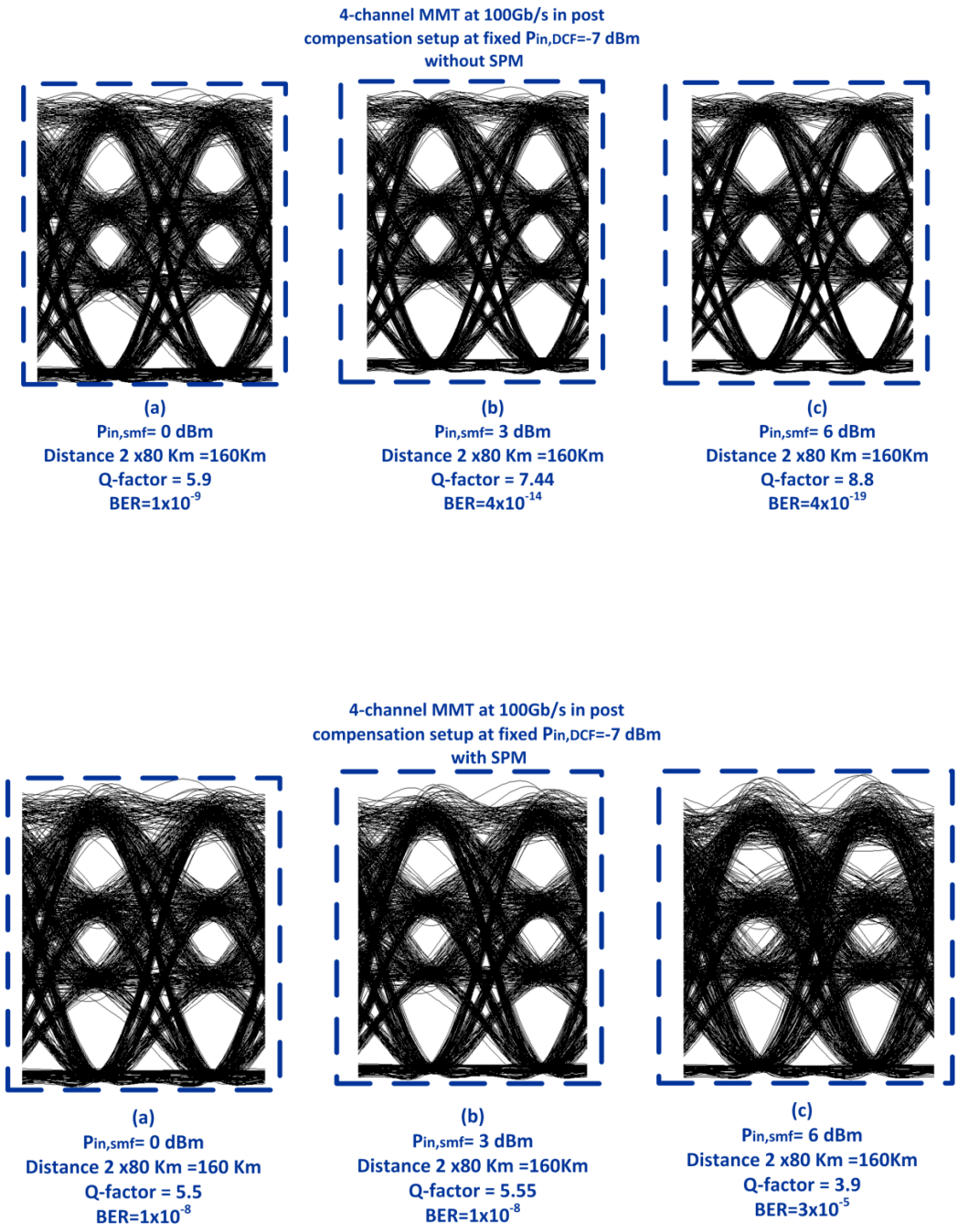

Figure 5.35 Eye diagrams comparison at 100Gb/s between 4-channel MMT in a configuration without enabling the SPM effect and with SPM enabled at various input SMF power at fixed (a) $P_{in,SMF} = 0dBm$, (b) $P_{in,SMF} = 3dBm$ and (c) $P_{in,SMF} = 6dBm$.

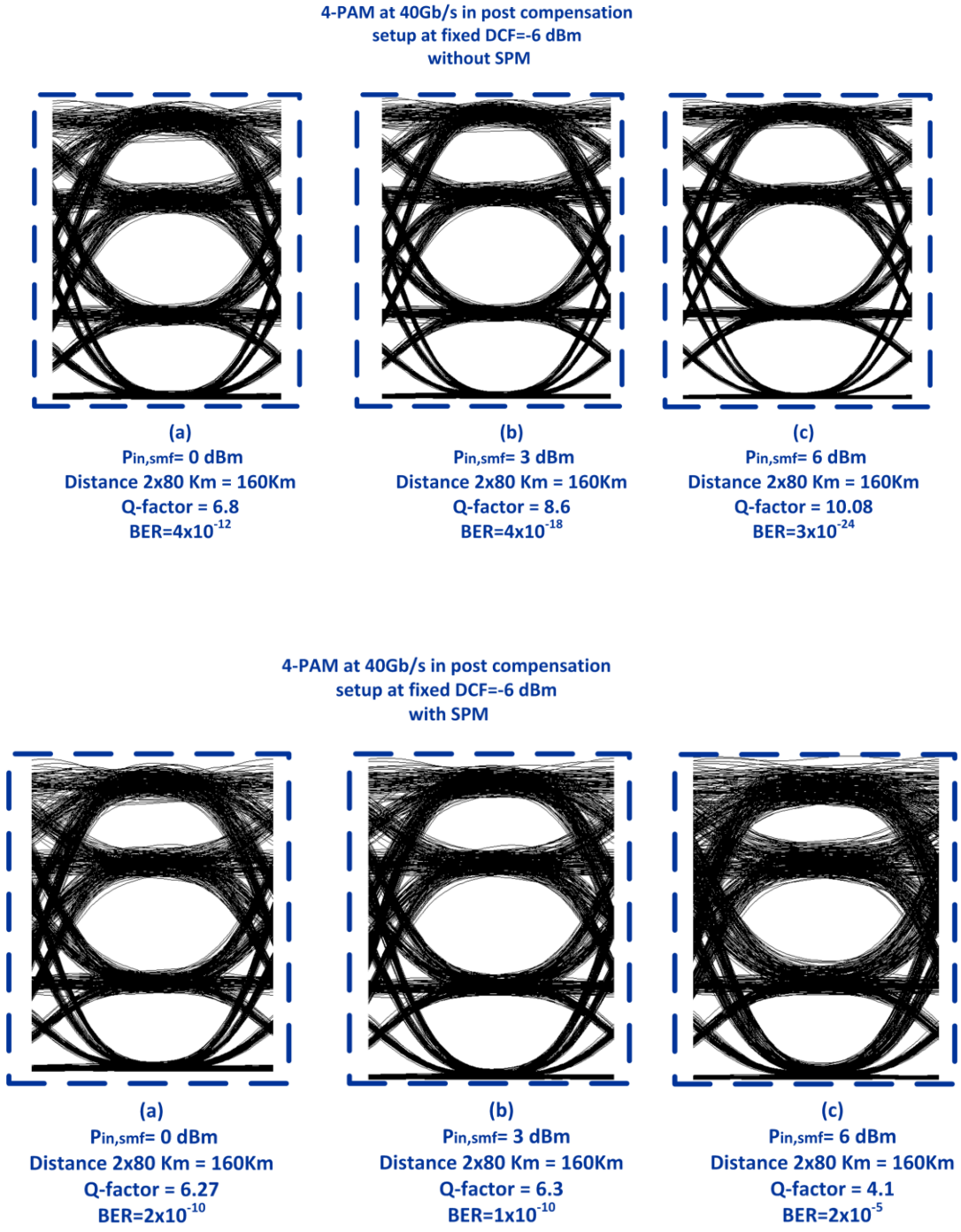

Figure 5.36 Eye diagrams comparison at 40Gb/s between 4-PAM in a configuration without enabling the SPM effect and with SPM enabled at various input SMF power at fixed,(a) $P_{in,SMF} = 0dBm$, (b) $P_{in,SMF} = 3dBm$ and (c) $P_{in,SMF} = 6dBm$.

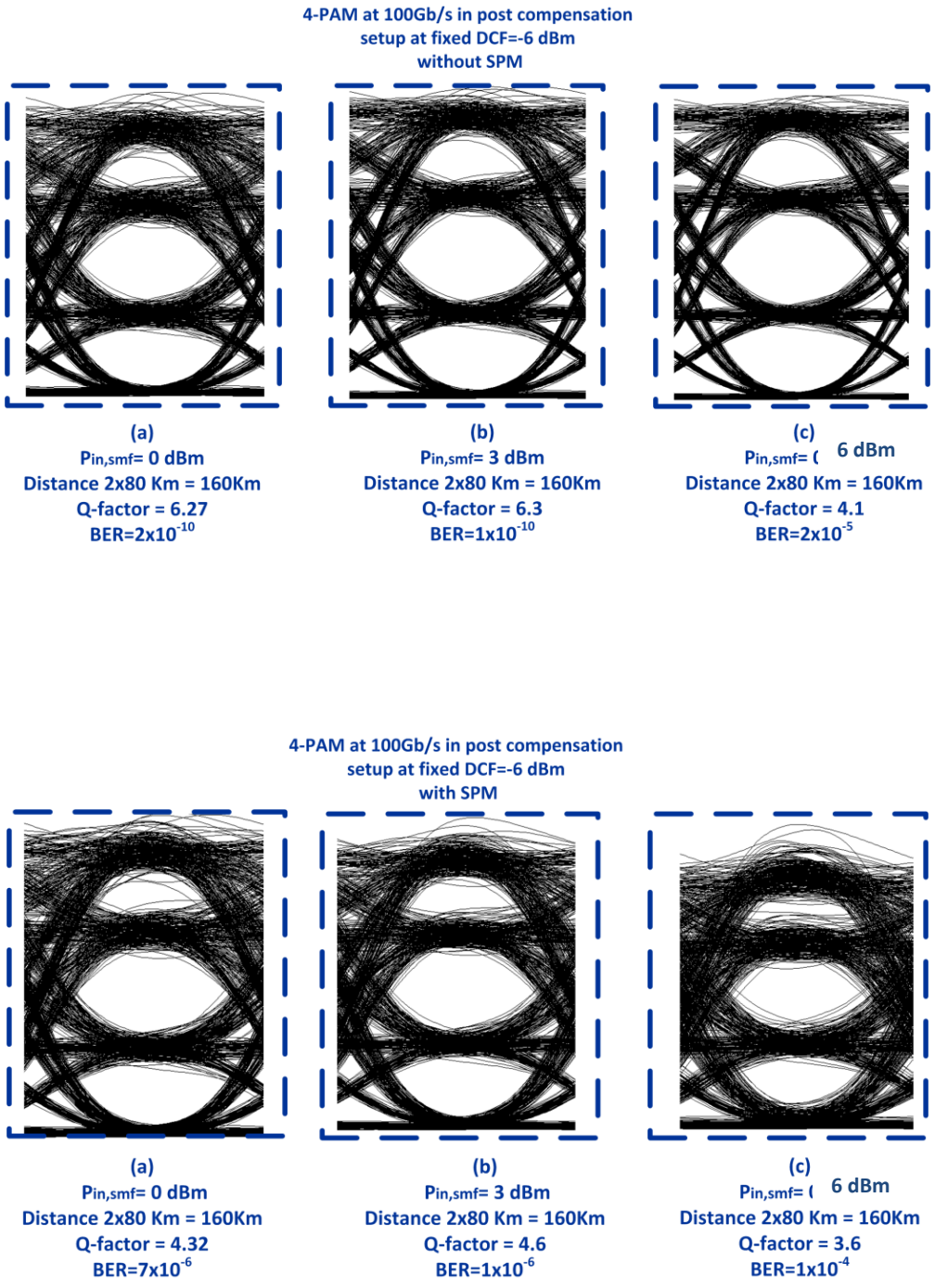

Figure 5.37 Eye diagrams comparison at 100Gb/s between 4-PAM in a configuration without enabling the SPM effect and with SPM enabled at various input SMF power at fixed, (a) $P_{in,SMF} = 0dBm$, (b) $P_{in,SMF} = 3dBm$ and (c) $P_{in,SMF} = 6dBm$.

5.3.2.8 MMT Maximum Reach for Metro Networks

In this section, the maximum system reach is identifyed and compared between 2-, 3-, 4-channel MMT and 4-PAM at 40Gb/s and 100Gb/s for metro-networks. The maximum transmission system reach can be defined as the link SMF transmission length in which the system obtain an acceptable reliable transmission at a Q-factor ≥ 5.9 equivalent to $\mathrm{BER} \leq 10^{-9}$. By applying forward error correction (FEC) codes and dispersion electronic equalization, a coding gain can be attained by reducing the signal to noise ratio required to attain a $\mathrm{BER} = 10^{-9}$ requirement and thus, increasing the maximum reach distance.

Figure 5.38 and figure 5.40 compare the relative performance of 2-, 3-, 4-channel MMT and 4-PAM with respect to the maximum reliable data transmission at 40Gb/s and 100Gb/s, respectively. In order to highlight the optical signal to Noise Ratio effect in obtaining a maximum transmission, figure 5.39 and figure 5.41 shows the corresponding OSNR requirement for variable number of spans transmission distances at 40Gb/s and 100Gb/s, respectively. The design setup is following the pre-post design, configuration due to its optimal performance, which is translated into maximization for the transmission reach, as discussed earlier.

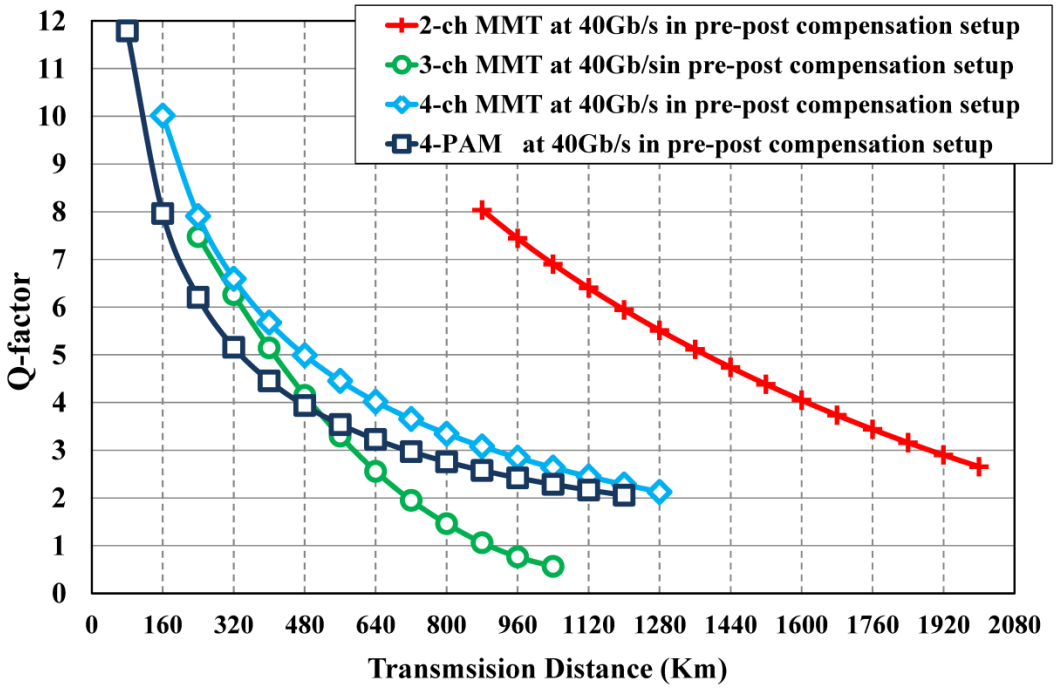

Figure5.38 Q-factor performance of N-channel MMT and 4-PAM as a function of the transmission distance at 40Gb/s aggregated bit rate.

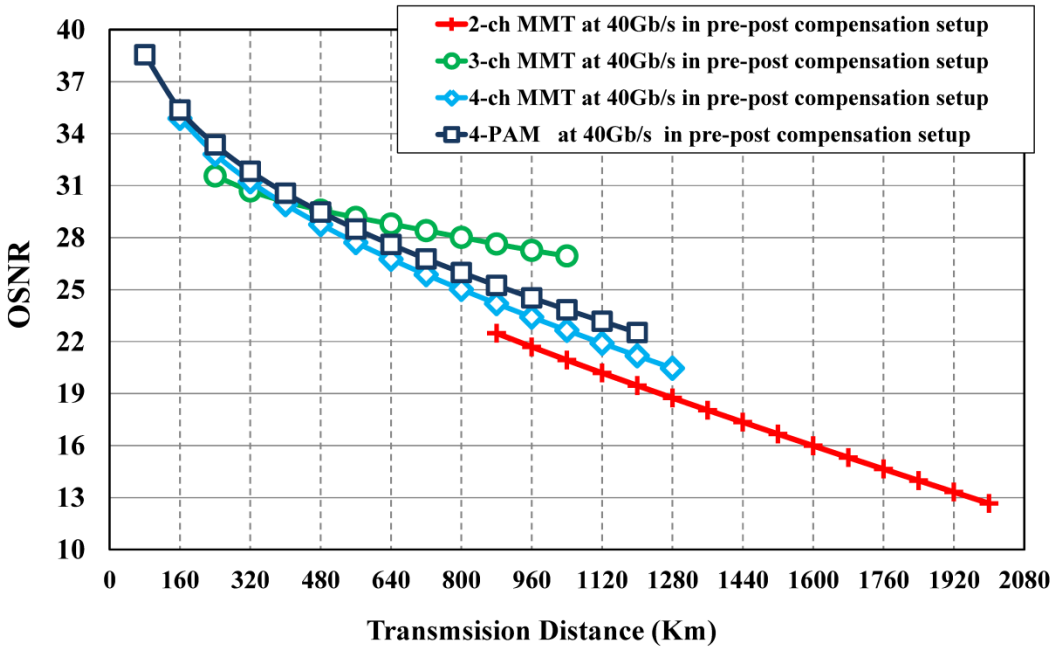

Figure 5.39 OSNR requirement of N-channel MMT and 4-PAM at variable transmission distances at 40Gb/s aggregated bit rate.

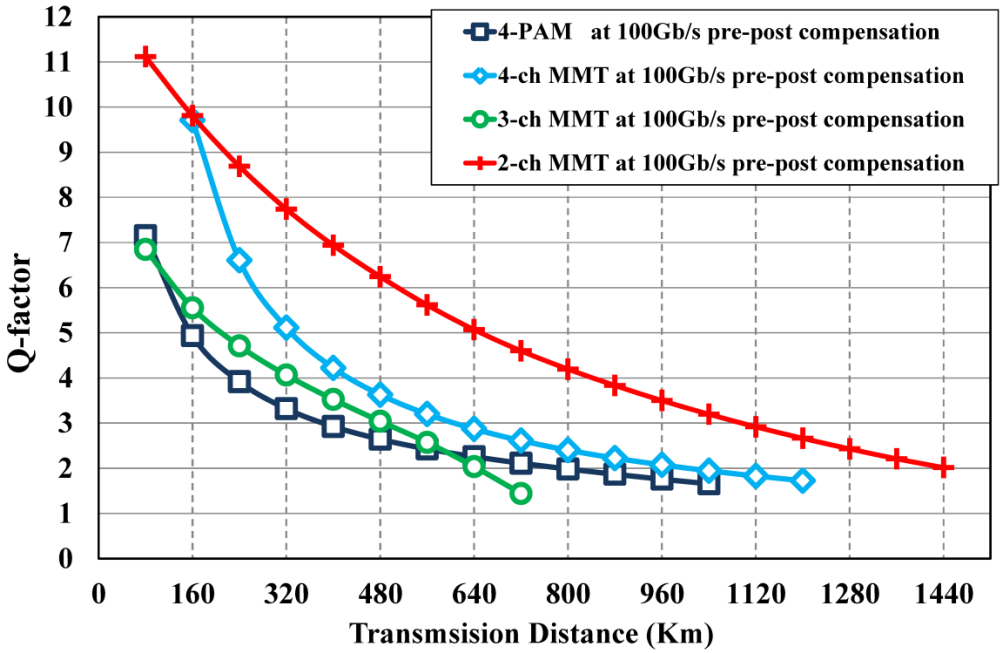

Figure 5.40 Q-factor performance of N-channel MMT and 4-PAM as a function of the transmission distance at 100Gb/s aggregated bit rate.

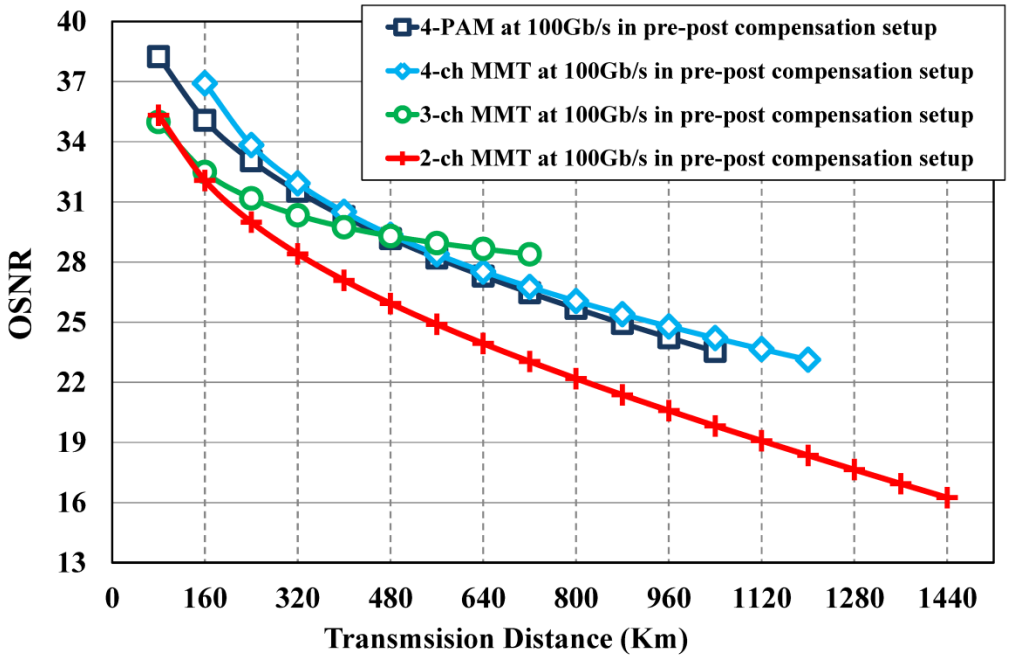

Figure 5.41 OSNR requirement of N-channel MMT and 4-PAM at variable transmission distances at 100Gb/s aggregated bit rate.

The results show that at 40 Gb/s system with baud rate = 20Gbaud/sec , 2-channel MMT with an input launched power of 2 dBm exhibits a maximum transmission distance of 1200Km, while at 100Gb/s with baud rate = 50Gbaud/sec, the maximum transmission distance have been reduced to 480Km. This is can be justified by looking in to the OSNR penalty difference between 2-channel MMT operating at 40Gb/s and 100Gb/s.

At 40Gb/s and 100Gb/s, figure 5.42 depicts the eye diagram of 2-channel MMT at various transmission distances. The symbol rate increase has induced more noise, which is translated into inter-symbol interference observed in the eye diagram for 2-channel MMT at both baud rates with variable increasing fiber distances. The in band noise and non-linearity effects are shown to scale with system baud rate. In addition, it is clear that at 40Gb/s the OSNR equivalent distance requirement is less for 2-channel MMT compared with increased number of levels formats. This can be justified by 2-channel MMT format structure exhibiting two levels, which is reflected in the eye opening of 2-channel MMT compared with 3-, 4-channel MMT and 4-PAM with four amplitude levels.

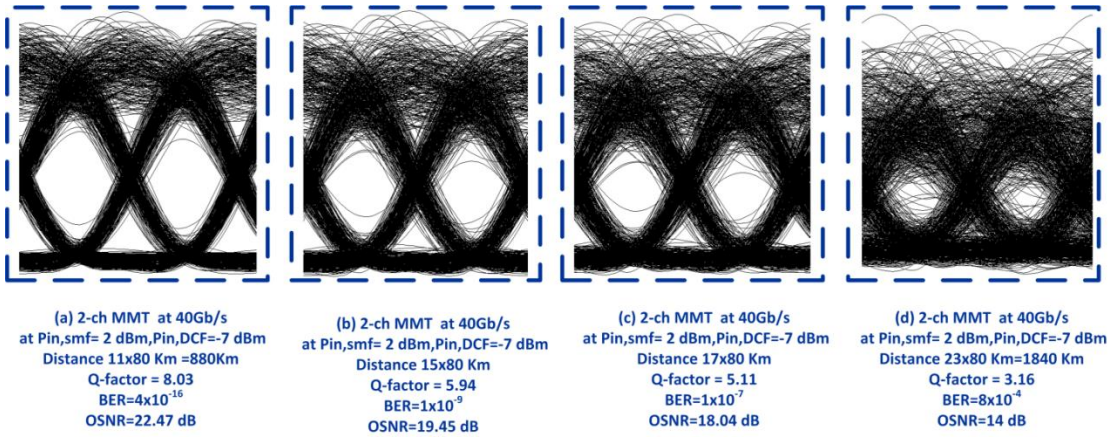

(i)2-channel MMT at 40Gb/s

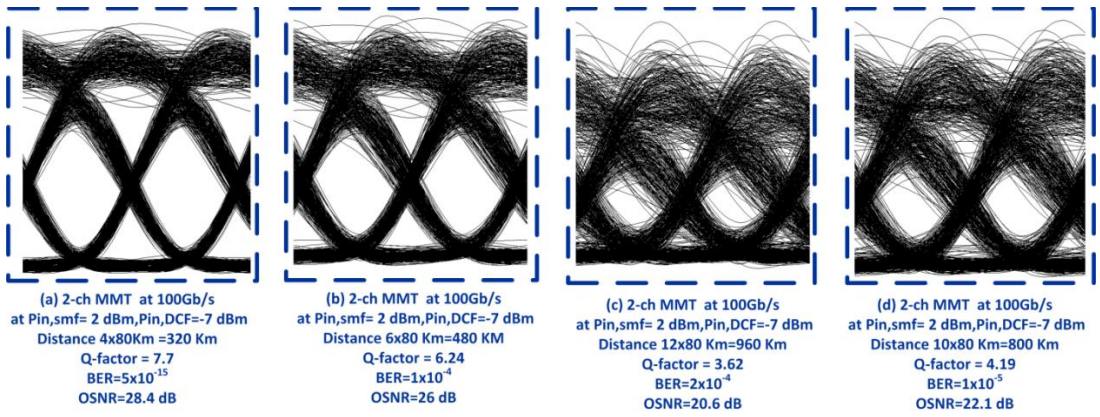

(ii)2-channel MMT at 100Gb/s

Figure 5.42 Eye diagram of 2-channel MMT transmission format with variable transmission distances at aggregated bit rates of (i)40Gb/s and (i)100 Gb/s

At an aggregated bit rate of 40Gb/s (baud rate = 13.3 Gbaud/sec), 3-channel MMT with a launched input power to the SMF = 1 dBm demonstrates a maximum reach of 320 Km, in which the transmission distance is reduced to 80Km for 100Gb/s aggregated bit rate with baud rate = 33.3 Gbaud/sec. The 3-channel MMT eye diagram degradation in performance for various transmission distances at both 40Gb/s and 100Gb/s are shown in figure 5.43. This can be justified as mentioned earlier by the nonlinear impairment penalties caused by the combination between SPM and intra channel non-linearities (IXPM and IFWM).

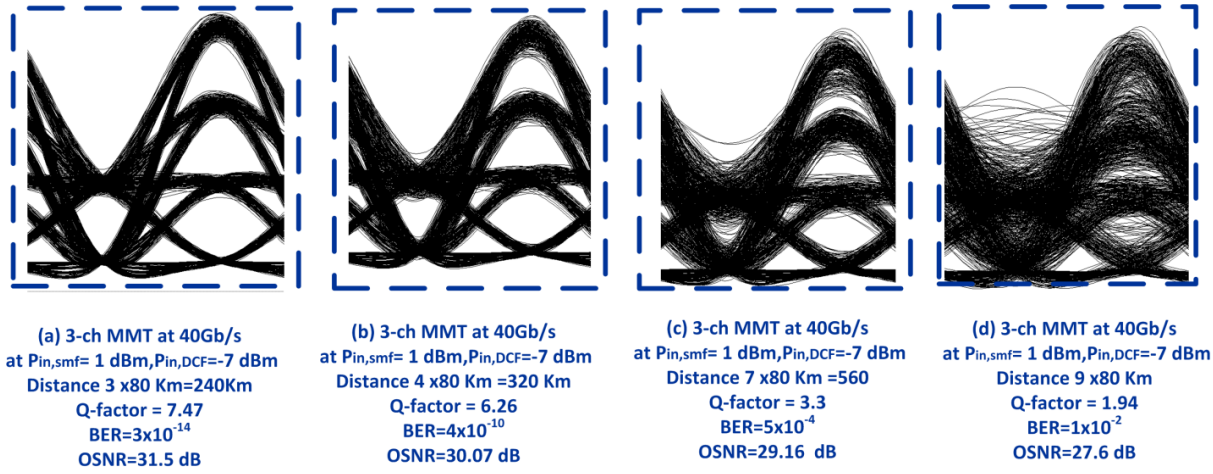

(a) 3-ch MMT at 40Gb/s
at $P_{in,smf}$= 1 dBm,$P_{in,DCF}$=-7 dBm
Distance 3 x80 Km=240Km
Q-factor = 7.47
BER=$3x10^{-14}$
OSNR=31.5 dB

(b) 3-ch MMT at 40Gb/s
at $P_{in,smf}$= 1 dBm,$P_{in,DCF}$=-7 dBm
Distance 4 x80 Km =320 Km
Q-factor = 6.26
BER=$4x10^{-10}$
OSNR=30.07 dB

(c) 3-ch MMT at 40Gb/s
at $P_{in,smf}$= 1 dBm,$P_{in,DCF}$=-7 dBm
Distance 7 x80 Km =560
Q-factor = 3.3
BER=$5x10^{-4}$
OSNR=29.16 dB

(d) 3-ch MMT at 40Gb/s
at $P_{in,smf}$= 1 dBm,$P_{in,DCF}$=-7 dBm
Distance 9 x80 Km
Q-factor = 1.94
BER=$1x10^{-2}$
OSNR=27.6 dB

(i)3-channel MMT at 40Gb/s

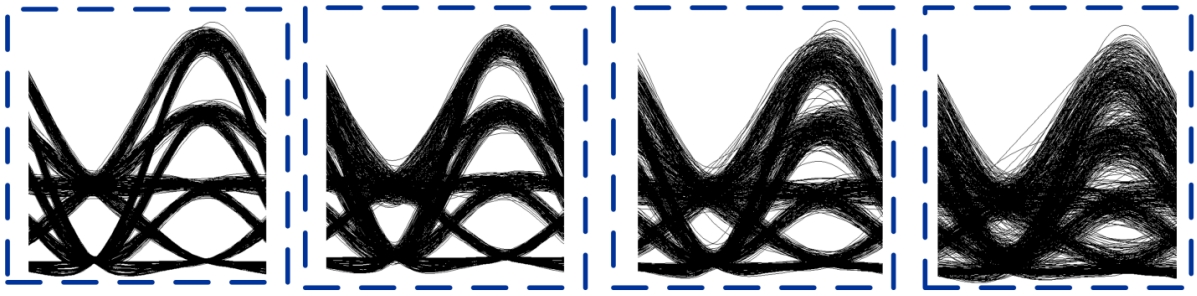

(a) 3-ch MMT at 100Gb/s
at $P_{in,smf}$= 1 dBm,$P_{in,DCF}$=-7 dBm
Distance 1 x80 Km
Q-factor = 7.47
BER=$3x10^{-13}$
OSNR=35 dB

(b) 3-ch MMT at 100Gb/s
at $P_{in,smf}$= 1 dBm,$P_{in,DCF}$=-7 dBm
Distance 2 x80 Km=160 Km
Q-factor = 6.2
BER=$1x10^{-10}$
OSNR=32.5 dB

(c) 3-ch MMT at 100Gb/s
at $P_{in,smf}$= 1 dBm,$P_{in,DCF}$=-7 dBm
Distance 5 x80 Km=400 Km
Q-factor = 3.3
BER=$4x10^{-4}$
OSNR=29.3 dB

(d) 3-ch MMT at 100Gb/s
at $P_{in,smf}$= 1 dBm,$P_{in,DCF}$=-7 dBm
Distance 7 x80 Km =560 Km
Q-factor = 1.9
BER=$2x10^{-2}$
OSNR=28.9 dB

(ii)3-channel MMT at 100Gb/s

Figure 5.43 Eye diagram of 3-channel MMT transmission format with variable transmission distances at aggregated bit rates of (i)40Gb/s and (i)100 Gb/s

For 4-channel MMT with an aggregated bit rate of 40Gb/s (baud rate = 10 Gbaud/sec), a maximum fiber reach of 320Km at an input launched power of 1 dBm is shown. While, at 100Gb/s (baud rate = 25 Gbaud/sec), a reduced fiber transmission reach of 240 Km is manifested at input launched power of 3 dBm. The eye diagram for 4-channel MMT generated at variable distance fiber reach for 40Gb/s and 100Gb/s aggregated bitrates is shown in figure 5.44.

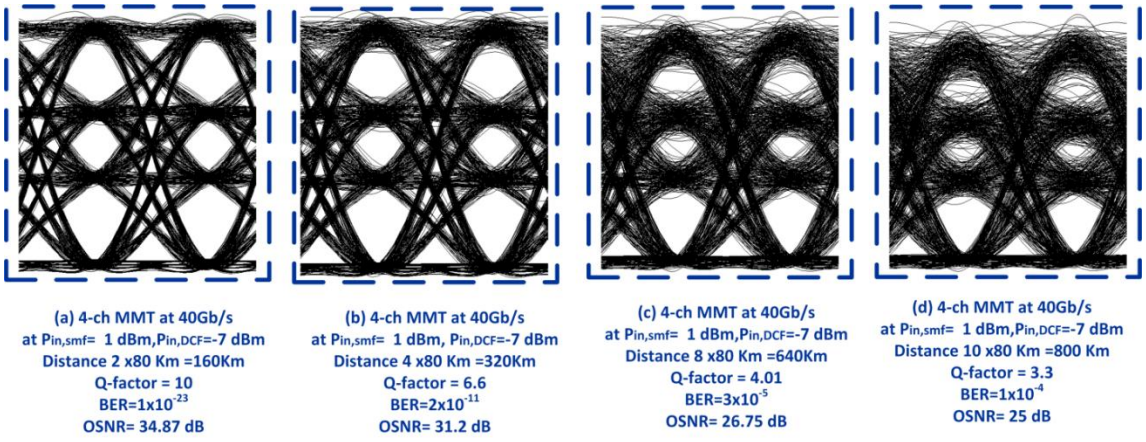

(i) 4-channel MMT at 40Gb/s

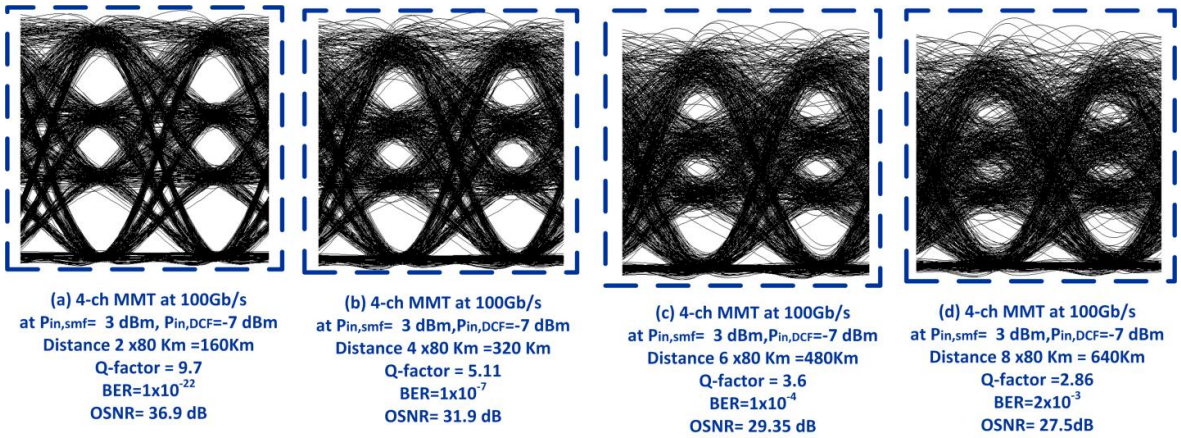

(ii) 4-channel MMT at 100Gb/s

Figure 5.44 Eye diagram of 4-channel MMT transmission format with variable transmission distances at aggregated bit rates of (i)40Gb/s and (i)100 Gb/s

For 4-PAM with an aggregated bit rate of 40Gb/s (baud rate = 20 Gbaud/sec), a maximum fiber reach of 240 Km at an input launched power of 4 dBm is observed. While, at 100Gb/s and baud rate = 50 Gbaud/sec, a reduced fiber transmission reach of 80 Km is show at the same input launched power equivalent to 4 dBm. The eye diagram for 4-PAM generated at variable distance fiber reach for 40Gb/s and 100Gb/s aggregated bit rates are depicted in figure 5.45.

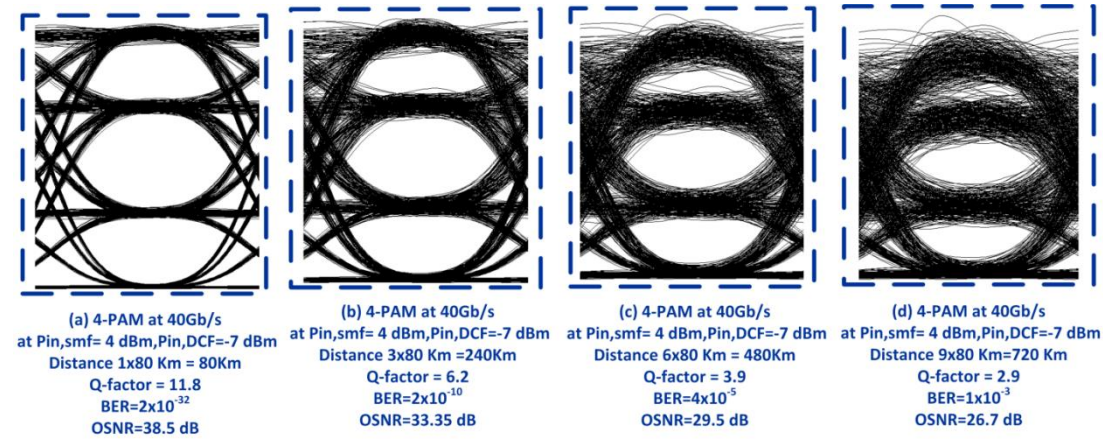

(i)4-PAM at 40Gb/s

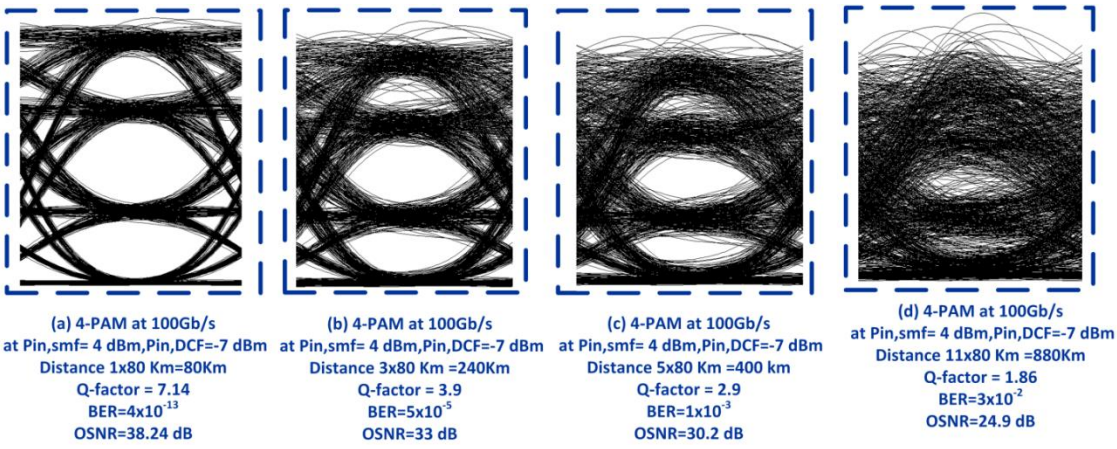

(ii) 4-PAM at 100Gb/s

Figure 5.45 Eye diagram of 4-PAM transmission format with variable transmission distances at aggregated bit rates of (i)40Gb/s and (ii)100 Gb/s

5.3.2.9 Stimulated Brillouin Scattering (SBS) Non-linear Effect

Although, Stimulated Brillouin Scattering (SBS) impose a non-linear impact on optical communication links, which is due to the interaction of light with acoustic modes in an optically transparent medium. However, optical system designers may overcome the effect of SBS by considering factors that help to overcome SBS reflections.

Accordingly, MMT design configuration employs a continuous wave laser with a wide spectral width (spectral linewidth f_{laser}=100MHz) taking advantage of the narrow gain bandwidth of the SBS (SBS gain bandwidth f_{SBS}=20 MHZ). In this case, most of the laser power will fall outside the SBS bandwidth spectrum region and the power threshold of SBS can be expressed by [55]

$$P_{SBS} \approx \frac{21b\,A_e}{g_B\,L_{eff}}\left(1+\frac{f_{laser}}{f_{SBS}}\right) \tag{5.7}$$

where f_{laser} is the spectral line width, A_e is the effective area of fiber, g_B is the Brillouin gain coefficient which equal to 5×10^{-11} m/W, $L_{eff} \approx 20Km$ for $L >> \frac{1}{\alpha_{dB}}$ and b take value between 1 and 2 depending on the relative polarizations of the pump and Stokes waves.

For MMT system setup parameters, $f_{laser} = 100MHz$, $A_e = 80um^2, b = 1,$ the SBS threshold power is equivalent to $P_{SBS} \approx 11dBm$. Since the input power to SMF for MMT system is less than the SBS threshold in the dispersion compensation configuration.

Consequently, the SBS nonlinear effect will not influence neither MMT or M-PAM configurations discussed.

5.4 Concluding Remarks

In this chapter, a numerical investigation on the suitability of N-channel MMT for deployment in metropolitan area networks in the presence of pre-amplified receiver has been presented. The investigation comprised a study on the interaction between signal format characteristics and their interplay with fiber linear and non-linear impairments with an exploration for the optimized maximum power regions. An optimization for system settings have been carried to acquire a maximum transmission reach in the presence of fiber intra-channel non-linearities and dispersion inherent impairments.

Table 5.4 summarizes the performance difference between N-channel MMT and M-PAM formats.

Beside refractive index related non-linearities, it was meaningful to highlight the impact of scattering related fiber non-linearities. After calculating the SBS threshold, it was demonstrated that N-channel MMT power regions of operation is below the SBS threshold. Thus, N-channel MMT will not be influenced by SBS reflection penalties.

Table 5.5 shows an overall comparison between the performance of N-channel MMT and other different modulation formats at aggregate bitrate of 40 Gb/s.

From these analysis, it is evident that at the same spectral efficiency and aggregated bit rate, N-channel MMT observe more nonlinear immunity to fiber non-linearity which is translated to a longer fiber reach when compared with 4-PAM. This is due to the 4-channel design main feature in scaling the baud rate at fraction equivalent to ¼ of the aggregated bit rate. It is verified that 8-PAM and 16-PAM are non-feasible for deployment in metro links due to their inherent high power penalty.

Table 5.4 Performance comparison with respect to system tolerance to linear and non-linear impairments for maximum system reaches at acceptable reliable transmission of BER = 10^{-9} in a pre-post compensation setup.

	Maximum System Reach (Km)		***Maximum Input Power (dBm)***		***Chromatic Dispersion Tolerance (ps/nm)***		***Information Capacity (bits/symbol)***	***Spectral Efficiency (b/s/Hz)***
	At 40 Gb/s	***At 100 Gb/s***	***At 40 Gb/s***	***At 100 Gb/s***	***At 40 Gb/s***	***At 100 Gb/s***		
2-channel MMT	1200	480	2	1	±158	±28	2 bits/symbol	0.5
3-channel MMT	320	80	1	1	±246	±40	3 bits/symbol	0.75
4-channel MMT	320	240	1	3	±460	±76	4 bits/symbol	1
4-PAM	240	80	4	4	±224	±36	2 bits/symbol	1
8-PAM	N/A	N/A	N/A	N/A	±40	N/A	3 bits/symbol	1.5
16-PAM	N/A	N/A	N/A	N/A	N/A	N/A	4 bits/symbol	2

Table 5.5 Comparison between N-channel MMT and different systems at 40 Gb/s bitrate

	Inform. Capacity (bits/ symbol)	CD (ps/nm)	Rx Sens. (dBm)	Optical Spectral Effic. (b/s/Hz)	Tx Complexity	Baud Rate (Gbaud/ s)	Ref.
NRZ-OOK	1 bits/symbol	±108 ps/nm	-29.5 dBm	0.5 b/s/Hz	Laser + MZM +Photodiode	40	[118]
Duo-binary	1 bits/symbol	±340 ps/nm	-31 dBm	1 b/s/Hz	Laser + MZM +Electrical pre-coder +Driver for modulator +Photodiode	40	[223], [224]
2-channel MMT	2 bits/symbol	±158 ps/nm	-30.7 dBm	0.5 b/s/Hz	Laser + MZM +Photodiode	20	-
3-channel MMT	3 bits/symbol	±246 ps/nm	-26 dBm	0.75 b/s/Hz	Laser + MZM +Photodiode	13.33	-
4-channel MMT	4 bits/symbol	±460 ps/nm	-22.8 dBm	1 b/s/Hz	Laser + MZM +Photodiode	10	-
4-PAM	2 bits/symbol	±224 ps/nm	-23.3 dBm	1 b/s/Hz	Laser + MZM +Photodiode	20	-
8-PAM	3 bits/symbol	±40 ps/nm	-14.3 dBm	1.5 b/s/Hz	Laser + MZM +Photodiode	13.33	-
16-PAM	4 bits/symbol	N/A	-5.3 dBm	2 b/s/Hz	Laser + MZM +Photodiode	10	-

6. Chapter 6: MMT Practical Consideration

Since, N-channel MMT has been proposed as a low cost modulation format, thus, it is meaningful to highlight the practical implementation consideration, applicability and feasibility of our MMT transceiver design.

The aim of this section is to highlight and emphasize on the practical applicability and availability of CMOS circuits adequate for future MMT transceiver implementation utilizing state of the art CMOS circuits technology. Moreover, the commercial components (with their part numbers) are demonstrated to verify the practicality of the MMT format presented.

6.1 MMT Cost Consideration

The four available paths to increase the capacity in optical communication systems were comprised in increasing either one or a combination of the following: the frequency, the number of fibers, the number of wavelength per fiber and/or the number of bits/symbol. By taking in to consideration the cost constraint in high-speed short and metro range optical networks, industry and academic researchers have explored the optimum trade-off that could acquire a low cost high capacity solution.

Optical components have been reported being the dominant cost element[30], [31]. Thus, in order to lower the cost of optical transceiver, reducing the number of optical components is essential. Accordingly, IEEE standardization groups have reported that the system cost is the lowest if (Ideally) the link comprised a single laser component and a receiver[31].

As such, standardization bodies have leveraged the employment of higher order modulation formats to transfer the complexity and cost from optics to electronics. This approach was driven by the huge advances and maturity of electronic signal processing techniques[225].

Silicon Photonics (SiP) technology is providing unprecedented level of optoelectronic components integration featuring a reduction in area, cost and power consumption[32], [34], [226]–[228]. Nowadays, SiP is able to integrate CMOS circuits, communication systems, signal processors, filters, dense memory elements, oscillators and photonic components (such as laser, modulators and photo detectors), all integrated on a single module[229]–[232]. This revolution enabled CMOS SiP to be considered as the most cost effective, mass production, richly function solution for high speed optical transceivers [229], [233]–[235].

Luxtera company has released a high speed optoelectronic transceiver based upon CMOS photonics achieving a cost value equivalent to less than 1$ per Gigabit/second[236]. In addition, the energy consumption of all these integrated components and systems, are in its lowest order compared with conventional stand-alone devices. This is due to the integration advantage in canceling the parasitic and low impedance components interfaces which impose power losses in conventional systems[227], [229], [233], [237]–[240].

As such and since the CMOS technology is mature enough to provide both low cost and low power consumption for multilevel signaling, hence, the practical consideration to implement MMT using CMOS circuits are presented.

6.2 MMT Transmitter based upon CMOS circuits

For the MMT transmitter, the MMT symbol is composed of a dual slot and multiple amplitude level. This is based upon the MMT amplitude waveform modulator which is governed by the mapping table 3.1 and eq.(3.17).

By employing CMOS technology, Figure 6.1 shows the proposed block diagram of 4-channel MMT, which can be further customized for 2- and 3-channel MMT. First, in order to generate an amplitude-modulated waveform, the first cluster for the first slot is encoded by using MOS Current Mode Logic (MCML). The MCML encoder converts the input channels data in to a thermometer code as discussed in [241]. The MCML output is then applied to D-flip-flop for synchronization purpose. Then, the thermometer coded current steering digital to analog converter (DAC) is present to generate the four level amplitude modulated waveform. Figure 6.2(a) shows the MCML logic gate design. Figure 6.2(b) shows the truth tables of MCML circuit and thermometer code DAC as discussed in [241].

The thermometer coded DAC circuit is composed of P-MOS or N-MOS CMOS switches operating in the linear region in order to guarantee high-speed switching feature needed for MMT system. Due to the dual slot design nature of MMT symbol, hence, a delay circuit equivalent to half of the symbol period is required for the second slot waveform. This delay can be implemented by employing an RC delay circuit as discussed in [242]. Another alternative CMOS circuit design for generation of MMT signal can be implemented by utilizing already reported Pulse Width Modulator (PWM) circuit which features a duty cycle controller to govern the amplitude modulated slot, as discussed in [242], [243]. Furthermore, other signal processing circuits (such-as pre-emphasis techniques, feed-back equalizers,…) can be added to reduce the inter-symbol interference (ISI) as discussed and reported in [244]–[246].

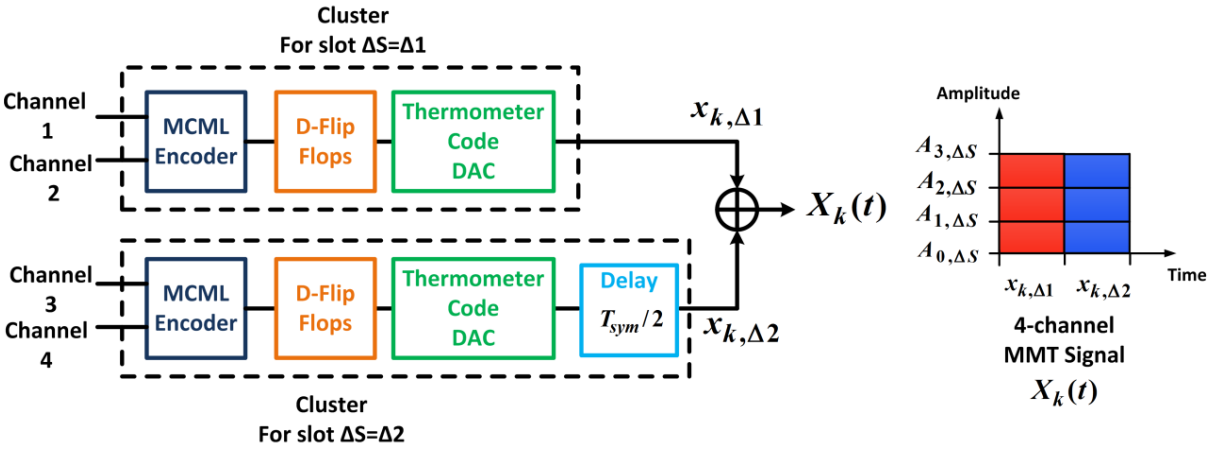

Figure 6.1 4-channel MMT generic transmitter block diagram based upon CMOS circuits.

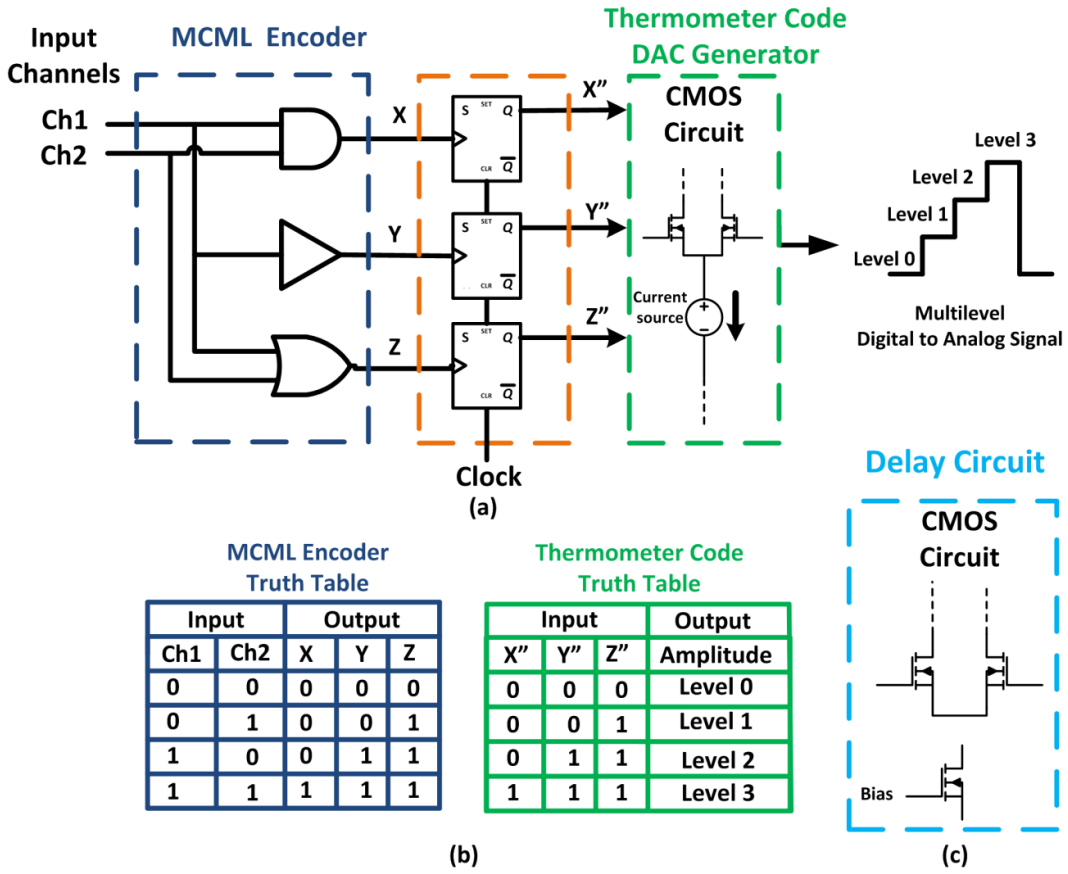

Input		Output		
Ch1	Ch2	X	Y	Z
0	0	0	0	0
0	1	0	0	1
1	0	0	1	1
1	1	1	1	1

Input			Output
X"	Y"	Z"	Amplitude
0	0	0	Level 0
0	0	1	Level 1
0	1	1	Level 2
1	1	1	Level 3

Figure 6.2 MMT Transmitter circuit blocks (a) MCML encoder, D-flip-flop and Thermometer Code DAC generator, (b) MCML and Thermometer Code truth tables, and (c) CMOS Delay Circuit.

6.3 MMT Receiver based upon CMOS circuits

The CMOS circuit consideration for MMT receiver threshold detection based (discussed on chapter 3, section 3.3.3.1), is demonstrated. A receiver that is based upon multilevel threshold detection of four level signal has been reported in [165], [247], [248]. Figure 6.3 shows the general proposed circuit design for MMT receiver. The threshold detection for a four level detected signal can be implemented by utilizing three comparators, which compare the detected signal against three voltage thresholds. The MMT employs two sampling instants for its dual slot MMT symbol structure. This can be realized by the employment of a recent multilevel dual sampling D-flip flop circuit that has been reported in [249]. The dual sampling flip-flop circuit outputs is driven to a decision and regeneration unit for the data recovery, according to pre-set defined de-mapping rules shown in table 3.2. Moreover, another alternative CMOS detection circuit can be considered for MMT receiver implementation utilizing InP/InGaAs Heterojunction Bipolar Transistors (HBTs) technology, has been reported in [248].

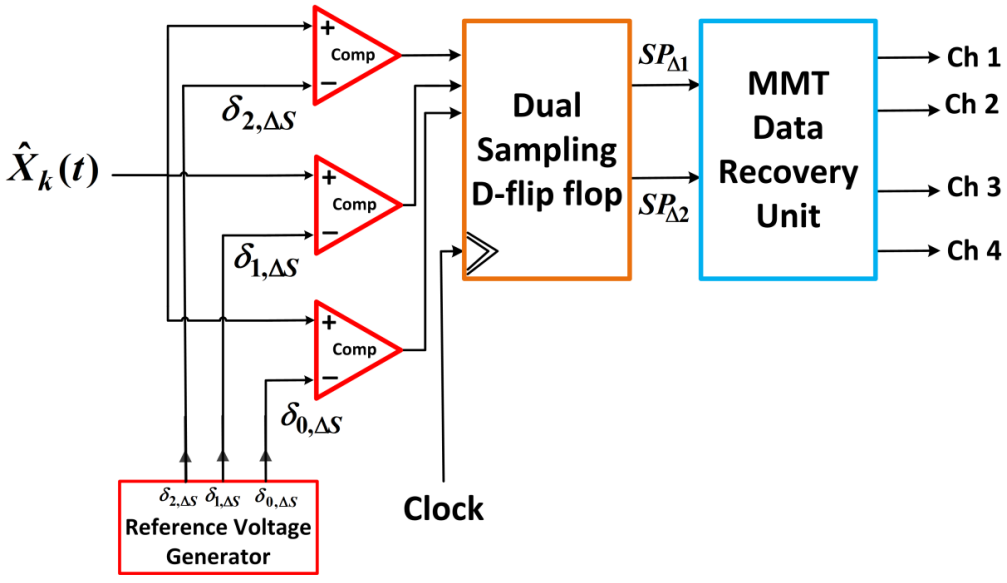

Figure 6.3 4-channel MMT generic receiver block diagram based upon CMOS circuits.

6.4 DSP Technologies enabling MMT

Digital Signal Processor (DSP) offers a high level of performance in integrating multiple signal processing circuits in one chip. This is enabled by the DSP richly-functions cost-effective signal processing solutions (i.e signal generation, encoding, decoding, error correction, noise cancellation, signal equalization, ..etc.)[235]. These features enable direct compensation for fiber impairments[225]. Moreover, it enables the implementation of customized advanced novel modulation formats that is able to satisfy the requirement and limitations for a particular targeted application.

As such mentioned features, this section aims to highlight on the practical applicability and availability of DSP technology for future implementation of MMT based DSP module.

Field Programmable Gate Arrays (FPGA) is promising high functionality signal processing chips, which features a customization capability according to a self-defined software algorithms[250], [251]. The software-defined characteristics of FPGA make it adequate to generate the MMT waveform based upon MMT waveform generator and mapping table defined earlier (*in section 3.3.2*). A multilevel real-time software for the generation of multilevel data transmission symbols has been realized operating with 28Gbaud by utilizing Xilinx Virtex5 FPGAs with the aid of MICRAM high speed DAC [252]. On a similar manner, the MMT symbols can be generated by utilizing FPGA device driven by MICRAM DAC as discussed in [252]. The system can multiplex the data from 4-channel MMT, which enable realizing MMT 112Gb/s system. Recently, DAC and ADC with a manufactured interface to FPGA chips have been released by MICRAM with sampling rate 30GS/s and 2 times interleaver ADC with sampling rate 60GS/s[253].

Although, FPGA provide adequate platform for a rapid prototyping of systems, however, the main drawbacks are classified in to, the high power consumption and high net system cost. Another mature technology that can be utilized for MMT implementation enabling low cost and low power consumption is Application Specific Integrated Circuits (ASIC) technology [254], [255]. Due to the custom design of Integrated Circuits (IC), thus, it provides the ultimate optimization for both the area and power.

6.5 System Requirements and Commercial components Enabling MMT

Table 6.1 compares between the system requirements to implement 4-channel MMT, 4-PAM and NRZ-OOK systems at 10Gb/s, 40Gb/s and 100Gb/s bitrates. Although, these requirements are based upon optimal industry standards and manufacturers application, however, these values may vary due to other dependent elements. For example , filters with fast roll off rate induces a narrower bandwidth requirement[256], [257]. Although, ideal oversampling ratio equivalent to 2 is optimal to guarantee non aliasing effect. However, practical systems employ a minimum oversampling ratio equivalent to 5/4[258]. It is clear that 4-channel MMT offer a relaxation in the optical system requirement compared with 4-PAM and NRZ-OOK. This advantage can be translated to a reduction overall system cost.

Table 6.1 show a comparison between 4-channel MMT, 4-PAM and NRZ-OOK with respect to system requirements.

	System Requirement				
	Bit Rate	**Baud Rate**	**DAC/ADC Sampling**	**Filter BW**	**TIA+ photodiode**
4-channel MMT	4x25= 100Gb/s	25 Gbaud/sec	Optimal=100GS/s Or Practical= 62.5GS/s	18.75 GHz	18.75 GHz
	4x10= 40Gb/s	10 Gbaud/sec	Optimal=40GS/s Or Practical= 25GS/s	7.5 GHz	7.5 GHz
	4x2.5= 10Gb/s	2.5 Gbaud/sec	Optimal=100GS/s Or Practical= 6.25GS/s	1.875 GHz	1.875 GHz
4-PAM	2x50= 100Gb/s	50 Gbaud/sec	Optimal=100GS/s Or Practical= 62.5GS/s	37.5 GHz	37.5 GHz
	2x20= 40Gb/s	10 Gbaud/sec	Optimal=40GS/s Or Practical= 25GS/s	15 GHz	15 GHz
	2x 5= 10Gb/s	5 Gbaud/sec	Optimal=100GS/s Or Practical= 6.25GS/s	3.75 GHz	3.75 GHz
NRZ-OOK	1x100= 100Gb/s	100 Gbaud/sec	Optimal=200GS/s Or Practical= 125GS/s	75 GHz	75 GHz
	1x40= 40Gb/s	40 Gbaud/sec	Optimal=80GS/s Or Practical= 50GS/s	30 GHz	30 GHz
	1x 10= 10Gb/s	10 Gbaud/sec	Optimal=10GS/s Or Practical= 12.5GS/s	7.5 GHz	7.5 GHz

For the above-mentioned requirement, it is meaningful to list state of the art commercial components that are adequate to enable the implementation of 4-channel MMT system. Table 6.2 list some of the commercial products fulfilling the requirements for the MMT system at 10Gb/s, 40Gb/s and 100Gb/s required optical components in MMT system.

Table 6.2 state of art commercial electrical and optical components.

Components	Commercial Products		Reference
	Company	Performance Specs	
DAC/ADC + DSP (Integrated)	***Fujitsu*®** 40nm-CMOS Technology (Part No.LEIA-DAC) (PartNo.LUKE-ES-ADC)	Sampling Rate= 65 GSa/s 8-bit resolution	[259],[260]
	***MICRAM*®** Vega-Technology (Part No. AWG6020)	Sampling Rate= 72 GSa/s DAC	[261]
	***Fujitsu*®** CHAIS- 65nm CMOS Technology	Sampling Rate= 56GSa/s ADC 6-bit resolution	[262]
	***Ciena*®** 65nm-CMOS Technology	Sampling Rate= 56GSa/s DAC 6-bit resolution	[263]
Photodetector	***Finisar*®** 1550nm/1330nm (Part No.XPDV412xR)	Cut-off frequency= 100GHz	[264]
	***Finisar*®** 1550nm/1330nm (Part No.XPDV2320R)	Cut-off frequency= 50GHz	[265]
	***Finisar*®** 1550nm/1330nm (Part No.XPDV3120R)	Cut-off frequency= 70GHz	[266]
	***Finisar*®** 1550nm (Part No.XPDV3120R)	Cut-off frequency= 35GHz	[267]
Trans-impedance Amplifier	***INPHI*®** Wide Band (Part No.IN2844TA)	Bandwidth=25GHz Trans-impedance Gain= 3KOhm at DC	[268]
	SIRENZA*® *MICRODEVICES InP HBT Technology	Bandwidth=60GHz Trans-impedance Gain= 3.6KOhm at DC	[269]
Photodetector+ Trans-impedance Amplifier	***INPHI*®** InP-HBT Technology	Bandwidth=38GHz Trans-impedance Gain= 1KOhm at DC	[270]
Laser	***Finisar*®** (Directly-Modulated DFB laser chip) CML Technology 1550nm (Part No.DM200-3/4)	Baud rate=10Gbaud Output Power= 0-3 dBm	[271]
	***Finisar*®**	Baud rate=10Gbaud	[272]

Laser	(CW Tunable Laser) CML Technology 1550nm (Part No. S7500)	Output Power= 9-13 dBm	
Optical External Modulators	***EOSpace*®** Li NbO_3 Intensity Modulator 1550nm	Bandwidth= 30GHz	[273]
	***Thorlabs*®** 20 GHz Analog Modulator 1550nm (Part No. LN58S-FC)	Bandwidth= 20GHz	[274]
Erbium Fiber Doped Amplifier (EDFA) "For Metro links"	***Finisar*®** 1550nm (Product: EDFA-PA-M)	Max Gain= 25 dB Noise Figure= 4.5 dB	[202]
Standard single-mode fibers (SMF)	***Corning*®** Product: SMF-28	Following ITU-T Recommendation G.652A–D	[113]
Dispersion Compensation Fiber (DCF) "For Metro links"	***Corning*®** Product: Pure-form DCM-SMF	Dispersion for 80KM span= -1314 ±26 ps/nm	[215]
PRBS Generator "For Test"	***Agilent*®** 40 Gb/s Based upon ASIC technology Product: Keysight N4974A	With maximum pattern length $2^{31}-1$	[199]
OSA Optical spectrum Analyzer "For Measurement"	***Agilent*®** Product: 71452B	High resolution 0.5nm	[201]
EDFA	***Optilab*®** C-band 1528nm-1563nm Pre-Amp EDFA	Maximum gain = 25 dB Noise Figure= 4.5 dB	[202]

7. Chapter 7: Conclusion and Future Directions

7.1 Conclusion

In this thesis, N-channel MMT has been proposed and investigated as a novel low-cost, power-efficient and high-capacity data transmission solution for short-haul and medium range optical links. The novel design has been motivated by the increase in power consumption that exists in high-speed and dense data centers interconnects and metropolitan area network. In this context, IM/DD system has been selected for N-channel MMT transmission since it exhibit the least cost and power consumption in contrast to coherent optical systems. The N-channel MMT has been compared with M-PAM, as both feature a capacity expansion advantage with the eligibility for scaling the baud rate with the limitations that exists in electronic and optical components operating at a fraction of the aggregated data rate.

In chapter 3, the thesis has started with a discussion on the methodology behind MMT format structure based upon Shannon channel capacity theory. Accordingly, the MMT structural design has considered the impactful trade-off between system parameters to satisfy the requirement and offer a solution to the thesis problem statement in realizing a high capacity transmission format accompanied by a reduced power budget. As such, N-channel MMT has been designed as joint multiplexing and modulation format utilizing two slots only and multiple levels dependent upon system information capacity (in bits/symbol) or channel count.

Afterwards, a benchmark classical methodology for modulation formats analytical evaluation utilizing signal space analysis has been performed for N-channel MMT. The signal space analysis has included the following:-

a) Orthonormal basis functions have been defined for N-channel MMT format in which a representation of MMT symbols with respect to the basis function is derived.

b) N-channel MMT has been conveyed in a multi-dimensional signal constellation following the optical channel non-negativity constraint.

Beside the signal space analysis, a development for the theory and governing rules behind the data multiplexing and modulation of N-channel MMT system was essential. The basic properties and waveform synthesis for 2-, 3-, and 4-channel MMT were defined. The thesis has proposed two receiver detection designs: Optimal detection receiver and threshold detection receiver. The optimal detection receiver was proposed based on the maximum likehood criterion, where an optimal assessment for MMT can be achieved. This model has been employed in chapter 4 analytical evaluation. The threshold detection receiver exhibits a low complex BER model based upon the MMT dual slot and multilevel MMT structure. This model has been adopted in chapter 5 numerical evaluation.

In chapter 4, analytical performance metrics have been employed to evaluate the performance of N-channel MMT. The signal space analysis has provided an appropriate level of abstraction in assessing the power efficiency of N-channel MMT compared with M-PAM. The evaluation metrics results and analysis can be summarized in the following:-

a) Since, the BER is a key figure of merit in transceiver systems assessments; hence, an explicit BER expression for computing the BER of 2-, 3-, and 4-channel MMT with respect to the received optical power has been derived.
b) For system information capacity of 2, 3 and 4 bits/symbol, 2-channel, 3-channel and 4-channel MMT formats have manifested a reduction in power penalty equivalent to $1.76\,dB$, $2.2\,dB$ and $4\,dB$ compared with 4-PAM, 8-PAM and 16-PAM, respectively relative to OOK format at fixed aggregated system bit rate.
c) For system information capacity of 2, 3 and 4 bits/symbol, 2-channel, 3-channel and 4-channel MMT formats have manifested a reduction in power penalty equivalent to 3.27 dB, 3.94 dB and 5.5 dB compared with 4-PAM, 8-PAM and 16-PAM, respectively relative to OOK format at fixed system baud rate.
d) At bit rates of 10Gb/s, 40Gb/s and 100Gb/s, the optical receiver sensitivity results have been calculated for N-channel MMT and M-PAM in the presence of directly

modulated fiber link noise model for short-haul optical links. The results confirm the optical sensitivity advantage of N-channel MMT compared with M-PAM.

e) A closed form expression to calculate the average electrical and optical power for N-channel MMT symbols has been derived. With respect to the same information capacity(in bits/symbol), the calculated results show that the energy per symbol and per bit is less than their counterparts in 4-, 8- and 16-PAM, respectively.

f) Asymptotic power efficiency evaluation between N-channel MMT and M-PAM has been demonstrated at both fixed bit rate and baud rate. The evaluation validated the derived BER model and manifested an agreement between analytical BER results and power efficiency asymptotic results relative to OOK.

g) The impact of the shot, thermal and relative intensity noise on N-channel MMT and M-PAM signal characteristics have been examined. Although, the results show that both formats exhibit different, but stable performance between each other against varied noise levels. However, the overall performance cannot be judged except by taking in consideration other dependent variables and system requirements such as bitrate, baud rate, bandwidth, availability of commercial optical components.

h) The electrical spectral efficiency has been calculated for M-PAM and N-channel MMT. At fixed information capacity, M-PAM exhibits less spectral width compared with N-channel MMT. Although, the transmission of 3 and 4 bits/symbol using 8-PAM and 16-PAM system has a spectral efficiency advantage over 3-channel and 4-channel MMT, respectively. However, 8-PAM and 16-PAM incur a significant power penalty disadvantage that act as a barrier between their realizations in practical systems. Un-coded 8-PAM and 16-PAM have been reported not practical for implementation in [11], [28], [30], [275], [276]. Although, for 8-PAM, a solution has been proposed to enhance the SNR by the addition of error correction techniques, as block coding or forward error correction codes (FEC). However, this caused an increase in one of the system trade-off parameters which is complexity[41], [48], [50].

i) The results show that 4-channel MMT against N-channel MMT formats and 4-PAM against M-PAM modulation formats exhibit superior performance and optimum compromise with respect to power penalties and trade-off parameters.

j) Although, 4-PAM exhibit less power penalty compared with 4-channel MMT at the same spectral efficiency. However, 4-PAM is operating at double the baud rate of 4-channel MMT, which implicate a rise in the fiber non-linearities impact that has strong direct proportional with the system baud rate of operation (as discussed in chapter 5) [108], [110]. In addition, 4-channel MMT operating at half the baud rate of 4-PAM offers a relaxation in the requirement of optical components characteristics. This constraint possessed the major challenge for the standardization of 100G and 400G Ethernet by IEEE Ethernet task forces [11], [30].

In chapter 5, a numerical investigation for the adequacy of N-channel MMT deployment in metropolitan area networks is presented. The investigation comprised a study on the interaction between signal format characteristics and their interplay with fiber linear and non-linear impairments. An optimization for system settings has been carried to acquire a maximum transmission reach in the presence of fiber intra-channel non-linearities and dispersion inherent impairments. The evaluation metrics results and analysis can be summarized in the following:-

a) At 40Gb/s and 100Gb/s, the receiver sensitivity for N-channel MMT has been examined in the presence of pre-amplified receiver. The results emphasize on the power penalty advantage of 2-, 3- and 4-channel MMT compared with 4-, 8- and 16-PAM. At 40Gb/s system bit rate, in comparison with M-PAM system, the transmission of 2, 3 and 4 bits/symbol employing N-channel MMT have manifested receiver sensitivity improvement equivalent to 7.4 dB, 11.3 dB, and 17.5 dB, respectively.

b) Quantitative comparison between N-channel MMT and M-PAM transmission formats in a back-to-back system configuration with respect to their tolerance against chromatic dispersion has been demonstrated. The tolerance results revealed that 4-channel MMT is outperform other N-channel MMT and M-PAM

formats with tolerances reaching ±460 and ±76 at 40Gb/s and 100Gb/s, respectively. At BER = 10^{-9}, the results have marked a degradation in chromatic dispersion tolerance for 8-PAM at 40Gb/s with tolerance ±40. In addition, 8-PAM at 100Gb/s and 16-PAM at both 40 and 100Gb/s showed a severe degradation in performance showing a BER floor = $6x10^{-6}$, $6x10^{-3}$ and $5x10^{-2}$, respectively.

c) Numerical exploration for the optimal dispersion compensation methodology (Post compensation and Pre-post compensation) to compensate for the residual dispersion in fiber spans for metro network data transmissions. The results revealed pre-post compensation display a longer transmission reach and more tolerance against fiber non-linearities

d) In this non-linearity investigation, the thesis has focused on the intra-channel non-linearities and their interaction with fiber linear impairment in the presence of pre-amplified receiver noise. Performance evaluation for N-channel MMT and M-PAM has been explored utilizing dispersion post compensation and dispersion pre-post compensation scenario in order to quantify the system tolerance to fiber non-linearities i.e Self Phase Modulation (SPM), Intra-channel Cross-Phase Modulation (IXPM) and Intra-channel Four-Wave Mixing (IFWM). The investigation has been adopted over different numbers of fiber spans for metro links applications. The results show that pre-post compensation configuration exhibit longer fiber reach, which can be translated to more tolerance to fiber non-linearities compared with post compensation.

e) By the employment of pre-post compensation to tolerate both residual chromatic dispersion and non-linearities, performance above acceptable reliable data transmission limit at 40Gb/s bit rate has been attained for 2-, 3- and 4-channel MMT over spans lengths of up to 1200Km, 320 Km and 320 Km, respectively. While, at an aggregated bit rate of 100 Gb/s, acceptable BER=10^{-9} data transmission can be achieved for 2-, 3- and 4-channel MMT over spans lengths of up to 480 Km, 80 Km and 160 Km, respectively.

f) The results clarified that at a high bitrate, the main dominant system limitation was due to the strong impact of IXPM and IFWM non-linearities. Hence, it is

desirable to embrace higher order modulation formats operating at a baud rate with a smaller fraction of the aggregated bit rates. As such, 4-channel MMT with information capacity equivalent to four bits/ symbol featuring a capability for scaling the system baud rate to ¼ of the aggregated bitrate, has shown superior performance. At information capacities of three and four-bits/ symbol, un-coded 8-PAM and 16-PAM has been verified non-feasible or applicable for deployment in metro links due to their inherent unambiguous high power budget.

g) By comparing 4-channel MMT and 4-PAM exhibiting an equivalence spectral efficiency at 40Gb/s and 100Gb/s, 4-channel MMT system has demonstrated better system immunity to fiber non linearities. This conjectured to 4-channel MMT baud rate advantage, where 4-channel MMT operate at half the baud rate compared with 4-PAM. Hence, the impact of intra-channel non-linearities on 4-PAM operating at 20Gbaud/sec and 50Gbaud/sec, is more than its counterpart 4-channel MMT exhibiting 10Gbaud/sec and 25Gbaud/sec systems.

h) Beside refractive index related non-linearities, it was meaningful to highlight the impact of scattering related fiber non-linearities. After calculating the SBS threshold, it was demonstrated that N-channel MMT power regions of operation is below the SBS threshold. Thus, N-channel MMT will not be manipulated by SBS reflection penalties.

In chapter 6, the thesis concluded by highlighting the practical applicability, feasibility and availability of state of the art CMOS circuits technology enabling future MMT transceiver implementation. In addition, a comparison between the system requirement for 4-channel MMT, 4-PAM and NRZ-OOK has been presented. The results have verified the potential advantage of 4-channel MMT offering a cost effective solution compared with 4-PAM and NRZ-OOK.

To conclude, with respect to system trade-off compromise between spectral efficiency, information capacity, power efficiency and immunity to fiber non-linearities, the thesis argues that 4-channel MMT exhibit supremacy against other higher order multilevel formats discussed in the thesis.

7.2 Future Directions

N-channel MMT being a novel power-efficient transmission format paves the way for its utilization in plenty of data transmission applications that are beyond the thesis objectives. MMT may be extended in future works into the following directions:-

- From both performance and implementation perspectives, CMOS Silicon Photonics is providing unprecedented levels of optoelectronic component integration with richly functional digital signal processing modules, featuring a reduction in area, cost and power consumption. In our discussion, the practical applicability and availability of CMOS circuits adequate for future MMT transceiver implementation utilizing state of the art CMOS technology has been highlighted. Other digital signal processing modules that are applicable for integration with MMT and feature enhancement in MMT signal characteristics can be classified into:-
    - ✓ *Forward error correction (FEC)* module has a good potential for employment with MMT. This is based upon the availability of a DSP chip with numerous functional capabilities beyond the MMT transmission format requirement. This will offer an enhancement in the overall MMT signal characteristics that is translated to a higher signal to noise ratio gain. This acquired robustness can be exploited to increase the fiber reach and/or tolerating imposed signal impairments.
    - ✓ *Electronic Dispersion Compensation (EDC)* is a powerful module that is able to overcome uncompensated chromatic dispersion effects. EDC exhibits a much lower cost compared with conventional DCF modules taking advantage of the cost effectiveness and richly functions of CMOS digital signal processors. Maximum-Likelihood Sequence Detection (MLSD) proposed for MMT optimal detection has been employed for EDC. In fact, MLSE does not compensate for chromatic dispersion, but take account for the dispersion effects during signal detection. MLSD has

been extensively reported as a detection technique for EDC modules [151], [159], [225].

- Although, in this thesis, N-channel MMT performance investigation has considered its deployment over SMF, however, MMT has a good potential to be transmitted over multi-mode fiber for short-high capacity optical links. This is due to the numerous commercial products and standardizations that are utilizing 4-PAM format over MMF[12], [100], [106], [277], [278]. As such, characterization for N-channel MMT tolerance to intermodal dispersion is an important figure of merit to evaluate the MMT performance for such short link applications over MMF.
- Although, performance investigations for MMT have been carried exhibiting a single wavelength channel due to cost constraints, however, with data hungry applications and internet services, the necessity is expected to grow for expanding the capacity in the order of 1T, 10T and beyond. As such, more investigations for N-channel MMT need to consider increasing the signal dimensionality. This can be achieved by the employment of a combination between Polarization Division-Multiplexing (PDM) and Dense Wavelength Division-Multiplexing (DWDM) with channel spacing in the order of 50GHz and 100GHz acquiring an overall system bit rate that can reach 3.2 T b/s, 6.4 T b/s and 12.8 Tb/s.
- The thesis has proposed a novel modulation format for applications related, but not limited to short-haul optical interconnects and metro networks. Since, N-channel MMT is an intensity-modulated format that follows the optical channel constraints, i.e. non-negativity constraint and average optical power constrained due to eye and skin safety consideration. Hence, N-channel MMT has a promising potential after further investigations in applying it for wireless optical applications such as visible indoor light communication and free space optical communications.

Appendix A

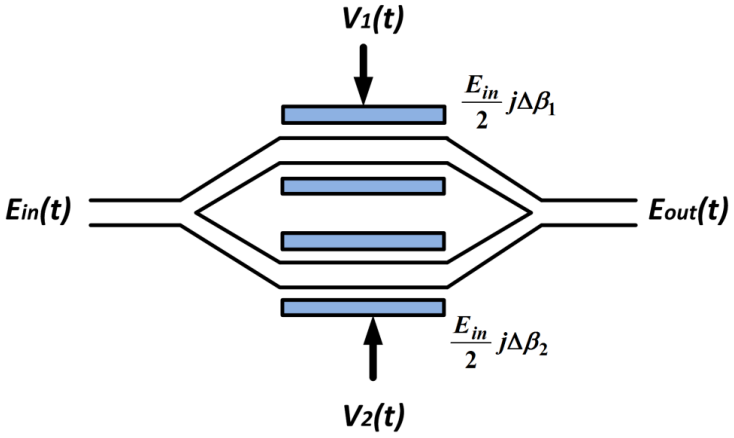

Figure A1.1 Dual-Drive Mach-Zehnder Modulator Configuration

As shown in figure A1.1, the Mach-Zehnder structure follow the two waveguide arms model discussed in section 2.5.1 .

In addition to many parameters, including the choice of the electro-optic wave guide material, the orientation of the crystal with respect to the external electric field, as well as to the polarization of the incoming light wave, the splitting ratios of the Y-branch divider and the differential length between the arms of the modulator. For modeling the output optical electrical field for the DD-MZ, The output of the modulator electric field can be represented by equation [211]:

$$E_o(V_1,V_2) = \frac{E_{in}}{1+SR}\left[SR\exp\left(-\left(\frac{\Delta\alpha_a(V_1)}{2}\right) + j\Delta\beta(V_1)L\right) + \exp\left(-\left(\frac{\Delta\alpha_a(V_2)}{2}\right) + j\Delta\beta(V_2)L - j\varphi_o\right)\right]$$

$$\equiv \sqrt{I(V_1,V_2)}\exp\left(j\phi(V_1,V_2)\right) \quad (6)$$

SR is the splitting ratio where $SR = P_2 / P_1$, $\alpha_a / 2$ represents the attenuation constant; ϕ is the phase of the output signal and φ_o is equal 0 or π radian for conventional modulator and phase-shift modulator, respectively . For $i = 1,2$

$$V_i(t) = V_{bias(i)} + V_{\mathrm{mod}(i)}\ v(t) \tag{7}$$

Where $V_{bias(i)}$ is the DC bias voltage, for specifying the quadrature point of the modulator; $V_{\mathrm{mod}(i)}$ peak amplitude of the modulating voltage; $v(t)$ is the peak amplitude of one and an average value of zero for the modulating voltage. The electrical input signal is normalized between 0.5 and -0.5. The model utilizes a single drive modulation, i.e., $V_{\mathrm{mod}(i)}$ is 0 in one of the arms. The model behavior resembles the measured experimental absorption and phase of optical signal on the applied voltage for each arm of a modulator.

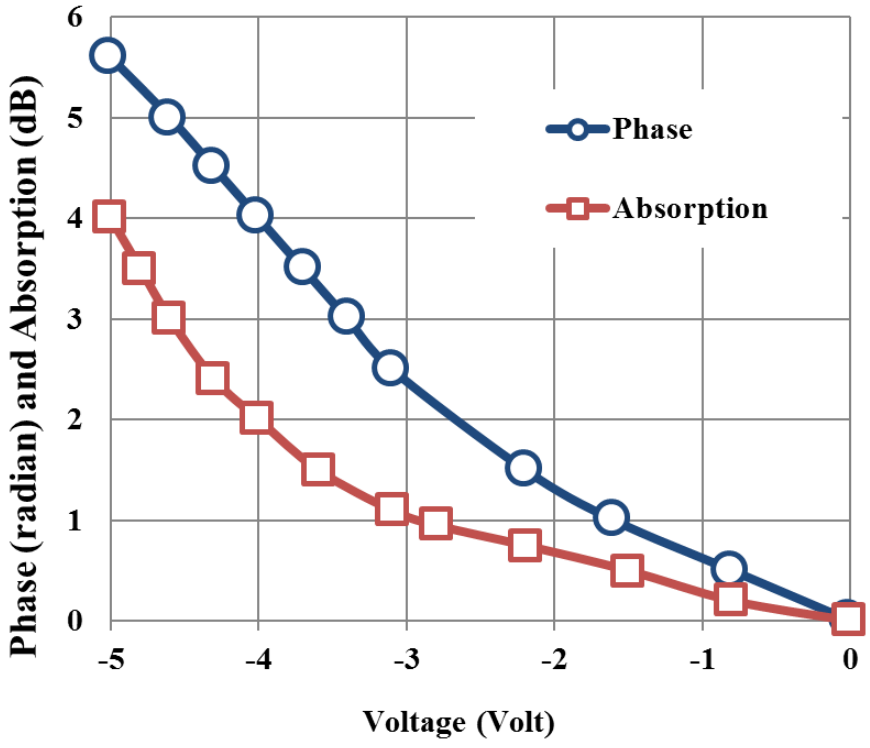

Figure A1.2 The MQW DD-MZ waveguide characteristics in terms of absorption (α_a) and phase difference ($\Delta\beta$) dependence of the material with varying the applied voltage[211].

Bibliography

[1] CISCO, “Cisco Visual Networking Index: Forecast and Methodology(2013–2018),” 2015.

[2] CISCO, “Cisco Visual Networking Index: Forecast and Methodology, 2014-2019,” 2015.

[3] Bell-Labs, “Metro Network Traffic Growth: an Architecture Impact Study: Strategic White Paper,” 2013.

[4] IEEE-802.3u-standard, “IEEE802.3u Standard,” 1995.

[5] G. Held, *Carrier Ethernet: Providing the Need for Speed*. CRC Press, 2008.

[6] “IEEE P802.3ba,” *IEEE P802.3ba 40Gb/s and 100Gb/s Ethernet Task Force*, 2009. [Online]. Available: http://www.ieee802.org/3/ba/PAR/P802.3ba_Objectives_0709.pdf.

[7] R. Rabinovich, “40Gb / s & 100Gb / s Ethernet Long-Reach Host Board Channel Design,” no. November, pp. 152–158, 2013.

[8] The IEEE Standards Association, “802.3ba-2010 standard,” *802.3ba-2010 - The IEEE Standards Association*, 2010. .

[9] “100G Ethernet Technology and Applications,” *ZTE Communications*, 2009.

[10] IEEE, “IEEE 802.3bm Standard,” 2015. [Online]. Available: https://standards.ieee.org/findstds/standard/802.3bm-2015.html.

[11] IEEE-400GBE-Taskforce, “400 Gb/s Ethernet Study Group,” *400 Gb/s Ethernet Study Group*, 2014. [Online]. Available: http://www.ieee802.org/3/400GSG/public/index.html.

[12] J. Wei, Q. Cheng, R. V Penty, I. H. White, and D. G. Cunningham, “400 Gigabit Ethernet using advanced modulation formats: Performance, complexity, and power dissipation,” *Commun. Mag. IEEE*, vol. 53, no. 2, pp. 182–189, 2015.

[13] Greenpeace International, “Make It Green - Cloud Computing and its Contribution to Climate Change,” *Forbes*, p. 12, 2010.

[14] GreanPeace, “How clean is your cloud?,” *GreenPeace Report*, 2012. [Online]. Available: http://www.greenpeace.org/international/Global/international/publications/climate/2012/iCoal/HowCleanisYourCloud.pdf.

[15] M. Erol-Kantarci and H. T. Mouftah, “Energy-Efficient Information and Communication Infrastructures in the Smart Grid: A Survey on Interactions and Open Issues,” *IEEE Commun. Surv. Tutorials*, vol. 17, no. 1, pp. 179–197, 2015.

[16] L. M. Hilty and B. Aebischer, “The Energy Demand of Data Centers,” in *ICT Innovations for Sustainability*, 2015, pp. 113–124.

[17] P. Wiatr, J. Chen, P. Monti, and L. Wosinka, “Energy Efficiency Versus Reliability Performance in Optical Backbone Networks,” *J. OPT. COMMUN. NETW.*, vol. 7, no. 3, pp. A482–A491, 2015.

[18] C. Gough, I. Steiner, and W. Saunders, “Why Data Center Efficiency Matters,” in *Energy Efficient Servers*, 2015.

[19] Greenpeace International, “How Companies are Creating the Green Internet,” 2015.

[20] CISCO, “Cisco Global Cloud Index: Forecast and Methodology, 2014–2019,” 2015.

[21] SMART2020, “Enabling the low carbon economy in the information age. A report by The Climate Group on behalf of the Global eSustainability Initiative (GeSI),” 2008.

[22] T. Gao, M. David, J. Geer, R. Schmidt, and B. Sammakia, “Experimental and numerical dynamic investigation of an energy efficient liquid cooled chiller-less data center test facility,” *Energy Build.*, vol. 91, pp. 83–96, 2015.

[23] C. Fiandrino, D. Kliazovich, P. Bouvry, and A. Zomaya, “Performance and Energy Efficiency Metrics for Communication Systems of Cloud Computing Data Centers,” *IEEE Trans. Cloud Comput.*, vol. PP, no. 99, pp. 1–1, 2015.

[24] L. Wang, F. Zhang, J. A. Aroca, A. V. Vasilakos, K. Zheng, C. Hou, D. Li, and Z. Liu, “GreenDCN: A general framework for achieving energy efficiency in data center networks,” *IEEE J. Sel. Areas Commun.*, vol. 32, no. 1, pp. 4–15, 2014.

[25] C. Kachris and I. Tomkos, “A Survey on Optical Interconnects for Data Centers - IEEE Communications Surveys & Tutorials.pdf,” vol. 14, no. 4, pp. 1021–1036, 2012.

[26] J. Arjona, A. Chatzipapas, A. F. Anta, and V. Mancuso, “A Measurement-based Analysis of the Energy Consumption of Data Center Servers,” in *5th international conference on future energy systems*, 2014, pp. 63–74.

[27] A. V. Krishnamoorthy, H. Schwetman, X. Zheng, and R. Ho, “Energy-Efficient Photonics in Future High-Connectivity Computing Systems,” *J. Light. Technol.*, vol. 33, no. 4, pp. 889–900, 2015.

[28] C. Cole, “Beyond 100G Client Optics,” *IEEE Commun. Mag.*, no. February, pp. 58–66, 2012.

[29] C. Kachris and I. Tomkos, “A survey on optical interconnects for data centers,” *IEEE Commun. Surv. Tutorials*, vol. 14, no. 4, pp. 1021–1036, 2012.

[30] C. Cole, I. Lyubomirsky, and F. Corp, “Higher-Order Modulation for Client Optics,” no. March, pp. 50–57, 2013.

[31] V. Bhatt, B. Dama, and G. Nicholl, “Update on Advanced Modulation for a Low Cost 100G Single Mode Fiber PMD,” no. July, pp. 1–20, 2012.

[32] D. V Plant, “Silicon Photonic Enabled 400G/1T Short Reach Optical Interconnects for Data Center Applications,” in *2015 IEEE Optical Interconnects Conference*, 2015, pp. 126 – 127.

[33] F. Karinou, R. Borkowski, D. Zibar, I. Roudas, K. G. Vlachos, and I. Tafur Monroy, “Advanced Modulation Techniques for High-Performance Computing Optical Interconnects,” *IEEE J. Sel. Top. Quantum Electron.*, vol. 19, no. 2, p. 3700614, 2013.

[34] Z. Zhou, Z. Tu, T. Li, and X. Wang, “Silicon Photonics for Advanced Optical Interconnections,” *J. Light. Technol.*, vol. 33, no. 4, pp. 928–933, 2015.

[35] and J. V. C. Absil, P. Verheyen, P. De Heyn, M. Pantouvaki, G. Lepage, J. De Coster, “Silicon photonics integrated circuits: a manufacturing platform for high density, low power optical I/O’s,” *Opt. Express*, vol. 23, pp. 9369–9378, 2015.

[36] J. Sangirov, I. A. Ukaegbu, T.-W. Lee, M. H. Cho, and H.-H. Park, “10 Gbps transimpedance amplifier-receiver for optical interconnects,” *J. Opt. Soc. Korea*, vol. 17, no. 1, pp. 44–49, 2013.

[37] W. Way, T. Chan, and A. Lebedev, “Technical Feasibility Study of 56Gb/s and 112Gb/s PAM-4 Transmission,” no. May, 2014.

[38] M. Traverso, M. Mazzini, M. Webster, C. Muzio, S. Anderson, P.-C. Sun, D. Siadat, D. Conti, A. Cervasio, S. Pfnuer, J. Stayt, C. Togami, T. Daugherty, and K. Yanushefski, "25GBaud PAM-4 Error Free Transmission over both Single Mode Fiber and Multimode Fiber in a QSFP form factor based on Silicon Photonics," *Opt. Fiber Commun. Conf. Post Deadline Pap.*, p. Th5B.3, 2015.

[39] K. Zhong, X. Zhou, T. Gui, L. Tao, Y. Gao, W. Chen, J. Man, L. Zeng, A. P. T. Lau, and C. Lu, "Experimental study of PAM-4, CAP-16, and DMT for 100 Gb/s Short Reach Optical Transmission Systems," *Opt. Express*, vol. 23, no. 2, p. 1176, 2015.

[40] T. Inoue and S. Namiki, "Dispersion Pre-Compensation for PAM Transmission System Using 1-sample / symbol DAC and IQ Modulator," pp. 7–9, 2015.

[41] "Fiber Optic Task Force and Next Generation Optical Ethernet Study Group," *IEEE 802.3bm 40 Gb/s and 100 Gb/s*. [Online]. Available: http://www.ieee802.org/3/bm/index.html.

[42] a. Boletti, P. Boffi, P. Martelli, M. Ferrario, and M. Martinelli, "Performance analysis of communication links based on VCSEL and silicon photonics technology for high-capacity data-intensive scenario," *Opt. Express*, vol. 23, no. 2, p. 1806, 2015.

[43] M. Morsy-Osman, M. Chagnon, M. Poulin, S. Lessard, and D. V. Plant, "224-Gb/s 10-km Transmission of PDM PAM-4 at 1.3 #x03BC;m Using a Single Intensity-Modulated Laser and a Direct-Detection MIMO DSP-Based Receiver," *J. Light. Technol.*, vol. 33, no. 7, pp. 1417–1424, 2015.

[44] R. Dubé-demers, C. S. Park, S. Larochelle, and W. Shi, "60 Gb / s PAM-4 Operation with a Silicon Microring Modulator," vol. 59, pp. 153–154, 2015.

[45] W. T. Beyene, Y. Hahm, D. Secker, D. Mullen, and N. Mayandi, "Measurement and Characterization of Backplanes for Serial Links Operating at 56 Gbps," pp. 512–517, 2015.

[46] J. Zhou, S. Member, C. Yu, S. Member, H. Kim, and S. Member, "Transmission Performance of OOK and 4-PAM Signals Using Directly Modulated 1 . 5- μ m VCSEL for Optical Access Network," *J. Light. Technol.*, vol. 33, no. 15, pp. 3243–3249, 2015.

[47] B. Teipen, N. Eiselt, A. Dochhan, H. Griesser, M. Eiselt, J. Elbers, A. Optical, and N. Se, "Investigation of PAM-4 for Extending Reach in Data Center Interconnect Applications," pp. 3–6, 2015.

[48] F. Karinou, C. Prodaniuc, N. Stojanovic, M. Ortsiefer, A. Daly, R. Hohenleitner, B. Kogel, and C. Neumeyr, "Experimental performance evaluation of equalization techniques for 56 Gb/s PAM-4 VCSEL-based optical interconnects," *2015 Eur. Conf. Opt. Commun.*, no. 2, pp. 1–3, 2015.

[49] D. Sadot, G. Dorman, A. Gorshtein, E. Sonkin, and O. Vidal, "Single channel 112Gbit/sec PAM4 at 56Gbaud with digital signal processing for data centers applications," *Opt. Express*, vol. 23, no. 2, pp. 991–997, 2015.

[50] K. Szczerba, P. Westbergh, M. Karlsson, P. A. Andrekson, and A. Larsson, "70 Gbps 4-PAM and 56 Gbps 8-PAM Using an 850 nm VCSEL," *J. Light. Technol.*, vol. 33, no. 7, pp. 1395–1401, 2015.

[51] IEEE Std 802.3-2012 Section Six, "IEEE Std 802.3-2012 Section Six," 2012.

[52] IEEE-802.3bj-standard, "IEEE 802.3bj-2014," 2014.

[53] J. R. Barry, *Wireless Infrared Communications*. M A Kluwer, 1994.

[54] S. B. Inphi, "PAM Modulation for 400G SMF 400GE Reach Objectives," no. May, 2014.

[55] R. Ramasawami, K. Sivarajan, and G. Sasaki, *Optical networks: a practical prespective*, Third. Morgan Kaufman, 2010.

[56] G. P. Agrawal, "Nonlinear Fiber Optics," pp. 195–211, 2000.

[57] S. Arnon, J. R. Barry, G. K. Karagiannidis, R. Schober, and M. Uysal, *Advanced wireless optical communication systems*. 2006.

[58] J. Karout, E. Agrell, K. Szczerba, and M. Karlsson, "Optimizing constellations for single-subcarrier intensity-modulated optical systems," *IEEE Trans. Inf. Theory*, vol. 58, no. 7, pp. 4645–4659, 2012.

[59] K. Szczerba, P. Westbergh, J. Karout, J. S. Gustavsson, Å. Haglund, M. Karlsson, P. a. Andrekson, E. Agrell, and A. Larsson, "4-PAM for High-Speed Short-Range Optical Communications," *J. Opt. Commun. Netw.*, vol. 4, no. 11, p. 885, 2012.

[60] J. M. Kahn and J. R. Barry, "Wireless Infrared Communications," vol. 9219, no. 97, 1997.

[61] P. Pathak, X. Feng, P. Hu, and P. Mohapatra, "Visible Light Communication, Networking and Sensing: A Survey, Potential and Challenges," *IEEE Commun. Surv. Tutorials*, no. c, pp. 1–1, 2015.

[62] H. C. Ji, H. Kim, and Y. C. Chung, "Full-duplex radio-over-fiber system using phase-modulated downlink and intensity-modulated uplink," *IEEE Photonics Technol. Lett.*, vol. 21, no. 1, pp. 9–11, 2009.

[63] W. Yan, T. Tanaka, B. Liu, M. Nishihara, L. Li, T. Takahara, Z. Tao, J. C. Rasmussen, and T. Drenski, "100 Gb/s Optical IM-DD Transmission with 10G-Class Devices Enabled by 65 GSamples/s CMOS DAC Core," *Opt. Fiber Commun. Conf. Fiber Opt. Eng. Conf. 2013*, p. OM3H.1, 2013.

[64] W. Yan, L. Li, B. Liu, H. Chen, Z. Tao, T. Tanaka, T. Takahara, J. C. Rasmussen, and T. Drenski, "80 km IM-DD transmission for 100 Gb/s per lane enabled by DMT and nonlinearity management," *Conf. Opt. Fiber Commun. Tech. Dig. Ser.*, pp. 4–6, 2014.

[65] X. Z. X. Zhu and J. M. Kahn, "Free-space optical communication through atmospheric turbulence channels," *IEEE Trans. Commun.*, vol. 50, no. 8, pp. 1293–1300, 2002.

[66] J. M. Kahn, K. Ho, and S. Member, "Spectral Efficiency Limits and Modulation / Detection Techniques for DWDM Systems," vol. 10, no. 2, pp. 259–272, 2004.

[67] M. S. Islim, D. Tsonev, and H. Haas, "Spectrally Enhanced PAM-DMT for IM/DD Optical Wireless Communications," *Int. Symp. Pers. Indoor Mob. Radio Commun.*, pp. 877–882, 2015.

[68] M. Presi, R. Corsini, M. Artiglia, F. Bottoni, G. Cossu, and E. Ciaramella, "Low-Cost 6 . 25 GHz UDWDM-PON based on Direct Intensity-Modulated Transmitters," pp. 6–8, 2015.

[69] R. P. Giddings, Y. Hong, X. Q. Jin, J. L. Wei, X. Zheng, and J. M. Tang, "First Experimental Demonstration of Low-Cost VCSEL- Intensity Modulated End-to-End Real-Time Optical OFDM Signal Transmission at 11 . 25Gb / s over 25km SSMFs," *Assembly*, pp. 25–27, 2011.

[70] J. Armstrong, B. J. C. Schmidt, D. Kalra, H. a. Suraweera, and A. J. Lowery, "Performance of asymmetrically clipped optical OFDM in AWGN for an intensity modulated direct detection system," *GLOBECOM - IEEE Glob. Telecommun. Conf.*, pp. 6–10, 2006.

[71] K. Szczerba, J. Karout, E. Agrell, P. Westbergh, P. Andrekson, and A. Larsson, "Chalmers Publication Library Copyright Notice Demonstration of 8-level subcarrier modulation sensitivity improvement in an IM / DD system," vol. 9, pp. 8–11.

[72] R. Ramirez-Iniguez, S. M. Idrus, and Z. Sun, *Optical Wireless communications : IR for wireless connectivity*. CRC Press, 2008.

[73] X. Li, J. Vucic, V. Jungnickel, and J. Armstrong, "On the Capacity of Intensity-Modulated Direct-Detection Systems and the Information Rate of ACO-OFDM for Indoor Optical Wireless Applications," *IEEE Trans. Commun.*, vol. 60, no. 3, pp. 799–809, 2012.

[74] ANSI, "Laser Standards and Classifications," *American National Standard for Safe Use of Lasers*, 2007. [Online]. Available: https://www.lia.org/PDF/Z136_1_s.pdf.

[75] Internationatal-Electrotechnical-Commission-(IEC), "Safety of laser products- Part12: Safety of Free space opticalk communication systems used for tranmssion of information," *Safety of laser products*, 2004. .

[76] F. Träger, "Springer Handbook of Lasers and Optics," *Springer Handb. Lasers Opt.*, vol. 72, p. 1332, 2007.

[77] IEC, "Safety of laser products - Part1: Equipment classification and requirements," *Int. Stand.*, vol. 05, pp. 1–13, 2014.

[78] S. Arnon, J. R. Barry, G. K. Karagiannidis, R. Schober, and M. Uysal, *Advanced Optical Wireless Communication Systems*. 2006.

[79] G. D. Forney and L. F. Wei, "Multidimensional Constellations-Part I: Introduction. Figures of Merit, and Generalized Cross Constellations," *IEEE J. Sel. Areas Commun.*, vol. 7, no. 6, pp. 877–892, 1989.

[80] L.-F. Wei, "Trellis-coded modulation with multidimensional constellations," *IEEE Trans. Inf. Theory*, vol. 33, no. 4, pp. 483–501, 1987.

[81] W. Mao and J. Kahn, "Lattice codes for amplified direct-detection optical systems," *IEEE Trans. Commun.*, vol. 56, no. 7, pp. 1137–1145, 2008.

[82] S. Hranilovic and F. R. Kschischang, "Capacity bounds for power- and band-limited optical intensity channels corrupted by Gaussian noise," *IEEE Trans. Inf. Theory*, vol. 50, no. 5, pp. 784–795, 2004.

[83] D. S. Shiu and J. M. Kahn, "Shaping and nonequiprobable signaling for intensity-modulated signals," *IEEE Trans. Inf. Theory*, vol. 45, no. 7, pp. 2661–2668, 1999.

[84] A. R. Calderbank and L. H. Ozarow, "Nonequiprobable Signaling on the Gaussian Channel," *IEEE Trans. Inf. Theory*, vol. 36, no. 4, pp. 726–740, 1990.

[85] R. Laroia, N. Farvardin, and S. A. Tretter, "On Optimal Shaping of Multidimensional Constellations," *IEEE Trans. Inf. Theory*, vol. 40, no. 4, pp. 1044–1056, 1994.

[86] M. S. Proakis, John G., *Digital Communications*. McGraw-Hill, 2008.

[87] K.-P. Ho, *Phase-Modulated Optical Communication Systems*. Springer Verlag, 2005.

[88] R.-J. Essiambre, G. Kramer, P. J. Winzer, G. J. Foschini, and B. Goebel, "Capacity Limits of Optical Fiber Networks," *J. Light. Technol.*, vol. 28, no. 4, pp. 662–701, 2010.

[89] L. Nguyen Binh, *Advanced digital optical communications*. CRC Press, 2015.

[90] J. B. Anderson, *Digital Transmission Engineering*. New Jersey: IEEE Press, 2005.

[91] P. J. Winzer and R. J. Essiambre, "Advanced modulation formats for high-capacity optical

transport networks," *Journal of Lightwave Technology*, vol. 24, no. 12. pp. 4711–4728, 2006.

[92] S. Dolinar, D. Divsalar, J. Hamkins, and F. Pollara, "Capacity of PPM on Gaussian and Webb channels," *2000 IEEE Int. Symp. Inf. Theory (Cat. No.00CH37060)*, no. 1, pp. 1–31, 2000.

[93] H. P. H. Park and J. R. Barry, "Modulation analysis for wireless infrared communications," *Proc. IEEE Int. Conf. Commun. ICC '95*, vol. 2, pp. 1182–1186, 1995.

[94] Z. Ghassemlooy, W. Popoola, and S. Rajbhandari, *Optical wireless communications: system and channel modelling with Matlab®*. 2012.

[95] J. R. Barry, *DIGITAL Communication*, Third Edit. Springer, 2004.

[96] K. Szczerba, P. Westbergh, J. Gustavsson, A. Haglund, J. Karout, M. Karlsson, P. Andrekson, E. Agrell, and A. Larsson, "30 Gbps 4-PAM transmission over 200m of MMF using an 850 nm VCSEL," *2011 37th Eur. Conf. Exhib. Opt. Commun.*, vol. 19, no. 26, pp. 1–3, 2011.

[97] R. Rodes, J. Estaran, B. Li, M. Mueller, J. B. Jensen, T. Gründl, M. Ortsiefer, C. Neumeyr, J. Rosskopf, K. J. Larsen, M.-C. Amann, and I. T. Monroy, "100 Gb/s single VCSEL data transmission link," *Opt. Fiber Commun. Natl. Fiber Opt. Eng. Conf.*, p. PDP5D.10, 2012.

[98] K. Szczerba, P. Westbergh, M. Karlsson, P. A. Andrekson, and A. Larsson, "60 Gbits error-free 4-PAM operation with 850 nm VCSEL," *Electron. Lett.*, vol. 49, no. 15, pp. 953–955, 2013.

[99] K. Szczerba, M. Karlsson, P. Andrekson, A. Larsson, and E. Agrell, "35.2 Gbps 8-PAMTransmission Over 100 m of MMF Using an 850 nm VCSEL," *39th Eur. Conf. Exhib. Opt. Commun.*, no. 2, p. Th.1.F.1, 2013.

[100] S. K. Pavan, J. Lavrencik, R. Shubochkin, Y. Sun, J. Kim, D. Vaidya, R. L. Jr, T. Kise, and S. E. Ralph, "50Gbit / s PAM-4 MMF Transmission Using 1060nm VCSELs with Reach beyond 200m," *Opt. Fiber Commun. Conf.*, no. 1, pp. 4–6, 2014.

[101] H. Zhang, S. Fu, J. Man, W. Chen, X. Song, and L. Zeng, "30km Downstream Transmission Using 4×25Gb/s 4-PAM Modulation with Commercial 10Gbps TOSA and ROSA for 100Gb/s-PON," *Opt. Fiber Commun. Conf.*, p. M2I.3, 2014.

[102] M. Poulin, C. Latrasse, J.-F. Gagne, Y. Painchaud, M. Cyr, C. Paquet, M. Morsy-Osman, M. Chagnon, S. Lessard, and D. V Plant, "107 Gb/s PAM-4 transmission over 10 km using a SiP series push-pull modulator at 1310 nm," in *Optical Communication (ECOC), 2014 European Conference on*, 2014, pp. 1–3.

[103] C. Prodaniuc, N. Stojanovic, F. Karinou, G. Goeger, and Z. Qiang, "56 Gb / s , PAM-4 Transmission Over 25 km , Using IQ Modulator and Unequally Spaced Levels," no. Cd, pp. 6–7, 2015.

[104] J. M. Castro, R. Pimpinella, B. Kose, Y. Huang, B. Lane, K. Szczerba, P. Westbergh, T. Lengyel, J. Gustavsson, A. Larsson, and P. A. Andrekson, "50 Gb/s 4-PAM over 200 m of High Bandwidth MMF using a 850 nm VCSEL," *Opt. Fiber Commun. Conf.*, vol. 6, p. W1D.1, 2015.

[105] J. Zhou, C. Yu, H. Kim, P. Krrqnlp, and N. Df, "1.5-μm, 21.4-Gbps 4-PAM VCSEL Link for Optical Access Applications," vol. 1, pp. 53–55, 2015.

[106] D. Patel, A. Samani, V. Veerasubramanian, S. Ghosh, and D. V Plant, "Silicon Photonic Segmented Modulator-Based Electro-Optic DAC for 100 Gb / s PAM-4 Generation," vol. 27, no. 23, pp. 2433–2436, 2015.

[107] J. C. Cartledge, "Comparison of Effective -Parameters for Semiconductor Mach – Zehnder Optical Modulators," vol. 16, no. 3, pp. 372–379, 1998.

[108] P. J. Winzer and R.-J. Essiambre, “Advanced optical modulation formats,” *Opt. Fiber Telecommun. V B Syst. Networks*, 2008.

[109] D. Feng, S. Liao, P. Dong, N. N. Feng, H. Liang, D. Zheng, C. C. Kung, J. Fong, R. Shafiiha, J. Cunningham, A. V. Krishnamoorthy, and M. Asghari, “High-speed Ge photodetector monolithically integrated with large cross-section silicon-on-insulator waveguide,” *Appl. Phys. Lett.*, vol. 95, no. 26, 2009.

[110] G. P. Agrawal, *Lightwave Technology: Telecommunication Systems*. John Wiley & Sons, Inc., 2005.

[111] J. L. Rebola and A. V. T. Cartaxo, “Gaussian approach for performance evaluation of optically preamplified receivers with arbitrary optical and electrical filters,” *IEE Proc. - Optoelectron.*, no. June, pp. 135–142, 2001.

[112] R. Hui and M. O’Sullivan, *Fiber Optic Measurement Techniques*. 2009.

[113] Corning, “Corning SMF -28 Ultra optical fiber.” [Online]. Available: https://www.corning.com/media/worldwide/coc/documents/Fiber/SMF-28 Ultra.pdf.

[114] G. P. Agrawal, *Fiber-Optic Communications Systems, Third Edition.*, vol. 6. 2002.

[115] E. Ip, A. P. T. Lau, D. J. F. Barros, and J. M. Kahn, “Coherent detection in optical fiber systems.,” *Opt. Express*, vol. 16, no. 2, pp. 753–791, 2008.

[116] T. Xu, G. Jacobsen, S. Popov, J. Li, E. Vanin, K. Wang, A. T. Friberg, and Y. Zhang, “Chromatic dispersion compensation in coherent transmission system using digital filters.,” *Opt. Express*, vol. 18, no. 15, pp. 16243–16257, 2010.

[117] G. P. Agrawal, *Fiber-Optic Communication Systems*. John Wiley & Sons, Inc., 2002.

[118] P. J. Winzer and R.-J. Essiambre, “Advanced Optical Modulation Formats,” *Proc. IEEE*, vol. 94, no. 5, pp. 952–985, 2006.

[119] S. Kumar, “Intrachannel Four-Wave Mixing in Dispersion Managed RZ Systems,” vol. 1135, no. August, pp. 800–802, 2001.

[120] B. Essiambre, R.-J., Raybon, G., and Mikkelsen, “Pseudo-linear transmission of highspeed TDM signals: 40 and 160 Gb/s,” in *Optical Fiber Telecommunications IV:*, T. Kaminow, I. P. and Li, Ed. Academic press, 2002.

[121] I. Djordjevic, W. Ryan, and B. Vasic, *Coding for Optical Channels*, no. 1. 2010.

[122] J. Takala, “Roles of pulse position modulation on intrachannel nonlinearities affected high-bit-rate optic fiber channel,” *2004 IEEE Int. Conf. Commun. (IEEE Cat. No.04CH37577)*, vol. 3, no. 1, pp. 1745–1749 Vol.3, 2004.

[123] R.-J. Essiambre, B. Mikkelsen, and G. Raybon, “Intra-channel cross-phase modulation and four-wave mixing in high-speed TDM systems,” *Electron. Lett.*, vol. 35, no. 18, pp. 1576–1578, 1999.

[124] M. Forzati, J. M??rtensson, A. Berntson, A. Djupsj??backa, and P. Johannisson, “Reduction of intrachannel four-wave mixing using the alternate-phase RZ modulation format,” *IEEE Photonics Technol. Lett.*, vol. 14, no. 9, pp. 1285–1287, 2002.

[125] S. Randel, B. Konrad, A. Hodlic, and K. Petermann, “Influence of Bitwise Phase Changes on the Performance of 160 Gbitls Transmission Systems,” in *European Conference of Optical Communication (ECOC)*, 2002, vol. 1, no. c, pp. 1–2.

[126] M. Khairuzzaman, C. Zhang, K. Igarashi, K. Katoh, and K. Kikuchi, “Fiber-nonlinearity equalization by maximum-likelihood-sequence estimation (MLSE) in digital coherent receivers,” *2009 14th Optoelectron. Commun. Conf. OECC 2009*, pp. 2–3, 2009.

[127] P. Zhou, X. Wang, and Z. Jiang, “Theoretical Study of the Threshold of Stimulated Brillouin Scattering in Multimode Fibers,” *Light. Technol. IEEE J.*, vol. 33, no. 21, pp. 4464–4470, 2015.

[128] T. Schneider, a. Wiatrek, and R. Henker, “Dispersion compensation by SBS based slow-light in an optical fiber,” *2009 Conf. Opt. Fiber Commun. - incudes post deadline Pap.*, no. 1, pp. 7–9, 2009.

[129] H. a Al-Asadi, M. H. Al-Mansoori, M. Ajiya, S. Hitam, M. I. Saripan, and M. a Mahdi, “Effects of pump recycling technique on stimulated Brillouin scattering threshold: a theoretical model.,” *Opt. Express*, vol. 18, no. 21, pp. 22339–47, 2010.

[130] N. Reinold, *Essentials of modern optical fiber communication*. Springer, 2010.

[131] C. E. Shannon, “A mathematical theory of communication,” *Bell Syst. Tech. J.*, vol. 27, no. July 1928, pp. 379–423, 1948.

[132] a. D. Ellis, J. Z. J. Zhao, and D. Cotter, “Approaching the Non-Linear Shannon Limit,” *J. Light. Technol.*, vol. 28, no. 4, pp. 423–433, 2010.

[133] A. Ellis, “Modulation Formats Which Approach the Shannon Limit,” *Opt. Fiber Commun. Conf. Natl. Fiber Opt. Eng. Conf.*, p. OMM4, 2009.

[134] J. D. Ambrosia, “400GbE Task Force Opening Report IEEE P802 . 3bs 400GbE Task Force,” pp. 1–7.

[135] D. Tse, “Fundamentals of Wireless Communications 12,” p. 646, 2004.

[136] M. a. Taubenblatt, “Optical Interconnects for High-Performance Computing,” *J. Light. Technol.*, vol. 30, no. 4, pp. 448–457, 2012.

[137] J. C. Cartledge and A. S. Karar, “100 Gb/s Intensity Modulation and Direct Detection,” *Light. Technol. J.*, vol. 32, no. 16, pp. 2809–2814, 2014.

[138] Steve Hranilovic, *Wireless Optical Communication Systems*. 2005.

[139] V. A. Kotelnikov, “The theory of optimum noise immunity,” Ph.D. dissertation, 1947.

[140] Shannon, “Communication in the Presence of Noise,” 1949.

[141] J. M. Wozencraft and I.M. Jacobs, “Principles of Communication Engineering.” John Wiley & Sons, Inc., Newyork, 1965.

[142] Xue-Bin Liang and Xiang-Gen Xia, “Unitary signal constellations for differential space-time modulation with two transmit antennas: parametric codes, optimal designs, and bounds,” *IEEE Trans. Inf. Theory*, vol. 49, no. 8, pp. 2291–2322, 2002.

[143] J.-K. K. and I. L. Jihoon Kim, Wonjun Lee, “On the symbol error rates for signal space diversity schemes over a rician fading channel,” *IEEE Trans. Commun.*, vol. 57, no. 8, pp. 2204–2209, 2009.

[144] S. H. and F. R. Kschischang, “Optical intensity-modulated direct detection channels: Signal space and lattice codes,” *IEEE Trans. Inf. Theory*, vol. 49, no. 6, pp. 1385–1399, 2003.

[145] S. and E. B. Benedetto, *Principles of Digital Transmission With Wireless Applications*. New York, NY: KLUWER ACADEMIC PUBLISHERS, 2002.

[146] A. V Oppenheim and R. W. Schafer, “Communication Systems,” 1987.

[147] B. Sklar, *Digital Communications: Fundamentals and Applications*, 2nd Editio. .

[148] M. Tavan, E. Agrell, J. Karout, and S. Member, “Bandlimited Intensity Modulation,” *IEEE Glob. Commun. Conf.*, pp. 1–28, 2011.

[149] A. Goldsmith, *Wireless communications*. Wiley, 2005.

[150] J. Proakis and M. Salehi, *Communication systems engineering*, 2nd Editio. 1994.

[151] O. E. Agazzi, M. R. Hueda, H. S. Carrer, and D. E. Crivelli, “Maximum-likelihood sequence estimation in dispersive optical channels,” *J. Light. Technol.*, vol. 23, no. 2, pp. 749–763, 2005.

[152] O. E. Agazzi, D. E. Crivelli, and H. S. Carrer, “Maximum likelihood sequence estimation in the presence of chromatic and polarization mode dispersion in intensity modulation/direct detection optical channels,” *2004 IEEE Int. Conf. Commun. (IEEE Cat. No.04CH37577)*, vol. 5, no. c, pp. 2787–2793, 2004.

[153] M. O. Damen, H. El Gamal, and G. Caire, “On maximum-likelihood detection and the search for the closest lattice point,” *IEEE Trans. Inf. Theory*, vol. 49, no. 10, pp. 2389–2402, 2003.

[154] D. Marsella, M. Secondini, and E. Forestieri, “Maximum Likelihood Sequence Detection for Mitigating Nonlinear Effects,” *Light. Technol. J.*, vol. 32, no. 5, pp. 908–916, 2014.

[155] Agrawal, *Fiber-Optic Communications Systems, Third Edition.*, vol. 6. 2002.

[156] E. A. Lee and D. G. Messerschmitt, *Digital Communication*. KLUWER ACADEMIC PUBLISHERS, 1994.

[157] A. . Fallis, “A COMPARISON OF CMOS AND BiCMOS ADD-COMPARE-SELECT CIRCUITS FOR MAXIMUM LIKELIHOOD SEQUENCE DETECTORS,” *J. Chem. Inf. Model.*, vol. 53, no. 9, pp. 1689–1699, 2013.

[158] G. Bosco and P. Poggiolini, “Long-distance effectiveness of MLSE IMDD receivers,” *IEEE Photonics Technol. Lett.*, vol. 18, no. 9, pp. 1037–1039, 2006.

[159] T. Foggi, E. Forestieri, G. Colavolpe, and G. Prati, “Maximum-likelihood sequence detection with closed-form metrics in OOK optical systems impaired by GVD and PMD,” *J. Light. Technol.*, vol. 24, no. 8, pp. 3073–3087, 2006.

[160] O. Software, “OptiSystem Publication References - 2014,” *OptiSystem Publication References - 2014*, 2015. .

[161] O. Software, “OptiSystem Version 12,” *Manual-OptiSystem Version 12*. [Online]. Available: http://optiwave.com.

[162] J. Salehi and M. Proakis, *Communication Systems Engineering*. 2002.

[163] W. Freude, R. Schmogrow, B. Nebendahl, M. Winter, A. Josten, D. Hillerkuss, S. Koenig, J. Meyer, M. Dreschmann, M. Huebner, C. Koos, J. Becker, and J. Leuthold, “Quality metrics for optical signals Eye diagram, Q-factor, OSNR, EVM and BER,” *Transparent Opt. Networks (ICTON), 2012 14th Int. Conf.*, vol. 1, pp. 1–4, 2012.

[164] S. Ibrahim and S. Bhandare, “Narrowband 2x10 Gbit/s Quaternary Intensity Modulation Based on Duobinary Modulation in Two Polarizations with Unequal Amplitudes,” *Opt. Fiber Commun.*, no. August, pp. 10–12, 2006.

[165] S. Walklin, J. Conradi, and S. Member, “Multilevel Signaling for Increasing the Reach of 10 Gb / s Lightwave Systems,” *Light. Technol. IEEE J.*, vol. 17, no. 11, pp. 2235–2248, 1999.

[166] Anritsu CORPORATION, “Q Factor/Eye Analysis Software,” 2000.

[167] B. Nebendahl, R. Schmogrow, T. Dennis, A. Josten, D. Hillerkuss, S. Koenig, J. Meyer, M. Dreschmann, M. Winter, M. Huebener, W. Freude, C. Koos, and J. Leuthold, “Quality Metrics in Optical Modulation Analysis: EVM and its relation to Q-factor, OSNR, and BER,” in *Asia Communications and Photonics Conference*, 2012, p. AF3G.2.

[168] Maxim Integrated, “Optical Modulation Amplitude (OMA) and Extinction Ratio,” pp. 1–5, 2008.

[169] D. Van Den Borne, *Robust Optical Transmission Systems: Modulation and Equalization*. 2008.

[170] E. FORESTIERI, *OPTICAL COMMUNICATION THEORY AND TECHNIQUES*. Springer US, 2005.

[171] OFSTP-4A, “Optical Eye Pattern Measurement Procedure,” 1997.

[172] GR-253-CORE, “Synchronous Optical Network (SONET) Transport Systems: Common Generic Criteria,” 1999.

[173] ITU-T-Recommendation-G.957, “Optical Interfaces for Equipments and Systems Relating to the Synchronous Digital Hierarchy,” 2006.

[174] IEC-61280-2-2:, “Fibre Optic Communication Subsystem Test Procedures - Part 2–2: Digital Systems - Optical Eye Pattern, Waveform, and Extinction Ratio Measurement,” 2008.

[175] G. Breed, “Using the Eye Diagram,” *High Freq. Electron.*, no. November, pp. 50–53, 2005.

[176] J. L. Rebola and A. V. T. Cartaxo, “Q-factor estimation and impact of spontaneous-spontaneous beat noise on the performance of optically preamplified systems with arbitrary optical filtering,” *J. Light. Technol.*, vol. 21, no. 1, pp. 87–95, 2003.

[177] S. Alexander, *Optical Communication Receiver Design*. London, UK: SPIE Press, 1997.

[178] K. Kikuchi and S. Tsukamoto, “Evaluation of Sensitivity of the Digital Coherent Receiver,” *J. Light. Technol.*, vol. 26, no. 13, pp. 1817–1822, 2008.

[179] E. Agrell and M. Karlsson, “Power-efficient modulation formats in coherent transmission systems,” *J. Light. Technol.*, vol. 27, no. 22, pp. 5115–5126, 2009.

[180] P. D. Townsend, P. Ossieur, and N. Quadir, “A 56Gb/s PAM-4 VCSEL driver circuit,” *IET Irish Signals Syst. Conf. (ISSC 2012)*, no. JUNE 2012, pp. 59–59, 2012.

[181] P. Moser, “oxide-confined VCSELs for optical interconnects in data centers and supercomputers,” no. April 2015.

[182] F. Gray, “Pulse code communication.” US Patent, 1953.

[183] E. Agrell, J. Lassing, E. G. Strom, and T. Ottosson, “On the Optimality of the Binary Reflected Gray Code,” *IEEE Trans. Inf. Theory*, vol. 50, no. 12, pp. 3170–3182, 2004.

[184] Z. Zalevsky, P. García-Martínez, and J. García, “Superresolution using gray level coding.,” *Opt. Express*, vol. 14, no. 12, pp. 5178–5182, 2006.

[185] S. Hranilovic, “Spectrally Efficient Signalling for Wireless Optical,” 2003.

[186] L. N. Binh, *Digital Processing Optical Transmission and Coherent Receiving Techniques*. CRC

Press, 2014.

[187] S. M. Park, J. Lee, and H. J. Yoo, "1-Gb/s 80-dBΩ fully differential CMOS transimpedance amplifier in multichip on oxide technology for optical interconnects," *IEEE J. Solid-State Circuits*, vol. 39, no. 6, pp. 971–974, 2004.

[188] C. DeCusatis, *HANDBOOK OF FIBER OPTIC DATA COMMUNICATION*, Second edi. Academic press, 2002.

[189] G. Boreman, *Basic Electro-optics for Electrical Engineers*. SPIE Press, 1998.

[190] M. I. Products, "Impact of Transmitter RIN on Optical Link Performance," pp. 1–7, 2008.

[191] J. Palais, *Fiber Optic Communications*. Prentice Hall, 2005.

[192] C. Science, *Fundamentals of Optical Communications*. Prentice Hall, 2005.

[193] L. A. N. Man, S. Committee, and I. Computer, *IEEE Standard for Ethernet Amendment 2 : Physical Layer Specifications and Management Parameters for 100 Gb / s Operation Over Backplanes and Copper Cables*, vol. 2014. 2014.

[194] E. Säckinger, *Broadband Circuits for Optical Fiber Communication*. 2005.

[195] C. M. DeCusatis and C. J. Sher DeCusatis, *Fiber Optic Essentials*. 2006.

[196] G. Nicholl and C. F. Cisco, "Update on technical feasibility for PAM modulation," no. March, 2012.

[197] M. A. Elsherif and A. Malekmohammadi, "Power Efficiency Evaluation of Mapping Multiplexing Technique and Pulse Amplitude Modulation for Noncoherent Systems," *IEEE Photonics J.*, vol. 7, no. 4, pp. 1–12, 2015.

[198] W. H. Press, S. a Teukolsky, W. T. Vetterling, and B. P. Flannery, *Numerical recipes in C (2nd ed.): the art of scientific computing*, vol. 29, no. 4. 1992.

[199] AGILENT, "Keysight N4974A PRBS Generator 40 Gb / s," *PRBS Keysight*. [Online]. Available: http://literature.cdn.keysight.com/litweb/pdf/N4974-91021.pdf?id=2217665.

[200] C.-F. Lin, *Optical Components for Communications: Principles and Applications*. Congress library, 2004.

[201] AGILENT, "Agilent 71452B Optical Spectrum Analyzer," *Optical Spectrum Analyzer*. [Online]. Available: http://cp.literature.agilent.com/litweb/pdf/5963-7148E.pdf.

[202] Optilab, "25 dB Gain Pre-Amp EDFA Module, C-band (EDFA-PA-M)," *EDFA*. [Online]. Available: http://www.optilab.com/products/category/module_edfa/25_d_gain_pre_amp_edfa_module_c_band/.

[203] THORLABS, "D400FC InGaAs Fiber Optic Photo Detector," *Photodetcttors*. [Online]. Available: https://www.thorlabs.de/thorcat/2100/D400FC-SpecSheet.pdf.

[204] J. Zhao, L. Huo, and C. Chan, "Analytical investigation of optimization, performance bound, and chromatic dispersion tolerance of 4-amplitude-shifted-keying format," *2006 Opt. Fiber Commun. Conf. Natl. Fiber Opt. Eng. Conf.*, p. 3 pp., 2006.

[205] M. Seimetz, *High-Order Modulation for Optical Fiber Transmission*. Berlin: Springer Germany, 2009.

[206] N. a. Olsson, “Lightwave systems with optical amplifiers,” *J. Light. Technol.*, vol. 7, no. 7, pp. 1071–1082, Jul. 1989.

[207] V. Ter-Mikirtychev, *Fundamentals of fiber lasers and fiber amplifiers*, vol. 181. Springer Series in Optical Sciences, 2014.

[208] Y. Chen, X. Zhou, X. Chen, J. Su, and C. Li, “A Cost-effective and Low-overhead Chromatic Dispersion Compensation Scheme in TDM PON Systems,” *2012 Second Int. Conf. Instrumentation, Meas. Comput. Commun. Control*, pp. 1069–1072, Dec. 2012.

[209] B. Konrad, K. Petermann, S. Member, J. Berger, R. Ludwig, C. M. Weinert, H. G. Weber, and B. Schmauss, “Impact of Fiber Chromatic Dispersion in High-Speed TDM Transmission Systems,” vol. 20, no. 12, pp. 2129–2135, 2002.

[210] J. M. Senior, *Optical Fiber Communications: Principles and Practice*. Pearson Education, 2009.

[211] J. C. Cartledge and S. Member, “Combining Self-Phase Modulation and Optimum Modulation Conditions to Improve the Performance of 10-Gb / s Transmission Systems Using MQW Mach – Zehnder Modulators,” *J. Light. Technol.*, vol. 18, no. 5, pp. 647–655, 2000.

[212] A. K. Somani, J. R. J. Endowed, and C. Engineering, *SURVIVABILITY AND TRAFFIC GROOMING IN WDM OPTICAL NETWORKS*. Cambridge University Press.

[213] M. D. Perry, T. Ditmire, and B. C. Stuart, “Self-phase modulation in chirped-pulse amplification.,” *Opt. Lett.*, vol. 19, no. 24, pp. 2149–51, 1994.

[214] G. P. Agrawal, “Self-phase modulation in optical fiber communications: good or bad?,” in *2007 Quantum Electronics and Laser Science Conference*, 2007, pp. 1–2.

[215] Corning, “Corning Pure-form SMF DCM Modules.” [Online]. Available: http://www.lightwavestore.com/product_datasheet/FSC-DCM-018C_pdf1.pdf.

[216] R. Lipsman and J. Rosenberg, *A Guide to MATLAB*, vol. 16. 2001.

[217] W. L. Martinez, A. R. Martinez, and H. Crc, “Computational Statistics Handbook with Matlab,” *New York*, vol. 65, no. 1, p. 616, 2002.

[218] A. Sahara, H. Kubota, and M. Nakazawa, “Q-factor contour mapping for evaluation of optical transmission systems: Soliton against NRZ against RZ pulse at zero group velocity dispersion,” *Electron. Lett.*, vol. 32, no. 10, pp. 915–916, 1996.

[219] G. Tzimpragos, C. Kachris, I. Djordjevic, M. Cvijetic, D. Soudris, and I. Tomkos, “A Survey on FEC Codes for 100G and Beyond Optical Networks,” *IEEE Commun. Surv. Tutorials*, no. c, pp. 1–1, 2014.

[220] N. Kikuchi and S. Sasaki, “Improvement of tolerance to fibre non-linearity of incoherent multilevel signalling for WDM transmission with 10-Gbit/s OOK channels,” *2009 35th Eur. Conf. Opt. Commun.*, pp. 4–5, 2009.

[221] G. Agrawal, “Nonlinear Fiber Optics,” *Nonlinear Sci. Daw. 21st Century*, pp. 195–211, 2000.

[222] M. f. Ferreira, *Nonlinear Effects in Optical Fibers*. New Jersey: John Wiley & Sons, Inc., 2011.

[223] X. Wei, X. Liu, S. Chandrasekhar, A. H. Gnauck, G. Raybon, J. Leuthold, and P. J. Winzer, “40 Gb/s Duobinary and Modified Duobinary Transmitter Based on an Optical Delay Interferometer,” *28th Eur. Conf. Opt. Commun.*, vol. 4, pp. 1–2, 2002.

[224] E. Pincemin, C. Gosset, N. Boudrioua, A. Tan, D. Grot, and T. Guillossou, “Experimental

performance comparison of Duobinary and PSBT modulation formats for long-haul 40 Gb/s transmission on G 0.652 fibre," *Opt. Express*, vol. 20, no. 27, pp. 28171–28190, Dec. 2012.

[225] M. Franceschini, G. Bongiorni, G. Ferrari, R. Raheli, F. Meli, and A. Castoldi, "Fundamental limits of electronic signal processing in direct-detection optical communications," *J. Light. Technol.*, vol. 25, no. 7, pp. 1742–1753, 2007.

[226] E. Kakoulli, V. Soteriou, C. Koutsides, and K. Kalli, "Design of high-performance, power-efficient optical NoCs using Silica-embedded silicon nanophotonics," *2015 33rd IEEE Int. Conf. Comput. Des.*, pp. 1–8, 2015.

[227] Y. a. Vlasov, "Silicon CMOS-integrated nano-photonics for computer and data communications beyond 100G," *IEEE Commun. Mag.*, vol. 50, no. 2, pp. 67–72, 2012.

[228] R. R. Panepucci, C. a Finardi, L. T. Zanvettor, D. S. Spozito, A. C. Gozzi, C. T. I. Centro, D. Tecnologia, I. Renato, R. Dom, and P. I. S.- Km, "Silicon Photonic Integrated Circuits," pp. 6–8, 2013.

[229] L. Tsybeskov, D. J. Lockwood, and M. Ichikawa, "Silicon Photonics: CMOS Going Optical [Scanning the Issue]," *Proc. IEEE*, vol. 97, no. 7, pp. 1161–1165, 2009.

[230] A. Biberman and K. Bergman, "Optical interconnection networks for high-performance computing systems," *Reports Prog. Phys.*, vol. 75, p. 046402, 2012.

[231] K. Ohashi, K. Nishi, T. Shimizu, M. Nakada, J. Fujikata, J. Ushida, S. Toru, K. Nose, M. Mizuno, H. Yukawa, M. Kinoshita, N. Suzuki, A. Gomyo, T. Ishi, D. Okamoto, K. Furue, T. Ueno, T. Tsuchizawa, T. Watanabe, K. Yamada, S. I. Itabashi, and J. Akedo, "On-chip optical interconnect," *Proc. IEEE*, vol. 97, no. 7, pp. 1186–1196, 2009.

[232] A. Malacarne, F. Gambini, S. Faralli, J. Klamkin, and L. Potì, "High-Speed Silicon Electro-Optic Microring Modulator for Optical Interconnects," *IEEE Photonics Technol. Lett.*, vol. 26, no. 10, pp. 1042–1044, 2014.

[233] D. Guckenberger, S. Abdalla, C. Bradbury, J. Clymore, P. De Dobbelaere, D. Foltz, S. Gloeckner, M. Harrison, S. Jackson, D. Kucharski, Y. Liang, C. Lo, M. Mack, G. Masini, A. Mekis, A. Narasimha, M. Peterson, T. Pinguet, J. Redman, S. Sahni, B. Welch, K. Yokoyama, and S. Yu, "Advantages of CMOS photonics for future transceiver applications," *36th Eur. Conf. Exhib. Opt. Commun.*, pp. 1–6, 2010.

[234] P. De Dobbelaere, S. Abdalla, S. Gloeckner, M. Mack, G. Masini, A. Mekis, T. Pinguet, S. Sahni, A. Narasimha, D. Guckenberger, and M. Harrison, "Si Photonics Based High-Speed optical Transceivers," *Eur. Conf. Exhib. Opt. Commun.*, no. 1, p. We.1.E.5, 2012.

[235] P. J. Winzer, "Modulation and Multiplexing in optical communication systems," *IEEE LEOS Res. Highligh*, 2009.

[236] A. Narasimha, S. Abdalla, C. Bradbury, A. Clark, J. Clymore, J. Coyne, A. Dahl, S. Gloeckner, A. Gruenberg, D. Guckenberger, S. Gutierrez, M. Harrison, D. Kucharski, K. Leap, R. LeBlanc, Y. Liang, M. Mack, D. Martinez, G. Masini, A. Mekis, R. Menigoz, C. Ogden, M. Peterson, T. Pinguet, J. Redman, J. Rodriguez, S. Sahni, M. Sharp, T. J. Sleboda, D. Song, Y. Wang, B. Welch, J. Witzens, W. Xu, K. Yokoyama, and P. De Dobbelaere, "An Ultra Low Power CMOS Photonics Technology Platform for H/S Optoelectronic Transceivers at Less than $1 per Gbps," *Opt. Fiber Commun. Conf.*, p. OMV4, 2010.

[237] N.-N. Feng and X. Sun, "Parallel Optical Interconnects Submodule Using Silicon Optical Bench," *J. Light. Technol.*, vol. 33, no. 4, pp. 811–813, 2015.

[238] O. Liboiron-ladouceur, "Design Approaches for Energy-Efficient Optical Interconnects in

Computing Platforms," p. 5369, 2010.

[239] J. Chen, "High Capacity and Energy Efficient Optical Interconnects at Top of the Rack in Datacentres," p. 2014, 2016.

[240] J. Chen, S. Member, Y. Gong, M. Fiorani, and S. Aleksic, "Optical Interconnects at Top of the Rack for Energy - Efficient Datacentres," no. August, pp. 140–148, 2014.

[241] S. Jung and J. Gao, "CMOS Multi-level signal transmitter for optical communicatio," in *The 47th IEEE International Midwest Symposium on Circuits and Systems*, 2004, pp. 185–188.

[242] J.-R. (J. H. R. . Schrader, E. A. M. Klumperink, J. L. Visschers, and B. Nauta, "Pulse-Width Modulation Pre-Emphasis Applied in a Wireline Transmitter, Achieving 33 dB Loss Compensation at 5-Gb/s in 0.13-μm CMOS," *IEEE J. Solid-State Circuits*, vol. 41, no. 4, pp. 990–999, 2006.

[243] H. Cheng and A. C. Carusone, "A 32/16 Gb/s 4/2-PAM transmitter with PWM pre-emphasis and 1.2 Vpp per side output swing in 0.13-??m CMOS," *Proc. Cust. Integr. Circuits Conf.*, no. Cicc, pp. 635–638, 2008.

[244] D. J. Foley and M. P. Flynn, "A low-power 8-PAM serial transceiver in 0.5- mu;m digital CMOS," *IEEE J. Solid-State Circuits*, vol. 37, no. 3, pp. 310–316, 2002.

[245] B. Song, K. Kim, J. Lee, and J. Burm, "A 0.18-?? m CMOS 10-Gb/s dual-mode 10-PAM serial link transceiver," *IEEE Trans. Circuits Syst. I Regul. Pap.*, vol. 60, no. 2, pp. 457–468, 2013.

[246] C. K. K. Yang, M. a. Horowitz, and H. Lee Thomas, "A 0.3-um CMOS 8-Gb/s 4-PAM serial link transceiver," *IEEE J. Solid-State Circuits*, vol. 35, no. 5, pp. 757–764, 2000.

[247] S. K. Ibrahim and S. Bhandare, "Performance of 20 Gb / s Quaternary Intensity Modulation Based on Binary or Duobinary Modulation in Two Quadratures With Unequal Amplitudes," no. August, pp. 596–602, 2006.

[248] P. Desrousseaux, P. André, M. Meghelli, A. Konczykowska, and J. Godin, "Multilevel Decoder-Decision Circuit for High Bitrate ETDM Transmission," in *European Solid-State Circuits Conference (ESSCIRC 1997)*, 1997, pp. 368–371.

[249] G. Byun and M. Navidi, "A Low-Power 4-PAM transceiver using a Dual-Sampling Technique for Heterogeneous Latency Sensitive Network-on-Chip," *IEEE Trans. Circuits Syst. II Express Briefs*, vol. PP, no. 99, pp. 1–1, 2015.

[250] S. Qasim, S. Abbasi, and A. Bandar, "Advanced FPGA Architectures for Efficient Implementation of Computation Intensive Algorithms: A State-of-the-Art Review," *MASAUM J. Comput.*, vol. 1, no. 2, pp. 300–303, 2009.

[251] H. G. Yang, "Overview: Emerging technologies on Giga-scale FPGA implementation," *ISCAS 2010 - 2010 IEEE Int. Symp. Circuits Syst. Nano-Bio Circuit Fabr. Syst.*, pp. 1428–1431, 2010.

[252] R. Schmogrow, D. Hillerkuss, M. Dreschmann, M. Huebner, M. Winter, J. Meyer, B. Nebendahl, C. Koos, J. Becker, W. Freude, and J. Leuthold, "Real-time software-defined multiformat transmitter generating 64QAM at 28 GBd," *IEEE Photonics Technol. Lett.*, vol. 22, no. 21, pp. 1601–1603, 2010.

[253] MICRAM, "60GS/s ADC and 30GS/s DAC MICRAM," 2015. .

[254] U. Meyer-Baese, *Digital signal processing with field programmable gate arrays*, 2nd Editio. Springer, 2013.

[255] C. Laperle, M. O. Sullivan, and K. Roberts, "Advances in High-Speed ADCs , DACs , and DSP for

Optical Transceivers," pp. 1–30, 2013.

[256] W. Paper, "NRZ Bandwidth (-3db HF Cutoff vs SNR) How Much Bandwidth is Enough ?," pp. 1–11, 2003.

[257] P. J. Winzer, M. Pfennigbauer, M. M. Strasser, and W. R. Leeb, "Optimum filter bandwidths for optically preamplified NRZ receivers," *J. Light. Technol.*, vol. 19, no. 9, pp. 1263–1273, 2001.

[258] J. Perin, M. Sharif, and J. Kahn, "Modulation Schemes for Single-Laser 100 Gbit/s Links: Multicarrier," *J. Light. Technol.*, pp. 1–1, 2015.

[259] Fujitsu-LEIA, "Digital to Analog Converter (DAC) 55 – 65 GSa/s 8-bit." [Online]. Available: http://www.fujitsu.com/uk/Images/c60.pdf.

[260] Fujitsu-LUKE-ES, "Analog to Digital Converter (ADC) 65 GSa/s 8 bit," *Optical Components*. [Online]. Available: http://www.fujitsu.com/uk/Images/c63.pdf.

[261] Micram-Instruments-AWG6020, "AWG6020 - 72 GS/s VEGA DAC," *DAC*. .

[262] Fujitsu, "The Fujitsu 56GSa/s Analog-to-Digital Converter Enables 100GbE Transport," *Fujitsu Technology Backgrounder*. [Online]. Available: http://www.funkschau.de/fileadmin/media/whitepaper/files/56gsa-tech-backgrounder.pdf.

[263] Y. M. Greshishchev, D. Pollex, S. C. Wang, M. Besson, P. Flemeke, S. Szilagyi, J. Aguirre, C. Falt, N. Ben-Hamida, R. Gibbins, and P. Schvan, "A 56GS/s 6b DAC in 65nm CMOS with 256x6b memory," *Dig. Tech. Pap. - IEEE Int. Solid-State Circuits Conf.*, pp. 194–195, 2011.

[264] FINISAR-XPDV412xR, "100 GHz Single High-speed Photodetector," *Optical Components*. .

[265] Finisar-XPDV2320R, "50 GHz 1310/1550nm Single High-speed Photodetector," *Optical Components*. [Online]. Available: https://www.finisar.com/optical-components/xpdv2320r.

[266] FINISAR-XPDV3120R, "70 GHz DWDM Single High-speed Photodetector," *High-Speed Detectors and Receivers*. [Online]. Available: https://www.finisar.com/optical-components/xpdv3120r.

[267] FINISAR-MPDV1120RA, "35 GHz Single High-speed Photodetector," *Optical Components*. [Online]. Available: https://www.finisar.com/optical-components/mpdv1120ra.

[268] INPHI-IN2844TA, "IN2844TA - 28 Gbps Quad Transimpedance Amplifier/ Limiting Amplifier," *Optical Components*. [Online]. Available: https://www.inphi.com/products/in2844ta.php.

[269] K. W. Kobayashi and S. Microdevices, "State-of-the-Art 60 GHz, 3.6 K-Ohm Transimpedance Amplifier for 40 Gb/s and Beyond," in *Radio Frequency Integrated Circuits (RFIC) Symposium*, 2003, pp. 3–6.

[270] T. P. E. Broekaert and M. W. Pospieszalski, "High gain (1 kOhm) high transimpedance bandwidth (38 GHz) transimpedance amplifier in InP-HBT technology," no. 805, pp. 38–40, 2002.

[271] Finisar, "10Gb/s 200km Telecom CMLTM 13pin-GPO Butterfly Transmitter," *DM200-01-3/4*. [Online]. Available: https://www.finisar.com/sites/default/files/downloads/dm200-01-3-4_10gbs_200km_telecom_cml_13pin-gpo_butterfly_transmitter_datasheet_reva.pdf.

[272] Finisar, "CW Tunable Laser – Butterfly Package-S7500," *CW Tunable Laser*. [Online]. Available: https://www.finisar.com/sites/default/files/downloads/finisar_s7500_cw_tunable_laser_butterfly_package_product_specification.pdf.

[273] Eospace, "Low-loss and wideband intensity modulators for OC-768 applications," *External*

Modulators. [Online]. Available: http://www.eospace.com/40G_modulator.htm.

[274] THORLABS, "20 GHz Analog Modulator," *Modulators*. [Online]. Available: https://www.thorlabs.de/newgrouppage9.cfm?objectgroup_id=3945.

[275] A. Ghiasi and B. Welch, "Investigation of 100GbE Based on PAM-4 and PAM-8," *IEEE 802.3bm Task Force*, 2012.

[276] J. Anderson and S. Anderson, "PAM MPI – Overview & Recommendations," *IEEE 802.3bm Task Force*, no. May, 2012.

[277] J. Anderson and M. Traverso, "Optical transceivers for 100 gigabit ethernet and its transport," *IEEE Commun. Mag.*, vol. 48, no. 3, pp. 35–40, 2010.

[278] J. M. Castro, R. Pimpinella, B. Kose, Y. Huang, B. Lane, K. Szczerba, P. Westbergh, T. Lengyel, J. S. Gustavsson, A. Larsson, and P. A. Andrekson, "48.7-Gb/s 4-PAM Transmission Over 200 m of High Bandwidth MMF Using an 850-nm VCSEL," *IEEE Photonics Technol. Lett.*, vol. 27, no. 17, pp. 1799–1801, 2015.

List of Publications, Awards and Grants

Patent

- A novel multilevel modulation scheme for high speed intensity modulated direct detection systems, "Mapping Multiplexing Technique", (MY PI2012700631).
- Accepted & presented in Tech-Connect World Innovation Conference and Exhibition, June 2015, Washington D.C, USA.

Peer Reviewed Publications

Journal Publications:-

[Paper-1] **Mohamed A. Elsherif** , and A. Malekmohammadi, " Power Efficiency Evaluation of Mapping Multiplexing Technique (MMT) and Pulse Amplitude Modulation (M-PAM) for Non-Coherent Systems," *IEEE Photonics Journal* , vol. 7(4), August 2015.

[Paper-2] **Mohamed A. Elsherif**, and A. Malekmohammadi, "Performance Enhancement of Mapping Multiplexing Technique (MMT) Utilizing Dual-Drive Mach-Zehnder Modulator for Metropolitan Area Networks," *IET Optoelectron*ics ,vol. 8, no. 6, Dec. 2014.

[Paper-3] A. MalekMuhammadi, **Mohamed A. Elsherif**, "A Novel Multilevel Coding Technique for High Speed Optical Fiber Communication Systems," *Optik - International Journal for Light and Electron Optics*, 2013.

International Conferences Publications:-

[Paper 4] Mohamed A. Elsherif , and A. Malekmohammadi, " Energy Efficient Transmission Scheme Alternative to M-PAM for Short Range Data Communication," *Tech Connect World Innovation Conference* , Taylor & Francis , Washington DC USA, June 2015.

[Paper 5] Mohamed A. Elsherif , and A. Malekmohammadi, " An Alternative to M-PAM Transmission System Featuring Improved Receiver Sensitivity for Optical Interconnects," in Proc. *IEEE Optical Interconnects* (OI), pp. 66-67, San Diego-USA, April 2015.

[Paper 6] Mohamed A. Elsherif ,A. MalekMuhammadi, "Performance Improvement of Mapping Multiplexing Technique (MMT) Using Dual-Drive Mach-Zehnder Modulator at 40 Gb/s" *in The IEEE 23rd Wireless and Optical Communication Conference (WOCC 2014)*, pp. 66-67, New-Jersey USA, May 2014.

[Paper 7] Mohamed A. Elsherif and A. MalekMohammadi, "Utilization of Dual-Drive Mach-Zehnder Modulator in Performance Improvement of Mapping Multiplexing Technique (MMT)" *In: The International Optical Society of America (OSA) Network of Students (IONS-14) Conference*, Torun Poland , 2013.

[Paper 8] Mohamed A. Elsherif and A. MalekMohammadi, "The Impact of Self-Phase Modulation on Dispersion Compensated Mapping Multiplexing Technique (MMT) *In: International Conference on Mobile, Wireless and Optical Communication*, *ICMWOC* 2013, Paris, France, 2013.

Funding Organizations

This work has been funded by both, ***The Ministry of Science, Technology and Innovation (MOSTI)*** and ***The University of Nottingham***.

Conference Meetings

- *Topical Meeting on Photonics*, Organized by IEEE Malaysia Chapter and IEEE Photonics Society, Aug. 2015.

Scholarship Grant & Awards

USA	**Best Poster Award Prize** The International Optical Society of America (OSA) Network of Students (IONS-14) Conference.
Malaysia	**Best Project Award** The International Engineering and Technology Exhibition (IETE 2015).
Malaysia	**PhD scholarship** • Funded by the Ministry of Science, Technology and Innovation (MOSTI), Malaysia.
Malaysia	**Research Assistant scholarship** • Tuition fees waiver funded by The University of Nottingham.

Certificates

1. Certified Fiber Optics Technical (**CFOT**) , *The Fiber optics Association of America (**FOA**)*, 2013.

2. Certificate of Competency in Fiber optics, *The Fiber Optic Association of Malaysia (**FOAM**)*, 2013.